



GEORG-AUGUST-UNIVERSITÄT
GÖTTINGEN

GGNB

Göttingen Graduate Center for
Neurosciences, Biophysics, and Molecular Biosciences

The role of GTPases in human mitochondrial ribosome biogenesis

Dissertation

for the award of the degree

“Doctor rerum naturalium”

of the Georg-August-Universität Göttingen

within the doctoral program: Molecular Biology of Cells
of the Georg-August University School of Science (GAUSS)

submitted by

Elena Lavdovskaia

from Druzhkivka, USSR

Göttingen, 2021

*Dedicated to my SUPERvisor Dr. Ricarda Richter-Dennerlein
and
to my husband MD Mikhail Lavdovskii.*

This work is yours as much as it is mine.

Thesis Advisory Committee (TAC)

Dr. Ricarda Richter-Dennerlein (Supervisor and First Referee)	University Medical Center Göttingen Department of Cellular Biochemistry Göttingen, Germany
Prof. Dr. Ralf Ficner	Georg-August University of Göttingen Institute for Microbiology and Genetics Department of Molecular Structural Biology Göttingen, Germany
Prof. Dr. Henning Urlaub (Second Referee)	Max Planck Institute for Biophysical Chemistry Department of Bioanalytical Mass Spectrometry Göttingen, Germany

Further Members of the Examination Board

Prof. Dr. Markus Bohnsack	University Medical Center Göttingen Department of Molecular Biology Göttingen, Germany
Prof. Dr. Jörg Stülke	Georg-August University of Göttingen Institute for Microbiology and Genetics Department of General Microbiology Göttingen, Germany
Prof. Dr. Hauke Hillen	University Medical Center Göttingen Department of Cellular Biochemistry Göttingen, Germany

Date of thesis submission: 9th June 2021

Date of oral examination: 27th July 2021

Table of Contents

Acknowledgments.....	5
List of Publications	7
Abbreviations.....	8
1 Abstract.....	11
2 Introduction.....	13
2.1 The mammalian mitochondrial ribosome: structure and function	13
2.1.1 Evolution of the mitochondrial ribosome.....	13
2.1.2 Structure of the mammalian mitochondrial ribosome	15
2.1.3 Functional sites on the mammalian mitochondrial ribosome	16
2.1.4 Mitochondrial translation	23
2.2 Mammalian mitochondrial ribosome assembly.....	29
2.2.1 Compartmentalization and kinetics	30
2.2.2 Assembly factors	33
2.3 GTP-binding proteins	37
2.3.1 Structure and molecular functions	37
2.3.2 Ribosome assembly GTPases.....	39
3 Aims and objectives.....	44
4 Results.....	45
4.1 Publication 1	45
4.2 Publication 2	65
4.3 Publication 3	94
5 Discussion	121
5.1 Identification of the human mitoribosome assembly GTPases	121
5.2 GTPBP6 and GTPBP10 as TRAFAC RA-GTPases	122
5.2.1 The structure of the GTPase domain	122
5.2.2 Recruitment to the mitoribosome and the GTPase cycle	123
5.3 The role of the Obg/HfiX superfamily GTPases in human mitoribosome biogenesis.....	125
5.3.1 The role of GTPBP10	125
5.3.2 The role of GTPBP6	127
5.4 GTPase-driven structural transitions during mtLSU biogenesis.....	128
5.5 Novel recycling pathway for human mitoribosomes	135
5.6 Structural basis of the dual function of GTPBP6 in human mitochondria....	138
6 Summary and outlook.....	140
7 References	142
List of figures.....	156
Curriculum Vitae.....	157

Acknowledgments

During my graduate work, I have enjoyed working with many amazing people and brilliant scientists to whom I am sincerely and deeply grateful.

First and foremost, I thank my supervisor Dr. Ricarda Richter-Dennerlein. Besides the formalities such as 'providing an opportunity to work on such an exciting project', I would like to thank you, Rica, for always being for me the most inspiring example of a woman in science. Your mentorship, continuous support, valuable scientific advices and warm-heartedness shaped me as a scientist and as a person during these years. I appreciate your trust while letting me travel to conferences and present our data in front of an experienced scientist in the mitochondrial field.

Second, but no less important, my sincere gratitude goes to my TAC members Prof. Dr. Ralf Ficner and Prof. Dr. Henning Urlaub. In general, thank you for the warm and encouraging atmosphere during my TAC meetings. In particular, thank you, Prof. Dr. Ficner, for your helpful advice regarding the mutational analysis of the mitoribosome assembly GTPases. Thank you, Prof. Dr. Urlaub, for providing me with the possibility to collaborate with your amazing team and to analyze hundreds of samples which I generated during my PhD work.

I am grateful to my examination board members Prof. Dr. Markus Bohnsack, Prof. Dr. Jörg Stülke and Prof. Dr. Hauke Hillen for their interest in my work.

I thank the entire GGNB team for their support during my PhD time, to answer my questions and guide me to the doctoral degree. I profited a lot from multiply workshops and courses as well as from GGNB retreats. Especially the scientific and personal support and encouragement from the 'Molecular Biology of Cells' program speaker, Prof. Dr. Markus Bohnsack, was outstanding.

Indeed, this thesis was a collaboration with brilliant researchers who contributed to my project progress. I would like to thank all of my collaborators, former and present, for making excellent science together, for their patience while discussing the results and experimental strategies. Special thanks to Prof. Dr. Hauke Hillen for introducing me to the exciting world of cryo-EM and to Dr. Kärt Denks for the replenishment of my knowledge of rapid kinetic measurements.

I am grateful to my dearest colleagues, former and present members of the NWG RRD: Elisa, Mandy, Emely, Franzi, Venkat, Marleen, Arun and Angi. Thank you, guys, for your contribution to my work and for providing a great working atmosphere. Thank you, Emely and Angi, for your excellent technical assistance! Special 'thank you' belongs to my lab partner in crime Franziska Nadler. Franzi, I know that I can rely on you both personally and

scientifically, and this is priceless. Thank you, Arun, for having fun together and for our exciting scientific discussions.

Also, I would like to thank my friends Dr. Natalia Pashkovskaia, Dr. Elisa Hanitsch, Dr. Daryna Tarasenko, Kseniia Lysakovskaia and Olexandr Dovgusha for sharing my ups and downs, for valuable advice regarding how to survive while writing the thesis, and for having my back.

List of Publications

Publication 1

Lavdovskaia, E., Kolander, E., Steube, E., Mai, M.M.-Q., Urlaub, H., and Richter-Dennerlein, R. (2018). The human Obg protein GTPBP10 is involved in mitoribosomal biogenesis. *Nucleic Acids Research* 46, 8471–8482. doi: 10.1093/nar/gky701

Publication 2

Lavdovskaia, E., Denks, K., Nadler, F., Steube, E., Linden, A., Urlaub, H., Rodnina, M.V., and Richter-Dennerlein, R. (2020). Dual function of GTPBP6 in biogenesis and recycling of human mitochondrial ribosomes. *Nucleic Acids Research* 48, 12929–12942. doi: 10.1093/nar/gkaa1132

Publication 3

Hillen, H., **Lavdovskaia, E.**, Nadler, F., Hanitsch, E., Linden, A., Bohnsack, K., Urlaub, H., and Richter-Dennerlein, R. (2021). Structural basis of GTPase-mediated mitochondrial ribosome biogenesis and recycling. *Nature Communications* 12. doi: 10.1038/s41467-021-23702-y.

Review article (not included in the thesis)

Maiti, P., **Lavdovskaia, E.**, Barrientos, A., and Richter-Dennerlein, R. (2021). Role of GTPases in Driving Mitoribosome Assembly. *Trends in Cell Biology* 31, 284–297. doi: 10.1016/j.tcb.2020.12.008

Abbreviations

(p)ppGpp	Guanosine pentaphosphate
3D	3-dimensional
A-site	Aminoacyl-site
aa-tRNA	Aminoacyl-tRNA
ANTAR	AmiR and NasR transcription antitermination regulators
ArfB	Alternative ribosome-rescue factor B
ATP	Adenosine triphosphate
ATP6/8	ATP synthase membrane subunit 6/8
<i>B. oleracea</i>	<i>Brassica oleracea</i>
<i>B. subtilis</i>	<i>Bacillus subtilis</i>
bp	Base pair(s)
C-terminus	Carboxyl-terminus
CLPP	Caseinolytic mitochondrial matrix peptidase proteolytic subunit
CO1-3	Cytochrome C oxidase subunit 1-3
CP	Central protuberance
Cryo-EM	Cryogenic electron microscopy
CTD	C-terminal domain
CYB	Cytochrome B
D-foci	Degradation-foci
DNA	Deoxyribonucleic acid
DAP3	Death associated protein 3, mS29
DDX28	DEAD-Box helicase 28
DHX30	DExH-Box helicase 30
DH-domain	Dibble-homology domain
<i>E. coli</i>	<i>Escherichia coli</i>
E-site	Exit-site
EF-G	Elongation factor G
EF-Tu	Elongation factor thermo unstable
ELAC2	ElaC gene family homolog protein 2
EngA/B	Essential neisserial GTP-binding protein A/B
Era	<i>E. coli</i> Ras-like protein
ERAL1	Era-like G-protein 1
FASTKD2	FAST kinase domain-containing protein 2
FLAG-tag	DYKDDDDK-Peptide tag
fMet	N-Formylmethionine
G-domain	GTPase domain
GAC	GTPase-associated center
GAP	GTPase activating protein
GDP	Guanosine diphosphate
GEF	Guanine nucleotide exchange factor
GST-tag	Glutathione-S-transferase tag
GTP	Guanosine triphosphate
GTPBP	GTP-binding protein
<i>H. sapiens</i>	<i>Homo sapiens</i>
H-strand	Heavy strand of mtDNA
HAS-GTPase	Hydrophobic amino acid substituted for catalytic glutamine GTPase
HEK293T	Human embryonic kidney 293 cells that express a mutant version of the SV40 large T antigen
HflX	High frequency of lysogenization, X-locus
IC	Initiation complex
ICT1	Immature colon carcinoma transcript-1
IF	Initiation factor
IMM	Inner mitochondrial membrane

kDa	Kilo Dalton
<i>L. Monocytogenes</i>	<i>Listeria monocytogenes</i>
L-strand	Light strand of mtDNA
<i>L. tarentolae</i>	<i>Leishmania tarentolae</i>
LRPPRC	Leucine rich pentatricopeptide repeat containing protein
MALSU1	Mitochondrial assembly of ribosomal large subunit protein 1
Mba1	Multi-copy bypass of AFG3 protein
MDa	Mega Dalton
METTL15	Methyltransferase Like 15
MPV17L2	MPV17 mitochondrial inner membrane protein like 2
MRG	Mitochondrial RNA granules
MRM1-3	Mitochondrial rRNA methyltransferase 1-3
mRNA	Messenger ribonucleic acid
MRP	Mitochondrial ribosomal protein
MRPL	Mitochondrial ribosomal protein of the large subunit
MRPP1-3	mitochondrial ribonuclease P protein 1-3
MRPS	Mitochondrial ribosomal protein of the small subunit
mt	Mitochondrial
mtACP	Mitochondrial acyl carrier protein 1
MTERF	Mitochondrial transcription termination factor
MTG1-3	Mitochondrial ribosome associated GTPase 1-3
(mt)LSU	(Mitochondrial) ribosomal large subunit
mtRBFA	Ribosome-binding factor A, mitochondrial
MTRES1	Mitochondrial transcription rescue factor 1
mtRF-R	Mitochondrial translation release factor in rescue
mtRNAP	Mitochondrial RNA polymerase
mtSSU	(Mitochondrial) ribosomal small subunit
N-terminal	Amino-terminal
NCR	Non-coding region
ND1-6	NADH dehydrogenase subunit 1-6
nDNA	Nuclear DNA
NGRN	Neugrin, neurite outgrowth associated
NOA1	Nitric oxide associated protein 1
NSUN4	NOL1/NOP2/Sun domain family member 4
NTP	Nucleoside triphosphate
Obg	spo0B-associated GTP-binding protein
OBGH	Obg-homolog, human
ORF	Open reading frame
Oxa1	Oxidase assembly 1
OXA1L	Oxidase assembly 1-like
OXPHOS	Oxidative phosphorylation
P-loop (GTPases)	Phosphate-loop
P-site	Peptidyl-site
PES	Polypeptide exit site
PET	Polypeptide exit tunnel
Pi	Inorganic phosphate
PIC	Pre-initiation complex
PNPase	Polynucleotide phosphorylase
POLRMT	DNA-directed RNA polymerase, mitochondrial
Poly-A	Poly-adenosine
PPR	Pentatricopeptide repeat
PTC	Peptidyl transferase centre
PTCD1/3	Pentatricopeptide repeat domain 1/3 protein
r-proteins	Ribosomal proteins
RA-GTPases	Ribosome-associated GTPases

Ras	Rat sarcoma protein
RbgA	Ribosome biogenesis GTPase A
RCC1L	RCC1-like G exchanging factor-like protein
REXO2	RNA exonuclease 2
RF	Release factor
RluC/D	Ribosomal large subunit pseudouridine synthase C/D
RNA	Ribonucleic acid
ROS	Reactive oxygen species
RPUSD3-4	RNA pseudouridine synthase D3-4
RRF	Ribosome recycling factor
RrmJ	Ribosomal RNA large subunit methyltransferase J
rRNA	Ribosomal ribonucleic acid
S	Svedberg unit
<i>S. aureus</i>	<i>Staphylococcus aureus</i>
<i>S. cerevisiae</i>	<i>Saccharomyces cerevisiae</i>
<i>S. scrofa</i>	<i>Sus scrofa</i>
<i>S. solfataricus</i>	<i>Sulfolobus solfataricus</i>
SD sequence	Shine–Dalgarno sequence
SILAC	Stable isotope labelling by amino acids in cell culture
SLIRP	Stem-loop-interacting RNA binding protein
Spp.	Several species
SRL	Sarcin-ricin loop
<i>T. thermophila</i>	<i>Tetrahymena thermophila</i>
<i>T. brucei</i>	<i>Trypanosoma brucei</i>
TEFM	Transcription elongation factor, mitochondrial
TFAM	Transcription factor A, mitochondrial
TFB1/2M	Transcription factor B1/2, mitochondrial
TIM44	Mitochondrial import inner membrane translocase subunit 44
TRAFAC class	Translation factors class of GTPases
trGTPases	Translational GTPases
TRMT2B	tRNA methyltransferase 2 homolog B
TRMT61B	tRNA methyltransferase 61B
tRNA	Transfer ribonucleic acid
TRNT1	tRNA nucleotidyl transferase 1
TRUB2	TruB pseudouridine synthase family member 2
UTR	Untranslated region
WBSCR16	Williams-Beuren syndrome chromosome region 16
WT	Wild type

Other abbreviations used in this thesis: amino acids are designated according to the one-letter or three-letter IUPAC code. Nucleotides are designated according to the standard IUPAC code.

1 Abstract

Mitochondria are essential organelles of eukaryotic cells, which produce the vast majority of the cellular ATP via oxidative phosphorylation (OXPHOS). The mitochondrial gene expression machinery contributes to the formation of the OXPHOS complexes by providing 13 core protein components synthesized by dedicated mitochondrial ribosomes (mitoribosomes). Despite the recent progress in our understanding of the mitoribosome structure and function, the assembly pathway of this ribonucleoprotein complex remains elusive. Furthermore, an increasing number of diseases are linked to defects in the mitochondrial translation apparatus but the molecular basis of these disorders is still unknown.

Mitoribosome biogenesis is facilitated by nuclear-encoded auxiliary factors required for the proper assembly and folding of RNAs and mitoribosomal proteins. The human genome encodes numeral GTP-binding proteins that are involved into the biogenesis of the mitoribosomal particles. However, the exact molecular functions of these proteins remain largely unknown. Using the combination of biochemical, mass spectrometry and structural biology methods, we identified the members of the Obg/HflX GTPases superfamily GTPBP6 and GTPBP10 as factors required for late stages of mitoribosomal large subunit (mtLSU) assembly. We showed that GTPBP10 associates with the other factors, including proteins required for the 16S rRNA processing, mitochondrial RNA granule components and late mitoribosome assembly factors such as the MALSU1 module and the MTERF4-NSUN4 complex to facilitate mtLSU maturation. Altogether, our data suggest that GTPBP10 is essential for mitoribosome biogenesis and thus for mitochondrial translation and OXPHOS complexes formation.

The other GTPase, GTPBP6 is homologous to bacterial HflX protein. We have shown that in humans GTPBP6 retains its conserved function as a ribosome recycling factor. Surprisingly, in contrast to its bacterial counterpart, GTPBP6 does fulfill an additional role as a mitoribosome biogenesis factor and is essential for cell growth and mitochondrial gene expression under physiological conditions. GTPBP6 ablation abolishes mitoribosome formation associated with the accumulation of the nearly matured subunits, thereby leading to mitochondrial translation deficiency. Loss of GTPBP6 stalls mtLSU maturation at a very late assembly stage when all of the mitoribosomal proteins are incorporated. Cryo-electron microscopy approach revealed that GTPBP6 is required for the final folding of the catalytic core of the ribosome – the peptidyl transferase center (PTC). Additionally, the analysis disclosed an interplay of the assembly factors during the PTC maturation. Thus, we have shown that GTPBP5 cooperates with MTERF4-NSUN4 complex to promote the PTC folding.

In summary, our data has revealed that GTPBP6 and GTPBP10 coordinate late steps of the PTC maturation in collaboration with the other assembly factors. This mode of the mitoribosome biogenesis is reminiscent of other ribosomes and highlights the evolutionary conserved mechanism of involved GTPases. Moreover, we have disclosed an alternative pathway for mitoribosome recycling mediated by GTPBP6.

2 Introduction

2.1 The mammalian mitochondrial ribosome: structure and function

2.1.1 Evolution of the mitochondrial ribosome

Ribosomes are large ribonucleoprotein complexes that catalyze protein synthesis in all living cells. A ribosome consists of two unequal subunits: a large ribosomal subunit (LSU) and a small ribosomal subunit (SSU) according to their sedimentation profile. The SSU provides the platform for mRNA binding and decoding while the LSU catalyzes the peptidyl transferase reaction leading to nascent peptide bond formation. Although ribosomes maintain a relatively conserved 'core' to fulfill universal translation function, they vary in their peripheral 'shelves' structure and composition between different domains of life, probably reflecting the specific adaptation to intracellular/intraorganellar environment and needs (reviewed by Márquez et al., 2011; Melnikov et al., 2012). Regardless of our rather detailed knowledge about bacterial and eukaryotic cytosolic ribosome structure and mechanism of action, insights about organellar ribosomes have been just started to emerge during the last decade.

The acquisition of organelles preconditioned the rise of the eukaryotic life. For example, mitochondria were gained as a product of endosymbiotic co-evolution between an α -proteobacterial cell and a host cell of archaeal lineage (Roger et al., 2017; Zaremba-Niedzwiedzka et al., 2017). Although the modern organelle fulfills a broad range of functions, its gene expression machinery, including the mitochondrial ribosomes (mitoribosomes), is entirely dedicated to the biosynthesis of the core components of the oxidative phosphorylation system (OXPHOS).

As the data obtained by comprehensive structural, genomic and proteomic studies have been accumulated during the last two decades, we can now postulate that although mitoribosomes from different eukaryotic lineages share bacterial ancestry, they are strikingly distinct in both general architecture and rRNA/protein content (Table 1) (reviewed by (Kummer and Ban, 2021; Waltz and Giegé, 2020). However, a few underlying principles exist that can be applied to all of the mitoribosomes characterized to date: (i) mitoribosomes have a dual genetic origin: the rRNA content is encoded solely by mtDNA and most (or even all) of the MRPs are products of the nuclear genome; (ii) mitoribosomes are porous complexes and their sizes are larger than that of the bacterial counterpart; (iii) mitoribosomes are enriched in their protein content and have acquired up to 70 additional proteins in different lineages in comparison to their bacterial ancestor; (iv) rRNAs mostly accumulate in the mitoribosomal core while the MRPs cover near the entire surface, protecting rRNAs from reactive oxygen species (ROS); (v) many MRPs are unique to mitochondria with no

homologs in bacterial or cytosolic ribosomes; (vi) certain conserved MRPs have acquired extra species-specific sequences on their N- or C-termini; (vii) 5S rRNA – a structural component of the central protuberance (CP) – was lost from all mitoribosomes (with an exception of the plant mitoribosome) and substituted either by a structural tRNA (mammals), rRNA extensions (fungi), or MRPs extensions (kinetoplastids); (viii) mitoribosomes are associated with the inner mitochondrial membrane (IMM) to enable co-translational insertion of the OXPHOS proteins (Amunts et al., 2015; Desai et al., 2017; Greber et al., 2015; Ramrath et al., 2018; Tobiasson and Amunts, 2020; Waltz et al., 2020).

Table 1. The diverse composition of mitochondrial ribosomes.

	Bacteria	Mammals	Fungi	Plants	Kinetoplastida	Ciliata
	<i>E. coli</i>	<i>H. sapiens</i> <i>S. scrofa</i>	<i>S. cerevisiae</i>	<i>B. oleracea</i>	<i>Trypanosoma spp.</i> , <i>L. tarentolae</i>	<i>T. thermophila</i>
Sedimentation coefficient	70S	55S	74S	78S	50S	80S
Molecular weight, MDa	2.3	2.7	~3-3.3	–	~4.5	~4
Number of rRNAs	3 (16S, 5S, 23S)	3 (12S, tRNA ^{Val/Phe} , 16S)	2 (15S, 21S)	3 (18S, 5S, 26S)	2 (9S, 12S)	2 (14S, 21S)
Number of proteins	54	82	73	~86	~122	92

Table is adapted from Kummer and Ban, 2021; Greber and Ban, 2016.

Mitoribosomes underwent two distinct evolutionary phases. The first constructive phase occurred before the divergence of the major eukaryotic lineages resulting in an extensive gaining of the mitoribosomal protein mass. The second reductive phase concerned metazoans and kinetoplastids and led to a nearly double diminution of the rRNA content (Petrov et al., 2018; van der Sluis et al., 2015; reviewed by Waltz and Giegé, 2020). However, despite the size reduction, the structural elements of the rRNAs comprising the ribosome catalytic core remain largely unaffected and resemble that of bacterial ribosomes.

The constructive phase was proposed to be driven by an accumulation of deleterious mutations and erosions in the genome of the pre-mitochondria, initiating the substantial incorporation of proteins to the mitoribosome to ‘patch’ the resulting instabilities (Petrov et al., 2018; van der Sluis et al., 2015). Some of them are conserved in all investigated eukaryotes (as CP components mL41 and mL46 and mtSSU structurally integrated GTPase mS29), while other novel MRPs only occur in specific lineages as an adaptation to distinct mitoribosomal properties (Desmond et al., 2011; Petrov et al., 2018). For example, MRPs mL57 and mL58 are only found in yeast and were recruited to stabilize fungi-specific rRNA expansions.

The primitive mitoribosomal ancestor comprised 54 MRPs, and the gaining of the 15 mitochondrial-specific MRPs has happened before the major divergence of the eukaryotic lineages. Subsequent recruitment and loss of MRPs were lineage-specific (Desmond et al., 2011; Petrov et al., 2018; Smits et al., 2007). What is the origin of the super numerous MRPs

in the mitoribosome? Some of the MRPs appeared as a result of gene duplication. The most striking example is the existence of the three isoforms for bS18 (MRPS18) (Koc et al., 2001a). bS18m (MRPS18C) and mS40 (MRPS18B) are components of the mtSSU, whereas the third isoform mL66 (MRPS18A) was recruited to the mtLSU (Amunts et al., 2015; Greber et al., 2015). Second, mitoribosome has engaged pre-existing proteins and adapted their functionality as structural components. For example, mL39 was acquired into the mitoribosome in the form of mitochondrial threonyl-tRNA synthetase, later losing its functional enzyme domains by adaptive evolution (reviewed by O'Brien, 2002). mS29, also known as DAP3 (death-associated protein 3), is implicated in apoptosis (Koc et al., 2001b); reviewed by O'Brien, 2002). The other example is the recruitment of a peptidyl-tRNA hydrolase mL62 (ICT1) as a structural element of the CP (Brown et al., 2014; Greber et al., 2014; Richter et al., 2010). Further analysis indicated that the incorporated copy of mL62 fulfills a structural function solely since it locates far away from the site of action of typical peptidyl-tRNA hydrolases (Akabane et al., 2014; Brown et al., 2014; Greber et al., 2014).

During the reductive phase, the diminution of the rRNA was accompanied by the loss of some proteins due to the contraction of their corresponding rRNA binding sites (Petrov et al., 2018; van der Sluis et al., 2015). Indeed, gaining of the compensative elements was a prerequisite of the rRNA/MRPs loss and was rather a result of a neutral evolution where structural features were fixed into mitoribosomes following codependent mutations without any apparent functional reason. Interestingly, evolutionary shaping of the mammalian mitochondrial ribosome was coupled with the gaining of the specific assembly factors as it was shown, for example, for certain RNA-binding enzymes (reviewed by van Esveld and Huynen, 2018).

2.1.2 Structure of the mammalian mitochondrial ribosome

A fully-assembled, mature mammalian mitoribosome has a sedimentation coefficient of 55S and a molecular mass of 2.7 MDa. The rRNA content of the 55S particle is reduced to an inner core extensively covered by a protein coat (Sharma et al., 2003). Thus, the loss of the rRNA segments and recruitment of novel proteins result in a protein to rRNA ratio of 2:1, which is reverse in ancestral 70S ribosomes. The mtSSU consists of 12S rRNA and 30 ribosomal proteins (r-proteins), 14 of which are mitochondrion-specific (Amunts et al., 2015; Greber et al., 2015). The mtLSU encompasses 2 RNA molecules – 16S rRNA and structural tRNA^{Val} or tRNA^{Phe} and 52 proteins with 22 mitochondrion-specific (Brown et al., 2014; Greber et al., 2014). In mammals, all of the 82 MRPs are encoded by the nuclear genome. The 36 mitochondrion-specific proteins form clusters that occupy the L7/L12 stalk, the central protuberance and the polypeptide exit site (PES) on the mtLSU as well as the head (mS29 cluster) and the foot (mS27 cluster) of the mtSSU (Figure 1).

The mitoribosome is a highly dynamic structure. Therefore, its functional integrity relies on intersubunit contacts at the subunit interface, namely intersubunit bridges. High resolution structures revealed that mitoribosomal subunits in mammals interact less extensively than in bacteria, forming 15 intersubunit bridges (Amunts et al., 2015; Greber et al., 2015; Sharma et al., 2003). Remarkably, most of the contacts are mediated by protein-protein (3) or protein-RNA (6) interactions, while in bacteria, intersubunit bridges are formed mainly via RNA-RNA contacts (Amunts et al., 2015; Greber et al., 2015; Liu and Fredrick, 2016; reviewed by Greber and Ban, 2016). Eight of these bridges are mitochondrion-specific since they are built by mitochondrion-specific proteins or mitochondrion-specific protein extensions (Amunts et al., 2015).

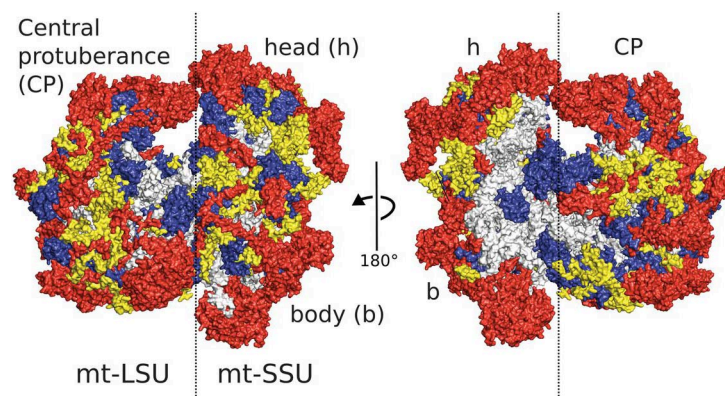


Figure 1. Overview of the human mitoribosome structure. rRNA core (grey), proteins conserved with bacteria (blue), extensions of homologous proteins (yellow) and mitoribosome-specific proteins (red). Figure is taken from Amunts et al., 2015. Reprinted with permission from AAAS (licence number 5084760494378).

2.1.3 Functional sites on the mammalian mitochondrial ribosome

Although the evolutionary process has significantly modified the mitoribosome architecture and composition, the functional centers crucial for the universal translation mechanism were preserved, albeit with novel structural features. In the next chapter, these functional sites will be described, and the structural divergence and conservation will be highlighted.

2.1.3.1 The central protuberance

The CP is an essential structural element of the mtLSU. It forms two mitochondrion-specific intersubunit bridges with the mtSSU head contacting the intrinsic GTPase mS29. The second crucial function of the CP is to hold intersubunit-bound tRNAs during translation. Generally, the CP of the mitoribosomes is highly remodeled (Aibara et al., 2020; Brown et al., 2014; Greber et al., 2014). It consists mainly of helices 80-88 of the 16S rRNA domain V and is characterized by a replacement of the backbone 5S rRNA by a structural tRNA^{Val} in human and tRNA^{Phe} in porcine. Remarkably, the arrangement of the structural tRNAs in a tRNA^{Phe}-

12S rRNA-tRNA^{Val}-16S rRNA polycistronic transcript features the engagement of the 5S rRNA in the same operon together with the other rRNA species in bacteria and thus allows their processing in stoichiometric amounts. On the organism level, a single type of these two structural tRNAs incorporates into the mtLSU in all tissues depending on the species. However, at least in humans the mitoribosome can switch to tRNA^{Phe} instead of tRNA^{Val} when the availability of the latter is compromised (Chrzanowska-Lightowlers et al., 2017; Rorbach et al., 2016).

Structurally, the mammalian CP consists of a partially conserved platform formed by uL18, bL27, mL38, mL52 and mL62 connected via tRNA^{Val/Phe} to the mitochondrion-specific cluster of mL40, mL46 and mL48 (Figure 2). The core architecture of the CP is maintained by mL38, which mimics the 5S rRNA function to connect the base of the CP to the 16S rRNA in the ribosome body.

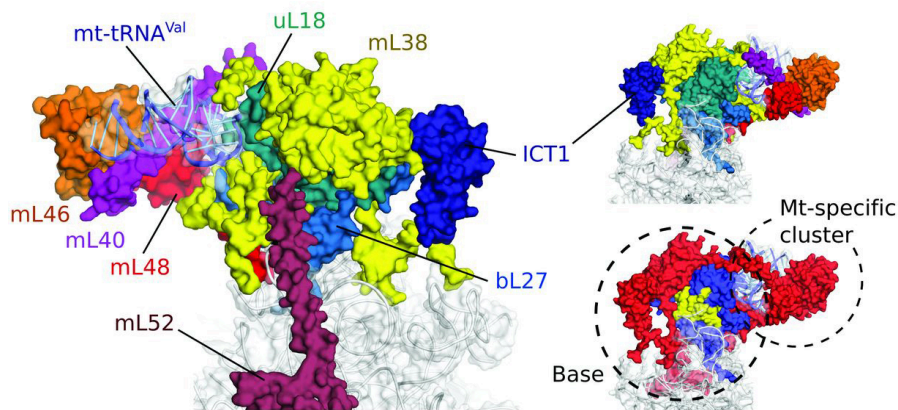


Figure 2. Structure of the human mitoribosomal central protuberance. Left panel: the CP is organized around the structural tRNA^{Val/Phe} (light blue) and consists of the base (uL18m, bL27m, mL38, mL52 and mL62 (ICT1)) and the recruited mitoribosomal-specific cluster (mL40, mL46 and mL48). The rRNA core is shown in pale grey. Right top panel: view of the CP rotated by 180°. Right bottom panel: protein composition of the CP colored according to homology to bacterial ribosomal proteins. Conserved (blue), mitochondrion-specific (red) and homologous proteins with mitochondrion-specific extensions (yellow). Figure is taken from Brown et al., 2014. Reprinted with permission from AAAS (licence number 5084761044145).

Evolutionary, the displacement of 5S rRNA was coupled with the universal loss of bL25 as the protein is tightly associated with this structural element. Considering the central role of the 5S rRNA in the CP structure and function, the prerequisite incorporation of the mL38, mL40 and mL46 was suggested for partial structural compensation (Petrov et al., 2018). Further shortening of the 16S rRNA segments involved in CP formation in mammals led to the incorporation of mL48 and the structural tRNA stabilized by pre-existing proteins uL18m and mL38.

2.1.3.2 The peptidyl transferase center

The peptidyl transferase center (PTC) locates on the subunit interface of the mtLSU beneath the CP. It comprises structural elements of the 16S rRNA (multi-branched central loop of the domain V of the rRNA) (Figure 3) and shows unprecedented homology to both bacterial and cytosolic ribosomes emphasizing the conserved catalytic function (Ban et al., 2000; Greber et al., 2014; Nissen et al., 2000; reviewed by Polacek and Mankin, 2005). Especially, the interactions stabilizing the conserved CCA tails of tRNAs in the A- (aminoacyl) and P- (peptidyl) sites have been retained and are mediated by the A-loop (helix 92) and P-loop (helix 80), respectively (Brown et al., 2014; Greber et al., 2014). For instance, bases U2993 (bacterial U2506) and A2938 (bacterial A2451) maintain the same structural orientation and reach the A- and P-site tRNAs, respectively (Greber et al., 2014; Voorhees et al., 2009). The only protein approaching the PTC rRNA is the N-terminal part of bL27m stabilizing the P-site tRNA acceptor arm (Aibara et al., 2020; Greber et al., 2014; 2015). In bacterial ribosomes, bL27 also contacts the PTC, but interacts with the A-site tRNAs (Voorhees et al., 2009). However, as it was shown for *E. coli* PTC, the protein does not contribute to the catalytic activity but rather implements structural function by holding rRNA elements together (Maracci et al., 2015).

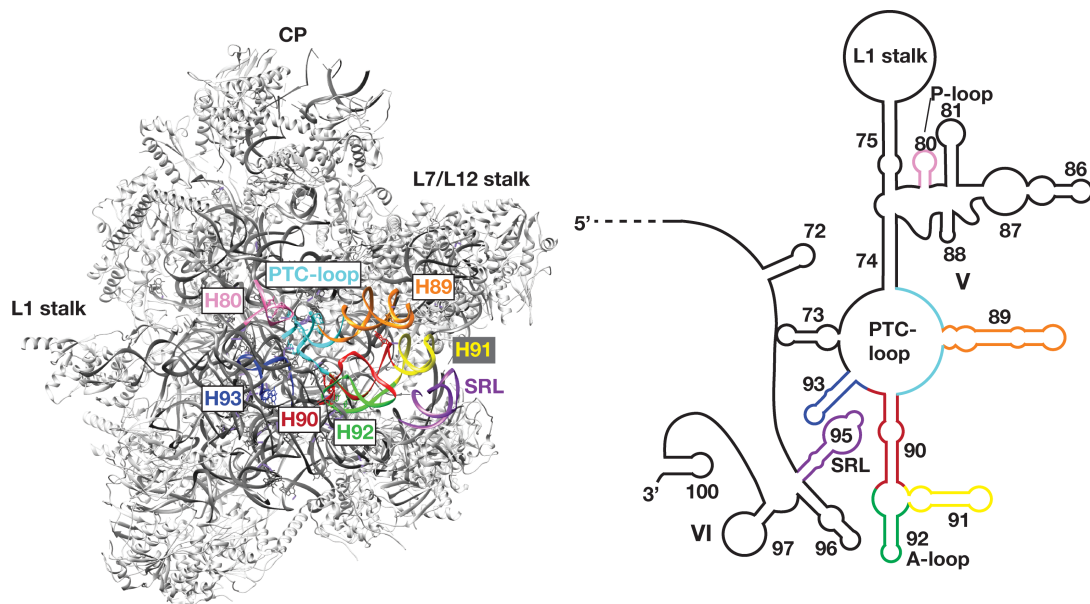


Figure 3. Schematic representation of the PTC structure. Left panel: relative position of the crucial 16S rRNA helices of the mtLSU core comprising the PTC and involved in polypeptide synthesis. Sarcin-ricin loop (SRL) belongs to the mtLSU GAC (GTPase-associated center) functionally closely interconnected with the PTC. Right panel: schematic depiction of the 16S rRNA domain V secondary structures which form the PTC as shown in the left panel. The colors of the 16S rRNA helices correspond to the left panel. The structure is visualized with UCSF Chimera (PDB: 3J7Y). 16S rRNA is shown in dark grey and proteins are shown in light grey.

2.1.3.3 The polypeptide exit tunnel

The polypeptide exit tunnel (PET) starts at the PTC and protrudes to the polypeptide exit site (PES). In contrast to the remodeled PET of the yeast mitoribosome, the mammalian counterpart uses the canonical PET path consisted of the bacterial/cytosolic homologous proteins, namely bL17m, uL22m, uL23m, uL24m and uL29m. The tunnel wall is highly hydrophobic, mainly due to exposure of hydrophobic residues of uL22m and mimics the IMM environment (Brown et al., 2014). However, the major structural divergences are observed close to the PES due to the massive depletion of the rRNA segments (domain I and III) and the recruitment of the novel mitochondrion-specific proteins mL39, mL41, mL44 and mL45. These are coupled with the specific adaptation of the mitochondrial translation apparatus to synthesize, extrude and insert hydrophobic OXPHOS proteins into the IMM (Brown et al., 2014; Greber and Ban, 2016; Greber et al., 2014; reviewed by Ott et al., 2016; Petrov et al., 2018; Bieri et al., 2018). The mitoribosome is tethered to the IMM via charge-based contact mediated by mL45 that is homologous to the mitochondrial IMM translocase subunit TIM44 and the yeast mitoribosome membrane anchor Mba1 (multi-copy bypass of AFG3 protein) (Englmeier et al., 2017; Kummer et al., 2018).

Remarkably, when the mitoribosome resides in an inactive state, the PET is entirely blocked by insertion of the mL45 N-terminal tail cemented by electrostatic interactions between the basic residues and 16S rRNA moieties and the PES is further obstructed by a protrusion of uL23m (Figure 4) (Itoh et al., 2021; Koripella et al., 2020; Kummer et al., 2018).

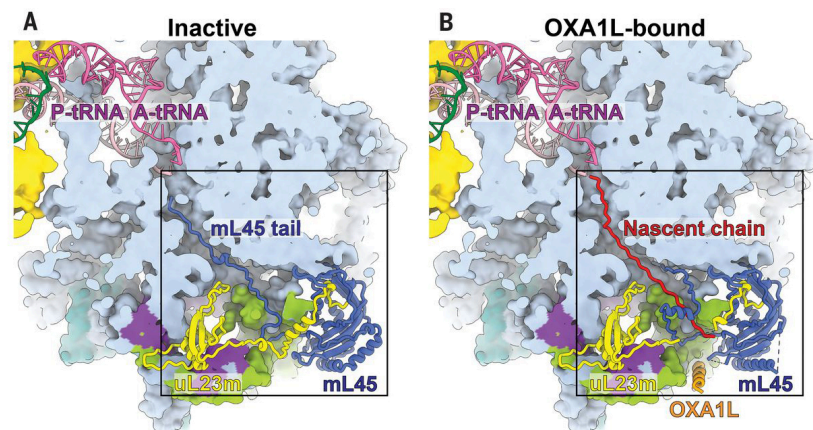


Figure 4. Structure of the human mitoribosome bound to the OXA1L insertase. In the inactive state (A) the PET is obstructed by insertion of mL45 tail (dark blue) and by a protrusion of uL23m (yellow). During translation elongation, when the nascent chain (red) is starting to emerge (B), mL45 interaction with OXA1L (orange) leads to displacement of mL45 N-terminal tail from the PET. Additional proteins involved into interaction with OXA1L are shown in green (uL24m) and violet (uL29m). Figure is taken from Itoh et al., 2021. Reprinted with permission from AAAS (licence number 5084761209867).

Recent studies have resolved a long-standing question of the exact mechanism of co-translational insertion of the nascent OXPHOS proteins into the IMM (Desai et al., 2020; Itoh et al., 2021). The insertion is carried out by the oxidase assembly 1-like (OXA1L) protein, a homolog of yeast Oxa1 and bacterial YidC (Haque et al., 2010a; 2010b). OXA1L interacts with the mitoribosome via three distinct contact sites. When bound to OXA1L during translation elongation, the rotation and displacement of the mL45 N-terminus followed by excision of the uL23m plug enable the growing peptide chain to leave the mitoribosome (Figure 4) (Itoh et al., 2021; Koripella et al., 2020; Kummer et al., 2018). Thus, in addition to its function as a mitoribosome membrane tether, mL45 guides the nascent chain to the exit of the tunnel and holds space between the PES and the IMM insertase to allow post-translational modification and folding of the newly synthesized polypeptides. Although it was suggested that the specific structure of the PET favors co-translation folding of the nascent OXPHOS components (reviewed by Bieri et al., 2018; Greber and Ban, 2016; Ott et al., 2016), the recent study argues that the constrictions observed in the tunnel would prevent the secondary structure formation until a protein does not reach the 'folding pocket' formed by mL45 and the IMM (Itoh et al., 2021).

2.1.3.4 The L7/L12 stalk and the ribosome GTPase-associated center

The L7/L12 stalk is an extended dynamic structure of the LSU. In bacteria, the stalk consists of several (typically 4, 6 or 8) copies of bL12 protein connected to the uL10 N-terminal domain (Davydov et al., 2019). The construct associates with respective 23S rRNA segments (domain II, helix 42-43) next to the uL11-binding site (helix 43-44), thereby forming a stalk base. The stalk is part of a ribosome site called the GTPase-associated center (GAC). The GAC is essential for protein synthesis, since together with helix 95 (sarcin-ricin loop, SRL), its function is to recruit translational GTPases and stimulate factor-dependent GTP hydrolysis. The computational approach allowed to predict a copy number of bL12m in mammalian mitochondria even before the first high-resolution structures of the mitoribosome stalk had been published (Davydov et al., 2019). Thus, three putative binding sites for bL12m dimers were allocated to uL10m. Indeed, recent structural findings revealed that the stalk comprises 6 N-terminal copies of the bL12 protein that bridges interactions with uL10m and mito-specific protein mL53 (Aibara et al., 2020).

Due to conserved crucial function, the structural elements of the 16S rRNA that comprise the L7/L12 stalk in mammals (helices 42-44) and the SRL are preserved and did not undergo reductive evolution (Brown et al., 2014; Petrov et al., 2018). However, the acquisition of the mitochondrion-specific proteins makes the structure more stable than in the other ribosomes owing to hydrophobic protein-protein interactions (Aibara et al., 2020; Brown et al., 2014). In mitoribosomes, the stalk is connected to the ribosome body via mL66 and mL53 as well as mitoribosome-specific N-terminal extension of uL10m (Aibara et al., 2020; Brown et al.,

2014). In addition, mL54 is involved in stabilizing interactions with uL11m (Aibara et al., 2020).

2.1.3.5 The mRNA channel and the mitoribosome decoding center

As mentioned before, there is a functional separation of the two mitoribosomal subunits during the translation process. The previously described mitoribosomal elements belong to the mtLSU and deal with polypeptides, whereas the mtSSU secures the interactions with the mRNA as well as cognate tRNA anticodon recognition and pairing. The mRNA enters and goes forward through the mitoribosome via the RNA-rich mRNA channel. Despite the functional parts of the channel, responsible for mRNA decoding, are relatively well conserved in the human mitoribosome, its entrance and exit sites are significantly remodeled due to the adaptation to translate short, mostly leaderless mitochondrial mRNAs (reviewed by (Temperley et al., 2010a).

The canonical ring-like structure at the entrance site, which possesses the RNA-helicase activity to unwind mRNA secondary structures in bacteria, is absent from the mammalian mitoribosome due to the loss of uS4 and shortening of the uS3m N-terminus (Amunts et al., 2015; Greber et al., 2015). Instead, the remodeled gate is partially formed by mitochondrion-specific expansion of uS5m and has a wider diameter, and a novel pentatricopeptide repeat (PPR) protein mS39 (PTCD3) is recruited to the solvent side of the mtSSU head (Figure 5) (Amunts et al., 2015; Greber et al., 2015). A recent study has revealed the mechanism of mRNA delivery to the mitoribosome (Aibara et al., 2020). In an actively translating mitoribosome, the LRPPRC/SLIRP complex bound to the mt-mRNA interacts with mS39 enabling mRNA engagement to the mtSSU.

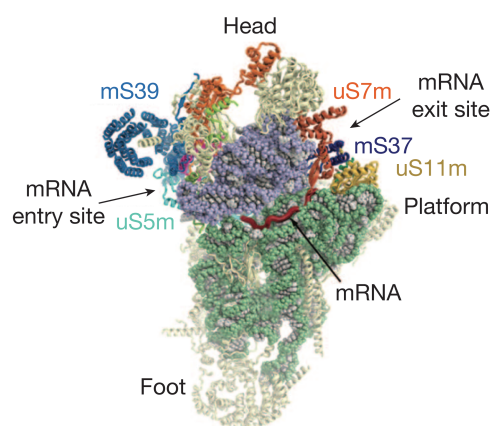


Figure 5. The mammalian mitochondrial mRNA channel. The channel surrounds the mtSSU neck and houses the conserved site for mRNA decoding. As a result of an adaptation to specific features of the mitochondrial mRNAs, the mRNA entry and exit sites are significantly remodeled compared to bacterial ribosomal SSU. The entry site is formed by the mitochondrion-specific extension of uS5m and a newly recruited MRP mS39. The fixation of mRNA 3' end is achieved at the exit site by interaction with mS37. mRNA is shown in red. Figure is modified from Greber et al., 2015.

As an adaptation to the absence of the Shine-Dalgarno sequence in mt-mRNAs, the exit part of the tunnel lacks the rRNA elements involved in rRNA-mRNA pairing in bacteria. Thus, the 3' end of the 12S rRNA is stably fixed by the association with mS37 (Figure 5) (Amunts et al., 2015; Greber et al., 2015; Kaushal et al., 2014). The exit is also surrounded by bS1m, uS7m, uS11m, bS18m and bS21m where the positively charged bS1m oligonucleotide-binding domain additionally stabilizes mRNA (Amunts et al., 2015; Greber et al., 2015).

The decoding center provides a platform for mRNA pairing with the cognate tRNA and ensures their correct interaction. The structural 12S rRNA motifs involved in the decoding center formation are highly conserved, suggesting that the mechanism employed by mitoribosomes resembles the decoding process in bacteria. The 3' minor domain of the 12S rRNA (helix 44) provides a structural scaffold for the main body of the mtSSU and encompasses the mRNA decoding site on the subunit interface (Greber et al., 2015; Kaushal et al., 2014). Adenine bases A1565 and A1566 (corresponding to bacterial A1492 and A1493) of the helix 44 serve to discriminate between correct and incorrect codon-anticodon pairs (Desai et al., 2020; Greber et al., 2015). They are inserted into the minor groove of the codon-anticodon helix in the mitoribosomal A-site in a way residing the analogous bacterial proof-reading system (Ogle et al., 2001; Yoshizawa et al., 1999). Another conserved interaction forms between the G903 (bacterial G530) of the 12S rRNA 5' domain and the codon-anticodon helix.

2.1.3.6 tRNA binding sites

During translation elongation tRNAs are bound to the three functional sites located at the intersubunit space. A-, P-, and E-sites are relatively similar to those in other ribosomes in nucleotide sequence and structure. However, the protein environment of the tRNA-binding positions is highly remodeled due to the adaptation to the considerably variable elbow regions of the human mitochondrial tRNAs with reduced or absent D- and/or T-loops (Helm et al., 2000). In addition, elimination of certain rRNA structural elements makes the tRNA binding sites prone to accommodate versatile structures of the tRNAs. For example, the A-site remodeling includes the loss of the conventional A-site finger formed by rRNA helix 38 and bL25 (Aibara et al., 2020; Brown et al., 2014; Greber et al., 2014; 2015). To compensate for the absence of the structural elements engaged in tRNA accommodation, the mitoribosome evolved a new element called P-site finger. It is formed by two proteins structurally belonging to the CP – mL40 and mL48. The finger is inserted between A- and P-sites where the N-terminal helix of mL40 interacts with A- and P-site tRNAs elbow regions (Aibara et al., 2020; Greber et al., 2015). mL48 does not touch tRNAs directly but forms hydrophobic contacts with mL40, thus securing its sustaining function (Aibara et al., 2020). The E-site, which is positioned close to the L1 stalk and ejects tRNAs from the ribosome, has lost essential rRNA elements involved into tRNA binding such as helices 76-77 (Brown et al.,

2014; Greber et al., 2014). The long C-terminal helix of the mitochondrion-specific MRP mL64 together with uS7m stabilizes the elbow region of E-site tRNA (Aibara et al., 2020; Greber et al., 2014).

2.1.4 Mitochondrial translation

Translation is the finalizing step of mitochondrial gene expression. As a basic matrix process, mitochondrial translation proceeds through three canonical steps assisted by a conserved set of translation factors encoded by nDNA: initiation, elongation and termination of the polypeptide synthesis followed by recycling of the mitoribosomes at the end of the translation cycle. Despite the bacterial origin of the mitochondrial translation apparatus, evolutionary divergence of the mitoribosome architecture, mitochondrial genetic code and specific features of the mt-mRNAs contribute to the remarkable differences between bacterial and mitochondrial translation processes. Strikingly, human mitochondria use alternative codons to initiate and terminate protein synthesis; mRNAs do not have 5' untranslated regions (UTRs) and 3' polyadenine (poly-A) tails are shortened; 2 mRNAs, ND4L/ND4 and ATP8/ATP6, are bi-cistronic and each of them contains two partially overlapping open reading frames (ORFs) (Figure 6) (reviewed by Temperley et al., 2010a; Hällberg and Larsson, 2014; Ott et al., 2016; Kummer and Ban, 2021). As the number of individual codons in mt-mRNAs exceeds the number of tRNAs, the latter often have a modified uridine base in the wobble position introduced by GTP-binding protein 3 (GTPBP3), allowing non-conventional base pairing (reviewed by Bohnsack and Sloan, 2018).

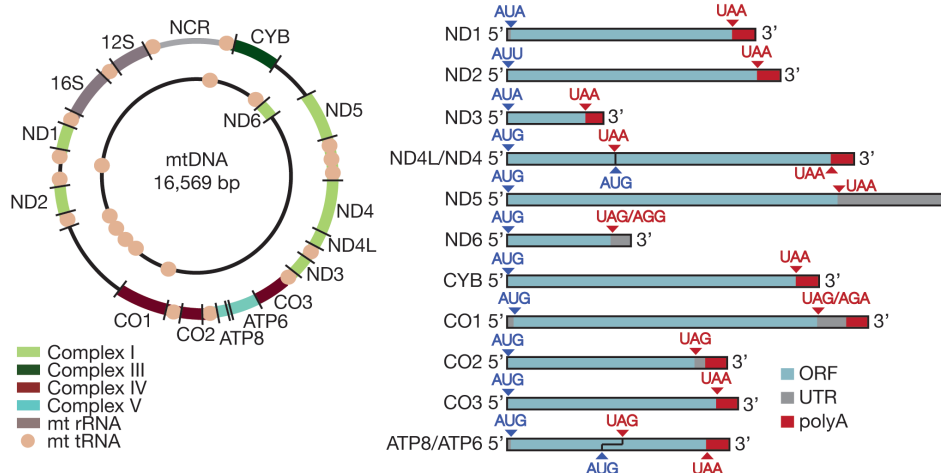


Figure 6. The mitochondrial genome and RNAs. Right panel: circular mtDNA consists of 2 strands: the heavy strand (H-strand) and the light strand (L-strand). L-strand encodes for 8 mitochondrial tRNAs (mt-tRNA, beige dots) and ND6 mRNA. H-strand contains a regulatory non-coding region (NCR, grey) and encodes for 12 mRNAs and 14 tRNAs as well as 12S rRNA and 16S rRNA (dark grey). Left panel depicts characteristic features of the mt-mRNAs, such as short or absent poly-A tails and absence of the 5' UTR. Two mRNAs are bi-cistronic (ND4L/ND4 and ATP8/ATP6). Figure is modified from Hällberg and Larsson, 2014 and Richter-Dennerlein et al., 2015).

2.1.4.1 Initiation

Translation initiation begins with the formation of the initiation complex on the SSU. In bacteria, it contains initiation factors IF1, IF2, IF3, mRNA and fMet-tRNA^{fMet} and proceeds through the formation of the distinct initiation complexes (IC) (reviewed by Rodnina, 2018). IF3 and IF2*GTP bind SSU and promote the recruitment of IF1, which preserves the A-site against premature tRNA accommodation; IF2*GTP recruits fMet-tRNA^{fMet} and IF3 monitors the P-site for the presence of mRNA start codon. Recruitment of a mRNA to the SSU via pairing of the Shine–Dalgarno (SD) sequence with anti-SD of the rRNA accomplishes the formation of the SSU IC. Remarkably, the factor recruitment does not always follow the same order, and mRNA can associate with the SSU even without any IF (Milón and Rodnina, 2012). After mRNA joining IF3 ensures the correct codon-anticodon interaction in the P-site and leaves the complex allowing LSU to join, resulting in 70S-IC formation. Further, IF1 leaves the complex allowing B2a intersubunit bridge formation (conserved in mitoribosome) (Kaledhonkar et al., 2019). During subunit joining IF2*GTP comes in close contact with the GAC, and thus GTP is hydrolyzed, allowing fMet-tRNA^{fMet} to release from IF2 interaction and accommodate the classical P/P state.

The process of leaderless mRNA engagement into translation complex appeared more complicated and not fully understood. These mRNAs can directly bind 70S ribosomes, and then fMet-tRNA^{fMet} is delivered by IF2 and IF3. To maintain the complex integrity, IF3 was suggested to adopt a non-canonical position preventing the ribosomal complex dissociation (reviewed by Rodnina, 2018). Perhaps, this situation is more applicable to the mitoribosomes since most of the mitochondrial mRNAs are leaderless.

Two alternative strategies for the initiation complex formation in mammalian mitochondria were recently suggested using *in vitro* reconstitution of the initiation complexes followed by cryo-EM analysis. The first model (Khawaja et al., 2020) claims that the pathway starts with the formation of the pre-IC1 complex consisted of mtSSU and mtIF3 (Figure 7). Interaction between mtIF3 and mS37 promotes conformational changes of the complex, thereby allowing the accommodation of mtIF2 and is designated as pre-IC2 (Figure 7). mtIF2 extension between domains II and III fulfills the function of the missing IF1 (Gaur et al., 2008; Kummer et al., 2018). Similarly to bacteria, mtIF2 is required for fMet-tRNA^{fMet} engagement to the P-site (Kummer et al., 2018). However, the positioning of extended N- and C-terminal domains of mtIF3 on the complex exclude the initiator fMet-tRNA^{fMet} binding. Therefore, mtIF3 must leave the complex before fMet-tRNA^{fMet} can be accommodated. Finally, pre-IC2 associates with the mtLSU, thus allowing initiator tRNA and leaderless mRNA to join. After mRNA is delivered to the mitoribosome by LRPPRC/SLIRP module, it becomes engaged into the mRNA tunnel via mS39 (Aibara et al., 2020; Kummer et al., 2018).

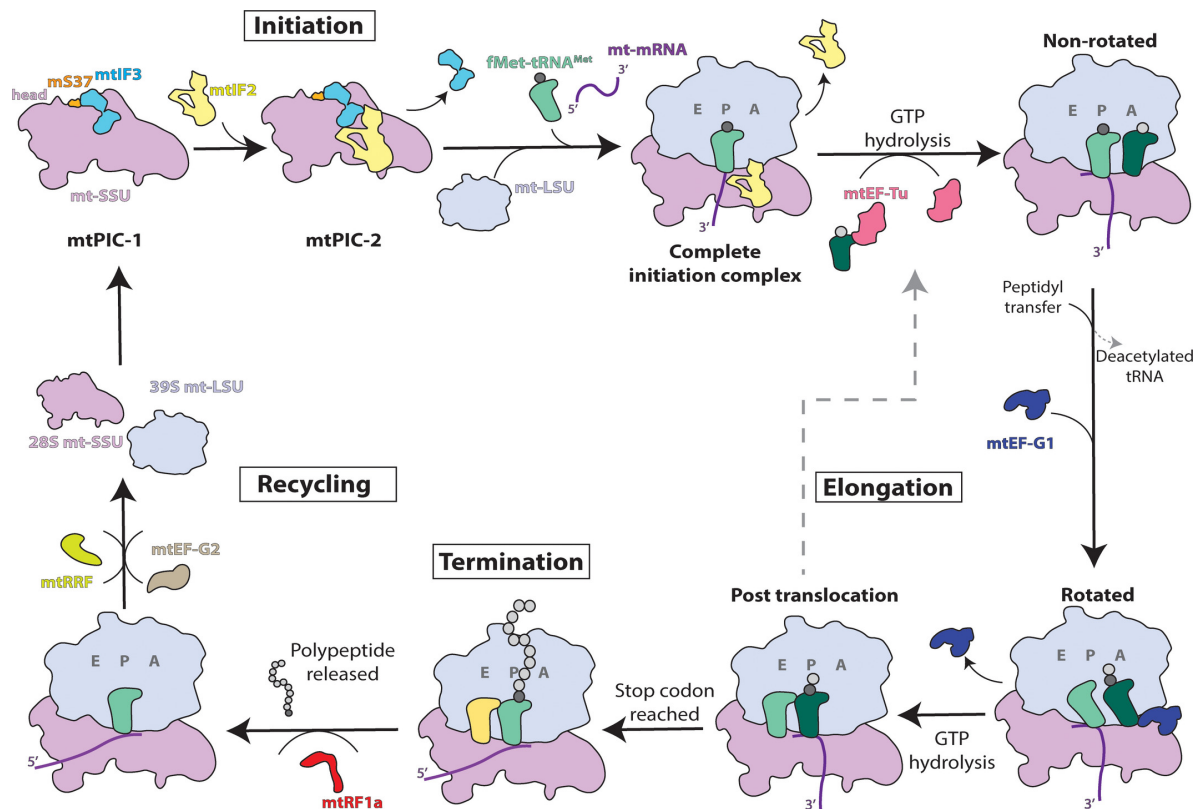


Figure 7. Translation cycle in human mitochondria. Initiation proceeds through the formation of 2 mitochondrial pre-initiation complexes when mtIF3 (mtPIC-1) and mtIF2 (mtPIC-2) subsequently bind to the mtSSU. Dissociation of mtIF3, binding of the mtLSU and loading of the mRNA and initiator fMet-tRNA^{fMet} accomplishes the IC formation. When fMet-tRNA^{fMet} accommodates in the P-site paired to the mRNA start codon, mtIF2 leaves the complex, and elongation starts with the delivery of the second tRNA by EF-Tu. Peptidyltransferase reaction between A- and P-site tRNAs and mtEF-G1 joining facilitates the rotated state of the mitoribosome, thus allowing translocation of tRNAs to the P- and E-sites, respectively. Termination is implemented by release factor(s) (for example, mtRF1a) and results in the ejection of the nascent polypeptide from the mitoribosome. Afterward, the mitoribosome undergoes recycling driven by mtRRF in a complex with mtEF-G2 while mtIF3 prevents premature subunit association. Figure is taken from Ferrari et al., 2021. Reprinted with permission from John Wiley and Sons, FEBS Letters (licence number 5084761436386).

The alternative model of the IC formation was a prerequisite of the aforementioned and is based on the biochemical *in vitro* studies (Ayyub et al., 2018; Bhargava and Spremulli, 2005; Christian and Spremulli, 2009; Haque et al., 2008) and cryo-EM analysis of the mtSSU*mtIF3 complex (Koripella et al., 2019a), and the most prominent differences concern the function of mtIF3 into the initiation complex formation. In contrast to the first model, mtIF3 is considered to be essential for positioning the leaderless mRNA in the P-site via C-terminal domain mitochondrion-specific KKGK motif. In addition, in the presence of mRNA the mtIF3 mitochondrion-specific N-terminal extension undergoes a significant shift, thus promoting the mtIF2*GTP*fMet-tRNA^{fMet} recruitment.

2.1.4.2 Elongation

During the elongation step, the translating complex moves along mRNA and converts the genetic information encoded by nucleotides into the corresponding polypeptide sequence. Elongation of the protein synthesis includes three cycles: mRNA decoding by cognate tRNA, peptide bond formation and translocation of the mRNA–tRNA module. The basic elongation mechanism remains conserved among all ribosomes (reviewed by Ott et al., 2016; Rodnina et al., 2017; 2018; 2019).

When the translationally competent mitoribosomal complex is finally formed, the A-site remains empty and the P-site is occupied by the mRNA start codon paired to fMet-tRNA^{fMet}. The second aminoacyl-tRNA (aa-tRNA) is delivered to the A-site by elongation factor mtEF-Tu*GTP where it recognizes the mRNA codon and adopts A/T state (Figure 7) (Desai et al., 2020; Kummer and Ban, 2020; reviewed by Kummer and Ban, 2021; Ferrari et al., 2021). aa-tRNA-mtEF-Tu*GTP recruitment is performed by L7/L12 stalk in a way reminiscent of bacteria. Dedicated rRNA helices in the mtSSU decoding center execute the quality screening to ensure the cognate aa-tRNA binding (please, refer to section 2.1.3.5). If the aa-tRNA fits, mtEF-Tu*GTP gets into close contact with the SRL, which mediates GTP hydrolysis; mtEF-Tu*GDP leaves the translation complex, allowing the delivered aa-tRNA to accommodate the canonical A/A position.

The correct accommodation of the aa-tRNA in the A-site authorizes the second step – peptidyl transferase reaction. The reaction is achieved by conserved elements of the 16S rRNA in the PTC, which facilitates the P-tRNA to occupy the position appropriate for a nucleophilic attack (please, refer to section 2.1.3.2). The α -amine of the A-site amino acid mediates a nucleophilic attack on the carbonyl carbon of the P-site amino acid, consequently breaking the ester bond between the amino acid and P-site tRNA and attaching the carbonyl carbon to the α -amine at the A-site; therefore, the growing peptide chain is transferred to the A-site and leaves the P-site tRNA deacetylated (Desai et al., 2020; Kummer and Ban, 2020). The deacetylated P-site tRNA enhances the formation of tRNA hybrid states. mRNA-tRNA movement from the A- and P-site to the P- and E-site, respectively, is facilitated by massive subunit rotation. On the mtLSU tRNAs CCA 3'-ends occupy the new positions corresponding to the P- and E-sites, whereas the anticodon stem loops lag and still hold A- and P-sites in the mtSSU, thus forming the hybrid states A/P and P/E (Desai et al., 2020). The binding of the mtEF-G1*GTP (elongation factor G1) stabilizes the hybrid state and induces the next step of translocation coupled with GTP-hydrolysis and GAC closure (Figure 7) (Desai et al., 2020; Koripella et al., 2020a; Kummer and Ban, 2020). The mtSSU body returns into the non-rotated position but the head swivels and thus finally repositions the anticodon stem loops to the P- and E-sites allowing tRNAs to accommodate the P/P and E/E states. The

translocation step accomplishes when the mtSSU head finally returns to the non-rotated position, E-site tRNA is ejected by the mitochondrial-specific element composed by mL64 and uS7m, and mtEF-G1*GDP leaves the translation complex. Thus, only the peptidyl tRNA stays bound in the P-site, and a new mRNA codon is present in the A-site for the next cycle of elongation (Koripella et al., 2020a; Kummer and Ban, 2020).

2.1.4.3 Termination

Translation termination initiates once a stop-codon occurs in the A-site. In bacteria, the canonical stop codons (UAA, UAG and UGA) are recognized by the release factors RF1 and RF2. The termination factors facilitate the hydrolysis of the ester bond between the peptidyl-tRNA and the nascent peptide chain mediated by their conserved GGQ motifs. Subsequently, the newly synthesized polypeptide leaves the ribosome complex, and RF3 induces the ejection of RF1/RF2 (reviewed by Rodnina, 2018). Mitochondria have an altered genetic code, and therefore, the translation termination mechanism evolved accordingly. For example, in human mitochondria, UGA encodes tryptophan instead of a stop codon, which might be the reason why no homologous RF2 has been identified in human mitochondria. In addition, two mitochondrial mRNAs (MT-CO1 and MT-ND6) carry alternative stop codons (AGA and AGG, respectively), which were suggested to require -1 frameshifting to be recognized by conventional termination mechanism (Temperley et al., 2010b, reviewed by Hällberg and Larsson, 2014; Ott et al., 2016; Temperley et al., 2010a).

Four putative translation termination factors have been described in mitochondria based on their homology to known bacterial release factors and the presence of the essential catalytic GGQ motif: mtRF1, mtRF1a, mL62 (ICT1) and C12ORF65 (mtRF-R, mitochondrial translation release factor in rescue). Only mtRF1 and mtRF1a possess all domains found in canonical release factors, whereas mL62 and C12ORF65 lack stop-codon recognition domains. So far, peptidyl hydrolase activity has been demonstrated for mtRF1a, mL62 and C12ORF65-MTRES1 (mitochondrial transcription rescue factor 1) complex (Akabane et al., 2014; Desai et al., 2020; Feaga et al., 2016; Kogure et al., 2014; Nozaki et al., 2008; Richter et al., 2010; Soleimanpour-Lichaei et al., 2007; Wesolowska et al., 2014). *In vitro* data demonstrate that mtRF1a can discriminate UAA and UAG (Soleimanpour-Lichaei et al., 2007) and were further supported by visualizing the factor bound to the terminating mitoribosomes with the UAA codon in the A-site (Kummer et al., 2021). mtRF1a utilizes essentially the same mechanism of stop codon recognition and polypeptide release as it was described for bacteria (Svidritskiy and Korostelev, 2018). Interestingly, mL62 was reported to act on canonical stop codons, non-canonical stop codons and ribosomes that lack a codon in the A-site using heterologous system with 70S bacterial ribosomes (Richter et al., 2010). Recent structural data has revealed that mL62 is involved in mitoribosome rescue scenario, being specifically bound to the mitoribosomes stalled on truncated mRNAs without a codon

in the A-site (Kummer et al., 2021).

C12ORF65 (mtRF-R) has been identified as a part of a mitoribosome-associated quality control pathway (Desai et al., 2020). Upon mitoribosome stalling during the elongation step, C12ORF65 (mtRF-R) cooperates with RNA-binding protein MTRES1 (C6ORF203) to release the nascent polypeptide chain from the mtLSU after mitoribosome splitting. Accordingly, no C12ORF65 (mtRF-R) was detected to be bound to the 55S mitoribosomes programmed with mRNAs bearing non-canonical stop codons or with truncated mRNA (Kummer et al., 2021).

2.1.4.4 Recycling

When translation is finished, mitoribosome undergoes recycling step, which includes the dissociation into the subunits and ejection of the remaining tRNA and mRNA. In bacteria, recycling is carried out by three factors: EF-G, the ribosome recycling factor RRF, and IF3 (Karimi et al., 1999). Collaborative action of EF-G and RRF splits the ribosome into subunits, whereas IF3 dissociates the remaining tRNA (reviewed by Rodnina, 2018). The canonical mitochondrial recycling system consists of mtRRF, mtEF-G2 and mtIF3 (Rorbach et al., 2008; Tsuboi et al., 2009; Christian and Spremulli, 2009; reviewed by Chicherin et al., 2019). Similarly to the bacterial recycling system, mtRRF binding to the mitoribosome require prerequisite deacylation of the P-site tRNA. Subsequent engagement of mtEF-G2 to the GAC induces large-scale rotation of mtRRF, thereby making the complex sterically incompatible with helix 44 of the 12S rRNA (Figure 7) (Kummer et al., 2021). Moreover, mtRRF embraces helix 69 of the 16S rRNA and altogether, this leads to disruption of the B2a intersubunit bridge (Kummer et al. 2021). After subunit splitting, mtIF3 stays bound to the mtSSU to prevent subunit association (Kummer et al., 2021; Ayyub and Varshney, 2019; Khawaja et al., 2020). However, the data obtained as a part of this thesis suggest the presence of an alternative recycling mechanism mediated by GTPBP6 and will be further introduced in the Discussion chapter as well as mechanistic details of both recycling systems (please, refer to section 5.5).

2.2 Mammalian mitochondrial ribosome assembly

In principle, the mitoribosome biogenesis can be divided into several distinct but interconnected steps: (i) transcription of the rRNAs and the structural tRNA from the mtDNA template; (ii) post-transcriptional processing of the rRNAs/tRNA^{Val/Phe}; (iii) synthesis of the MRPs on cytosolic ribosomes and their import into mitochondria; (iv) assembly of 12S rRNA and 30 MRPS (MRPs of the SSU) and 16S rRNA, tRNA^{Val/Phe} and 52 MRPL (MRPs of the LSU) into mature subunits; (v) assembly of the 55S mitoribosome from the subunits as a step of translation initiation. Thus, the assembly of the mitoribosome essentially relies on the coordinated expression of both nuclear and mitochondrial genomes and requires the assistance of at least 250-300 nuclear-encoded factors (reviewed by Pearce et al., 2017). The process is spatially-temporally organized within different sub-compartments in the mitochondrial matrix (Figure 8).

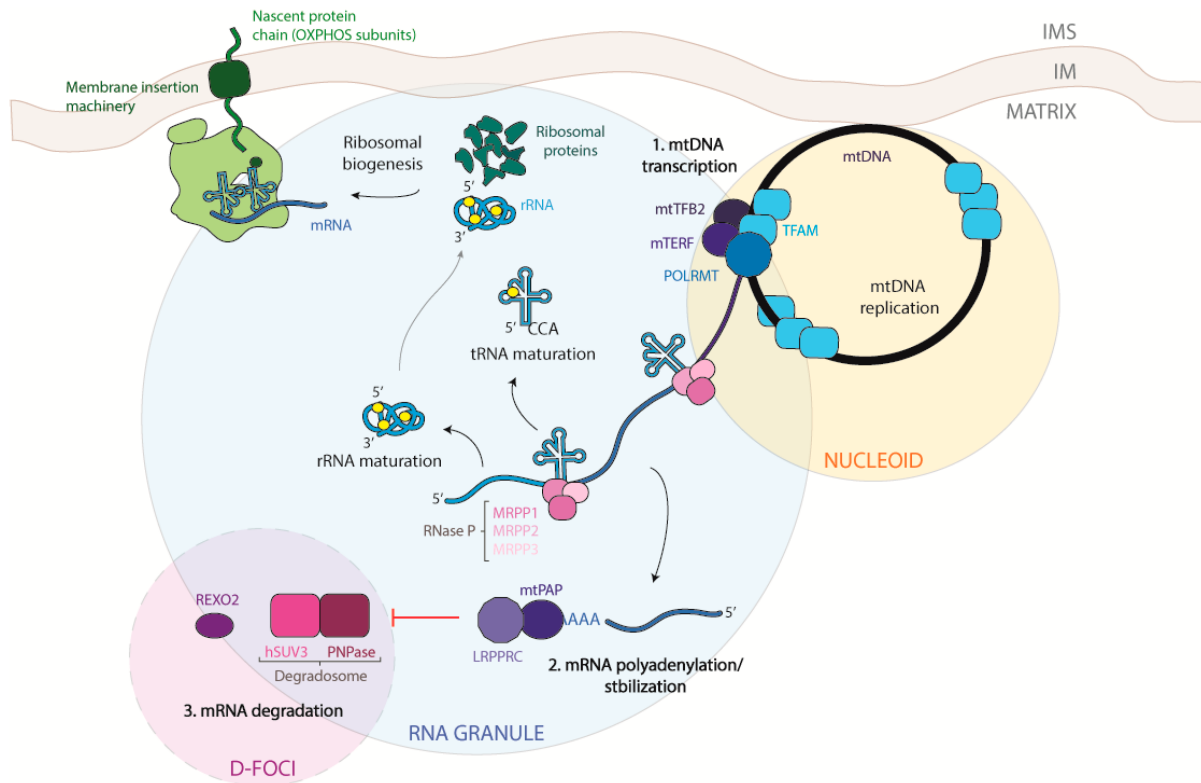


Figure 8. Compartmentalization of the mitochondrial gene expression. mtDNA replication and transcription are coupled with initial steps of the mitochondrial ribosome assembly and take place within the nucleoid. Further, mt-RNA processing and maturation continues within the RNA granules where structural ribosomal RNAs (12S and 16S rRNA and tRNA^{Val/Phe}) associate with MRPs. Degradation of the RNA species is performed by the degradosome complex localized in D-foci. Figure taken from Barchiesi and Vascotto, 2019. Reprinted with permission from MDPI open access Creative Common CC BY provided that any part of the article may be reused without special permission.

2.2.1 Compartmentalization and kinetics

2.2.1.1 Compartmentalization of the mitochondrial ribosome assembly

The nucleoid

The very first steps of mitoribosome assembly involve the transcription of the rRNAs and the structural tRNA from the mtDNA template and occur within foci called nucleoid (Figure 8) (reviewed by Barrientos, 2015; Bogenhagen et al., 2014). The multilayer architecture of the compartment includes an inner core region which comprises the circular double-stranded mtDNA compactly packed by mitochondrial transcription factor A (TFAM) and key mtDNA-associated proteins involved in mtDNA maintenance, replication and transcription (Ekstrand et al., 2004; Kukat et al., 2015; reviewed by Bonekamp and Larsson, 2018; Farge and Falkenberg, 2019; Lee and Han, 2017).

The diverged mitochondrial transcription machinery is driven by a single subunit mitochondrial RNA polymerase (mtRNAP or POLRMT). *In vitro* reconstitution suggests that mtRNAP in mammals requires just a few co-factors to initiate and maintain the RNA synthesis: TFAM and mitochondrial transcription factor B2 (TFB2M) form the initiation complex and TEFM stabilizes the elongation step (Falkenberg et al., 2002; Litonin et al., 2010; Agaronyan et al., 2015; Hillen et al., 2017a; 2017b). Both strands of the mtDNA are transcribed, resulting in the formation of two nearly genomic-sized polycistronic transcripts. The peripheral part of the nucleoid comprises proteins involved in RNA processing and partially overlaps with the mitochondrial RNA granules (MRGs) – the centers for RNA maturation.

Mitochondrial RNA granules

Further steps of the mitoribosome assembly require the hierarchical processing of the ribosomal RNAs and their incorporation into the growing mitoribosomal particles together with MRPs. In order to sequester and process the newly synthesized transcripts, mitochondria have evolved specialized non-membrane compartments (MRGs) (Figure 8) (Antonicka et al., 2013; Jourdain et al., 2013; Antonicka and Shoubridge, 2015; reviewed by Jourdain et al., 2016). Recently, using super-resolution microscopy techniques, RNA granules were shown to exhibit the properties of fluid condensates and localize in close vicinity to the IMM (Rey et al., 2020). They consist of compacted RNA species covered by RNA-binding proteins (Antonicka and Shoubridge, 2015; Rey et al., 2020).

Dedicated mitochondrial ribonucleases drive generation of individual functional RNA species from 2 polycistronic transcripts. Ribonuclease P (mtRNase P) complex (MRPP1, MRPP2 and MRPP3) cleaves the 5' ends while ELAC2 (RNase Z) processes at the 3' ends of the tRNAs that punctuate most of the ORFs (so-called 'tRNA punctuation' model) (Brzezniak et al.,

2011; Holzmann et al., 2008; Ojala et al., 1981; Sanchez et al., 2011). However, it is evident from the mtDNA genetic composition that not all of the transcripts are primed with tRNAs (Figure 6). The excision of these transcripts requires other mechanisms that remain to be clarified (reviewed by D'Souza and Minczuk, 2018; Kummer and Ban, 2021; Barchiesi and Vascotto, 2019).

In principle, the initial cleavage of the transcript containing tRNA^{Phe}-12S rRNA-tRNA^{Val}-16S rRNA sequence should result in the formation of individual rRNAs and a structural tRNA^{Val/Phe} since it satisfies the classical tRNA punctuation model. It remains a mystery whether incorporation of the MRPs to the rRNA scaffold happens after the complete release of 12S and 16S rRNAs or can occur already before or during the cleavage. Experimental data suggest that MRP clusters are able to occupy non-cleaved rRNAs, although to a lower extent, but the formation of the complete mitoribosome is abolished (Rackham et al., 2016). The post-transcriptional chemical modification of rRNAs is vital for ensuring the stability and functionality of mitoribosomes and will be reviewed further (please, refer to section 2.2.2). Cryo-EM analysis of the mtLSU has revealed that the structural tRNA^{Val/Phe} follows the common pattern of tRNA post-transcriptional modifications such as an addition of the CCA 3' end essential for cognate amino acid accommodation added by tRNA-nucleotidyltransferase 1 (TRNT1) (Greber et al., 2014; Nagaike et al., 2001) and methylation of the A9 base (m¹A9) by MRPP1/MRPP2 (Vilardo et al., 2012).

The surveillance and degradation of the mt-RNAs are regulated by several mechanisms, which in principle should be applicable to all of the RNA species. However, the current knowledge is mostly restricted to mRNA metabolism. Excess and aberrant RNAs are subjected to degradosome, which in mammals is a complex of polynucleotide phosphorylase (PNPase) and the RNA helicase SUV3. The degradosome resides in the distinct foci within the mitochondrial RNA granules (D-foci) (Figure 8) (Borowski et al., 2013). The PNPase/SUV3 complex is accompanied by REXO2 exoribonuclease capable of degrading very short RNA molecules (Bruni et al., 2013).

2.2.1.2 Kinetics of the mitoribosome assembly

The bacterial ribosome assembly pathway is well resolved both *in vivo* and *in vitro*. Pioneering classical studies performed by Nierhaus and Nomura revealed that the building of the ribosome includes both parallel and hierarchical incorporation of the individual r-proteins and protein clusters (Dohme and Nierhaus, 1976; Nierhaus and Dohme, 1974; Traub and Nomura, 1968). Thus, the r-proteins were classified as primary-binding that associate directly with rRNAs, thereby facilitating the recruitment of the secondary (dependent on primary r-proteins) and tertiary (dependent on secondary r-proteins) binders. More recent studies resolved the assembly of the 70S ribosome *in vivo* using SILAC (stable isotope labeling by

amino acids in cell culture) combined with mass spectrometry approach (Chen and Williamson, 2013). The study revealed that consistent with the *in vitro* reconstitution, protein clusters assemble in a hierarchical order. A combination of the biochemical and cryo-EM approaches further confirmed that r-proteins binding drives folding of the rRNA structure and induces conformational changes to create new binding sites for secondary proteins. Notably, the formation of the crucial functional sites on the ribosome, such as the CP and the PTC are defined as rate-limiting steps and accomplishes the assembly process (Nikolay et al., 2018). In contrast to *in vitro* studies *in vivo* assembly involve numerous assembly factors and emphasizes that bacterial ribosome assembly starts co-transcriptionally (Chen and Williamson, 2013; reviewed by Davis and Williamson, 2017). Yeast mtLSU biogenesis resembles the bacterial pathway and proceeds through the hierarchical incorporation of preassembled MRP modules into the growing particle (Zeng et al., 2018). In addition, homologs of the bacterial 50S LSU assembly factors have been defined to act in similar stages in the yeast mtLSU assembly.

The first assembly map of the human mitoribosome has been obtained using SILAC pulse-labeling in combination with the analysis of protein-protein interaction surfaces in the mitoribosome structure (Bogenhagen et al., 2018). MRPs form assembly clusters, which join the growing mitoribosomal particles in a coordinated manner following the same tendency observed during bacterial and yeast (mito)ribosome biogenesis (Figure 9). Early-assembly MRPs are enriched into the nucleoid fraction and often share extensive interactions with the rRNAs (Bogenhagen et al., 2014; 2018). The intermediate-binding proteins have less direct contact with the rRNA, and their incorporation relies on protein-protein interactions with the primary binders as well as on rRNA remodeling induced by incorporation of the early clusters. Late biogenesis stages are accompanied by the tuning of the intersubunit interface, where the late MRPs join the growing particle.

Insights into late stages of human mtLSU assembly also have been gained using single-particle cryo-EM. The analysis of the native assembly intermediates revealed that similarly to bacterial ribosome biogenesis, the folding of the intersubunit rRNA and the maturation of the PTC complete the mtLSU assembly (Brown et al., 2017).

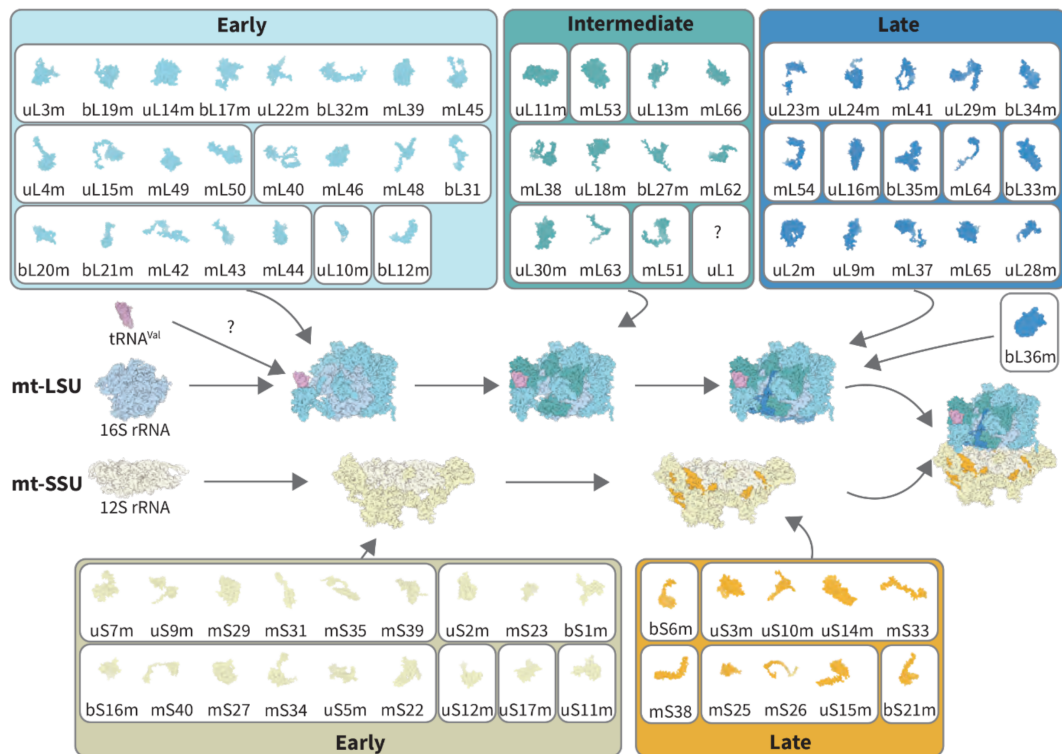


Figure 9. The assembly map of the human mitoribosome. MRPs form assembly clusters, which join the growing particles in a hierarchical order. mtLSU MRPs can be classified as early-, intermediate- or late-binding, while mtSSU MRPs represent 2 major groups of early- or late-binding proteins. Figure is based on the data obtained by Bogenhagen et al., 2018 and is taken from Lopez Sanchez et al., 2021. Reprinted with permission from MDPI open access Creative Common CC BY provided that any part of the article may be reused without special permission.

2.2.2 Assembly factors

Numerous assembly factors orchestrate the biogenesis process of the mitoribosome. The growing list includes RNA helicases and modifying enzymes, GTPases and other factors involved in RNA/protein chaperoning, that ensure the proper folding of the RNA and protein components into the maturing mitoribosomal particles.

2.2.2.1 RNA helicases

RNA helicases are known for their essential function in RNA metabolism pathways, including ribosome biogenesis in all domains of life. The enzymes bind and remodel ribonucleoprotein complexes allowing to accommodate new proteins and facilitate RNA-protein interactions (reviewed by Martin et al., 2013). In humans, two putative DExH/D-box RNA helicases DHX30 and DDX28 were identified as essential components of the MRGs (Antonicka and Shoubridge, 2015). DHX30 is involved presumably in early stages of the mitoribosome biogenesis, acting on a nascent rRNA (Antonicka and Shoubridge, 2015; Minczuk et al., 2011). Similarly, DDX28 acts relatively early during mtLSU assembly and stabilizes 16S rRNA (Tu and Barrientos, 2015).

2.2.2.2 Methyltransferases

There are two universally conserved methylated residues in the mtSSU rRNA, N⁶-dimethylated adenines m⁶₂A1583 and m⁶₂A1584 (m⁶₂A1518 and m⁶₂A1519 in *E. coli* 16S rRNA numbering) located in helix 45. Methylation at these sites facilitates contact between helices 44 and 45, thereby stabilizing the decoding center of the ribosome in both bacteria and human mitochondria (Demirci et al., 2010; Liu et al., 2019). In mammals, the modification is installed by TFB1M (transcription factor B, mitochondrial) (Metodiev et al., 2009). Dimethylation requires the presence of the mitochondrial ribosome binding factor A (mtRBFA), which binds directly to the methylation sites and promotes TFB1M activity (Rozanska et al., 2017).

The methyltransferase NSUN4 (NOL1/NOP2/Sun domain family member 4) modifies a m⁵C base at a position C1488 in human 12S rRNA (Metodiev et al., 2014). The equivalent modification of the 16S rRNA in bacteria (C1404) catalyzed by RsmF presumably occurs during late stages of ribosome assembly (Demirci et al., 2010). Similarly, in mice NSUN4 ablation leads to impaired 55S formation accompanied by accumulation of the nearly matured subunits (Metodiev et al., 2014). Interestingly, NSUN4 lacks RNA-binding domain and *in vitro* studies suggest that NSUN4 affinity to the 12S rRNA is increased by another factor MTERF4 (mitochondrial transcription termination factor 4) (Yakubovskaya et al., 2012).

Methyl-5-uridine (m⁵U) modification at the position U1076 of 12S rRNA is installed by TRMT2B (tRNA methyltransferase 2 homolog B) (Laptev et al., 2020b; Powell and Minczuk, 2020). However, in contrast to the other 12S rRNA modifying enzymes, no significant defect into mitoribosome assembly and function was detected upon TRMT2B loss in cultured human cells (Powell and Minczuk, 2020).

The 12S rRNA m⁴C1486 is introduced by the methyltransferase-like 15 enzyme METTL15 (Chen et al., 2020; Van Haute et al., 2019; reviewed by Laptev et al., 2020a; Lopez Sanchez et al., 2020). Although the methylation site is not conserved among ribosomes, the loss of m⁴C1486 modification leads to aberrant assembly of the mtSSU and accumulation of late-stage assembly intermediates (Chen et al., 2020; Van Haute et al., 2019). Notably, decreased C1486 methylation negatively affects the m⁵C1488 modification catalyzed by NSUN4, suggesting a potential interdependence of these two nearby residues (Chen et al., 2020; Van Haute et al., 2019).

The mtLSU 16S rRNA contains two universally conserved 2'-O-ribose methylations, Gm2815 and Um3039 (Gm2251 and Um2552 in *E. coli*) located in the P-loop and A-loop, respectively. The Gm2815 modification is introduced by mitochondrial rRNA methyltransferase 1 (MRM1) in human mitochondria. MRM1 is enriched in the nucleoid fraction, suggesting its involvement in early stages of mtLSU biogenesis (Lee and Bogenhagen, 2014; Lee et al.,

2013). U3039 is modified by MRM2 (Lee and Bogenhagen, 2014; Lee et al., 2013; Rorbach et al., 2014). MRM2 depletion strongly affects the mtLSU maturation and consequently impairs mitochondrial translation and OXPHOS function (Rorbach et al., 2014). Akin to human MRM2, the bacterial homolog RrmJ/FtsJ/RlmE acts late during LSU formation modifying U2552 (Arai et al., 2015; Bügl et al., 2000). Intriguingly, overexpression of the two GTPases ObgE and EngA suppresses the negative effect of RrmJ/FtsJ/RlmE depletion and stimulates the LSU assembly to proceed further even in the absence of the modification (Tan et al., 2002). The third site for 2'-O-ribose methylation in the 16S rRNA is G3040 modified by MRM3. Although Gm3040 modification is not conserved, it is critical for the mtLSU biogenesis (Lee et al., 2013; Rorbach et al., 2014).

The 16S rRNA base methylation of A2617 requires the action of TRMT61B (tRNA methyltransferase 61B). The event is probably coupled with early maturation of the 16S rRNA since TRMT61B is able to modify naked rRNA *in vitro* (Bar-Yaacov et al., 2016). This base contributes to the formation of the B3 intersubunit bridge and therefore stabilizes the mitoribosome (Bar-Yaacov et al., 2016; Greber et al., 2015).

2.2.2.3 Pseudouridine synthase module

The only pseudouridine conversion is identified at position U1397 in the 16S rRNA introduced by RPUSD4. The enzyme is an essential component of the MRGs and its deficiency leads to the aberrant assembly of the mtLSU and dramatically decreased levels of the 55S mitoribosome (Antonicka et al., 2017; Zaganelli et al., 2017). RPUSD4 is a part of a functional pseudouridine synthase module together with RPUSD3, TRUB2, NGRN, WBSCR16 (RCC1L, RCC1-like G exchanging factor-like protein), FASTKD2 and PTC1 (Arroyo et al., 2016; Perks et al., 2018). Ablation of any of these factors impairs the 16S rRNA stability and compromises mtLSU formation, although their precise role in 16S rRNA metabolism remains elusive.

2.2.2.4 Endoribonuclease

YbeY is a highly conserved endoribonuclease that is involved in the late biogenesis steps of the SSU in bacteria providing a quality control function to ensure the correct maturation of the 16S rRNA (Babu et al., 2020; Jacob et al., 2013). In human mitochondria, YbeY is believed to regulate the stability of the 12S rRNA and incorporation of the uS11m (D'Souza et al., 2021; Summer et al., 2020). Although the endoribonuclease activity of YbeY was confirmed using total RNA isolated from human cells (Ghosal et al., 2017), its substrate specificity and potential mechanism of action in humans needs to be further characterized.

2.2.2.5 Other assembly factors

MALSU1 (mitochondrial assembly of ribosomal large subunit 1) is essential for mtLSU biogenesis and promotes the incorporation of uL14m into the growing particle (Fung et al., 2013; Rorbach et al., 2012; Wanschers et al., 2012). Despite a relatively early association of MALSU1 with the mtLSU intermediate, the factor stays bound to the 39S particle until complete maturation. Recent cryo-EM findings resolved this discrepancy and demonstrated that MALSU1 forms a complex with LOR8F8 and mt-ACP (mitochondrial acyl carrier protein) which eliminates the possibility of the immature mtLSU to associate with mtSSU (Brown et al., 2017). Interestingly, the MALSU1/LOR8F8/mt-ACP anti-association function is not restricted to mitoribosome biogenesis but also plays an important role in a mitoribosome recycling. The complex was found to be associated with the mtLSU particle undergoing post-splitting quality control (Desai et al., 2020).

In addition of its function in 12S rRNA maturation and, thus, in mtSSU assembly, NSUN4 also interacts with the mtLSU in a complex with MTERF4. The complex was suggested to target the mtLSU for the 55S mitoribosome formation (Cámara et al., 2011; Metodiev et al., 2014; Spåhr et al., 2012). However, the precise role of the MTERF4-NSUN4 dimer into mitoribosome assembly remained unclear for a long time and was revealed as a part of this study (please, refer to Discussion chapter, section 5.4).

MPV17L2 (Mpv17-like protein 2) localizes to the inner mitochondrial membrane and associates with both mtLSU and 55S mitoribosome (Dalla Rosa et al., 2014). Thus, MPV17L2 is probably involved in the late stages of the mitoribosome maturation. Depletion of MPV17L2 results in decreased levels of the mitoribosomal particles and negatively affects protein synthesis.

2.3 GTP-binding proteins

GTP-binding proteins (GTPBPs) or GTPases are a superclass of hydrolase enzymes that are characterized by their ability to bind GTP and hydrolyze it to GDP by evolutionary conserved GTP-binding domain (G-domain) and participate in virtually all fundamental processes within the cell (Leipe et al., 2002; reviewed by Verstraeten et al., 2011). TRAFAC (named after translational factors) GTPases represent the main focus of this chapter since they are largely involved into translation machinery biogenesis and function.

2.3.1 Structure and molecular functions

Analysis of the available 3D structures suggests that despite of low primary sequence homology, GTPBPs possess highly conserved architecture of the functional motifs. The ~20 kD G-domain carries out GTP-binding and hydrolysis and therefore represents the minimal functional core of a GTPase (reviewed by Bourne et al., 1991; Vetter and Wittinghofer, 2001). Typically, it consists of 6 hydrophobic β -strands alternated with 5 amphipathic α -helices and connected by linker loops (Figure 10). G-domain includes 4 to 5 conserved sequence motifs (named G1-G5 after guanine-nucleotide binding) (Leipe et al., 2002; Vetter and Wittinghofer, 1999; Wittinghofer and Vetter, 2011). However, due to circular permutations, the order of the motifs does not always correspond to their numbering. Initially identified in Ras (Rat sarcoma protein), G1-G4 are the most conserved among GTPases, while G5 is highly variable and sometimes not present. Remarkably, G1-G3 variations were defined in all NTP-binding proteins and serve as a foothold for phosphate binding, while G4-G5 are responsible for the guanine base recognition.

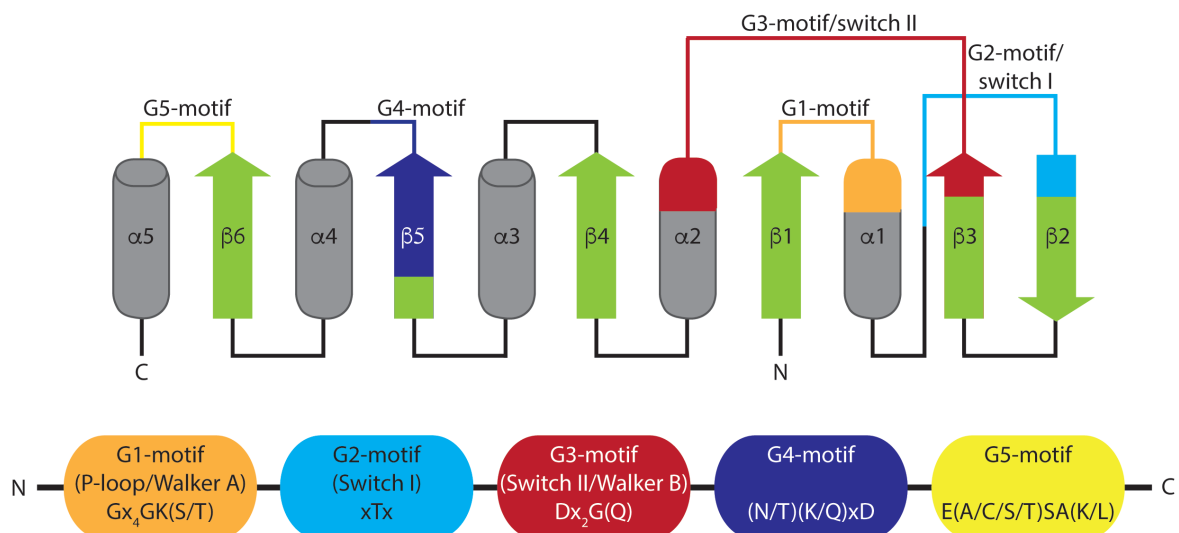


Figure 10. Structure of the G-domain. Upper panel: The canonical structure of the G-domain based on GTPase Ras. α -helices are shown in green and β -strands in gray. Lower panel: Conserved sequence motifs of the TRAFAC GTPases G-domain. x corresponds to any amino acid.

The G1 motif, or the P-loop (also known as Walker A motif) connects the first β -strand with the following α -helix. G1 consensus $Gx_4GK(S/T)$ (where x corresponds to any amino acid) is highly conserved in all NTP utilizing proteins, including GTPases as well as ATPases. Structurally it forms a pocket for nucleotide-phosphate binding. More precisely, the interaction with the α - and β -phosphate of the NTP is ensured by the main chain amino-groups of Gly and Lys as well as side chain amino-group of Lys that connects β - and γ -phosphates. Ser/Thr residue is involved in the coordination of the magnesium ion, an essential NTPase co-factor that bridges β - and γ -phosphates.

The G2 motif involves the N-terminal end of the β_2 strand and a part of the loop that anticipates it. Upon nucleotide binding the G2 motif considerably changes its architecture and therefore is called switch I region, reflecting its ability to sense the nucleotide-bound state. Despite maintaining the same function, the primary amino acid sequence of this region is highly variable among the P-loop GTPase superclass but tends to be conserved within every individual (sub)family. The only amino acid which sustains in all of the members of TRAFAC class is Thr. This residue forms main-chain hydrogen bonds to the tertiary phosphate of the bound NTP and coordinates the Mg^{2+} ion via hydroxyl group, thereby stabilizing the γ -phosphate.

The G3 motif (also known as Walker B motif) is settled in the C-terminal part of the β_3 strand and extends to the following loop. It overlaps partially with the region known as switch II and possesses the same function as switch I. G3 conserved primary sequence is $Dx_2G(Q)$, where Asp indirectly connects with the Mg^{2+} and Gly interacts with the γ -phosphate via hydrogen bonds. The Gln belongs to switch II and fulfills essential catalytic function into GTP hydrolysis.

The G4 motif consists of 4 hydrophobic or non-polar residues of the β_5 strand and followed by $(N/T)(K/Q)x_D$ consensus. Asp and Gln form hydrogen bonds to the O5 of the guanine ring via its carboxy oxygens and Asn contacts the purine base. In TRAFAC GTPases G4 cooperates with G1 motif to promote nucleotide binding (via Lys of G4 and Gly of G1).

The G5 motif, which is situated on the loop connecting β_6 strand with α_5 helix, is not particularly conserved; however, structural evidence suggests that main chain amino group of Ala of its consensus $E(A/C/S/T)SA(K/L)$ connects to the O6 of the guanine ring. The extensive hydrogen bonds network built by G4/G5 motifs and the guanine base sterically and electrostatically excludes an interaction of a GTPase G-domain with ATP.

The classical paradigm suggests that GTPases accomplish their function as molecular switchers cycling between inactive GDP-bound state, transient 'empty' state and structurally distinct active GTP-bound state (Bourne et al., 1991; 1990; Vetter and Wittinghofer, 2001).

GTP-binding, therefore, facilitates the GTPase interaction with its effector molecules and triggers a cellular response. With certain exceptions, the basic GTPase cycle is relatively slow due to the low intrinsic rate of GTP hydrolysis and GDP/GTP exchange. To facilitate the processes, GTPBPs cooperate with guanine nucleotide exchange factors (GEFs) and GTPase activating proteins (GAPs) (Figure 11).

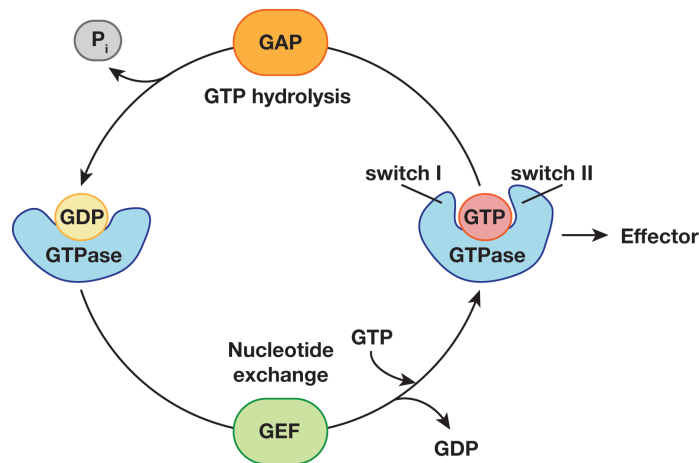


Figure 11. The GTPase cycle. GTPase oscillates between an active (GTP-bound) and inactive (GDP-bound) state. GTP hydrolysis is stimulated by the GTPase activating protein (GAP) and GDP/GTP exchange is performed by guanine nucleotide exchange factor (GEF). In case of TRAFAC GTPases, the ribosome serves as a GAP and nucleotide exchange usually occurs spontaneously without assistance of a GEF. Switch I and switch II regions considerably change their conformation upon GTP binding.

Conversion of a GTPase from an inactive GDP-bound state (OFF state) to an active GTP-bound conformation (ON state) is called GTPase switch (Figure 11). The mechanism is conserved and involves functionally significant structural rearrangements of the switch I and switch II regions. Nucleotide exchange by trGTPases/RA-GTPases is usually very fast and spontaneous due to the high intracellular GTP concentration and to weak nucleotide binding (reviewed by Bennison et al., 2019; Maiti et al., 2021; Maracci and Rodnina, 2016; Verstraeten et al., 2011). Substitution of GDP with GTP is achieved by destabilization of the Mg^{2+} ion in the nucleotide-binding pocket which leads to GDP release. Intrinsic GTPase activity of the trGTPases and TRAFAC GTPases involved into (mito)ribosome assembly is very low and accelerates significantly upon binding to the ribosome, which serves as a GAP (reviewed by Bennison et al., 2019a; Maiti et al., 2021; Maracci and Rodnina, 2016; Rodnina et al., 2000).

2.3.2 Ribosome assembly GTPases

To date, GTPases represent the most abundant class of the mitoribosome biogenesis factors. In total, six GTPases were identified to play an essential role in mitoribosome biogenesis in humans, namely MTG3, ERAL1, GTPBP5-7 and GTPBP10 (reviewed by Maiti

et al., 2021). The factors mentioned above have bacterial homologs and belong to several superfamilies of the TRAFAC GTPases class (Leipe et al., 2002; reviewed by Verstraeten et al., 2011). Since GTPBP6 and GTPBP10 were characterized as a part of this doctoral study (Lavdovskaia et al., 2020; 2018) and represent the direct contribution of the author to the scientific field, these GTPases will be introduced into the Discussion chapter (please, refer to section 5).

2.3.2.1 Era family (related to ERAL1)

In bacteria, Era (*E. coli* Ras-like protein) is involved in diverse intracellular functions, including ribosome assembly. Era comprises two functional domains: N-terminal GTP-binding domain and a unique C-terminal domain involved in RNA-binding (KH motif) (Figure 12) (reviewed by Bennison et al., 2019; Britton, 2009; Goto et al., 2013; Karbstein, 2007; Verstraeten et al., 2011).

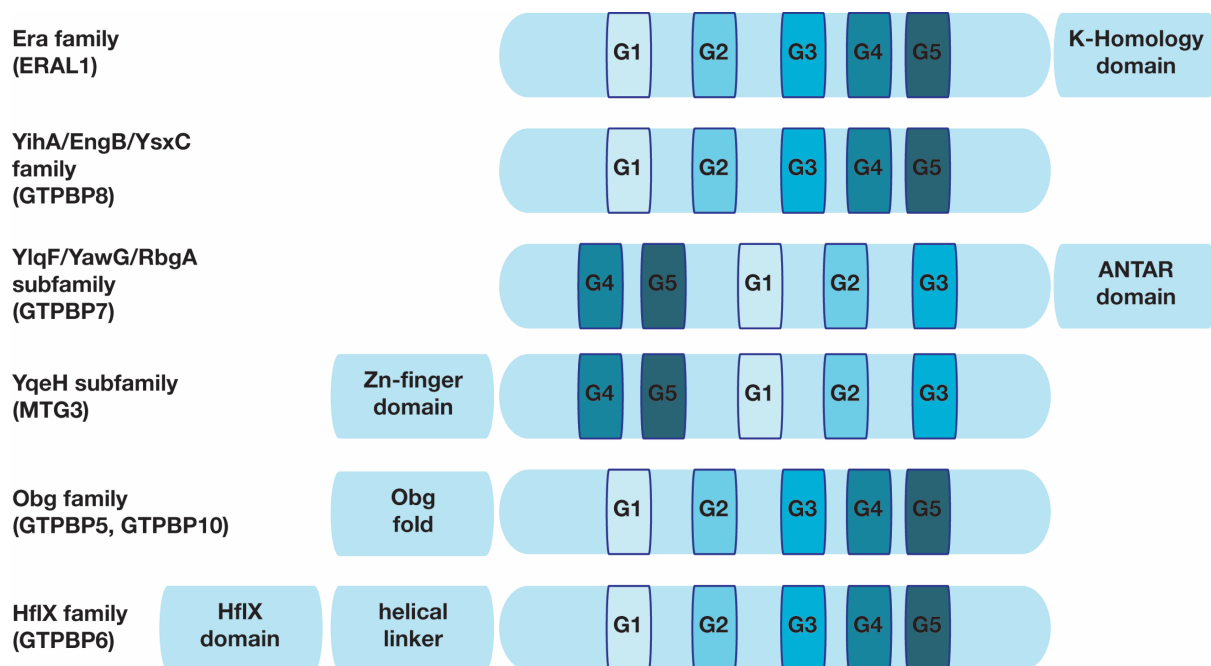


Figure 12. The domain architecture of the ribosome assembly GTPases. Conserved sequence motifs of the GTPase domain (G1 – G5) are shown as boxes in different shades of blue. The RbgA/YqeH subfamily GTPases are characterized by circular permutation of the motifs. Additional known structural features/domains characteristic to each GTPase family are indicated.

Era is involved in the assembly and maturation of the bacterial SSU and acts presumably as a rRNA chaperone specifically interacting with the anti-SD sequence of the SSU rRNA. In addition, the binding of Era is structurally incompatible with bS1 protein and IF3, thus keeping the SSU in a conformation unfavorable for premature LSU and mRNA association (reviewed by Bennison et al., 2019; Goto et al., 2013; Karbstein, 2007; Verstraeten et al., 2011). Remarkably, under physiological conditions addition of Era alone was efficient to

reconstitute the SSU assembly *in vitro* (Tamaru et al., 2018).

Similarly to its bacterial counterpart, human ERAL1 (Era-like G-protein 1) was suggested to act as an RNA chaperone since it binds to the 3' end of the 12S rRNA near to the conserved adenines dimethylated by TFB1M (Dennerlein et al., 2010). Both ablation and overexpression of ERAL1 are detrimental for mitoribosome biogenesis. Thus, depletion of the protein leads to the 12S rRNA instability, thereby negatively affecting the mtSSU formation (Dennerlein et al., 2010). In line with the function of its bacterial homolog, an elevated level of ERAL1 arising due to defects in its controlling CLPP (caseinolytic peptidase proteolytic subunit) protease inhibits the incorporation of the bS1m to the mtSSU particle (Szczepanowska et al., 2016).

2.3.2.2 YihA/YsxC/EngB family (related to GTPBP8)

Bacterial YihA/YsxC/EngB (essential neisserial GTP-binding protein B) was found to be essential for the late stages of LSU biogenesis (Schaefer et al., 2006). GTP hydrolysis by YsxC is stimulated by mature 50S LSU and to a lower extent by immature LSU particles (Ni et al., 2016).

A human homolog of EngB – GTPBP8 has been suggested to be a component of MRGs as it was identified among the DDX28 interaction partners (Maiti et al., 2018; Tu and Barrientos, 2015). However, currently, there is no evidence of GTPBP8 involvement in mitoribosome biogenesis in mammals. In *T. brucei* and *P. falciparum* EngB/YihA associates with mtLSU in a GTP-dependent manner and is involved into the maturation of the domain II of the mtLSU rRNA together with the other GTPases (Gupta et al., 2020; Jaskolowski et al., 2020).

2.3.2.3 YlqF/YawG/YqeH family

YlqF/YawG/YqeH GTPases represent a separate family within the TRAFAC class characterized by circularly permuted GTPase domain (G4-G5-G1-G2-G3) (Figure 12).

YlqF/YawG/RbgA subfamily (related to GTPBP7)

YlqF/YawG/RbgA subfamily proteins comprise the N-terminal circularly permuted GTPase domain and the C-terminal AmiR–NasR Transcription Antitermination Regulator (ANTAR) domain implicated into RNA binding (reviewed by Bennison et al., 2019; Gulati et al., 2013; Leipe et al., 2002). RbgA (ribosome biogenesis GTPase A) GTPase activity is stimulated by binding to the mature LSU and 70S ribosome, but not to the immature LSU particles (Achila et al., 2012; Ni et al., 2016). Biochemical studies combined with mass spectrometry revealed that RbgA is a late LSU biogenesis factor and ablation of the protein leads to the formation of the immature LSU particles missing uL16, bL27 and bL36 and severely depleted bL28, bL33 and bL35 (reviewed by Goto et al., 2013; Jomaa et al., 2014). Cryo-EM analysis shows that

RbgA stabilizes rRNA involved into the CP and the PTC formation, thus allowing the recruitment of the aforementioned r-proteins into the structure (Seffouh et al., 2019).

GTPBP7 (MTG1) is homologous to bacterial RbgA and *S.cerevisiae/T.brucei* Mtg1p, where the latter is involved in the PTC maturation forming an extensive network with the other assembly factors such as mtEngA (Barrientos et al., 2003; Jaskolowski et al., 2020; Tobiasson et al., 2021). Similarly, in humans, GTPBP7 acts at late stages of mtLSU biogenesis and is essential for mitochondrial translation (Kim and Barrientos, 2018). According to the model suggested by the authors, GTPBP7 is required for the proper folding of the 16S rRNA and uL19m and its release from the mtLSU is coupled with GTP hydrolysis and mB6 intersubunit bridge formation.

YqeH subfamily (related to MTG3)

YqeH is involved in early stages of SSU biogenesis, and its GTPase activity is stimulated by the ribosomal protein bS5 (Anand et al., 2009). Depletion of the protein abolishes the 70S ribosome formation accompanied by an accumulation of the free LSU. However, no free SSU particles were detected, and the accumulation of the SSU rRNA precursor was observed (Loh et al., 2007).

MTG3 (mitochondrial ribosome associated GTPase 3)/NOA1 (nitric oxide associated-1)/C4orf14 is a mammalian mitochondrial homolog of the bacterial YqeH and yeast Mtg3p. Mtg3p was proposed to be involved into the maturation of the mtSSU rRNA precursor (Paul et al., 2012). In mammals, the ablation of MTG3 leads to mitochondrial translation deficiency and causes global OXPHOS defect associated with impaired 55S mitoribosome formation and accumulation of the mtSSU precursor (He et al., 2012; Kolanczyk et al., 2011).

2.3.2.4 Obg/HflX superfamily

Obg/HflX superfamily share a glycine-rich sequence (GAX₂GxGxGx₃I, where I is one of the aliphatic residues Ile, Leu, or Val) after the G3 motif and a YxFxTx₅G sequence in the G2 motif (Leipe et al., 2002; reviewed by Verstraeten et al., 2011).

Obg (ObgE/CtgA) family (related to GTPBP5 and GTPBP10)

The Obg (*spo0B*-associated GTP-binding protein) family is characterized by a unique N-terminal glycine-rich Obg-fold (Figure 12) (Bennison et al., 2019; Leipe et al., 2002; reviewed by Verstraeten et al., 2011). Obg family proteins are conserved among different life domains and are involved in many crucial processes in bacteria including ribosome biogenesis (reviewed by Bennison et al., 2019; Verstraeten et al., 2011). ObgE/CtgA is essential for cell viability, and expression of mutant variants of ObgE causes an accumulation of the LSU/SSU rRNA precursors and non-mature LSU particles enriched with maturation factors RrmJ (ribosomal RNA large subunit methyltransferase J) and RluC (ribosomal large subunit

pseudouridine synthase C) and partially lacking uL16, bL33 and bL34 (Jiang et al., 2006). The Obg-fold is thought to be crucial for mediating protein-protein interactions by ObgE and mimics tRNA structure (Feng et al., 2014; Lee et al., 2010). The structure of the ObgE-50S LSU complex revealed that ObgE locates close to the methylation sites modified by RrmJ, RluD and RluC (Feng et al., 2014). Thus, the structural data suggest that ObgE monitors the methylation status of the PTC rRNA helices. Additionally, the factor prevents premature subunit association. More recent findings provide insights into the cooperative action of ObgE together with the other biogenesis factors, including methyltransferase RluD, during the maturation of the LSU active sites and suggest that incorporation of the late-binding r-proteins uL16 and bL36 triggers GTPase activity of ObgE (Nikolay et al., 2021).

GTPBP5 (ObgH1, MTG2) and GTPBP10 (ObgH2) are human homologs of the bacterial ObgE GTPase, which are involved into mtLSU biogenesis. GTPBP5 is required for the late stages of the mtLSU assembly and specifically interacts with the 16S rRNA and MRM2 (Cipullo et al., 2021b; Maiti et al., 2020). As a result, GTPBP5 ablation leads to accumulation of the nearly matured mtLSU particles enriched with late biogenesis factors such as MTERF4-NSUN4, GTPBP7, GTPBP10 and MALSU1 (Cipullo et al., 2021b; Maiti et al., 2020). The late-binding protein bL36 is missing from the complex as well as Um3039 modification introduced by MRM2 (Maiti et al., 2020). Thus, GTPBP5 was proposed to be required for the PTC folding preceding methylation of the U3039 and incorporation of bL36m. In yeast, Mtg2p promotes mitoribosome assembly and its overexpression partially rescues *mrm2* depletion phenotype (Datta et al., 2005).

HflX family (related to GTPBP6)

The HflX-related GTPases structure comprises the specific N-terminal domain of the protein (HflX domain or ND1, HflX for high frequency of lysogenization, X-locus) connected to the canonical G-domain (ND2) via a long flexible glycine-rich linker (Figure 12). The C-terminal GTPase domain is not conserved and sometimes even absent (reviewed by Verstraeten et al., 2011; Wittinghofer and Vetter, 2011). HflX is widely present in nearly all domains of life, excluding fungi, and is non-essential in bacteria under physiological conditions. HflX was found to be associated with both 70S ribosomes and 50S LSU (Zhang et al., 2015). However, despite HflX association with ribosomal particles, there is no direct evidence of its role in ribosome biogenesis in bacteria. Instead, the protein is required to rescue ribosomes stalled under stress conditions possessing both ATPase activity of HflX domain to unwind altered rRNA (Dey et al., 2018; Ghosh et al., 2016) and GTPase activity to dissociate from the LSU (Coatham et al., 2016; Rudra et al., 2020; Zhang et al., 2015). The preferable substrate for HflX is vacant ribosomes or translation complexes with deacylated tRNA in the P-site (Zhang et al., 2015). HflX*GTP binds stalled complexes and induces the disruption of the conserved intersubunit bridge B2a (Zhang et al., 2015).

3 Aims and objectives

Despite the available detailed structure of the mammalian mitoribosome, the biogenesis process of this ribonucleoprotein machinery remains largely elusive. The insights into the ancestral bacterial ribosome assembly pathway have been gained extensively both *in vivo* and *in vitro*; however, they cannot be directly applied to the mitochondrial counterpart due to substantial structural differences. The ribosome maturation process requires several auxiliary factors to facilitate the folding of rRNA and proteins into the growing particles. Among those factors, TRAFAC GTPases represent one of the major groups. For example, the Obg/HflX superfamily members are known to be involved into ribosome biogenesis and function in bacteria. Based on sequence similarities, human GTPBP10 and GTPBP6 were classified as members of the Obg/HflX superfamily with a putative role in mitoribosome biogenesis and function; however, experimental evidence of their involvement in mitochondrial gene expression is missing. To functionally investigate GTPBP6 and GTPBP10, we addressed the following questions:

Question 1: Where do the GTPases localize in human cells?

Question 2: Do GTPBP6 and GTPBP10 associate with the 55S mitoribosome or with the small or large ribosomal subunit?

Question 3: What are the consequences of the loss of function of these factors?

- Are they essential for cell growth?
- Are they required for mitochondrial gene expression?
- Are they a requisite for mitoribosome biogenesis?

Question 4: What is their molecular function during mitoribosome assembly?

Question 5: Does GTPBP6 retain its function as a ribosome recycling factor in human mitochondria as its bacterial counterpart HflX?

4 Results

4.1 Publication 1

Lavdovskaia, E., Kolander, E., Steube, E., Mai, M.M.-Q., Urlaub, H., and Richter-Dennerlein, R. (2018). The human Obg protein GTPBP10 is involved in mitoribosomal biogenesis. *Nucleic Acids Research* 46, 8471–8482. doi: 10.1093/nar/gky701

Copyright license number: 5081350530640. Obtained on 03 June, 2021 from *Nucleic acid research, Oxford University Press* via Copyright Clearance Center's RightsLink®.

Authors contribution:

Figure 1. Cluster analysis of the Obg GTPase family, amino acids sequence alignment of GTPBP10 and its homologs (R.R.-D.); isolation of mitochondria, mitochondrial localization assay and carbonate extraction of mitochondrial membrane proteins (E.L.).

Figure 2. Generation of HEK293T *Gtpbp10*^{64R65K} mutant cell line, western blot analysis, [³⁵S]Methionine *de novo* labeling of mitochondrial translation products, northern blot analysis of mt-DNA encoded RNAs steady-state levels (E.L.); cell counts (E.S.).

Figure 3. Generation of HEK293T cell lines expressing FLAG-tagged proteins (GTPBP10^{FLAG}, mL62^{FLAG} and mS40^{FLAG}) (E.L., R.R.-D.); sucrose gradient analysis of mitochondrial ribosomal complexes isolated from WT human mitochondria/mitoplasts, western blot (E.L.); FLAG-immunoprecipitation of mitoribosomal complexes (E.L., M.M.); mass-spectrometry and data analysis of GTPBP10 protein interactome (R.R.-D., H.U., E.L.).

Figure 4. Steady state analysis of mitochondrial ribosomal proteins and assembly factors in HEK293T *Gtpbp10*^{64R65K} cells, sucrose gradient analysis of mitochondrial ribosomal complexes isolated from HEK293T *Gtpbp10*^{64R65K} cells (E.L.).

Figure 5. Generation of GTPBP10^{G82E-FLAG} and GTPBP10^{S325P-FLAG} mutant cell lines, cell counts (E.L., E.S.); western blot, [³⁵S]Methionine *de novo* pulse-chase labeling of mitochondrial translation products in cells expressing GTPBP10^{G82E-FLAG} or GTPBP10^{S325P-FLAG}, FLAG-immunoprecipitation of mitochondrial ribosomal complexes via GTPBP10^{G82E-FLAG} or GTPBP10^{S325P-FLAG} (E.L.).

Figure S1: Sequence analysis of *Gtpbp10*^{64R65K} cell line, alignment of *Gtpbp10*^{64R65K} vs. WT cell line (E.L.)

Figure S2: Expression titration of HEK293T GTPBP10^{FLAG} cell line (E.L.).

Figure S3: Co-immunoprecipitation of mitochondrial ribosomal complexes via uL1m protein (E.K.).

Non-experimental contribution: data analysis and visualization (E.L., R.R.-D. and H.U); conceptualization and supervision of the study (R.R.-D.); manuscript writing (R.R.-D. with the contribution of all the co-authors).

The human Obg protein GTPBP10 is involved in mitoribosomal biogenesis

Elena Lavdovskaia¹, Elisa Kolander¹, Emely Steube¹, Mandy Mong-Quyen Mai¹, Henning Urlaub^{2,3} and Ricarda Richter-Dennerlein^{1,*}

¹Department of Cellular Biochemistry, University Medical Center Göttingen, D-37073 Göttingen, Germany,

²Bioanalytical Mass Spectrometry Group, Max Planck Institute for Biophysical Chemistry, D-37077 Göttingen,

Germany and ³Bioanalytics, Institute for Clinical Chemistry, University Medical Center Göttingen, D-37073 Göttingen, Germany

Received May 17, 2018; Revised July 19, 2018; Editorial Decision July 20, 2018; Accepted July 23, 2018

ABSTRACT

The human mitochondrial translation apparatus, which synthesizes the core subunits of the oxidative phosphorylation system, is of central interest as mutations in several genes encoding for mitoribosomal proteins or translation factors cause severe human diseases. Little is known, how this complex machinery assembles from nuclear-encoded protein components and mitochondrial-encoded RNAs, and which ancillary factors are required to form a functional mitoribosome. We have characterized the human Obg protein GTPBP10, which associates specifically with the mitoribosomal large subunit at a late maturation state. Defining its interactome, we have shown that GTPBP10 is in a complex with other mtLSU biogenesis factors including mitochondrial RNA granule components, the 16S rRNA module and late mtLSU assembly factors such as MALSU1, SMCR7L, MTERF4 and NSUN4. GTPBP10 deficiency leads to a drastic reduction in 55S monosome formation resulting in defective mtDNA-expression and in a decrease in cell growth. Our results suggest that GTPBP10 is a ribosome biogenesis factor of the mtLSU required for late stages of maturation.

INTRODUCTION

Mammalian mitochondrial ribosomes (mitoribosomes) are essential as they synthesize the mitochondrial DNA (mtDNA)-encoded core subunits of the oxidative phosphorylation (OXPHOS) system. The significance of this machinery is demonstrated by a growing number of patients with severe mitochondrial diseases associated with mutations in genes encoding for mitoribosomal proteins (MRPs) (1). Although mitoribosomes derived from a bacterial ancestor, there are substantial differences in structure and

composition comparing the 55S human mitoribosome and the 70S bacterial ribosome. The 70S particle, composed of a 30S small ribosomal subunit (SSU) and a 50S large ribosomal subunit (LSU), shows a very compact structure with approximately 70% rRNA and 30% proteins. The 55S mitoribosome, which consists of a 28S mitochondrial SSU (mtSSU) and a 39S mitochondrial LSU (mtLSU), exhibits a more porous structure with a reverse rRNA:protein ratio (2). During evolution the human mitoribosome acquired additional proteins and N- and C-terminal extension to the pre-existing ones leading to ~50% of the MRPs being unique to the 55S without any homologue in bacteria. Additionally, the 55S is of dual genetic origin, meaning the rRNA (12S and 16S rRNA) and the tRNA of the central protuberance are encoded by the mtDNA, whereas all the 82 MRPs are encoded by the nucleus suggesting a complex assembly pathway with the requirement of coordinated communication between different cellular compartments. In the last decades the bacterial ribosome was extensively studied in its function and assembly *in vitro* and *in vivo* (3). Having a common ancestor, similarities in the assembly pathway comparing the 70S and the 55S particles are expected. However, due to the aforementioned differences in structure and composition, significant differences are highly likely to be present for the assembly of this complex machinery. For the *in vivo* assembly of the 70S ribosome several ancillary factors are required including RNA helicases, RNA modifying enzymes, chaperones and GTPases (3). The GTPases comprise the highly conserved Obg family, whose members are present in bacteria, but also in eukaryotes. It has been demonstrated in various bacterial species that Obg proteins associate with the LSU (4–8), however, the molecular function of Obg proteins in ribosome biogenesis is still elusive. Feng *et al.* have suggested that the *E. coli* Obg protein (ObgE) acts as an anti-association factor to prevent the formation of the 70S ribosome. Thus, ObgE might function as a quality control factor in late assembly stages of the LSU in bacteria (9). In human, there are

*To whom correspondence should be addressed. Tel: +49 551 395913; Fax: +49 551 395979; Email: ricarda.richter@med.uni-goettingen.de

two homologues of ObgE, namely GTPBP5 (OBGH1) and GTPBP10 (OBGH2) (10). Both exhibit GTPase activity *in vitro* and complemented ObgE deleted *E. coli* strains suggesting conserved function of Obg proteins throughout evolution. However, while GTPBP5 was localized to mitochondria, associating with the mtLSU, GTPBP10 was proposed to be present in the nucleolus suggesting different functions of the human Obg proteins (10,11).

Here, we show that GTPBP10 is a mitochondrial protein, peripherally associated with the inner mitochondrial membrane. GTPBP10 associates with the mtLSU at a late maturation state, but not with the mtSSU or with the assembled 55S monosome. The loss of GTPBP10 leads to a significant decrease in monosome formation associated with reduced steady state levels of selected MRPs as well as of 16S rRNA leading to ablated mtDNA gene expression. In addition, we show that both the N-terminal Obg domain, and also the GTPase domain of GTPBP10 are required for mtLSU binding. In contrast to previous observations, our data suggest that both human Obg homologues and not only GTPBP5 localize to mitochondria (10) and that GTPBP10 is required for mtLSU biogenesis at a late assembly stage.

MATERIALS AND METHODS

Cell culture

The cultivation media and chemicals were purchased by Sigma or GIBCO unless specified otherwise. Human embryonic kidney cell lines (HEK293-Flp-In T-Rex; HEK293T), 143B wild-type, and 143B Rho⁰ cells were cultured in Dulbecco's modified Eagle's medium (DMEM) supplemented with 10% fetal bovine serum (FBS), 2 mM L-glutamine, 1 mM Sodium pyruvate, 50 µg/ml uridine, 100 units/ml Penicillin and 100 µg/ml Streptomycin at 37°C under 5% CO₂ humidified atmosphere. Cells were systematically tested for the presence of Mycoplasma. For testing cell growth 7.5 × 10⁴ cells were seeded into 6-well plates and cell number was monitored after 1, 2 and 3 days using a Neubauer chamber.

Stable inducible HEK293T cell lines expressing C-terminal FLAG tagged mS40 and GTPBP10 wild type (WT) or mutated variants of GTPBP10 were generated as described previously (12,13). Briefly, HEK293T cells were simultaneously transfected with pOG44 and pcDNA5/FRT/TO plasmids containing the respective FLAG construct using GeneJuice (Novagen) or Superfect (Qiagen) as transfection reagent according to manufacturer's instructions. Selection of clones with FLAG construct insertion was started on the second day after transfection using Hygromycin B (100 µg/ml) and Blasticidin S (5 µg/ml). After approximately two weeks, single clones were isolated, induced with tetracycline and analysed for expression by Western blotting.

Gtpbp10^{64R65K} HEK293T cell line was generated applying the CRISPR/Cas9 technology as previously described (13,14). HEK293T cells were transfected with pX330-gRNA-GTPBP10 plasmid containing guide RNA sequence targeting *Gtpbp10* gene (CCAGCCACAAACCGTTTCCG AGG) and with the pEGFP-N1 plasmid for GFP-mediated single cell sorting. Resulting clones were subjected to pri-

mary screening by immunoblotting and the mutation in the GTPBP10 coding sequence was analysed by sequencing.

Cell lysates, mitochondria isolation from cultured cells and mitoplasts preparation

Cells were lysed in NP-40 containing lysis buffer (50 mM Tris/HCl pH 7.4, 130 mM NaCl, 2 mM MgCl₂, 1% NP-40, 1 mM PMSF and 1× Protease inhibitor cocktail (Roche)), vortexed for 30 s, centrifuged for 2 min at 560 g and supernatant saved for further analyses.

Mitochondria were isolated as described previously (15). Briefly, cells were resuspended in homogenization buffer (300 mM Trehalose, 10 mM KCl, 10 mM HEPES pH 7.4) with addition of 1 mM PMSF and 0.2% BSA and potted with Homogen^{plus} Homogenizer (Schuett-Biotec, Germany). Suspension was subjected to differential centrifugation and isolated mitochondria were pelleted at 11 000 g for 10 min, washed with homogenization buffer and subjected to further analyses. For mitoplasts preparation, mitochondria were resuspended in homogenization buffer containing 0.1% Digitonin, incubated on ice for 30 min and treated with proteinase K for 15 min. After blocking Proteinase K with 2 mM PMSF, resulting mitoplasts were washed five times prior further analyses.

Protein localization assays

Proteinase K assay and Carbonate extraction of membrane proteins were executed as previously described (16).

Immunodetection of proteins

Primary antibodies used in this study were: rabbit anti-GTPBP10 (Novusbio NBP1-85055), rabbit anti-uL1m (PRAB4964), rabbit anti-uL3m (ProteinTech 16584-1-AP), rabbit anti-bL12m (ProteinTech 14795-1-AP), rabbit anti-uL13m (ProteinTech 16241-1-AP), rabbit anti-u23m (PRAB1716), rabbit anti-bL32m (PRAB4957), rabbit anti-mL44 (ProteinTech 16394-1-AP), rabbit anti-mL62 (10403-1-AP), rabbit anti-uS14m (ProteinTech 16301-1-AP), rabbit anti-bS15m (ProteinTech 17006-1-AP), rabbit anti-bS16m (ProteinTech 16735-1-AP), rabbit anti-mS27 (ProteinTech 17280-1-AP), rabbit anti-mS40 (ProteinTech 16139-1-AP), rabbit anti-MALSU1 (ProteinTech 22838-1-AP), rabbit anti-NGRN (ProteinTech 14885-1-AP), rabbit anti-GTPBP7 (ProteinTech 13742-1-AP), mouse anti-SDHA (Invitrogen 459200), mouse anti-GAPDH (Santa Cruz sc-32233), mouse anti-COX1 (Invitrogen 459600), mouse anti-COX2 (ab110258), rabbit anti-MFN2 (ProteinTech 12186-1-AP), rabbit anti-TIM23 (PRAB1527), rabbit anti-TIM44 (ProteinTech 13859-1-AP).

[³⁵S]Methionine *de novo* synthesis

Labeling was performed as described previously (16,17). Prior to labeling, cells were treated with 100 µg/ml emetine (Invitrogen) or anisomycin to inhibit cytosolic translation. Mitochondrial translation products were labeled with 0.2 mCi/ml [³⁵S]Methionine for 1 h (pulse labeling), separated on 10–18% Tris-Tricine gel, blotted, visualized by

Typhoon imaging system (GE Healthcare) and quantified using ImageQuant TL. For pulse-chase experiments media was changed after 1 h pulse labeling and cells were further incubated for 3, 6 or 24 h prior analysis.

Co-immunoprecipitation

Immunoprecipitation of FLAG-tagged proteins were performed as described (13) with some modifications. Mitochondrial lysates were prepared in buffer containing 50 mM Tris/HCl [pH 7.4]; 100 mM NH₄Cl; 10 mM MgCl₂; 10% glycerol; 1 mM PMSF and 1% digitonin. After centrifugation at 16 000 g at 4°C for 10 min supernatants were subjected to co-immunoprecipitation using either anti-FLAG M2 Affinity Gel (Sigma) or specific or control antibodies conjugated to ProteinA-sepharose columns (GE Healthcare) for 1h. Elution of co-purified proteins was achieved by FLAG peptides or by pH-shift.

Isokinetic sucrose gradient analysis

Lysed mitoplasts (500 µg in 3% sucrose, 100 mM NH₄Cl, 20 mM MgCl₂, 20 mM Tris-HCl, pH 7.5, 1% Digitonin, 1 × PI-Mix, 0.08 U/µl RiboLock RNase Inhibitor) or affinity purified native complexes were separated by linear sucrose gradient centrifugation (5–30% (w/v) in 100 mM NH₄Cl, 20 mM MgCl₂, 20 mM Tris-HCl pH 7.5, 1 × Protease inhibitor cocktail (Roche)) at 79 000 g, 4°C for 15 h using SW41 Ti (Beckman Coulter). Fractions (1-16) were collected applying BioComp fractionator and analysed by western blot.

RNA isolation and northern blot

RNA was isolated from whole cell extracts using TRIzol reagents (Invitrogen), following the manufacturer's instructions. RNA separation on a denaturing formaldehyde/formamide 1.2% agarose gel was performed as previously described (18). [³²P]-radiolabeled probes were generated utilizing T4 Polynucleotide Kinase (Thermo Scientific) according to the manufacturer's instructions. Imaging was performed with Typhoon imaging system (GE Healthcare).

Quantitative mass spectrometry analyses

SILAC experiments were performed as described previously (13). In brief, cells were cultured for five passages in DMEM containing either 'light' or 'heavy' (¹³C₆¹⁵N₄-arginine ¹³C₆¹⁵N₂-lysine, Cambridge Isotope Laboratories, Tewksbury, MA, USA) labeled amino acids supplemented with 10% dialyzed FBS and 600 mg/l proline.

Equal amounts of isolated mitochondria from differentially SILAC-labeled HEK293T wild type cells and cells expressing GTPBP10^{FLAG} were mixed prior to immunoprecipitation. Purified protein complexes were separated on a 4–12% Nu-PAGE (Invitrogen) and gel slices were digested with trypsin (Sigma Aldrich) and subjected to quantitative mass spectrometry as described previously (19) using Orbitrap Fusion (ThermoFisher). Data were analyzed using Max Quant (version 1.6.0.1) utilizing the human Uniprot database (version 24.11.16) as a reference.

Proteins with a mean ratio ≥ 2 and a *P*-value ≤ 0.05 were considered to be specifically associated with GTPBP10 complexes.

Quantification and statistical analysis

Western blots and northern blots were quantified with Typhoon imaging system and ImageJ software. The protein and RNA levels are presented as percentages relative to WT control. Error bars indicate the SEM from the mean of *n* experiments (see figure legends for details).

RESULTS

GTPBP10 is a mitochondrial protein homologous to bacterial Obg proteins

As Obg proteins are highly conserved GTPases and present in both, prokaryotes and eukaryotes, we performed cluster analysis showing that both human Obg proteins GTPBP5 as well as GTPBP10 group together with *E. coli* ObgE (Figure 1A). Both proteins share ~30% identities with ObgE (GTPBP5: 32.7% and GTPBP10: 31.2%) and show high similarities in the Obg fold region at the N-terminus and in the GTPase domain, whereas the C-terminal domain appears to be more diverse (Figure 1B). In contrast to GTPBP5, which localizes to mitochondria, GTPBP10 was shown to be present in the nucleolus (10). However, a recent genome-wide CRISPR 'death screen' suggested that GTPBP10 is required for mitochondrial OXPHOS function (20). Based on this observation we investigated the localization of GTPBP10 biochemically performing a Proteinase K treatment on intact mitochondria and mitoplasts. Interestingly, GTPBP10 followed the same pattern as the matrix marker uS14m and was protected against Proteinase K even in the absence of the outer mitochondrial membrane (Figure 1C). To assess whether GTPBP10 is an integral membrane protein or a soluble matrix protein we performed sodium carbonate extraction at different pH (Figure 1D). At lower pH a significant portion of GTPBP10 remained in the membrane-containing pellet fraction, but was almost completely extracted at a higher pH similarly to TIM44, a component of the mitochondrial protein import motor associated with the inner mitochondrial membrane (21,22). These results demonstrate that GTPBP10 is a mitochondrial matrix protein peripherally attached to the inner mitochondrial membrane.

GTPBP10 is required for mitochondrial gene expression

As GTPBP10 is present in mitochondria and has been suggested to be required for mitochondrial OXPHOS function (20), we asked whether GTPBP10 is maintained in OXPHOS deficient cells lacking mtDNA (ρ^0). Interestingly, GTPBP10 is significantly reduced in ρ^0 cells (Figure 2A), which is reminiscent to other proteins required for mitochondrial gene expression including MRPs and ribosome biogenesis factors such as MALSU1, DDX28 or mtRBFA (23,24).

Based on this observation, we speculated that GTPBP10 is involved in mitochondrial gene expression. To address this further we aimed to analyze the consequences of the

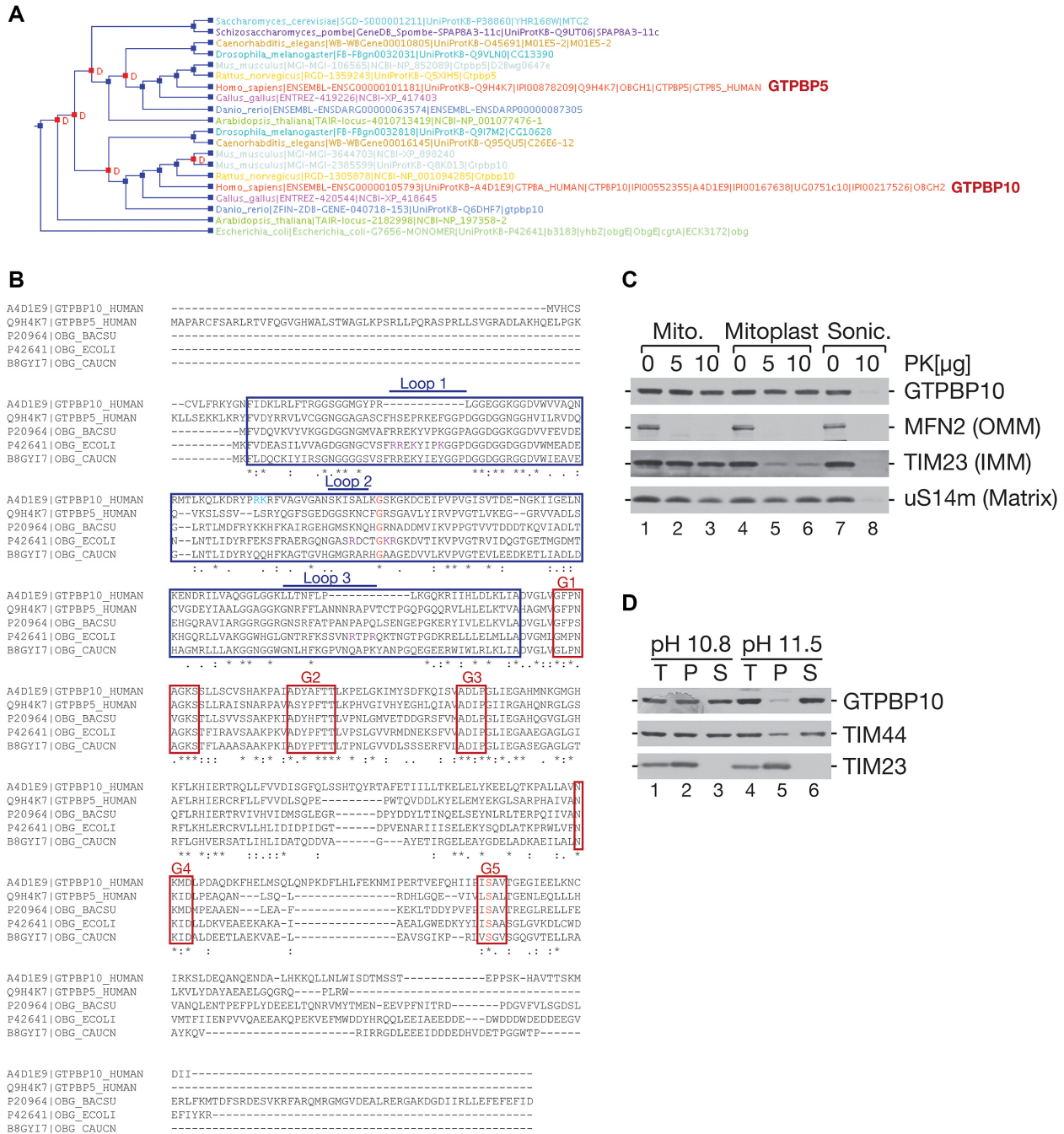


Figure 1. GTPBP10 is a peripheral protein of the inner mitochondrial membrane belonging to the Obg-subfamily. (A) Cluster analysis of the Obg GTPase family based on P-POD – Princeton Protein Orthology Database (<http://ppod.princeton.edu/>). Human GTPBP5 and GTPBP10 are indicated in red. (B) Amino acid sequence alignment of GTPBP5 and GTPBP10 and their bacterial homologues. Blue and red boxes indicate Obg domain and the five motifs of the GTPase domain (G1–G5), respectively. Arginine 64 and lysine 65 (*Gtbbp10*^{64R65K}), which were deleted in GTPBP10 using CRISPR/Cas9 (see below in the text), are labeled in blue. Amino acid substitutions for GTPBP10^{G82E}-FLAG and GTPBP10^{S325P}-FLAG are indicated in red. Purple shows amino acid substitutions in the *E. coli* ObgE protein, which abolish its function in bacterial ribosome assembly (9). (C) Localization of the GTPBP10. Isolated intact mitochondria (lanes 1-3), mitoplasts (lanes 4-6) and sonicated mitochondria (lanes 7,8) from HEK293T WT cells were treated with proteinase K as indicated. MFN2, TIM23 and uS14m were used as markers of the outer mitochondrial membrane (OMM), inner mitochondrial membrane (IMM) and matrix fraction, respectively. (D) GTPBP10 is a peripherally associated protein of the mitochondrial inner membrane. Carbonate extraction of mitochondrial membrane proteins at different pH from HEK293T WT cells. Fractions (T-total, P-pellet, S-supernatant) were analyzed by western blotting with specific antibodies as indicated.

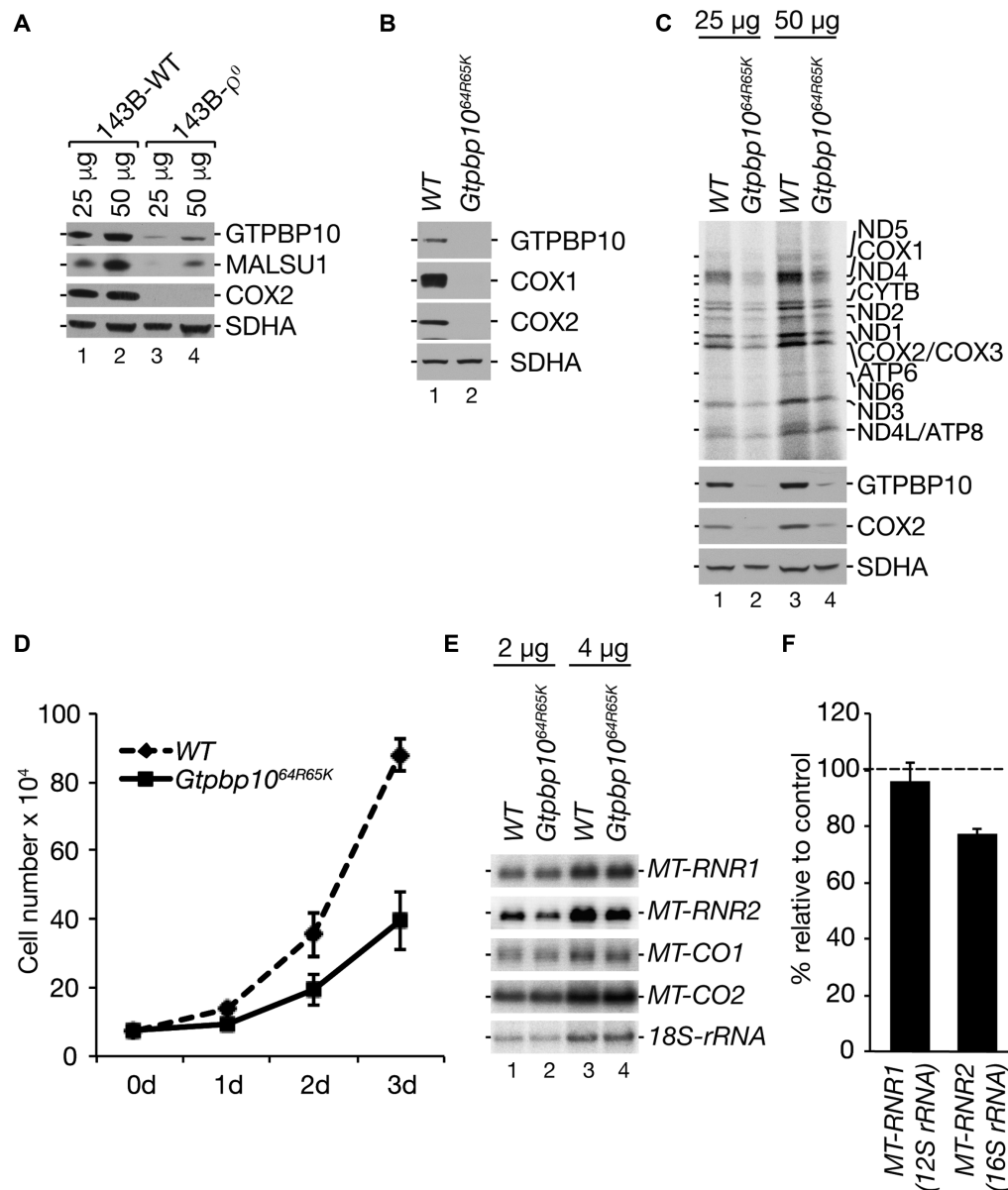


Figure 2. GTPBP10 is involved in mitochondrial gene expression. (A) GTPBP10 is unstable in the absence of mtDNA. Protein steady state levels from 143B wild type (WT) or 143B- ρ^0 cells were analyzed by western blotting. (B) Altered mitochondrial gene expression in *Gtpbp10*^{64R65K} cells. Steady state levels of mtDNA-encoded proteins (COX1 and COX2) isolated from HEK293T WT or *Gtpbp10*^{64R65K} cells. SDHA is used as a loading control. (C) *Gtpbp10*^{64R65K} cells exhibit diminished mitochondrial translation. [³⁵S]methionine *de novo* synthesized mtDNA-encoded proteins from HEK293T WT cells or *Gtpbp10*^{64R65K} cells were visualized by autoradiography (upper panel) or with designated antibodies (lower panel). SDHA is used as a loading control ($n = 3$). (D) Ablation of GTPBP10 reduces growth rate. Equal numbers of HEK293T WT and *Gtpbp10*^{64R65K} cells were seeded on day 0 (0d) and counted after 1 day (1d), 2 days (2d) and 3 days (3d) (mean \pm SD, $n = 3$). (E and F) GTPBP10 is required for 16S rRNA stability. (E) Steady state levels of mtDNA-encoded RNAs extracted from HEK293T WT and *Gtpbp10*^{64R65K} cells were analyzed by Northern blot with indicated probes. *MT-RNR1*: 12S rRNA; *MT-RNR2*: 16S rRNA; *MT-CO1*: mRNA encoding COX1; *MT-CO2*: mRNA encoding COX2. *18S-rRNA* was used as a loading control. (F) *MT-RNR1* and *MT-RNR2* were quantified using ImageJ and normalized to *18S-rRNA* (mean \pm SEM; $n = 3$).

loss of function of GTPBP10 on mitochondrial protein synthesis. In order to generate a stable knockout cell line we applied CRISPR/Cas9 technology, however, we failed to gain a complete loss of GTPBP10 as residual protein levels were still detectable, but were significantly reduced in the obtained clone (Figure 2B). Sequencing analysis revealed a deletion of six nucleotides (190–195) leading to the deletion of two amino acids at position 64 (R) and 65 (K) in the Obg fold domain (Supplementary Figure S1 and Figure

1B). As especially lysine at position 65 is conserved between human GTPBP10 and ObgE it is tempting to speculate that this deletion compromises function and thus leads to the instability of GTPBP10 and therefore represents a good tool to analyze the function of GTPBP10 in human mitochondria further. In order to address the effect of functional loss of GTPBP10 in this mutant cell line (*Gtpbp10*^{64R65K}) we performed *de novo* mitochondrial translation assays and observed an overall significant reduction of newly synthe-

sized mtDNA-encoded proteins leading to reduced protein steady state levels as represented by COX1 and COX2 (Figure 2B and C). The ablation of GTPBP10 and its accompanied decreased mitochondrial protein synthesis lead to a significant reduced cell growth as demonstrated by cell counts for one to three days in glucose containing media (Figure 2D). We asked further whether the reduced levels of mtDNA-encoded proteins were due to decreased levels of mitochondrial transcripts and analyzed isolated RNA from wild type and *Gtpbp10*^{64R65K} cells via Northern blot (Figure 2E). Interestingly, the levels of the mitochondrial rRNA of the mtSSU, 12S rRNA (*MT-RNR1*) and of mitochondrial mRNAs encoding COX1 (*MT-CO1*) and COX2 (*MT-CO2*) remained stable suggesting that GTPBP10 does not affect mitochondrial gene expression at the level of transcription. However, the mitochondrial rRNA of the mtLSU, 16S rRNA (*MT-RNR2*) was significantly reduced suggesting defects in mtLSU and thus in mitoribosome stability or biogenesis, which might explain the diminution in mitochondrial translation (Figure 2F).

GTPBP10 associates specifically with the mtLSU at a late maturation state

As the 16S rRNA was significantly reduced in *Gtpbp10*^{64R65K}, we speculated that GTPBP10 plays a role in the biogenesis of the mtLSU. In order to address this possibility, first, we analyzed whether GTPBP10 interacts with the mitoribosome. Applying sucrose density gradient centrifugation GTPBP10 mostly migrated in the less dense fractions, however, a portion of GTPBP10 clearly co-fractionated with proteins of the mtLSU, but not with the monosome (Figure 3A). To assess a possible interaction of GTPBP10 with the mtLSU, we performed co-immunoprecipitation experiments using C-terminal FLAG-tagged mL62 (13), a structural component of the central protuberance of the mtLSU (25–27). Utilizing mL62^{FLAG} as bait, we were able to isolate the mtLSU and the 55S monosome as demonstrated by the co-isolation of MRPs of the mLSU and mtSSU (Figure 3B). Interestingly, GTPBP10 was also significantly enriched in the elution fraction of mL62^{FLAG}, which is in agreement with the co-sedimentation of GTPBP10 with the mtLSU on sucrose gradients. To exclude the association of GTPBP10 with the 55S monosome or the mtSSU we performed similar immunoprecipitation experiments using mS40^{FLAG}, a component of the mtSSU (Figure 3C). Under those conditions we expect to co-isolate the mtSSU and the 55S monosome, but no free mtLSU. Indeed, we did not detect any GTPBP10 in this elution fraction indicating that GTPBP10 exclusively interacts with the mtLSU, but not with the mtSSU or the assembled 55S monosome. To directly address whether GTPBP10 interacts only with the completely assembled mtLSU or also with assembly intermediates and other ribosome biogenesis factors, we generated a stable cell line inducibly expressing a C-terminal FLAG-tagged GTPBP10 to determine its interactome via co-immunoprecipitation experiments. To avoid overexpression of GTPBP10^{FLAG}, we titrated the concentration of the inducer tetracycline to a minimum (Supplementary Figure S2). Western blot analysis of

co-immunoprecipitation experiments using GTPBP10^{FLAG} as bait confirmed the association of GTPBP10 with the mtLSU as all the tested MRPs of the mtLSU were enriched in the eluate of GTPBP10^{FLAG} (Figure 3D). In agreement with our previous observations GTPBP10^{FLAG} did not co-isolate components of the mtSSU confirming that GTPBP10 does not interact with the mtSSU or with the 55S mitoribosome. Interestingly, we detected also a number of known ribosome biogenesis factors including GTPBP7 (MTG1), NGRN and MALSU1 (11,20,28,29).

To comprehensively determine the interactome of GTPBP10^{FLAG} we performed quantitative mass spectrometry analyses. We identified 51 of 52 MRPs of the mtLSU (Figure 3E, Supplementary Table S1). Only bL36m was not detected, which seems to be a common problem as it was also not detected in other mitoribosome analyses (30). None of the MRPs of the mtSSU were enriched under our set thresholds. Most interestingly, we identified a number of mtLSU assembly factors and mtRNA granule proteins, which are involved in the processing and maturation of the 16S rRNA indicating that GTPBP10 is indeed involved in the biogenesis of the mtLSU (Table 1). The most enriched associated factors of GTPBP10^{FLAG} were SMCR7L and MALSU1. Both proteins were shown to be part of a late mtLSU assembly intermediate as shown by cryo-EM analyses (31), suggesting that GTPBP10 might act late in the mtLSU biogenesis. In agreement with such a hypothesis is the association with MTERF4, which targets NSUN4, also identified in the complex with GTPBP10, to the mtLSU at a late maturation state to form the 55S monosome (32,33). To support this observation, we performed a FLAG-immunoprecipitation of GTPBP10 and analyzed native isolated complexes via sucrose gradient (Figure 3F). We tested a number of mitoribosomal proteins of the mtLSU including uL1m and uL23m, which can be usually also detected in less dense fractions presumably presenting assembly intermediates (Figure 3A). However, apart from GTPBP10 itself, we did not observe any other protein including uL1m and uL23m in the less dense fractions suggesting that GTPBP10 does not associate with early mtLSU assembly intermediate complexes. All tested MRPs, which were co-purified with GTPBP10 sediment in the higher dense fractions indicating that GTPBP10 associates either with a very late assembly intermediate or with the matured mtLSU.

Loss of GTPBP10 affects mitoribosome assembly

As GTPBP10 associates exclusively with the mtLSU, it is tempting to speculate that GTPBP10 has a role in the biogenesis of the mtLSU potentially at a late assembly stage. Hence, we aimed to analyze the consequences of the loss of GTPBP10 on the biogenesis of the mtLSU and the 55S monosome. First, we tested GTPBP10 ablation on the protein steady state level and observed a decrease in certain mitoribosomal proteins, especially from the mtLSU, namely uL3m, uL13m and mL62m (Figure 4A and C). Interestingly, we noticed a decrease of NGRN as well, but not of GTPBP7 or MALSU1 (Figure 4B and C), which were all identified to be in complex with GTPBP10 (Figure 3D and F) and are suggested to be involved in the as-

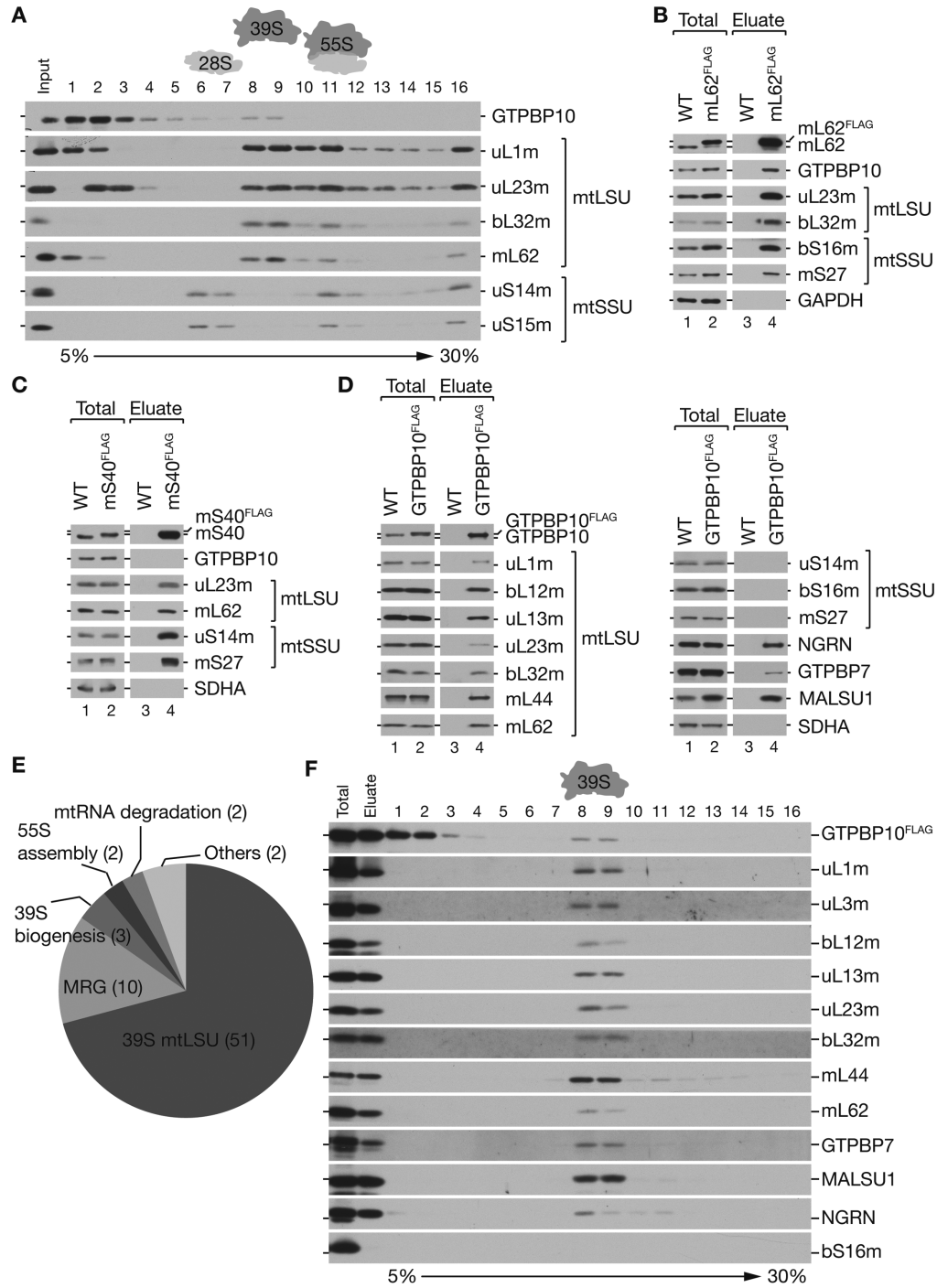


Figure 3. GTPBP10 interacts with the mtLSU and assembly factors. (A) GTPBP10 co-fractionates with mtLSU. Native protein complexes were isolated from HEK293T WT mitoplasts and separated by 5–30% sucrose gradient centrifugation. Fractions (1–16) were visualized by western blot with antibodies against mtLSU (uL1m, uL23m, bL32m, mL62) and mtSSU (uS14m, uS15m). (*n* = 4). (B–C) GTPBP10 associates specifically with mtLSU. Co-immunoprecipitation of FLAG-tagged mL62 (B) and mS40 (C). GAPDH and SDHA were used as negative controls for unspecific binding. Total, 3%; Eluate, 100% (*n* = 3). (D) Mitochondrial proteins and biogenesis factors of the mtLSU co-purify with GTPBP10^{FLAG}. Mitochondrial protein complexes containing GTPBP10 were co-purified via FLAG-tagged GTPBP10. Total, 3%; Eluate, 100% (*n* = 3). (E) The interactome of GTPBP10^{FLAG}. Equal amounts of differentially labeled mitochondria from HEK293T WT and GTPBP10^{FLAG} cells were mixed and applied to FLAG-immunoprecipitation. Native eluted complexes were analyzed by quantitative mass spectrometry. Diagram represents the results from four experiments (including label switch). *P* < 0.05; mean ratio ≥ 2 (*n* = 4). (F) GTPBP10 associates with mtLSU at a late assembly stage. FLAG-immunoprecipitation via GTPBP10^{FLAG} was performed as in (D). Native eluate was subjected to 5–30% Sucrose gradients. Fractions were analyzed by western blot with specific antibodies against mitochondrial proteins of the mtLSU and mtSSU, and assembly factors. Total (FLAG-immunoprecipitation input), 1%; Eluate (FLAG-immunoprecipitation eluate = gradient input), 10% (*n* = 3).

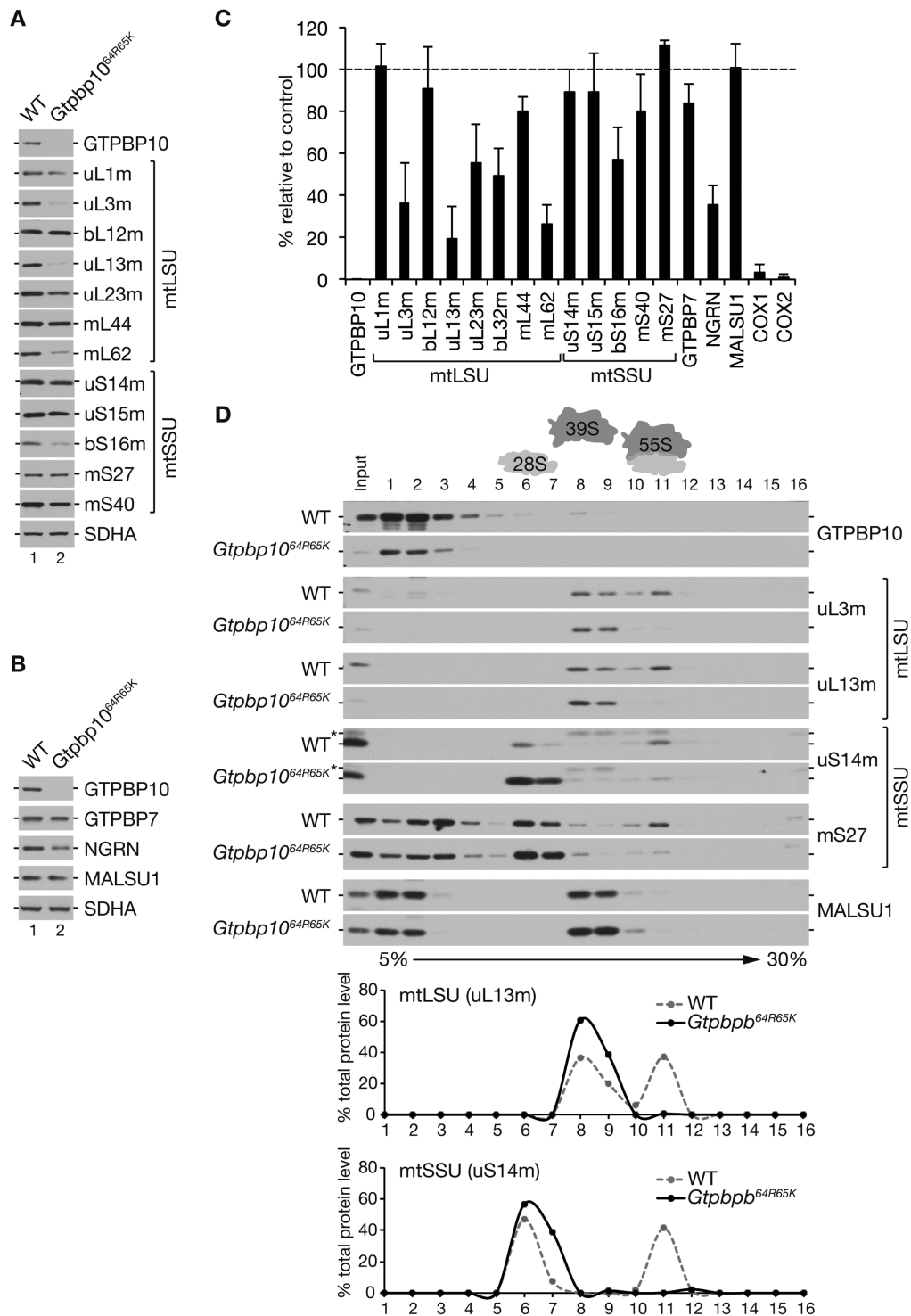


Figure 4. GTPBP10 is required for 55S monosome formation. (A-C) *Gtpbp10*^{64R65K} leads to reduced protein levels of selected MRPs (A) and ribosome biogenesis factors (B). (C) Quantification of steady state analysis of MRPs and biogenesis factors in *Gtpbp10*^{64R65K} cells relative to HEK293T WT control. SDHA was used as a loading control. ($n = 3$, mean \pm SEM). (D) Ablation of GTPBP10 reduces monosome formation. Protein complexes from HEK293T WT and *Gtpbp10*^{64R65K} mitoplasts were separated on 5–30% sucrose gradients and fractions (1–16) were analyzed by western blot with specific antibodies against mtSSU and mtLSU components and MALSU1. Protein distributions for uL13m (mtLSU) and uS14m (mtSSU) are presented as percentage of the total protein abundance. (*) indicates residual signals of bL32m.

Table 1. GTPBP10-associated factors

Name	Accession	Mean ratio	P-value
SMCR7L	L0R8F8	4.68	0.00015
MTERF4	Q7Z6M4	4.38	0.00031
MALSU1	Q96EH3	4.29	0.00038
DDX28	Q9NUL7	4.10	0.00055
NSUN4	Q96CB9	3.85	0.00102
TRUB2	O95900	3.36	0.00330
YARS2	Q9Y2Z4	3.32	0.00365
NGRN	Q9NPE2	3.19	0.00513
RNMTL1/MRM3	Q9HC36	3.13	0.00593
GTPBP7/MTG1	Q9BT17	3.13	0.00590
PTCD1	O75127	3.10	0.00635
FASTKD2	Q9NYY8	3.04	0.00770
WBSCR16/RCC1L	Q96I51	2.98	0.00874
SUPV3L1	Q8IYB8	2.95	0.00944
MTERF3	Q96E29	2.89	0.01210
TRMT61B	Q9BVS5	2.64	0.02145
RPUSD4	Q96CM3	2.56	0.02982
HSPA9/mtHSP70	P38646	2.56	0.02582
RPL22L1	Q6P5R6	2.56	0.02608
PNPT1/PNPASE	Q8TCS8	2.35	0.04580
PMPCA/MPPA	Q10713	2.34	0.04656

Mean ratio ≥ 2 ; P-value ≤ 0.05 .

Identified proteins of the mtLSU (51/52) are excluded from this table (see Supplementary Table S1).

sembly of the mtLSU. Our data indicate that GTPBP10 is required for the stability of certain mitoribosomal proteins and of mtLSU biogenesis factor NGRN and that the loss of GTPBP10 impairs mitoribosome maturation. To support this hypothesis we analyzed the formation of the 55S monosome by co-immunoprecipitation of uL1m, a core component of the mtLSU, which remains stable in the absence of GTPBP10 (Figure 4A and C). As expected in the absence of GTPBP10 the level of monosome formation decreases as demonstrated by the reduced level of co-immunoprecipitated mtSSU protein mS27 whereas components of the mtLSU including uL3m and uL13m remain associated to uL1m (Supplementary Figure S3).

In addition, we analyzed the consequences of the loss of GTPBP10 on mtLSU assembly and monosome formation via sucrose gradient centrifugation (Figure 4D). In agreement with the aforementioned co-immunoprecipitation experiments of uL1m, GTPBP10 ablation leads clearly to a drastic reduction of the 55S monosome, explaining the significant decrease in mitochondrial gene expression. All mitoribosomal proteins tested in these experiments were accumulating in the mtLSU or mtSSU, respectively. Thus, GTPBP10 influences mitoribosome biogenesis at a very late stage and loss of GTPBP10 leads to the accumulation of mtSSU and mtLSU with reduced 55S monosome formation.

GTPBP10 mutants are impaired in mtLSU binding

As GTPBP10 is homologous to bacterial ObgE, containing Obg domain as well as a functional GTPase domain (10), we asked whether both domains are required for mitoribosome biogenesis. To address this question, we generated two inducible stable cell lines expressing a FLAG tagged Obg domain mutant, namely GTPBP10^{G82E-FLAG} and a FLAG tagged GTPase domain mutant GTPBP10^{S325P-FLAG}. Both variants represent mutants with the replacement of a sin-

gle highly conserved amino acid in the respective domain (Figure 1B). Respective mutations in Obg proteins were reported to have an effect on ribosome biogenesis and cellular function in different bacterial strains (8,34). Interestingly, the induced expression of both mutants led to a significant reduction in cell growth monitored by decreased cell numbers in comparison to HEK293T wild type or GTPBP10^{WT-FLAG} cells (Figure 5A). To address the cause of this growth defect we analyzed the protein steady state levels of mtDNA-encoded proteins and indeed, we observed a significant reduction in COX1 and COX2 levels in both mutants of which the Obg mutant GTPBP10^{G82N-FLAG} showed the strongest effect (Figure 5B). The observed decrease in COX1 and COX2 levels suggest impaired mitochondrial gene expression in GTPBP10 mutants. Hence, we analyzed the *de novo* synthesis of mtDNA-encoded proteins by [³⁵S]Methionine labeling. Although we monitored a reduction in mitochondrial protein synthesis upon overexpression of GTPBP10^{WT-FLAG}, we observed a more drastic decrease in mitochondrial translation in the GTPBP10 mutant cell lines which might lead to a progressively reduction in the steady state level of mtDNA-encoded proteins (Figure 5C). To exclude that the reduction in COX1 and COX2 are due to decreased stability of newly synthesized mtDNA-encoded proteins, we performed [³⁵S]Methionine pulse-chase labeling experiments (Figure 5D). As the stability of newly synthesized mtDNA-encoded proteins are only marginally affected in the GTPBP10 mutants compared to the wild type cell line it is reasonable to suggest that reduced COX1 and COX2 levels are mainly caused by decreased mitochondrial translation.

As GTPBP10 binds the mtLSU at a late assembly state it is tempting to speculate that mtLSU biogenesis is impaired upon expression of GTPBP10 mutants. Thus, we analyzed whether GTPBP10 mutants maintained the ability to bind to the mtLSU. To this end, we performed FLAG-

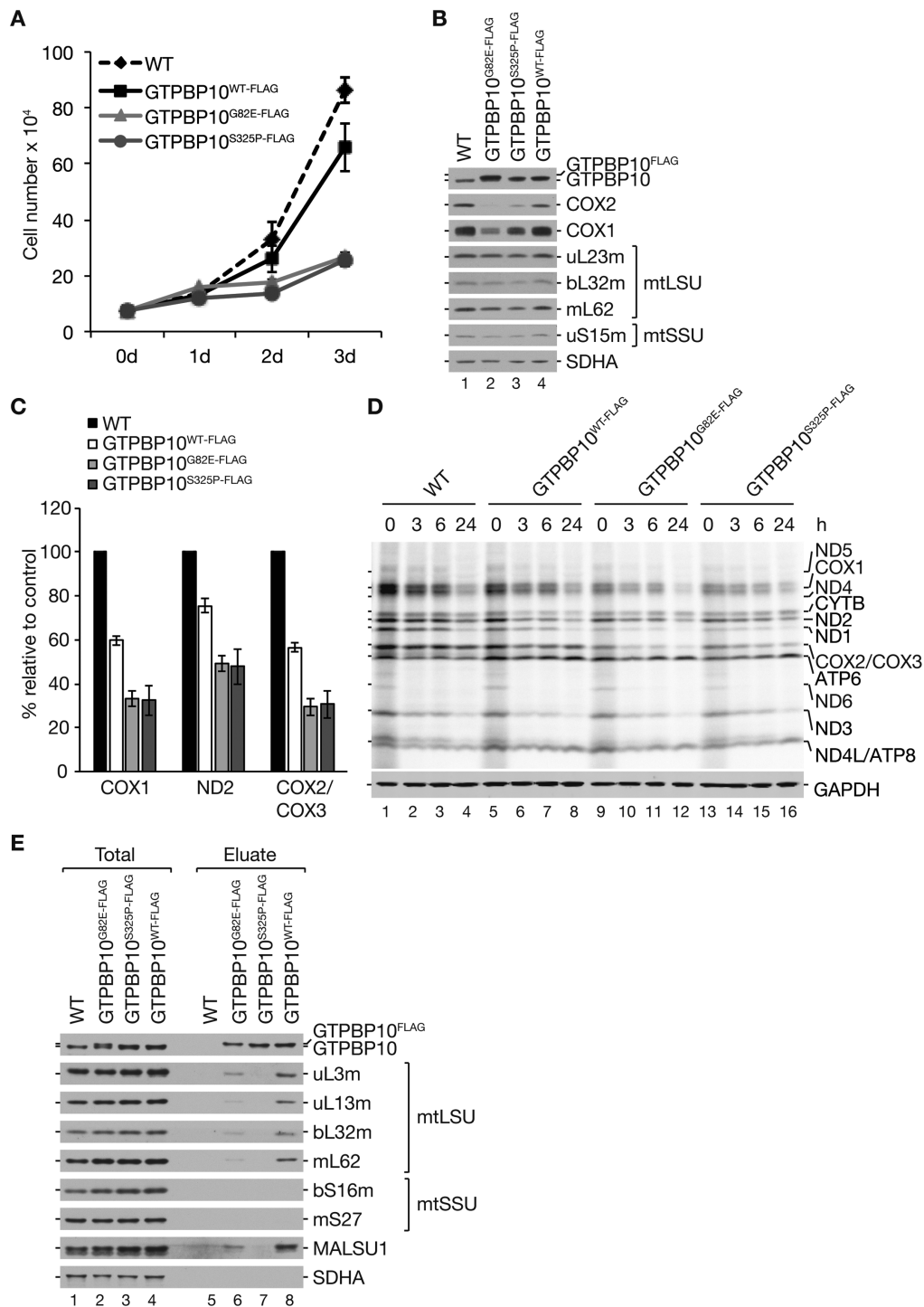


Figure 5. Expression of Obg and GTPase domain mutants negatively affect the function of GTPBP10. (A) GTPBP10^{G82E} and GTPBP10^{S325P} affect cell growth. Equal numbers of HEK293T WT, GTPBP10^{G82E-FLAG}, GTPBP10^{S325P-FLAG} and GTPBP10^{WT-FLAG} cells were seeded on day 0 (0d) and counted after 1 day (1d), 2 days (2d) or 3 days (3d) ($n = 3$, mean \pm SD). (B) GTPBP10^{G82E} and GTPBP10^{S325P} affect the steady state level of mtDNA-encoded proteins. Proteins were extracted from indicated cell lines and analyzed by western blot. SDHA was used as a loading control. (C and D) Synthesis and stability of mtDNA-encoded proteins in GTPBP10 mutants. Cells were pulse labeled for 1h in the presence of [³⁵S]Methionine (lanes 1, 5, 9 and 13) and chased for the indicated time points. Mitochondrial translation products from HEK293T WT cells or GTPBP10^{G82E-FLAG}, GTPBP10^{S325P-FLAG} and GTPBP10^{WT-FLAG} cells were visualized by autoradiography (D, upper panel). GAPDH was used as a loading control. Newly synthesized COX1, ND2 and COX2/COX3 were quantified after 1h pulse labeling using ImageQuant TL (C) (mean \pm SEM, $n = 4$). (E) GTPBP10 mutants show reduced mtLSU binding capacity. Lysed mitochondria from cell lines expressing FLAG-tagged GTPBP10^{G82E}, GTPBP10^{S325P} or wild type GTPBP10 were subjected to FLAG-immunoprecipitation. Samples were analyzed by western blot using indicated antibodies. SDHA was used as a negative control for unspecific binding. Total, 3%; Eluate, 10% ($n = 2$).

immunoprecipitation experiments with GTPBP10^{WT-FLAG} and the Obg and GTPase mutants. All FLAG-tagged versions of GTPBP10 were expressed at a similar level comparable to the endogenous level (Figure 5E). In contrast to GTPBP10^{WT-FLAG} both mutants showed a reduction in mtLSU association as demonstrated by decreased or non-detectable levels of co-immunoprecipitated mitoribosomal proteins of the mtLSU, where the GTPase mutant GTPBP10^{S325P-FLAG} revealed the most drastic reduction in mtLSU binding capacity. These data suggest that both the Obg domain as well as the GTPase domain are required for mtLSU binding and consequently for mitoribosome biogenesis and therefore for mitochondrial gene expression.

DISCUSSION

The two human homologues of bacterial ObgE, namely GTPBP5 and GTPBP10, were previously shown to localize to different cellular compartments. While GTPBP5 was demonstrated to be present within mitochondria, GTPBP10 was shown to localize to the nucleolus using fluorescence microscopy (10). Our studies provide evidence that GTPBP10 is a mitochondrial matrix protein, peripherally associated with the inner mitochondrial membrane, which is also in agreement with data by Arroyo *et al.* showing that GTPBP10 is required for OXPHOS function using a genome wide CRISPR ‘death screen’. Applying CRISPR/Cas9 technology we generated a GTPBP10 mutant with a deletion of arginine and lysine at position 64 and 65 within the Obg domain leading to the instability of the protein. This mutant cell line clearly demonstrated a mtDNA-expression defect, which also explains the requirement for OXPHOS function and concomitantly for cell growth for this factor. In addition, the overexpression of an Obg and a GTPase mutant variant also led to a reduction in mtDNA-expression with a progressively decrease in mtDNA-encoded proteins accompanied with a cell growth defect. What is the cause of this translation defect? Similarly to other mitochondrial GTP binding proteins such as GTPBP5 and GTPBP7 we show that GTPBP10 specifically associates with the mtLSU, but not with the mtSSU or the assembled monosome (11). For the association of GTPBP10 with the mtLSU both the Obg as well as the GTPase domain are required as mutants loose mtLSU binding capacity. Defining the interactome of GTPBP10 we identified besides the proteins of the mtLSU also components of the mitochondrial RNA granules and the 16S rRNA regulatory module such as DDX28, NGRN, WBSR16, RPUSD4, TRUB2, and FASTKD2 (20,23,35–38) suggesting the involvement of GTPBP10 in the biogenesis of the mtLSU. The ablation of GTPBP10 leads to a reduction of NGRN, which might also explain the partial decrease in the steady state level of 16S rRNA and some mitoribosomal proteins as NGRN depletion is associated with 16S rRNA diminishment (20). Interestingly, two of the most enriched proteins found in a complex with GTPBP10 were MALSU1, which was previously suggested to be a ribosome assembly or stability factor involved in mtLSU function (28,29), and SMCR7L. Both factors were identified in a late assembly intermediate of the mtLSU by cryo-EM (31). In addition MTERF4 and NSUN4 were also found to be

part of a GTPBP10 containing complex. As MTERF4 and NSUN4 together associate with a late matured mtLSU facilitating monosome formation (33), it is tempting to speculate that GTPBP10 is also involved in the late steps of mtLSU biogenesis, which would be also in agreement with its interaction with the late assembly factors MALSU1 and SMCR7L. Similar to the loss of either MTERF4 or NSUN4, GTPBP10 deficiency leads to a reduction in 55S monosome and thus to a decrease in mtDNA-expression at the translational level (32,33). What is the role of GTPBP10 in mtLSU biogenesis? The bacterial homologue ObgE has been suggested to be an anti-association factor preventing the formation of a monosome with irregular LSU particles (9). A temperature sensitive bacterial ObgE mutant affects rRNA processing and decreases 70S formation (8), reminiscent to the phenotypes in GTPBP10 deficient cells. As GTPBP10 associates with the mtLSU at a late assembly stage it is tempting to speculate that GTPBP10 might also act as a quality control factor for mtLSU maturation. Although both GTPBP5 and GTPBP10 complement Δ ObgE in *E. coli* (10), both are required in mitochondria as loss of either GTPBP5 (11) or GTPBP10 affect mitochondrial translation suggesting that they do not have overlapping function in human. Interestingly, GTPBP10 shows two deletions in the Obg domain in loop 1 and loop 3 in comparison to bacterial Obg proteins or human GTPBP5 (Figure 1B). As the human mitoribosome differs substantially from its bacterial counterpart these rearrangements in the Obg fold of GTPBP10 might reflect co-evolutionary changes and might explain the requirement for two Obg proteins in human mitochondria.

SUPPLEMENTARY DATA

Supplementary Data are available at NAR Online.

ACKNOWLEDGEMENTS

We thank Peter Rehling and Sven Dennerlein for critical reading of the manuscript and for discussions, Peter Rehling for providing antibodies, and Abhishek Aich for his guidance in CRISPR/Cas9 technology. We are thankful to Monika Raabe and Annika Kühn for technical assistance in mass spectrometry.

FUNDING

Deutsche Forschungsgemeinschaft [SFB860-A10 to H.U., SFB860 to R.R.-D., SFB1190-Z02 to H.U., SFB1190 to R.R.-D.]; Max Planck Society (to H.U.). Funding for open access charge: Deutsche Forschungsgemeinschaft.

Conflict of interest statement. None declared.

REFERENCES

1. Boczonadi, V. and Horvath, R. (2014) Mitochondria: impaired mitochondrial translation in human disease. *Int. J. Biochem. Cell Biol.*, **48**, 77–84.
2. Greber, B.J. and Ban, N. (2016) Structure and function of the mitochondrial ribosome. *Annu. Rev. Biochem.*, **85**, 103–132.
3. Shajani, Z., Sykes, M.T. and Williamson, J.R. (2011) Assembly of bacterial ribosomes. *Annu. Rev. Biochem.*, **80**, 501–526.

4. Kint, C., Verstraeten, N., Hofkens, J., Fauvart, M. and Michiels, J. (2014) Bacterial Obg proteins: GTPases at the nexus of protein and DNA synthesis. *Crit. Rev. Microbiol.*, **40**, 207–224.
5. Jiang, M., Sullivan, S.M., Wout, P.K. and Maddock, J.R. (2007) G-protein control of the ribosome-associated stress response protein SpoT. *J. Bacteriol.*, **189**, 6140–6147.
6. Wout, P., Pu, K., Sullivan, S.M., Reese, V., Zhou, S., Lin, B. and Maddock, J.R. (2004) The *Escherichia coli* GTPase CgtAE cofractionates with the 50S ribosomal subunit and interacts with SpoT, a ppGpp synthetase/hydrolase. *J. Bacteriol.*, **186**, 5249–5257.
7. Jiang, M., Datta, K., Walker, A., Strahler, J., Bagamasbad, P., Andrews, P.C. and Maddock, J.R. (2006) The *Escherichia coli* GTPase CgtAE is involved in late steps of large ribosome assembly. *J. Bacteriol.*, **188**, 6757–6770.
8. Sato, A., Kobayashi, G., Hayashi, H., Yoshida, H., Wada, A., Maeda, M., Hiraga, S., Takeyasu, K. and Wada, C. (2005) The GTP binding protein Obg homolog ObgE is involved in ribosome maturation. *Genes Cells*, **10**, 393–408.
9. Feng, B., Mandava, C.S., Guo, Q., Wang, J., Cao, W., Li, N., Zhang, Y., Zhang, Y., Wang, Z., Wu, J. *et al.* (2014) Structural and functional insights into the mode of action of a universally conserved Obg GTPase. *PLoS Biol.*, **12**, e1001866.
10. Hirano, Y., Ohniwa, R.L., Wada, C., Yoshimura, S.H. and Takeyasu, K. (2006) Human small G proteins, ObgH1, and ObgH2, participate in the maintenance of mitochondria and nucleolar architectures. *Genes Cells*, **11**, 1295–1304.
11. Kotani, T., Akabane, S., Takeyasu, K., Ueda, T. and Takeuchi, N. (2013) Human G-proteins, ObgH1 and Mtg1, associate with the large mitochondrial ribosome subunit and are involved in translation and assembly of respiratory complexes. *Nucleic Acids Res.*, **41**, 3713–3722.
12. Mick, D.U., Dennerlein, S., Wiese, H., Reinhold, R., Pacheu-Grau, D., Lorenzi, I., Sasarman, F., Weraarpachai, W., Shoubridge, E.A., Warscheid, B. *et al.* (2012) MITRAC links mitochondrial protein translocation to Respiratory-Chain assembly and translational regulation. *Cell*, **151**, 1528–1541.
13. Richter-Dennerlein, R., Oeljeklaus, S., Lorenzi, I., Ronsör, C., Bareth, B., Schendzielorz, A.B., Wang, C., Warscheid, B., Rehling, P. and Dennerlein, S. (2016) Mitochondrial protein synthesis adapts to influx of Nuclear-Encoded protein. *Cell*, **167**, 471–483.
14. Ran, F.A., Hsu, P.D., Wright, J., Agarwala, V., Scott, D.A. and Zhang, F. (2013) Genome engineering using the CRISPR-Cas9 system. *Nat Protoc.*, **8**, 2281–2308.
15. Callegari, S., Richter, F., Chojnacka, K., Jans, D.C., Lorenzi, I., Pacheu-Grau, D., Jakobs, S., Lenz, C., Urlaub, H., Dudek, J. *et al.* (2016) TIM29 is a subunit of the human carrier translocase required for protein transport. *FEBS Lett*, **590**, 4147–4158.
16. Dennerlein, S., Oeljeklaus, S., Jans, D., Hellwig, C., Bareth, B., Jakobs, S., Deckers, M., Warscheid, B. and Rehling, P. (2015) MITRAC7 acts as a COX1-specific chaperone and reveals a checkpoint during cytochrome c oxidase assembly. *Cell Rep.*, **12**, 1644–1655.
17. Chomyn, A. (1996) In vivo labeling and analysis of human mitochondrial translation products. *Methods Enzymol.*, **264**, 197–211.
18. Chrzanoska-Lightowlers, Z.M., Preiss, T. and Lightowlers, R.N. (1994) Inhibition of mitochondrial protein synthesis promotes increased stability of nuclear-encoded respiratory gene transcripts. *J. Biol. Chem.*, **269**, 27322–27328.
19. Bareth, B., Nikolov, M., Lorenzi, I., Hildenbeutel, M., Mick, D.U., Helbig, C., Urlaub, H., Ott, M., Rehling, P. and Dennerlein, S. (2016) Oms1 associates with cytochrome c oxidase assembly intermediates to stabilize newly synthesized Cox1. *Mol. Biol. Cell.*, **27**, 1570–1580.
20. Arroyo, J.D., Jourdain, A.A., Calvo, S.E., Ballarano, C.A., Doench, J.G., Root, D.E. and Mootha, V.K. (2016) A Genome-wide CRISPR death screen identifies genes essential for oxidative phosphorylation. *Cell Metab.*, **24**, 875–885.
21. Blom, J., Kübrich, M., Rassow, J., Voos, W., Dekker, P.J., Maarse, A.C., Meijer, M. and Pfanner, N. (1993) The essential yeast protein MIM44 (encoded by MPI1) is involved in an early step of preprotein translocation across the mitochondrial inner membrane. *Mol. Cell Biol.*, **13**, 7364–7371.
22. Schneider, H.C., Berthold, J., Bauer, M.F., Dietmeier, K., Guiard, B., Brunner, M. and Neupert, W. (1994) Mitochondrial Hsp70/MIM44 complex facilitates protein import. *Nature*, **371**, 768–774.
23. Tu, Y.-T. and Barrientos, A. (2015) The human mitochondrial DEAD-Box protein DDX28 resides in RNA granules and functions in mitoribosome assembly. *Cell Rep.*, **10**, 854–864.
24. Rozanska, A., Richter-Dennerlein, R., Rorbach, J., Gao, F., Lewis, R.J., Chrzanoska-Lightowlers, Z.M. and Lightowlers, R.N. (2017) The human RNA-binding protein RBFA promotes the maturation of the mitochondrial ribosome. *Biochem. J.*, **474**, 2145–2158.
25. Richter, R., Rorbach, J., Pajak, A., Smith, P.M., Wessels, H.J., Huynen, M.A., Smeitink, J.A., Lightowlers, R.N. and Chrzanoska-Lightowlers, Z.M. (2010) A functional peptidyl-tRNA hydrolase, ICT1, has been recruited into the human mitochondrial ribosome. *EMBO J.*, **29**, 1116–1125.
26. Greber, B.J., Boehringer, D., Leibundgut, M., Bieri, P., Leitner, A., Schmitz, N., Aebersold, R. and Ban, N. (2014) The complete structure of the large subunit of the mammalian mitochondrial ribosome. *Nature*, **515**, 283–286.
27. Brown, A., Amunts, A., Bai, X.-C., Sugimoto, Y., Edwards, P.C., Murshudov, G., Scheres, S.H.W. and Ramakrishnan, V. (2014) Structure of the large ribosomal subunit from human mitochondria. *Science*, **346**, 718–722.
28. Rorbach, J., Gammage, P.A. and Minczuk, M. (2012) C7orf30 is necessary for biogenesis of the large subunit of the mitochondrial ribosome. *Nucleic Acids Res.*, **40**, 4097–4109.
29. Wanschers, B.F.J., Szklarczyk, R., Pajak, A., van den Brand, M.A.M., Gloerich, J., Rodenburg, R.J.T., Lightowlers, R.N., Nijtmans, L.G. and Huynen, M.A. (2012) C7orf30 specifically associates with the large subunit of the mitochondrial ribosome and is involved in translation. *Nucleic Acids Res.*, **40**, 4040–4051.
30. Bogenhagen, D.F., Ostermeyer-Fay, A.G., Haley, J.D. and Garcia-Diaz, M. (2018) Kinetics and mechanism of mammalian mitochondrial ribosome assembly. *Cell Rep.*, **22**, 1935–1944.
31. Brown, A., Rathore, S., Kimanius, D., Aibara, S., Bai, X.-C., Rorbach, J., Amunts, A. and Ramakrishnan, V. (2017) Structures of the human mitochondrial ribosome in native states of assembly. *Nat. Struct. Mol. Biol.*, **24**, 866–869.
32. Cámara, Y., Asin-Cayuela, J., Park, C.B., Metodiev, M.D., Shi, Y., Ruzzenente, B., Kukat, C., Habermann, B., Wibom, R., Hultenby, K. *et al.* (2011) MTERF4 regulates translation by targeting the methyltransferase NSUN4 to the mammalian mitochondrial ribosome. *Cell Metab.*, **13**, 527–539.
33. Metodiev, M.D., Spähr, H., Loguercio Polosa, P., Meharg, C., Becker, C., Altmueller, J., Habermann, B., Larsson, N.-G. and Ruzzenente, B. (2014) NSUN4 is a dual function mitochondrial protein required for both methylation of 12S rRNA and coordination of mitoribosomal assembly. *PLoS Genet.*, **10**, e1004110.
34. Datta, K., Skidmore, J.M., Pu, K. and Maddock, J.R. (2004) The *Caulobacter crescentus* GTPase CgtAC is required for progression through the cell cycle and for maintaining 50S ribosomal subunit levels. *Mol. Microbiol.*, **54**, 1379–1392.
35. Antonicka, H. and Shoubridge, E.A. (2015) Mitochondrial RNA granules are centers for posttranscriptional RNA processing and ribosome biogenesis. *Cell Rep.*, **10**, 920–932.
36. Antonicka, H., Choquet, K., Lin, Z.-Y., Gingras, A.-C., Kleinman, C.L. and Shoubridge, E.A. (2017) A pseudouridine synthase module is essential for mitochondrial protein synthesis and cell viability. *EMBO Rep.*, **18**, 28–38.
37. Zaganelli, S., Rebelo-Guiomar, P., Maundrell, K., Rozanska, A., Pierredon, S., Powell, C.A., Jourdain, A.A., Hulo, N., Lightowlers, R.N., Chrzanoska-Lightowlers, Z.M. *et al.* (2017) The pseudouridine synthase RPUSD4 is an essential component of mitochondrial RNA granules. *J. Biol. Chem.*, **292**, 4519–4532.
38. Jourdain, A.A., Popow, J., la Fuente, de, M.A., Martinou, J.-C., Anderson, P. and Simarro, M. (2017) The FASTK family of proteins: emerging regulators of mitochondrial RNA biology. *Nucleic Acids Res.*, **45**, 10941–10947.

The human Obg protein GTPBP10 is involved in mitoribosomal biogenesis

Elena Lavdovskaia¹, Elisa Kolander¹, Emely Steube¹, Mandy Mong-Quyen Mai¹, Henning Urlaub^{2,3} and Ricarda Richter-Dennerlein^{1,*}

¹ Department of Cellular Biochemistry, University Medical Center Göttingen, D-37073 Göttingen, Germany

² Bioanalytical Mass Spectrometry Group, Max Planck Institute for Biophysical Chemistry, D-37077 Göttingen, Germany

³ Bioanalytics, Institute for Clinical Chemistry, University Medical Center Göttingen, D-37073 Göttingen, Germany

* To whom correspondence should be addressed. Tel: +49 (0)551 395913, Fax: +49 (0)551 395979, Email: ricarda.richter@med.uni-goettingen.de

SUPPLEMENTARY DATA

Table S1: Interactome of GTPBP10

Related to Table 1.

Figure S1: Sequence alignment of Gtpbp10-WT and *Gtpbp10*^{64K65R} mutant

Genomic DNA (gDNA) or RNA were isolated from wild type and *Gtpbp10*^{64K65R} mutant HEK293T cell lines. PCR amplicons from the respective gDNA or generated cDNA covering the guide RNA region were sequenced and analyzed using Geneious.

Figure S2: Expression titration of GTPBP10^{FLAG}

HEK293T cells expressing GTPBP10FLAG were induced with different concentration of tetracycline as indicated. Protein extracts were analyzed by immunoblotting. Relative expression level of GTPBP10 was compared to endogenous GTPBP10 of HEK293T WT cells.

Figure S3: Co-immunoprecipitation of uL1m

Isolated mitochondria from HEK293T WT and *Gtpbp*^{64R65K} cells were lysed and subjected to co-immunoprecipitation using uL1m antibodies and control IgGs. Protein complexes were eluted via pH-shift and analyzed by western blotting. Total, 5%; Eluate, 100%.

Table S1: Interactome of GTPBP10

Related to Table 1.

Protein	Gene names	Majority protein IDs	mean ratio	p-value
GTPBP10	GTPBP10	A4D1E9;C9JEQ8;C9J8R7;C9JN11	5.677	0.000129
SMCR7L	SMCR7L	L0R8F8	4.681	0.000155
bL20m	MRPL20	Q9BYC9	4.525	0.000259
mL44	MRPL44	A0A024R473;Q9H9J2	4.495	0.000266
uL15m	MRPL15	Q9P015;B2R739;E5RIZ4;E5RHF4	4.440	0.000305
mL52	MRPL52	A8K7J6;Q86TS9;G3V3U6;G5E9P5	4.436	0.000287
bL21m	MRPL21	Q7Z2W9;B4DXI4;A0A024R5G7;F5H7V8	4.427	0.000293
bL27m	MRPL27	Q9P0M9;D6RAN8;H7C5U8	4.425	0.000274
mL65	MRPS30	Q9BUN6;Q9NP92;Q53H77	4.421	0.000328
mL49	MRPL49	A0A024R578;Q13405;H0YDP7;E9PNF1;Q59GE9	4.415	0.000286
mL63	MRP63; MRPL57	A0A024RDM4;Q9BQC6	4.408	0.000313
uL13m	MRPL13	Q9BYD1;E5RJ17	4.400	0.000305
mL42	MRPL42	S4R360;J3KPP0;A0A024RBG3;S4R2Z7;Q9Y6G3	4.393	0.000335
mL50	MRPL50	Q8N5N7	4.385	0.000324
MTERF4	MTERF4	Q7Z6M4;B4DFP7;C9JNJ7;B4DKD5;H7C316	4.377	0.000310
uL4m	MRPL4	A0A024R7C5;Q9BYD3;K7ES61;X6RAY8;K7ELQ0	4.372	0.000323
mL43	MRPL43	H0Y6Y8;B1AL05;Q8N983;H0YBU8	4.372	0.000300
uL30m	MRPL30	Q8TCC3	4.371	0.000341
uL18m	MRPL18	A8K9D2;Q9H0U6	4.369	0.000301
mL38	MRPL38	Q96DV4	4.334	0.000325
uL14m	MRPL14	A0A024RD78;Q6P1L8	4.330	0.000336
MALSU1	MALSU1	Q96EH3	4.295	0.000377
mL45	MRPL45	A0A087X2D5;B4DEF8;Q9BRJ2;A0A0G2JMS5;A0A087WU62	4.284	0.000400
uL11m	MRPL11	Q9Y3B7;Q53G19	4.265	0.000408
bL28m	MRPL28	Q13084;A2IDC6;Q4TT37;A2IDC7	4.258	0.000429
mL51	MRPL51	Q4U2R6	4.228	0.000416
mL66	MRPS18A	Q9NVS2;Q5QPA5	4.224	0.000439
bL19m	MRPL19	A8K5D5;P49406;B4DIG4;S4R3W9	4.197	0.000453
bL17m	MRPL17	Q9NRX2;E9PKV2	4.157	0.000491
bL35m	MRPL35	Q9NZE8;D3YTC1	4.151	0.000512
uL3m	MRPL3	H0Y9G6;E7ETU7;P09001;B4DKM0;B4DW56;D6RC14;E9PF06	4.131	0.000546
uL2m	MRPL2	Q5T653;A0A024RD44	4.122	0.000526
uL29m	MRPL47	Q9HD33	4.106	0.000613
DDX28	DDX28	Q9NUL7	4.104	0.000548
mL41	MRPL41	Q8IXM3	4.102	0.000602
uL24m	MRPL24	Q96A35;X6RJ73	4.101	0.000573
mL39	MRPL39	Q9NYK5;C9JG87	4.066	0.000609
uL23m	MRPL23	A0A024RCB2;Q16540;B2R9J4;A6NJD9;A8MVT4;A8MYK1;H7C2P7	4.052	0.000632
uL16m	MRPL16	Q9NX20;E9PI14	4.040	0.000663
uL1m	MRPL1	A0PJ79;Q9BYD6;H0Y8N7	3.991	0.000790
bL12m	MRPL12; MRPL7/ L12	P52815;Q96Q74	3.980	0.000821
mL54	MRPL54	Q6P161	3.944	0.000808
uL22m	MRPL22	E7ESL0;J3KQY1;Q9NWU5	3.929	0.000845
mL53	MRPL53	Q96EL3	3.910	0.000885
mL64	GADD45 GIP1	Q8TAE8;Q7LAX7	3.888	0.000978
bL32m	MRPL32	A4D1V4;Q9BYC8	3.877	0.001055
mL62	ICT1	J3KS15;Q14197	3.868	0.001742
bL34m	MRPL34	A0A024R7J4;M0R226;Q9BQ48	3.851	0.001102
NSUN4	NSUN4	Q96CB9;A8K8I8;B3KUM0	3.851	0.001023
mL37	MRPL37	Q9BZE1;S4R369	3.677	0.001508
bL33m	MRPL33	O75394	3.507	0.002385
TRUB2	TRUB2	A0A024R886;O95900	3.361	0.003298
YARS2	YARS2	Q9Y2Z4;H0YHS6	3.325	0.003652
bL9m	MRPL9	Q9BYD2;Q5SZR1	3.244	0.004687
uL10m	MRPL10	B4DEH0;Q7Z7H8	3.238	0.005836
NGRN	NGRN	Q9NPE2	3.186	0.005129
RNMTL1	RNMTL1	Q9HC36;I3L443	3.132	0.005932
GTPBP7	MTG1	A8K900;U3KQ69;E9PI62;Q9BT17;B4DF93;B3KWF9;E7EVK2	3.130	0.005905
PTCD1	PTCD1;	Q3ZB84;A4D273;G3V325;B4DJ38;O75127;B3KMD7;Q3SYP6	3.103	0.006355

	ATP5J2-PTCD1			
FASTKD2	KIAA0971; FASTKD2	A0A024R419;Q9NYY8;B3KMB8	3.039	0.007697
WBSCR16	WBSCR16	Q96I51;B2RXG5	2.978	0.008737
SUPV3L1	SUPV3L1	Q8IYB8;B7Z611	2.955	0.009437
MTERF3	MTERF3/ MTERFD1	Q96E29;E5RIK9;E5RIY4	2.895	0.012104
mL46	MRPL46	Q9H2W6	2.876	0.011337
mL48	MRPL48	Q96GC5;F5H702;F5H8D0	2.862	0.011761
bL31m	MRPL55	A0A024R3R0;Q7Z7F7	2.854	0.012008
mL40	MRPL40	Q9NQ50	2.800	0.014138
TRMT61B	TRMT61B	Q9BVS5;F8WDR2	2.641	0.021453
RPUSD4	RPUSD4	A0A024R3K2;Q96CM3;B4DUN4	2.563	0.029822
mtHSP70	HEL-S- 124m; HSPA9	B7Z4V2;V9HW84;P38646;Q8N1C8;B7Z4T3;B7Z1V7	2.561	0.025818
RPL22L1	RPL22L1	C9JYQ9;H0Y8C2;Q6P5R6	2.559	0.026083
PNPT1	PNPT1	Q8TCS8	2.352	0.045804
PMPCA	PMPCA	Q10713;B4DRK5	2.344	0.046558

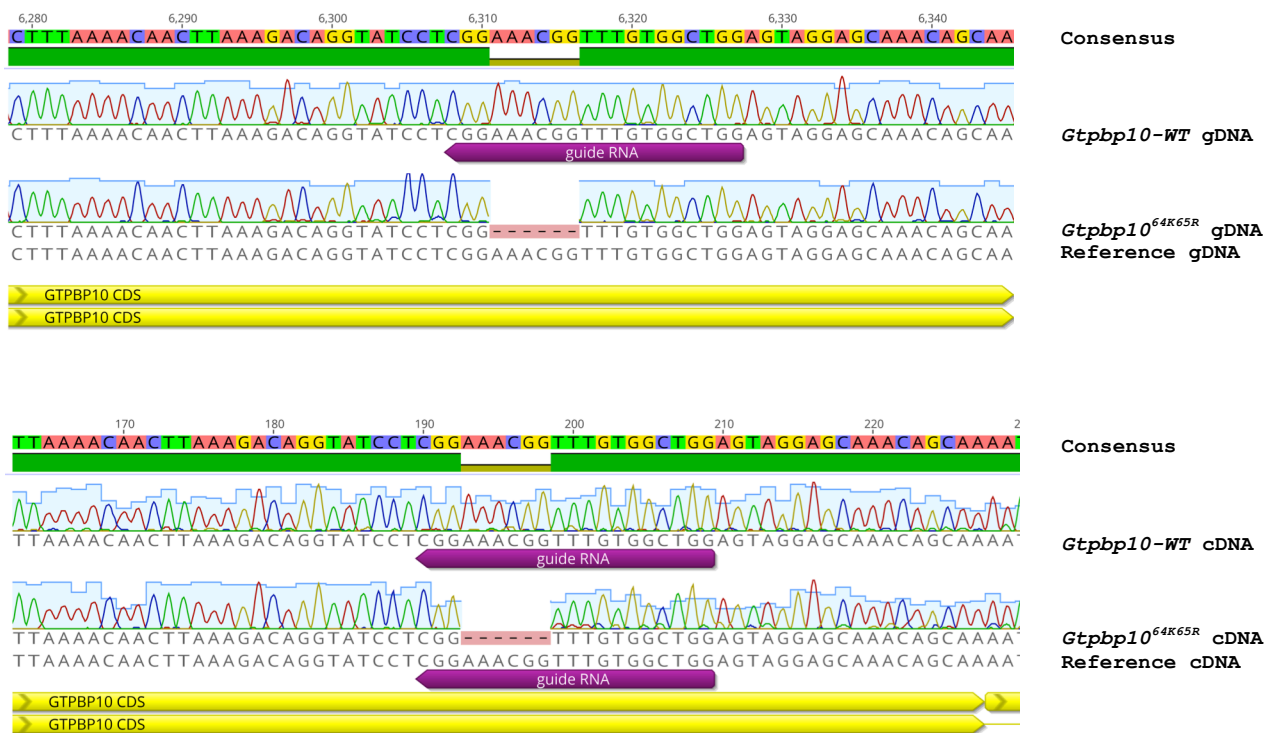


Figure S1: Sequence alignment of *Gtpbp10*-WT and *Gtpbp10*^{64K65R} CRISPR mutant
 Genomic DNA (gDNA) or RNA were isolated from wild-type and *Gtpbp10*^{64K65R} mutant cell lines. PCR amplicons from respective genomic DNA or generated cDNA covering the guide RNA region were sequenced and analysed using Geneious.

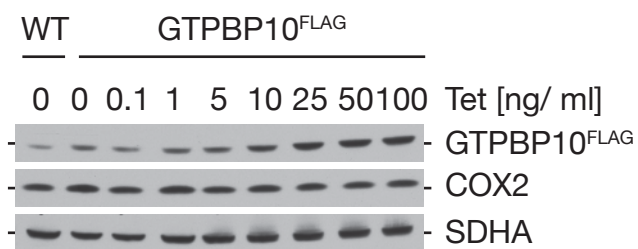


Figure S2: Expression titration of GTPBP10^{FLAG}

HEK293T cells expressing GTPBP10^{FLAG} were induced with different concentration of tetracycline as indicated. Protein extracts were analyzed by immunoblotting. Relative expression level of GTPBP10 was compared to endogenous GTPBP10 of HEK293T WT cells.

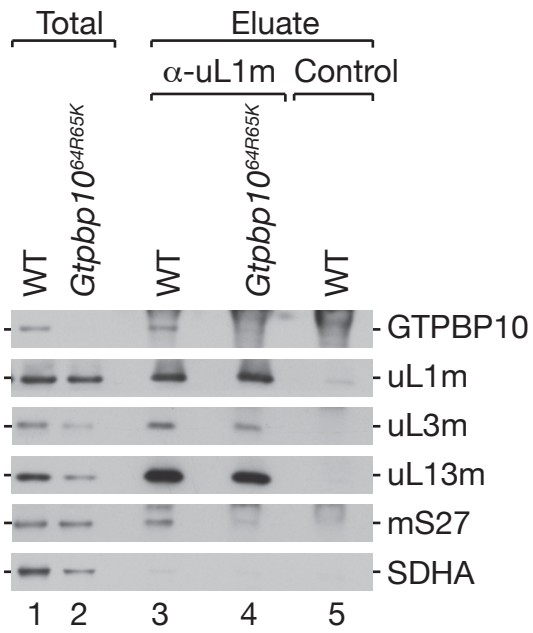


Figure S3: Co-immunoprecipitation of uL1m

Isolated mitochondria from HEK293T WT and *Gtpbp*^{64R65K} cells were lysed and subjected to co-immunoprecipitation using uL1m antibodies and control IgGs. Protein complexes were eluted via pH-shift and analyzed by western blotting. Total, 5%; Eluate, 100%.

4.2 Publication 2

Lavdovskaia, E., Denks, K., Nadler, F., Steube, E., Linden, A., Urlaub, H., Rodnina, M.V., and Richter-Dennerlein, R. (2020). Dual function of GTPBP6 in biogenesis and recycling of human mitochondrial ribosomes. *Nucleic Acids Research* 48, 12929–12942. doi: 10.1093/nar/gkaa1132

Copyright license: according to the publisher's web-site and Copyright Clearance Center's RightsLink[®], this is an open access article distributed under the terms of the [Creative Commons CC BY](https://creativecommons.org/licenses/by/4.0/) license, which permits unrestricted use, distribution, and reproduction in any medium, provided the original work is properly cited.

Authors contribution:

Figure 1. Cluster analysis of HflX GTPase family (R.R.-D.), generation of HEK293T cell line expressing GTPBP6^{FLAG}, isolation of mitochondria, mitochondrial localization assay and carbonate extraction of mitochondrial membrane proteins (E.L.).

Figure 2. FLAG-immunoprecipitation of mitochondrial ribosomal complexes associated with GTPBP6, western blot, cell counts, sucrose gradient analysis of mitochondrial ribosomal complexes isolated from cells overexpressing GTPBP6^{FLAG}, [³⁵S]Methionine *de novo* labeling of mitochondrial translation products in cells overexpressing GTPBP6^{FLAG} (E.L.).

Figure 3. Purification of recombinant GST-tagged GTPBP6 WT protein (E.L., E.S., R.R.-D.); Preparation of 70S ribosomal complexes, light-scattering experiments (K.D.).

Figure 4. Generation of *Gtpbp6*^{-/-} cell line, steady state analysis of mitochondrial ribosomal proteins in HEK293T *Gtpbp6*^{-/-} cells, [³⁵S]Methionine *de novo* labeling of mitochondrial translation products in *Gtpbp6*^{-/-} cells (E.L.); cell counts (R.R.-D.).

Figure 5. Sucrose gradient analysis of mitochondrial ribosomal complexes isolated from cells lacking GTPBP6, steady state analysis of mitochondrial ribosomal biogenesis factors in HEK293T *Gtpbp6*^{-/-} cells (EL); mass-spectrometry analysis of the mtLSU composition in GTPBP6-deficient cells (A.L.).

Figure 6. Purification of recombinant GST-tagged GTPBP6 mutant protein variants (E.L., E.S., R.R.-D.); light-scattering experiments (K.D.), [³⁵S]Methionine *de novo* labeling of mitochondrial translation products in cells bearing mutant GTPBP6 variants, sucrose gradient analysis of mitochondrial ribosomal complexes isolated from *Gtpbp6*^{-/-} cells or cells bearing FLAG-tagged variants of GTPBP6 (E.L., F.N.).

Figure S1. Sequence alignment of GTPBP6 and its homologs (R.R.-D.).

Figure S2. Sucrose gradient analysis of mitochondrial ribosomal complexes isolated from cells overexpressing GTPBP6^{FLAG} (E.L.).

Figure S3. Preparation of 70S ribosomal complexes, light-scattering experiments (K.D.).

Figure S4. Sequence analysis of *Gtpbp6*^{-/-} cell line, alignment of *Gtpbp6*^{-/-} vs. WT cell line, northern blot analysis of mtDNA-encoded RNAs steady-state levels in *Gtpbp6*^{-/-} cell line, expression titration of HEK293T *Gtpbp6*^{-/-} + GTPBP6^{FLAG} (rescue) cell line (E.L.).

Figure S5. Superimposition of 39S mtLSU with 50S *E. coli* LSU and analysis of the structural features (K.D.).

Non-experimental contribution: data analysis and visualization (E.L., K.D., A.L. and R.R.-D.); project supervision (R.R.-D., M.V.R. and H.U.); study conceptualization (R.R.-D.), manuscript writing (R.R.-D. with the contribution of all the co-authors).

Dual function of GTPBP6 in biogenesis and recycling of human mitochondrial ribosomes

Elena Lavdovskaia^{1,2}, Kärt Denks^{2,3}, Franziska Nadler¹, Emely Steube¹,
Andreas Linden^{4,5}, Henning Urlaub^{4,5}, Marina V. Rodnina^{2,3} and
Ricarda Richter-Dennerlein^{1,2,*}

¹Department of Cellular Biochemistry, University Medical Center Goettingen, D-37073 Goettingen, Germany, ²Cluster of Excellence ‘Multiscale Bioimaging: from Molecular Machines to Networks of Excitable Cells’ (MBExC), University of Goettingen, Goettingen, Germany, ³Department of Physical Biochemistry, Max Planck Institute for Biophysical Chemistry, D-37077 Goettingen, Germany, ⁴Bioanalytical Mass Spectrometry Group, Max Planck Institute for Biophysical Chemistry, D-37077 Goettingen, Germany and ⁵Bioanalytics, Institute for Clinical Chemistry, University Medical Center Goettingen, D-37073 Goettingen, Germany

Received July 29, 2020; Revised October 19, 2020; Editorial Decision November 03, 2020; Accepted November 09, 2020

ABSTRACT

Translation and ribosome biogenesis in mitochondria require auxiliary factors that ensure rapid and accurate synthesis of mitochondrial proteins. Defects in translation are associated with oxidative phosphorylation deficiency and cause severe human diseases, but the exact roles of mitochondrial translation-associated factors are not known. Here we identify the functions of GTPBP6, a homolog of the bacterial ribosome-recycling factor HflX, in human mitochondria. Similarly to HflX, GTPBP6 facilitates the dissociation of ribosomes *in vitro* and *in vivo*. In contrast to HflX, GTPBP6 is also required for the assembly of mitochondrial ribosomes. GTPBP6 ablation leads to accumulation of late assembly intermediate(s) of the large ribosomal subunit containing ribosome biogenesis factors MTERF4, NSUN4, MALSU1 and the GTPases GTPBP5, GTPBP7 and GTPBP10. Our data show that GTPBP6 has a dual function acting in ribosome recycling and biogenesis. These findings contribute to our understanding of large ribosomal subunit assembly as well as ribosome recycling pathway in mitochondria.

INTRODUCTION

The biogenesis and the function of the mitochondrial ribosome is of central importance for the fitness and viability of eukaryotic cells, and mutations in genes encoding for mitochondrial ribosomal proteins or translation factors lead to severe human diseases (1,2). Although the human mitochondrial genome (mtDNA) encodes only thir-

teen polypeptides, all of which are subunits of the oxidative phosphorylation (OXPHOS) system, ~25% of the mitochondrial proteome is dedicated to the task of mtDNA gene expression (3). More than 12% of the mitochondrial proteome form the translational apparatus to synthesize those thirteen mtDNA-encoded proteins. How the mitochondrial ribosome assembles and which auxiliary factors are required for its function is poorly understood. Even though the human mitochondrial ribosome evolved from a bacterial ancestor, there are significant differences in structure and composition between mitochondrial and bacterial ribosomes. The 55S mitochondrial ribosome is composed of a 28S small ribosomal subunit (mtSSU) with the 12S rRNA and 30 proteins, and a 39S large ribosomal subunit (mtLSU) with the 16S rRNA, the tRNA^{Val} or tRNA^{Phe} in the central protuberance and 52 proteins. The 55S ribosome is a protein-rich particle, with a protein:RNA ratio of 70%:30%, which is reversed compared to the bacterial ribosome (4). Approximately 50% of mitochondrial ribosomal proteins lack a bacterial homolog. Thus, it is likely that the assembly of the mitochondrial ribosome differs from that of the bacterial one and requires additional ancillary biogenesis factors. Although a number of assembly factors have been identified, including RNA helicases, RNA modifying enzymes, chaperones and GTPases, the list of factors required for mitochondrial ribosome biogenesis and function is far from complete (5). Recently, the role of GTPases in human mitochondrial ribosome biogenesis has received particular attention as their loss affects various cellular functions. For example, GTPases ERAL1 and NOA1/C4ORF14 are required for 12S rRNA stability and mtSSU assembly (6–9). GTPBP5, GTPBP7 and GTPBP10 are required for late maturation stages of the mtLSU (10–16): GTPBP7 couples mtLSU assembly to intersubunit bridge formation and

*To whom correspondence should be addressed. Tel: +49 551 395913; Fax: +49 551 395979; Email: ricarda.richter@med.uni-goettingen.de

governs a quality control checkpoint for mtLSU biogenesis (12). GTPBP10 acts in a complex with other late assembly factors such as NSUN4, MTERF4, MALSU1 and SMCR7L (13–15). GTPBP5, which acts subsequently to GTPBP10, is required for MRM2-catalyzed 16S methylation at position U1369 (16,17). GTPBP5 loss results in an accumulation of a late assembly intermediate containing GTPBP10, MALSU1 and MTERF4, but missing bL36m. Ablation of all these GTPases leads to loss of 55S ribosomes and to mitochondrial translation deficiency.

Human GTPBP6 is a poorly studied member of the translational GTPase family. The function of the factor in human cells is not known. It is homologous to the bacterial GTPase HflX, which is a ribosome-recycling factor facilitating dissociation of 70S ribosomes into subunits (18–20). HflX is not required for *Escherichia coli* viability under laboratory conditions of rapid growth, but becomes essential during heat shock where it helps to recycle damaged ribosomes (18). In addition, HflX may act as an ATP-dependent RNA helicase capable of remodeling damaged rRNA and thus restoring heat-inactivated ribosomes (20).

In the present study, we reveal the function of GTPBP6 in human mitochondria. Elevated levels of GTPBP6 cause an accumulation of mtSSU and mtLSU, suggesting that GTPBP6 facilitates 55S mitochondrial ribosome dissociation *in vivo*. We further validate the activity of GTPBP6 as a ribosome-recycling factor *in vitro* using real-time kinetic assays. GTPBP6 ablation leads to a drastic deficiency in mitochondrial translation due to defects in mitochondrial ribosome assembly resulting in accumulation of mtLSU intermediates at a late maturation stage when MTERF4, NSUN4, MALSU1, GTPBP5, GTPBP7 and GTPBP10 are bound to the mtLSU. Our results suggest that human GTPBP6 has a dual function in facilitating the recycling and biogenesis of mitochondrial ribosomes.

MATERIALS AND METHODS

Key reagents

A list of antibodies, oligonucleotides and other materials used within this study is provided in Supplementary Table S1.

Cell culture

Human embryonic kidney cell line (HEK293-Flp-In T-Rex, HEK293T) was cultured in Dulbecco's modified Eagle's medium (DMEM) supplemented with 10% FBS (Sigma), 2 mM L-glutamine, 1 mM sodium pyruvate, 50 μ g/ml uridine, 100 U/ml penicillin and 100 μ g/ml streptomycin (GIBCO) under standard cultivation conditions (37°C under 5% CO₂ humidified atmosphere). Cells were systematically confirmed to be negative for the presence of Mycoplasma by GATC Biotech.

For cell counts cells were grown on standard DMEM as described above or in medium containing 0.9 mg/l galactose. Cells (7.5×10^4 to 1×10^5) were seeded on day 0 of the experiment, and were counted on day 1, day 2 and day 3.

Stable inducible cell lines expressing C-terminal FLAG-tagged versions of proteins were generated as described previously (21,22) using GeneJuice (Novagen) or Lipofectamine 3000 (Invitrogen) as transfection reagents following the manufacturer's instructions.

Gtpbp6^{-/-} cell line was generated utilizing Alt-R CRISPR–Cas9 system (Integrated DNA Technologies) according to the manufacturer instructions. Briefly, cells were co-transfected with Cas9 enzyme and crRNA–tracrRNA duplex. crRNA was designed to target the first exon of the *Gtpbp6* gene. Clones were screened for mutations in GTPBP6 gene using the Alt-R Genome Editing Detection Kit (Integrated DNA Technologies) and the presence of mutations leading to premature stop codons formation in *Gtpbp6* were confirmed by Sanger sequencing.

Cell lysates and western blotting

Cells were lysed in nonionic lysis buffer (50 mM Tris–HCl pH 7.4, 130 mM NaCl, 2 mM MgCl₂, 1% NP-40, 1 mM PMSF and 1× Protease Inhibitor Cocktail (Roche)). Cell lysates were separated on 10–18% Tris–Tricine gel, transferred to nitrocellulose blotting membrane Amersham™ Protran™ 0.2 μ m NC (GE Healthcare) and visualized using specific antibodies.

Northern blotting

Total RNA was isolated from whole cell extracts using TRIzol reagent (Invitrogen), loaded onto a denaturing formaldehyde/formamide 1.2% agarose gel and blotted to Amersham Hybond™-N membrane (GE Healthcare). After UV-crosslinking, the membranes were incubated with [³²P]-radiolabelled probes targeting the specific mitochondrial RNAs and scanned with Typhoon imaging system (GE Healthcare).

[³⁵S]Methionine *de novo* synthesis

[³⁵S]Methionine labeling was performed as described previously (23,24). To monitor *de novo* mitochondrial protein synthesis cells were treated with 100 μ g/ml emetine (Roth) to block cytosolic translation and incubated in the presence of 0.2 mCi/ml [³⁵S]Methionine for 1 h. Mitochondrial translation products were visualized with Typhoon imaging system (GE Healthcare).

Mitochondria isolation and sucrose density gradient ultracentrifugation

Mitochondria isolation from cultured cells was performed as described (13). Briefly, cells were homogenized in trehalose buffer (300 mM trehalose, 10 mM KCl, 10 mM HEPES–KOH pH 7.4, 1 mM PMSF and 0.2% BSA) using Homogenplus Homogenizer (Schuett-Biotec, Germany). After lysis (3% sucrose, 100 mM KCl, 10 mM MgCl₂, 20 mM HEPES–KOH, pH 7.4, 1% digitonin, 1× Protease inhibitor cocktail (Roche) and 0.08 U/ μ l RiboLock RNase Inhibitor) 500 μ g mitochondria were separated by sucrose gradient ultracentrifugation (5–30% sucrose (w/v) in 100 mM KCl, 10 mM MgCl₂, 20 mM HEPES/KOH, pH 7.4,

1% digitonin, 1× Protease inhibitor cocktail (Roche)) at 79 000 × g, 4°C for 15 h using SW41 Ti rotor (Beckman Coulter). Fractions (1-16) were collected with BioComp fractionator, ethanol precipitated and analyzed by western blotting or mass spectrometry.

Quantitative mass spectrometry analyses

Precipitated proteins of three biological replicates of each condition (Gradient fraction #8 of *Gtpbp6*^{-/-} and WT) were dissolved with 4 M urea in 50 mM ammonium bicarbonate pH 8.0 and diluted to a final concentration of 1 M urea and 50 mM ammonium bicarbonate. Proteins were reduced and alkylated with 5 mM TCEP and 20 mM chloroacetamide, respectively. Proteins were digested with trypsin in an enzyme-to-protein ratio of 1:50 at 37°C overnight. Peptides were acidified with trifluoroacetic acid (TFA) to a final concentration of 0.5% (v/v), desalted via MicroSpin Columns (Harvard Apparatus) following manufacturer's instructions and vacuum dried. Peptides were resuspended in 2% acetonitrile/0.05% TFA and subjected to LC-MS/MS.

Peptides were measured in technical duplicates via an Q Exactive HF mass spectrometer coupled to a Dionex Ultimate 3000 UHPLC system (both Thermo Fisher Scientific) equipped with an in house-packed C18 column. Separation of peptides was accomplished via the following gradient: mobile phase A consisted of 0.1% formic acid (FA, v/v), mobile phase B of 80% ACN/0.08% FA (v/v). The gradient started at 5% B, increasing to 10% B within 3 min, followed by a continuous increase to 46% B within 74 min, then keeping B constant at 90% for 5 min. After each gradient the column was again equilibrated to 5% B for 6 min. The flow rate was set to 300 nl/min. MS1 survey scans were acquired with a resolution of 60 000, an injection time (IT) of 50 ms and an automatic gain control (AGC) target of 1 × 10⁶. Dynamic exclusion was set to 30 s and the 30 most abundant precursor ions were considered for fragmentation. MS2 spectra were acquired with a resolution of 15 000, IT was set to 128 ms and the AGC target 1 × 10⁵. Fragmentation was enforced by higher-energy collisional dissociation (HCD) at 30% normalized collision energy.

Raw files were analyzed by MaxQuant (v. 1.6.0.1, (25)). Default settings were applied with carbamidomethylation of cysteines as fixed and oxidation of methionines as variable modifications, FDR was set to 0.01. The label-free quantification (LFQ) algorithm was enabled. MS data were searched against all reviewed human proteins according to UniProt (26 530 entries, February 2020). Perseus (v. 1.6.0.7, (26)) was used for data analysis. Three LFQ values in at least one group (WT and/or *Gtpbp6*^{-/-}) were considered for further processing. Missing values were imputed based on normal distribution of LFQ values in each group. A two-sample Student's *t*-test (S0 2, permutation-based FDR 0.01 with 250 randomizations) was applied to assess statistical significance.

Protein localization assays

Intracellular GTPBP6 localization was determined as described (24). Briefly, isolated mitochondria or mitoplasts

from GTPBP6^{FLAG} tagged cell line were treated with or without Proteinase K. Samples were separated on a gel and analyzed by western blotting. To dissect whether GTPBP6 is integrated or associated with the inner mitochondrial membrane, mitochondria isolated from GTPBP6^{FLAG} cell line were incubated in 0.1 M Na₂CO₃ at different pH values. Samples were centrifuged at 41,000 rpm using TLA55 rotor (Beckman Coulter) for 1h. Obtained fractions were analyzed by western blotting.

Co-immunoprecipitation

FLAG co-immunoprecipitation of GTPBP6^{FLAG}-associated protein complexes was performed as described (22). Isolated mitochondria (1 mg) were lysed (20 mM HEPES-KOH pH 7.4; 100 mM KCl; 10 mM MgCl₂; 10% glycerol; 1 mM PMSF and 1% digitonin) prior centrifugation at 16 000 × g at 4°C for 10 min. Lysates were incubated with anti-FLAG M2 Affinity Gel (Sigma) for 1h. GTPBP6^{FLAG}-bound protein complexes were eluted using FLAG peptides.

Protein purification

Escherichia coli BL21 strains were transfected with plasmids (pGex-6P-1) containing N-terminal GST-tagged wild type and mutant variants of GTPBP6Δ43. Cells were grown until OD₆₀₀ = 0.6, induced with 1 mM IPTG and cultured overnight at 16°C. Obtained bacterial pellets were lysed in lysis buffer (50 mM Tris-HCl, pH 7.4, 300 mM KCl, 1× protease inhibitor cocktail (Roche), 1 mM PMSF) using EmulsiFlex-C3 (Avestin). Cleared cell lysates were incubated in the presence of 600 mM KCl to reduce contamination with bacterial ribosomes and ultra-centrifuged for 1 h at 250 000 × g (Rotor Type 70Ti, Beckman Coulter). Salt concentration was diluted to 300 mM prior subjecting samples to Glutathione Sepharose™ 4B beads (GE Healthcare). After overnight binding at 4°C, beads were washed seven times with buffer A (50 mM Tris-HCl, pH 7.4, 300 mM KCl, 1 mM PMSF, 2 mM DTT) and three times with buffer B (50 mM Tris-HCl, pH 7.4, 70 mM NH₄Cl, 30 mM KCl, 7 mM MgCl₂) and incubated overnight in buffer C (50 mM Tris-HCl, pH 7.4, 70 mM NH₄Cl, 30 mM KCl, 7 mM MgCl₂, 1 mM EDTA, 1 mM DTT) with addition of 100 U of PreScission™ protease (GE Healthcare) per 2 ml of beads suspension. Next day elutions were collected and samples were concentrated with Amicon® Centrifugal Filter Units Ultracel-10K (Merck Millipore) and stored in 50 mM Tris-HCl, pH 7.4, 70 mM NH₄Cl, 30 mM KCl, 7 mM MgCl₂, 1 mM DTT and 10% Glycerol at -80°C.

Escherichia coli initiation factors, EF-Tu, EF-G and RRF were purified according to published protocols (27–30).

Preparation of ribosome complexes

70S ribosomes were purified from *E. coli* MRE600; f³H]Met-tRNA^{Met} and [¹⁴C]Glu-tRNA^{Glu} were produced according to the published protocols (30–32).

Initiation complexes (IC) and ternary complexes were reconstituted as in (28) with following modifications. For IC,

1.5 μM of 70S ribosomes mixed with 3 μM mRNA encoding MEK peptide, 2.6 μM of initiation factor each (IF1, IF2, IF3), 1 mM DTT, 1 mM GTP and 4.5 μM of [^3H]Met-tRNA^{Met} were incubated at 37°C for 5 min. For ternary complex, 18 μM of EF-Tu was combined with 1 mM GTP, 1 mM DTT, 3 mM phosphoenol pyruvate, 0.1 mg/ml pyruvate kinase, and after 15 min of incubation at 37°C [^{14}C]Glu-tRNA^{Glu} was added. Translation was performed at 37°C for 5 min after mixing 0.75 μM IC with 9 μM of ternary complex and 0.2 μM EF-G. Resulting pre-hydrolysis complexes were purified through 1.1 M sucrose cushion for 2 h at 201 000 \times g. Translation efficiency was estimated by nitrocellulose filtration followed by scintillation counting of ribosome-bound tRNAs (28).

Post-hydrolysis complexes were produced when incubating pre-hydrolysis complexes with 0.1 mM puromycin at 37°C for 10 min. Efficiency of [^3H]Met-[^{14}C]Glu-puromycin formation was estimated by reverse-phase high performance liquid chromatography using Cromolith RP-8e 100–4.6 mm column (Merck) and quantified with scintillation counting.

Rapid kinetic measurements

The dissociation of 70S to subunits was monitored using Rayleigh light scattering at 325 nm using stopped flow apparatus (Applied Photophysics) (18,19,33). Experiments were performed in buffer A (50 mM Tris-HCl pH 7.5; 70 mM NH_4Cl ; 30 mM KCl and 7 mM MgCl_2) at 37°C. 70S ribosomes or pre- and post-hydrolysis complexes (0.05 μM) were rapidly mixed with 1 μM of GTPBP6 (if not indicated otherwise) in the presence of 0.5 mM GTP. In control reactions, buffer A or EF-G (2 μM) and RRF (2.5 μM) were used instead of GTPBP6. To assess the nucleotide dependence of GTPBP6 induced 70S recycling, GTP was replaced with either GDP, GTP γ S, ADP or ATP (each 0.5 mM) or buffer A. Phosphoenol pyruvate (3 mM) and pyruvate kinase (0.1 $\mu\text{g}/\mu\text{l}$) were used in experiments to determine the K_d of 70S and GTPBP6. All concentrations are indicated as the final concentrations after mixing. The reaction was recorded for at least 75 s and data fitting was performed on normalized curves obtained by averaging of 5–8 traces with GraphPad Prism 5.0 for Windows (GraphPad Software, www.graphpad.com) or with TableCurve 2D (Systat Software).

Quantification and statistical analysis

The protein and RNA levels were measured from western blots and northern blots using Typhoon imaging system (GE Healthcare) and quantified with ImageQuant TL software (GE Healthcare). The results from 3 independent experiments are presented as percentages relative to wild type control \pm SEM (see figure legends for details).

RESULTS

GTPBP6, a homolog of bacterial HflX, is a mitochondrial matrix protein

Cluster analysis of human GTPBP6 reveals that this GTPase is highly conserved and homologous to the bacterial

ribosome-recycling factor HflX (Figure 1A). *E. coli* HflX contains two nucleotide-binding domains, an N-terminal putative ATP-dependent RNA helicase domain (ND1) and a C-terminal GTPase domain (ND2) connected by an α -helical linker (20) (Figure 1B). Human GTPBP6 and *E. coli* HflX share \sim 30% sequence identity and have a similar domain arrangement (Supplementary Figure S1). Human MitoCarta2.0 database and MitoProt II (v1.101) suggest that GTPBP6 is a mitochondrial protein. To validate the mitochondrial localization, we tested the sensitivity of GTPBP6 to Proteinase K digestion in isolated mitochondria and mitoplasts. As antibodies against the endogenous GTPBP6 are unavailable, we ectopically expressed a C-terminal FLAG-tagged version of GTPBP6 and tested the protein localization in mitochondria isolated from these cells. GTPBP6^{FLAG} appears to be inside mitochondria as it is protected against Proteinase K treatment even when the outer membrane has been removed, similar to the matrix marker uL3m (Figure 1C). Sodium carbonate extraction experiments with isolated mitochondria show that some GTPBP6^{FLAG} is still present in the membrane fraction at pH 11.5, but it is completely extracted at higher pH, similar to TIM44, a protein of the import motor peripherally associated to the inner mitochondrial membrane (Figure 1D) (34,35). These data suggest that GTPBP6 is a mitochondrial matrix protein peripherally associated to the inner mitochondrial membrane like other mitochondrial GTPases such as GTPBP5 or GTPBP10 (13,16).

Excess GTPBP6 inhibits mitochondrial translation by promoting ribosome dissociation

Bacterial HflX preferentially associates with the large ribosomal subunit (LSU) (18,36,37). By analogy, we tested the interaction of GTPBP6 with the mitochondrial ribosome by performing FLAG immunoprecipitation. GTPBP6^{FLAG} used as a bait co-precipitates all tested ribosomal proteins suggesting that GTPBP6 binds either to both ribosomal subunits or to the assembled 55S complex (Figure 2A). Induction of GTPBP6^{FLAG} expression results in a slower cell growth and rapid media acidification. This phenotype is even more pronounced in galactose-containing media that was used to force mitochondria to produce ATP via OXPHOS (Figure 2B), resulting in a significant (by 2.9-fold) reduction of growth rate, suggesting that GTPBP6 overexpression negatively affects mitochondrial function. To test whether GTPBP6 overexpression has a direct effect on mitochondrial translation, we performed [^{35}S]Methionine ([^{35}S]Met) labeling of *de novo*-synthesized mtDNA-encoded proteins. Synthesis of mtDNA-encoded proteins is markedly decreased upon overexpression of GTPBP6^{FLAG} compared to wild type, resulting in reduced protein steady state levels as shown for COX1 and COX2 (Figure 2C).

HflX acts as a ribosome-recycling factor (18,19,38–40). To test whether also GTPBP6 might facilitate ribosome dissociation into subunits, we performed sucrose density gradient centrifugation to analyze the ratio of mtLSU and mtSSU relative to 55S ribosomes (Figure 2D, Supplementary Figure S2). Indeed, the fraction of free mtLSU and mtSSU increases upon overexpression of GTPBP6^{FLAG} at

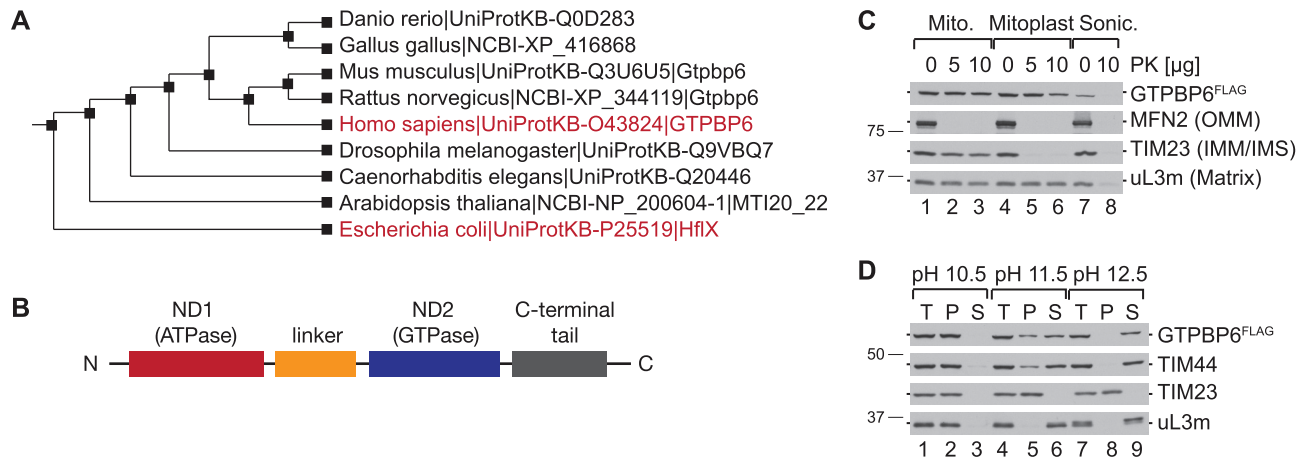


Figure 1. GTPBP6 is a mitochondrial protein homologous to bacterial HflX. (A) Cluster analysis of human GTPBP6 and bacterial HflX using P-POD (Princeton Protein Orthology Database (<http://ppod.princeton.edu/>)). (B) Domain arrangement of HflX and GTPBP6. Nucleotide binding domains (ND1 and ND2) are indicated in red and blue, respectively, the α -helical linker in orange and the C-terminal tail in grey. (C) Human GTPBP6 is a mitochondrial matrix protein. Mitochondria were isolated from HEK293T cells expressing C-terminal FLAG tagged GTPBP6. Intact mitochondria (lane 1–3), mitoplasts (lane 4–6) and sonicated mitoplasts (lane 7–8) were treated with Proteinase K (PK) as indicated. Samples were analyzed by western blotting using antibodies against MFN2, TIM23 and uL3m as markers for the outer mitochondrial membrane (OMM), the inner mitochondrial membrane (IMM), the intermembrane space (IMS), and the matrix, respectively. GTPBP6^{FLAG} was detected using antibodies against the FLAG epitope. (D) GTPBP6 is peripherally associated with the inner mitochondrial membrane. Mitochondrial membrane proteins were extracted using sodium carbonate solutions with different pH. Samples (total, T; pellet, P; and supernatant, S) were analyzed by western blotting using antibodies as indicated.

the cost of 55S ribosomes (Figure 2D, E). Quantification of the ribosome profiles yields the ratio of mtSSU:mtLSU:55S of 1.2:1.7:1 in wild type cells, which increases to 2.7:3.3:1 upon GTPBP6 overexpression (Figure 2E), suggesting that mtSSU and mtLSU accumulate in GTPBP6^{FLAG} expressing cells. Thus, the decrease of mitochondrial gene expression can be explained by the reduced number of translationally active 55S mitochondrial ribosomes caused by the ribosome-recycling activity of GTPBP6.

GTPBP6 dissociates 70S ribosomes *in vitro*

We next validated the ribosome-recycling activity of GTPBP6 *in vitro*. As a reconstituted *in vitro* translation system with 55S ribosomes is not available, we tested the ribosome dissociation activity of purified recombinant GTPBP6 using isolated 70S ribosomes from *E. coli*. Such hybrid systems have been successfully utilized to investigate the functions of human mitochondrial translation factors such as mtIF2, mtEFTu, mtEFG2, mtRF1a or ICT1 (41–44).

Ribosome dissociation to subunits can be monitored as a change in the intensity of scattered light (18,19,45). To monitor the dissociation in real time, we rapidly mixed 70S ribosomes with increasing concentrations of GTPBP6 in the presence of excess GTP in a stopped-flow apparatus and recorded the change in light scattering (Figure 3A). GTPBP6 facilitated ribosome dissociation in a concentration dependent manner. The apparent rate constants (k_{app}) of reactions were plotted as a function of GTPBP6 concentration (Figure 3B), and the slope of the linear fit provided the association rate constant of about $0.13 \mu\text{M}^{-1}\text{s}^{-1}$. The dissociation rate constant of the 70S-GTPBP6 complex, determined from the Y-axis intercept, is about 0.09 s^{-1} . The K_d of $0.7 \mu\text{M}$, which was calculated from both rate constants, is comparable to the K_d value of 1.0 – $1.5 \mu\text{M}$ that was reported for the HflX-70S complex (18).

The dissociation of 70S by GTPBP6 was independent of GTP hydrolysis (Figure 3C), as the reaction with non-hydrolysable GTP analog GTP γ S was as efficient as with GTP. In contrast, the reaction with GDP-bound or apo-GTPBP6 was very slow (Figure 3C), suggesting that the ribosome recycling activity of GTPBP6 depends on GTP binding, but not on GTP hydrolysis. As GTPBP6 contains a putative ATP-dependent RNA-helicase domain (46), we also tested whether ATP affects GTPBP6-facilitated ribosome dissociation and found that neither ATP nor ADP can replace GTP (Figure 3D).

To analyze GTPBP6 action on functional ribosome complexes, we utilized 70S ribosomes programmed with mRNA and carrying fMet-Glu-tRNA^{Glu} in the P site (pre-hydrolysis complex, preHC) or 70S ribosomes with deacylated tRNA^{Glu} in the P site (post-hydrolysis complex, postHC); both complexes had an empty A site. Similarly to bacterial recycling factor RRF together with EF-G (Supplementary Figure S3B), GTPBP6 facilitated rapid dissociation of postHC or vacant 70S ribosomes, but was less efficient on ribosomes with a peptidyl-tRNA in the P site (Figure 3E, Supplementary Table S2), suggesting that GTPBP6 activity is inhibited on translationally active ribosomes. These data show that GTPBP6 indeed acts as a ribosome-recycling factor facilitating the dissociation of vacant ribosomes as well as postHC into subunits in a GTP-dependent manner.

GTPBP6 loss stalls mtLSU biogenesis

To test whether GTPBP6 is essential in mitochondria, we generated knockout cell lines applying CRISPR/Cas9 technology. For detailed analysis, we have chosen two clones, both containing mutations in exon 1 leading to premature stop codons (Supplementary Figure S4A–C). Analysis of steady-state protein levels in the deletion clones shows

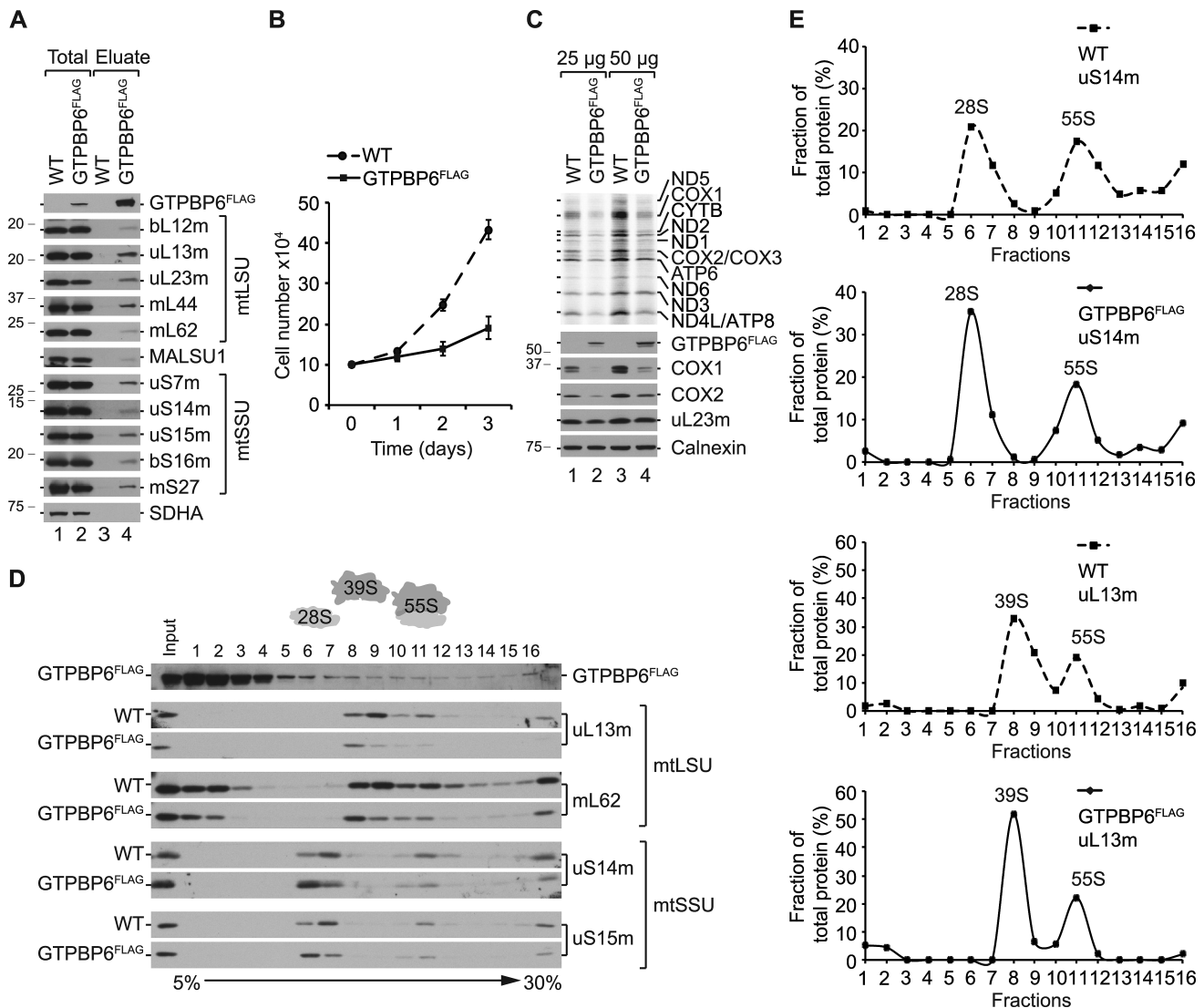


Figure 2. Elevated levels of GTPBP6 affect mitochondrial translation. (A) GTPBP6 interacts with the mitochondrial ribosome. Lysed mitochondria (1 mg) isolated from HEK293T-GTPBP6^{FLAG} and -wild type (WT) cells were subjected to FLAG-immunoprecipitation. Complexes were eluted using FLAG peptide. Samples (3% total; 100% eluate) were analyzed by western blotting using specific antibodies as indicated. SDHA (Subunit A of the succinate dehydrogenase) was used as a negative control. (B) GTPBP6 overexpression affects cell growth. HEK293T-GTPBP6^{FLAG} and wild type (WT) cells were cultured in galactose-containing media in the presence of 500 ng/ml tetracycline. Cells were counted after 1d, 2d and 3d. ($n = 3$; mean \pm SD). (C) Elevated GTPBP6 protein levels reduce mtDNA expression. Synthesis of mtDNA-encoded proteins in HEK293T-GTPBP6^{FLAG} and wild type (WT) cells was analyzed by [³⁵S]Methionine *de novo* incorporation. Samples were subjected to SDS-PAGE followed by autoradiography and western blot analyses. Calnexin was used as loading control. (D) Overexpression of GTPBP6 results in accumulation of mtSSU and mtLSU. Ribosome profiles were analyzed by sucrose density gradient centrifugation using lysed mitochondria (0.5 mg) isolated from HEK293T-GTPBP6^{FLAG} and wild type (WT) cells. Fractions (1-16) were analyzed by western blotting using antibodies as indicated (Input, 10% of material applied on a sucrose gradient). (E) Quantification of the relative distribution of mtSSU, mtLSU and 55S ribosomes using antibodies against uS14m and uL13m, respectively (100% = total protein in all fractions of tested cell line).

a complete lack of mtDNA-encoded proteins COX1 and COX2, suggesting that GTPBP6 is required for mitochondrial gene expression (Figure 4A). Ablation of GTPBP6 inhibits cell growth by \sim 2-fold compared to wild type (Figure 4B) and generally abolishes mtDNA expression as monitored by [³⁵S]Met *de novo* incorporation *in vivo* (Figure 4C).

To validate that the loss of GTPBP6, rather than an off-target effect, leads to the inhibition of mitochondrial translation, we generated rescue cell lines by integrating FLAG-tagged GTPBP6 into the Flp-In cassette of the

HEK293T *Gtpbp6*^{-/-} cell lines allowing inducible expression of GTPBP6^{FLAG}. Because overexpression of GTPBP6 has a negative effect on mitochondrial translation (Figure 2C), we titrated the inducer to a minimum to avoid false-negative results (Supplementary Figure S4D, E). Indeed, low-level expression of GTPBP6^{FLAG} restored the phenotype in *Gtpbp6*^{-/-} clone 1 confirming the specificity of the knockout and the functionality of the FLAG tagged variant of GTPBP6 (Figure 4C). In clone 2, mitochondrial translation was only partially restored possibly because the expres-

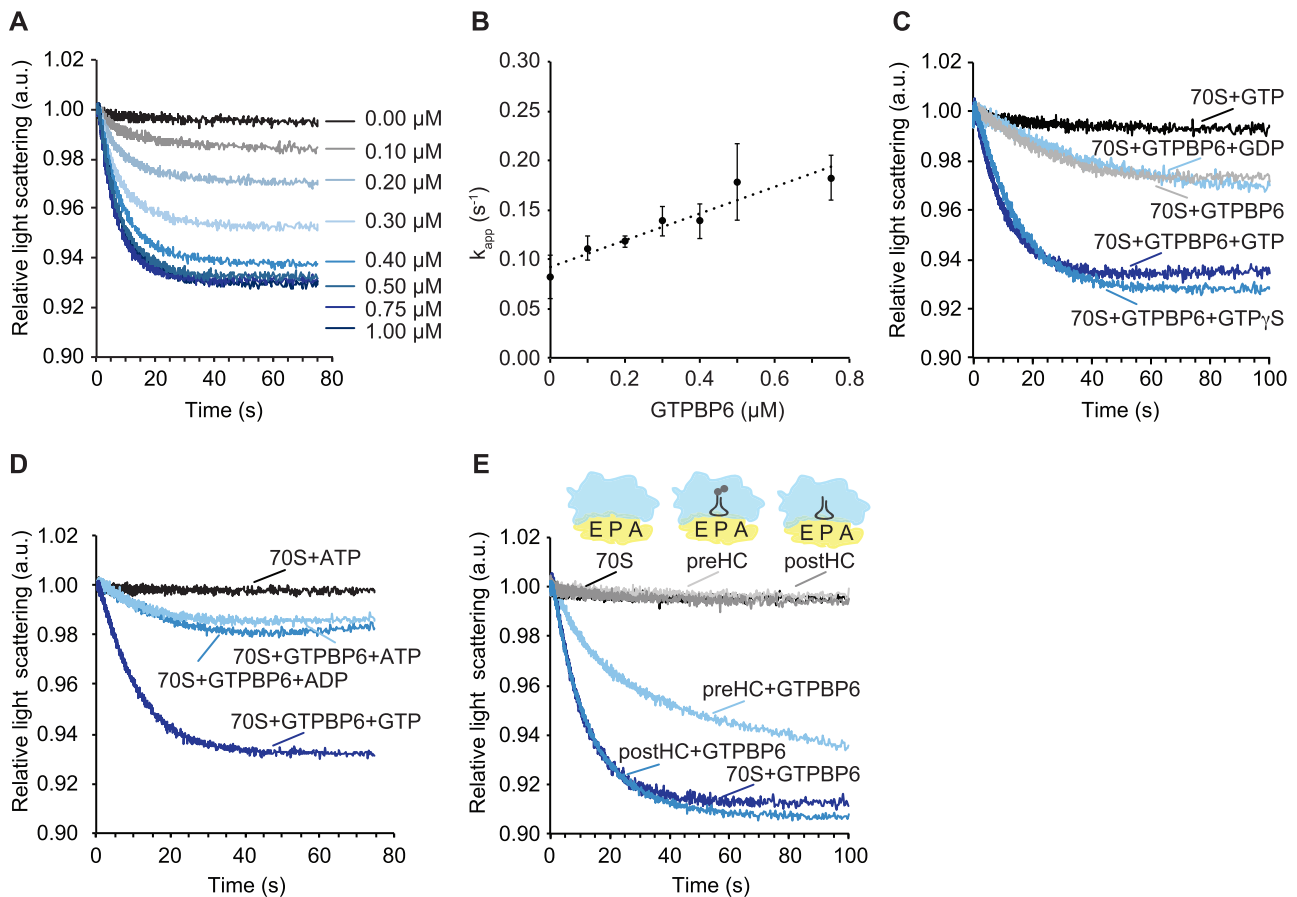


Figure 3. GTPBP6 splits 70S ribosomes *in vitro*. (A) Change in light scattering as a response to GTPBP6-induced dissociation of 70S ribosomes into subunits. 70S ribosomes ($0.05 \mu\text{M}$) were rapidly mixed with indicated concentrations of GTPBP6 in the presence of 0.5 mM GTP. The scattered light intensity at 325 nm was measured in a stopped-flow apparatus. Each curve represents the average of 5–8 individual traces. (B) GTPBP6 concentration dependence of 70S ribosome recycling. The apparent rate constants (k_{app}) obtained by fitting the light scattering curves on Figure 3A with one-exponential function, were plotted against GTPBP6 concentration. As k_{app} showed linear dependence of GTPBP6 concentration, linear fitting provided dissociation and association constants (intercept and slope), ratio of which represents K_d of reaction. (C) Dissociation of 70S ribosomes by GTPBP6 depends on GTP-binding but not on GTP-hydrolysis. 70S ribosomes ($0.05 \mu\text{M}$) were mixed rapidly with GTPBP6 ($1 \mu\text{M}$) in the absence or presence of GDP, GTP or GTP γ S (0.5 mM each). k_{app} was estimated to be $0.09 \pm 0.01 \text{ s}^{-1}$ in the presence of GTP and $0.08 \pm 0.01 \text{ s}^{-1}$ in the presence of GTP γ S. (D) GTPBP6 does not require ATP for 70S dissociation. Experiments were performed as in (A) and (C) in the presence of GTP, ATP or ADP (0.5 mM each). (E) GTPBP6 splits post-hydrolysis complexes. Dissociation of vacant 70S *E. coli* ribosomes (70S), pre-hydrolysis complexes (preHC) and post-hydrolysis complexes (postHC) ($0.05 \mu\text{M}$ each) by GTPBP6 ($1 \mu\text{M}$) was determined in the presence of GTP (0.5 mM).

sion of GTPBP6^{FLAG} was somewhat higher, which could have an inhibitory effect on translation.

To test whether mtDNA expression deficiency is due to defects in mitochondrial translation, transcription or mt-RNA stability, we quantified the steady-state levels of the mitochondrial rRNAs, *MTRNR1* (12S rRNA) and *MTRNR2* (16S rRNA), and of mitochondrial mRNAs, *MTCO1* (COX1 mRNA) and *MTCO2* (COX2 mRNA) by Northern blotting (Supplementary Figure S4F, G). We did not observe significant changes in the steady-state levels of tested mt-RNAs suggesting that the defects in mtDNA expression are specific for mitochondrial translation. We also did not detect severe changes in the steady state levels of ribosomal proteins in clone 1 (Figure 4D, E). However, when we tested whether these proteins assemble into a functional mitochondrial ribosome, we found a significant reduction in the fraction of 55S ribosomes and a considerable accumulation of 28S mtSSU and 39S mtLSU, which

can explain the defects in mitochondrial translation (Figure 5A, B). Notably, we observed a strong enrichment of NSUN4, MTERF4, MALSU1 and the GTPases GTPBP5, GTPBP7 and GTPBP10 in the 39S mtLSU fractions, which suggests accumulation of mtLSU assembly intermediate(s) at a late stage of maturation (12,13,16,47,48). The steady-state protein levels of NSUN4, MALSU1 and GTPBP10 were significantly increased in *Gtpbp6*^{-/-} cells compared to wild type (Figure 5C). To determine the composition of the complexes accumulating in fraction 8 (Figure 5A) we applied a label-free mass spectrometry approach. Interestingly, all 52 ribosomal proteins of the mtLSU were detected in WT and *Gtpbp6*^{-/-} samples and in most cases were even enriched in the absence of GTPBP6 (Figure 5D, Supplementary Table S3). This also includes bL36m, one of the last assembled ribosomal proteins (16) suggesting that the mtLSU in *Gtpbp6*^{-/-} cells represents an almost matured mtLSU with a complete set of ribosomal proteins.

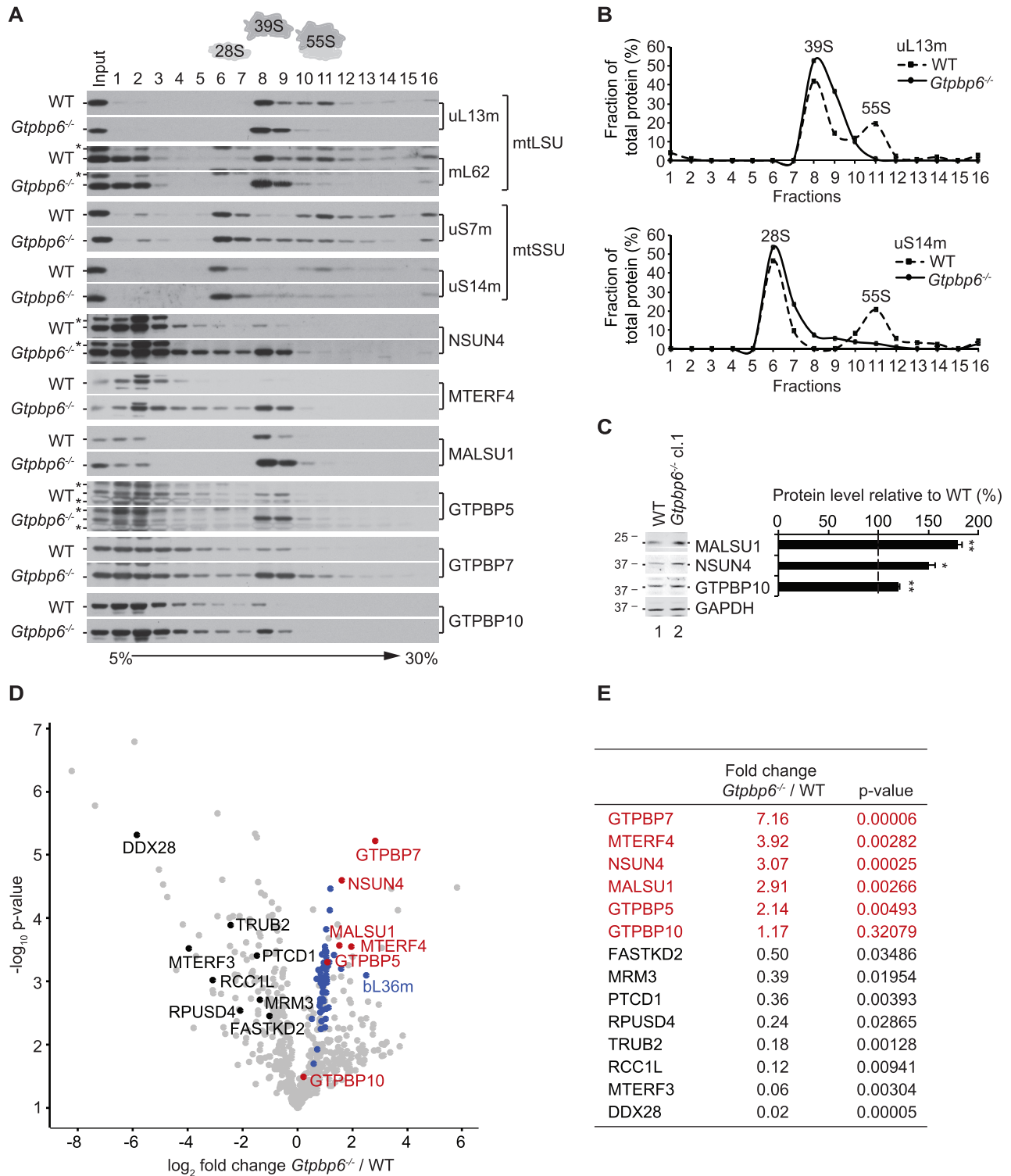


Figure 5. GTPBP6 is required for 55S ribosome assembly. (A) GTPBP6 ablation results in accumulation of mtSSU and mtLSU. Mitochondria (0.5 mg) were isolated from HEK293T-wild type (WT) and *Gtpbp6*^{-/-} cells (cl. 1). Ribosomes and ribosomal subunits were separated by sucrose density gradient centrifugation. Fractions (1-16) were analyzed by western blotting using antibodies as indicated. (*) indicates unspecific signal. (B) Distribution of mtSSU, mtLSU and 55S ribosomes calculated as percentage of uS14m and uL13m in each fraction. (C) GTPBP6 loss affects mitochondrial ribosome assembly factors. Cell lysates isolated from HEK293T-wild type (WT) and *Gtpbp6*^{-/-} cells (cl. 1) were analyzed as described in Figure 4E (*n* = 3; mean ± SEM; * *P* < 0.05; ** *P* < 0.01). (D, E) mtLSU composition in *Gtpbp6*^{-/-} cells. Proteins isolated from fraction 8 corresponding to mtLSU were analyzed by label-free quantitative mass spectrometry (*Gtpbp6*^{-/-} versus WT). Ribosomal proteins of mtLSU are labeled in blue, assembly factors accumulating in *Gtpbp6*^{-/-} are indicated in red and factors, which are reduced upon GTPBP6 ablation are marked in black (*n* = 3).

We tested mutant cell lines for *de novo* synthesis of mtDNA-encoded proteins by [³⁵S]Met incorporation (Figure 6A, B). GTPBP6 with a K187A mutation was as active in alleviating the inhibitory effect of GTPBP6 deletion as wild type protein. The D199A and S437P mutants restored mitochondrial translation, albeit not to the same extent as wild type GTPBP6^{FLAG}. The G352P mutant did not rescue the *Gtpbp6*^{-/-} phenotype. Interestingly, assembly factors NSUN4 and MALSU1 accumulated in G352P mutant similarly as in *Gtpbp6*^{-/-} cells suggesting that maturation of the mtLSU is blocked (Figure 6A, B). Accordingly, the profile of mitochondrial ribosome assembly revealed the accumulation of mtLSU intermediates that are incompetent in 55S ribosome formation in G352P mutants comparable to *Gtpbp6*^{-/-} cells (Figure 6C), suggesting the cause for the overall translation defect.

Next, we tested these mutant variants of GTPBP6 in their activity to facilitate 70S ribosome dissociation *in vitro*. In contrast to the wild type GTPBP6, mutant variants D199A and S437P lost the ability to split vacant 70S ribosomes. However, mutant G352P facilitated ribosome dissociation as efficient as wild type GTPBP6. Mutant K187A was even more active than the wild type GTPBP6 (Figure 6D). The results with the D199A and S437P mutants suggest that the loss of *in vitro* ribosome-recycling activity of GTPBP6 is not detrimental for mitochondrial translation. *Vice versa*, the intact recycling activity of the G352P mutant is not sufficient to restore mitochondrial translation. Thus, it is likely that the two activities of GTPBP6, as a ribosome biogenesis factor and as ribosome recycling factor, are physically separated and require different regions of the factor.

DISCUSSION

We show that GTPBP6, a so far uncharacterized human protein, localizes to mitochondria where it plays a role in ribosome assembly, in addition to facilitating ribosome recycling. Unlike its bacterial homolog HflX, which is non-essential at normal growth conditions, GTPBP6 is required for mitochondrial gene expression and cell survival. Its exact concentration in the cell is crucial as also elevated GTPBP6 levels in human cells are harmful for mitochondrial translation and cell growth due to depletion of the translating ribosomes pool and accumulation of mtSSU and mtLSU.

Our findings establish that the ribosome-recycling activity of GTPBP6/HflX is a conserved feature across different domains of life. Experiments in heterologous *in vitro* system demonstrate that GTPBP6 promotes rapid dissociation of *E. coli* vacant ribosomes and ribosomes with a deacylated tRNA at the P site like canonical ribosome recycling factor RRF that operates together with EF-G. Also human mitochondria employ mtRRF and mtEFG2 (42,51) and it is unclear whether GTPBP6 fulfills a complementary and/or specific role in recycling specific ribosomal complexes. HflX has been proposed to rescue ribosomes arrested at stress conditions (18,39,40). Stalled ribosomal complexes are formed if the mRNA is degraded from the 3' end, aminoacyl tRNAs are depleted, during certain antibiotic treatments or under heat shock condi-

tions. Neither GTPBP6 (this study) nor HflX (18) split the 70S ribosomes with a peptidyl-tRNA in the P site (preHC) as efficiently as ribosomes with a deacylated tRNA in the P site (postHC). It was proposed that the preceding action of peptidyl-tRNA hydrolases like ArfB or ArfA-RF2 might be required before HflX is able to recycle ribosomes (18). Also human mitochondria contain peptidyl-tRNA hydrolases such as C12ORF65 and ArfB homolog ICT1 (mL62) which may act on translationally arrested ribosomes (52–54). C12ORF65 and ICT1 belong to the same protein family as bacterial termination factors 1 and 2 that catalyze peptidyl-tRNA hydrolysis during termination of translation. However, C12ORF65 and ICT1 lack motifs for stop codon-specific translation termination activity, which prompted the suggestion that they might be involved in ribosome rescue in mitochondria (44,55–57). Although ICT1 has been identified as a ribosomal protein located in the central protuberance of the mtLSU (44,58,59), it has also been shown to exhibit codon-independent, but ribosome-dependent peptidyl release activity *in vitro* (44). It is possible that a free pool of ICT1 is available to terminate arrested ribosomes (60) that could be then recycled by GTPBP6. HflX has been shown to recycle ribosomes in different bacterial species (18,19,38–40). The functional importance and regulation of HflX is different depending on the organism. In *E. coli* and *S. aureus* expression of HflX is upregulated during heat stress (18,38). In *Listeria monocytogenes* macrolides and lincosamides promote ribosome stalling which in turn induces the expression of HflX (39). In contrast, human GTPBP6 is probably expressed constitutively in all tissues (46) and its expression must be tightly controlled, as abnormally high GTPBP6 levels in lymphoblasts have been associated with language impairment in men with Klinefelter's syndrome (61).

In contrast to the 70S splitting activity of *E. coli* RRF, which depends on GTP hydrolysis by EF-G (Supplementary Figure S3A) (28), GTPBP6 requires only GTP binding but not hydrolysis to dissociate the 70S ribosomes. It is possible that GTP hydrolysis induces the release of GTPBP6 from the LSU, as suggested for HflX (18). This indicates that GTPBP6 could act as an anti-association factor before GTP is hydrolyzed. Nonetheless, the rapid kinetics of 70S ribosome dissociation by GTPBP6 is typical for a recycling factor and differs from the slow reaction caused by bacterial anti-association factor IF3, which binds to already dissociated subunits and prevents their re-association (Supplementary Figure S3C) (28). It is reasonable to assume that GTPBP6 can act both as a recycling and as an anti-association factor.

Although the binding site of GTPBP6 on the bacterial or the mitochondrial ribosome is yet to be determined, it is feasible to assume that as a translational GTPase with conserved G-motifs GTPBP6 binds to the GTPase associated centre of the ribosome. The ribosome splitting function indicates that GTPBP6 might also reside at the interface of the two subunits. Thus, GTPBP6 probably binds on the 50S subunit to the similar location as HflX or a canonical ribosome recycling factor such as mtRRF (18,62). Superimposed *E. coli* HflX-bound 50S and human 39S mtLSU demonstrate structural conservation along the HflX bind-

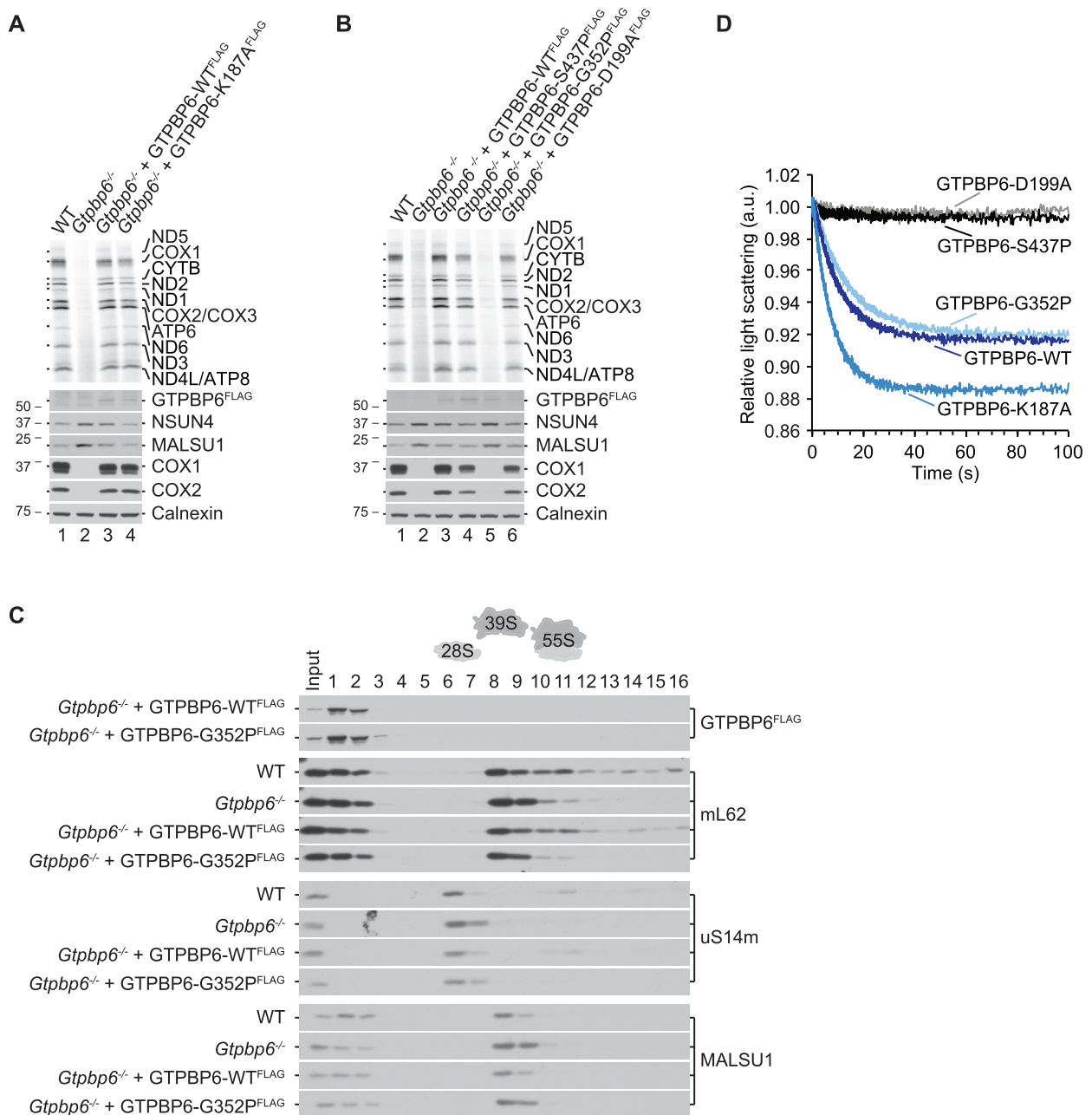


Figure 6. Mutation analyses of GTPBP6. (A, B) Residue G352 is required for GTPBP6 acting as a ribosome biogenesis factor. *Gtpbp6*^{-/-} cells expressing wild type or mutant variants of GTPBP6 were analyzed by [³⁵S]Methionine *de novo* incorporation. GTPBP6^{FLAG} protein expression was induced with tetracycline (GTPBP6-WT: 1 ng/ml; -K187A: 1 ng/ml; -D199A: 12 ng/ml; -G352P: 10 ng/ml; -S437P: 25 ng/ml) and adjusted to the level comparable to the one in Figure 4C, lane 3. All mutants were generated in *Gtpbp6*^{-/-} cl. 1. Samples were analyzed by autoradiography and western blotting. (C) GTPBP6-G352P mutant is incompetent in forming functional 55S ribosomes. Mitochondrial lysates (0.5 mg) from WT, *Gtpbp6*^{-/-} (cl. 1), *Gtpbp6*^{-/-} + GTPBP6-WT^{FLAG} and *Gtpbp6*^{-/-} + GTPBP6-G352P^{FLAG} were analyzed by sucrose density gradient centrifugation as in Figure 5A. (D) GTPBP6 mutants G352P and K187A facilitate dissociation of 70S ribosomes into subunits. Purified mutant and the wild type proteins (1 μM) were mixed with 70S ribosomes (0.05 μM) in the presence of GTP (0.5 mM GTP) as described in Figure 3, and the dissociation was monitored by a change in light scattering.

ing site that encompasses A- and P-loops at the PTC, helix 89, which connects the PTC to the sarcin-ricin loop (SRL), and SRL (Supplementary Figure S5). Thus, it is conceivable that GTPBP6 might act on a similar position on the bacterial 50S as well as on the 39S mtLSU.

Most importantly, we demonstrate that human GTPBP6 has acquired an additional role as a ribosome biogenesis

factor. Although it has been proposed that also HflX might play a role in ribosome assembly in *E. coli* (37), it is unlikely that HflX is a *bona fide* ribosome biogenesis factor as HflX loss does not show any assembly defect under laboratory growth conditions and its expression is induced by heat shock (18). In contrast, ablation of GTPBP6 leads to stalled mitochondrial ribosome biogenesis although all 52 riboso-

mal proteins of the mtLSU are assembled. GTPBP6 loss is characterized by an accumulation of mtLSU complex(es), enriched in NSUN4-MTERF4, MALSU1 and the GTPases GTPBP5, GTPBP7 and GTPBP10 (Figure 5A, D, E). These factors are required for mtLSU assembly at late maturation stages and thus for 55S ribosome formation (12–14,16,47,48,63,64). A similar assembly intermediate also accumulates upon loss of GTPBP5, which is required for 16S modification within the peptidyl transferase center (PTC) catalyzed by MRM2 (16,17). It has been proposed that GTPBP5 is part of a quality control system monitoring the maturation of the PTC to prevent premature subunit joining (16). It is tempting to speculate that GTPBP6 might also act as an anti-association factor to ensure late maturation steps of the mtLSU. However, in contrast to GTPBP5 loss, GTPBP6 deficiency results in the accumulation of mtLSU complex(es) containing bL36m suggesting that GTPBP6 acts downstream of GTPBP5, GTPBP7 and GTPBP10. Although we showed that only GTP-bound GTPBP6 dissociates the ribosomes efficiently, it is tempting to assume that GTP is also required for the late maturation steps of the ribosome. As proposed for other mitochondrial GTPases (12,16), GTPBP6 release from the mtLSU, likely coupled to GTP hydrolysis, might facilitate mtSSU joining.

It is reasonable to assume that the ribosome recycling and biogenesis activities of GTPBP6 are independent of each other and employ different structural elements of the factor. Ribosome recycling is likely catalyzed by the conserved GTPase ND2 domain of GTPBP6/HflX (65), whereas the variable ATP binding domain ND1 might have acquired different specialized functions in various organisms (46). In *E. coli* ND1 appears to act as an ATP-dependent RNA helicase rescuing heat-damaged ribosomes, whereas the archaeon *S. solfataricus* lacks the domain altogether (20,66). Our data indicate that the mutation in the ND2 domain which impairs GTP hydrolysis in *S. solfataricus* HflX (49), does not impair GTPBP6-dependent recycling of 70S ribosomes *in vitro*, but fails to rescue the mitochondrial ribosome assembly deficiency. If the G352 residue is indeed important for the GTPase activity of GTPBP6, this finding suggests that GTP hydrolysis is required either for the specific function of GTPBP6 in ribosome biogenesis, or for GTPBP6 dissociation from the ribosome. Contrary to the G352P mutation, D199A and S437P replacements abolish the activity of GTPBP6 in ribosome recycling, however, they are able to restore the mitochondrial translation phenotype in *Gtpbp6*^{-/-} cells. Thus, ribosome-recycling activity might not be an essential function of GTPBP6, possibly because it can be covered by mtRRF-mtEFG2. However, it might be crucial under certain stress conditions like in bacteria or when the canonical recycling machine mtRRF-EFG2 is non-functional. In summary, our findings demonstrate that GTPBP6 is a versatile protein with a dual function in human mitochondria and suggest that its role in ribosome biogenesis is essential for mitochondrial translation.

SUPPLEMENTARY DATA

Supplementary Data are available at NAR Online.

ACKNOWLEDGEMENTS

We thank Peter Rehling for providing antibodies; Sandra Kappler, Olaf Geintzer, Vanessa Herold, Tessa Hübner, Christina Kothe, Anna Pfeifer, Lena Preiser, Theresia Steiger and Michael Zimmermann for technical assistance; and Bee-Zen Peng, Frank Peske and Ekaterina Samatova for their advice.

Author contributions: Conceptualization, R.R.-D.; Investigation, E.L., K.D., F.N., E.S., A.L.; Writing – Original Draft, R.R.-D.; Writing – Review & Editing, K.D., E.L., M.V.R., R.R.-D.; Visualization, E.L., R.R.-D., K.D.; Supervision, R.R.-D., M.V.R., H.U.

FUNDING

Deutsche Forschungsgemeinschaft by the Emmy-Noether grant [RI 2715/1-1 to R.R.-D.]; Excellence Cluster [EXC 2067/1-390729940 to R.R.-D. and M.V.R.]; Collaborative Research Center [SFB860 to M.V.R., H.U. and R.R.-D.]; Max Planck Society (to M.V.R. and H.U.). Funding for open access charge: Deutsche Forschungsgemeinschaft and Open Access Publication Funds of the Göttingen University.

Conflict of interest statement. None declared.

REFERENCES

- De Silva, D., Tu, Y.-T., Amunts, A., Fontanesi, F. and Barrientos, A. (2015) Mitochondrial ribosome assembly in health and disease. *Cell Cycle*, **14**, 2226–2250.
- Richter-Dennerlein, R., Dennerlein, S. and Rehling, P. (2015) Integrating mitochondrial translation into the cellular context. *Nat. Rev. Mol. Cell Biol.*, **16**, 586–592.
- Morgenstern, M., Stiller, S.B., Lübbert, P., Peikert, C.D., Dannenmaier, S., Drepper, F., Weill, U., Höß, P., Feuerstein, R., Gebert, M. *et al.* (2017) Definition of a high-confidence mitochondrial proteome at quantitative scale. *Cell Rep.*, **19**, 2836–2852.
- Greber, B.J. and Ban, N. (2016) Structure and function of the mitochondrial ribosome. *Annu. Rev. Biochem.*, **85**, 103–132.
- Pearce, S.F., Rebelo-Guiomar, P., D'Souza, A.R., Powell, C.A., Van Haute, L. and Minczuk, M. (2017) Regulation of mammalian mitochondrial gene expression: recent advances. *Trends Biochem. Sci.*, **42**, 625–639.
- Dennerlein, S., Rozanska, A., Wydro, M., Chrzanoska-Lightowlers, Z.M.A. and Lightowlers, R.N. (2010) Human ERAL1 is a mitochondrial RNA chaperone involved in the assembly of the 28S small mitochondrial ribosomal subunit. *Biochem. J.*, **430**, 551–558.
- Uchiyama, T., Ohgaki, K., Yagi, M., Aoki, Y., Sakai, A., Matsumoto, S. and Kang, D. (2010) ERAL1 is associated with mitochondrial ribosome and elimination of ERAL1 leads to mitochondrial dysfunction and growth retardation. *Nucleic Acids Res.*, **38**, 5554–5568.
- Kolanczyk, M., Pech, M., Zemojtel, T., Yamamoto, H., Mikula, I., Calvaruso, M.-A., van den Brand, M., Richter, R., Fischer, B., Ritz, A. *et al.* (2011) NOA1 is an essential GTPase required for mitochondrial protein synthesis. *Mol. Biol. Cell*, **22**, 1–11.
- He, J., Cooper, H.M., Reyes, A., Di Re, M., Kazak, L., Wood, S.R., Mao, C.C., Fearnley, I.M., Walker, J.E. and Holt, I.J. (2012) Human C4orf14 interacts with the mitochondrial nucleoid and is involved in the biogenesis of the small mitochondrial ribosomal subunit. *Nucleic Acids Res.*, **40**, 6097–6108.
- Hirano, Y., Ohniwa, R.L., Wada, C., Yoshimura, S.H. and Takeyasu, K. (2006) Human small G proteins, ObgH1, and ObgH2, participate in the maintenance of mitochondria and nucleolar architectures. *Genes to Cells*, **11**, 1295–1304.
- Kotani, T., Akabane, S., Takeyasu, K., Ueda, T. and Takeuchi, N. (2013) Human G-proteins, ObgH1 and Mtg1, associate with the large

- mitochondrial ribosome subunit and are involved in translation and assembly of respiratory complexes. *Nucleic Acids Res.*, **41**, 3713–3722.
12. Kim, H.-J. and Barrientos, A. (2018) MTG1 couples mitoribosome large subunit assembly with intersubunit bridge formation. *Nucleic Acids Res.*, **46**, 8435–8453.
 13. Lavdovskaia, E., Kolander, E., Steube, E., Mai, M.M.-Q., Urlaub, H. and Richter-Dennerlein, R. (2018) The human Obg protein GTPBP10 is involved in mitoribosomal biogenesis. *Nucleic Acids Res.*, **46**, 8471–8482.
 14. Maiti, P., Kim, H.-J., Tu, Y.-T. and Barrientos, A. (2018) Human GTPBP10 is required for mitoribosome maturation. *Nucleic Acids Res.*, **46**, 11423–11437.
 15. Busch, J.D., Cipullo, M., Atanassov, I., Bratic, A., Silva Ramos, E., Schöndorf, T., Li, X., Pearce, S.F., Milenkovic, D., Rorbach, J. et al. (2019) MitoRibo-Tag mice provide a tool for in vivo studies of mitoribosome composition. *Cell Rep.*, **29**, 1728–1738.
 16. Maiti, P., Antonicka, H., Gingras, A.-C., Shoubridge, E.A. and Barrientos, A. (2020) Human GTPBP5 (MTG2) fuels mitoribosome large subunit maturation by facilitating 16S rRNA methylation. *Nucleic Acids Res.*, **48**, 95.
 17. Rorbach, J., Boesch, P., Gammage, P.A., Nicholls, T.J.J., Pearce, S.F., Patel, D., Hauser, A., Perocchi, F. and Minczuk, M. (2014) MRM2 and MRM3 are involved in biogenesis of the large subunit of the mitochondrial ribosome. *Mol. Biol. Cell.*, **25**, 2542–2555.
 18. Zhang, Y., Mandava, C.S., Cao, W., Li, X., Zhang, D., Li, N., Zhang, Y., Zhang, X., Qin, Y., Mi, K. et al. (2015) HflX is a ribosome-splitting factor rescuing stalled ribosomes under stress conditions. *Nat. Struct. Mol. Biol.*, **22**, 906–913.
 19. Coatham, M.L., Brandon, H.E., Fischer, J.J., Schümmer, T. and Wieden, H.-J. (2016) The conserved GTPase HflX is a ribosome splitting factor that binds to the E-site of the bacterial ribosome. *Nucleic Acids Res.*, **44**, 1952–1961.
 20. Dey, S., Biswas, C. and Sengupta, J. (2018) The universally conserved GTPase HflX is an RNA helicase that restores heat-damaged Escherichia coli ribosomes. *J. Cell Biol.*, **217**, 2519–2529.
 21. Mick, D.U., Dennerlein, S., Wiese, H., Reinhold, R., Pacheu-Grau, D., Lorenzi, I., Sasarman, F., Weraarpachai, W., Shoubridge, E.A., Warscheid, B. et al. (2012) MITRAC Links mitochondrial protein translocation to respiratory-chain assembly and translational regulation. *Cell*, **151**, 1528–1541.
 22. Richter-Dennerlein, R., Oeljeklaus, S., Lorenzi, I., Ronsör, C., Bareth, B., Schenzielorz, A.B., Wang, C., Warscheid, B., Rehling, P. and Dennerlein, S. (2016) Mitochondrial protein synthesis adapts to influx of nuclear-encoded protein. *Cell*, **167**, 471–483.
 23. Chomyn, A. (1996) In vivo labeling and analysis of human mitochondrial translation products. *Meth. Enzymol.*, **264**, 197–211.
 24. Dennerlein, S., Oeljeklaus, S., Jans, D., Hellwig, C., Bareth, B., Jakobs, S., Deckers, M., Warscheid, B. and Rehling, P. (2015) MITRAC7 acts as a COX1-specific chaperone and reveals a checkpoint during cytochrome c oxidase assembly. *Cell Rep.*, **12**, 1644–1655.
 25. Cox, J. and Mann, M. (2008) MaxQuant enables high peptide identification rates, individualized p.p.b.-range mass accuracies and proteome-wide protein quantification. *Nat. Biotechnol.*, **26**, 1367–1372.
 26. Tyanova, S., Temu, T., Sinitcyn, P., Carlson, A., Hein, M.Y., Geiger, T., Mann, M. and Cox, J. (2016) The Perseus computational platform for comprehensive analysis of (prote)omics data. *Nat. Methods*, **13**, 731–740.
 27. Cunha, C.E., Belardinelli, R., Peske, F., Holtkamp, W., Wintermeyer, W. and Rodnina, M.V. (2013) Dual use of GTP hydrolysis by elongation factor G on the ribosome. *Translation (Austin)*, **1**, e24315.
 28. Peske, F., Rodnina, M.V. and Wintermeyer, W. (2005) Sequence of steps in ribosome recycling as defined by kinetic analysis. *Mol. Cell*, **18**, 403–412.
 29. Rodnina, M.V., Savelsbergh, A., Matassova, N.B., Katunin, V.I., Semenov, Y.P. and Wintermeyer, W. (1999) Thiostrepton inhibits the turnover but not the GTPase of elongation factor G on the ribosome. *Proc. Natl. Acad. Sci. U.S.A.*, **96**, 9586–9590.
 30. Rodnina, M.V. and Wintermeyer, W. (1995) GTP consumption of elongation factor Tu during translation of heteropolymeric mRNAs. *Proc. Natl. Acad. Sci. U.S.A.*, **92**, 1945–1949.
 31. Caliskan, N., Wohlgenuth, I., Korniy, N., Pearson, M., Peske, F. and Rodnina, M.V. (2017) Conditional switch between frameshifting regimes upon translation of dnaX mRNA. *Mol. Cell*, **66**, 558–567.
 32. Rodnina, M.V., Semenov, Y.P. and Wintermeyer, W. (1994) Purification of fMet-tRNA(fMet) by fast protein liquid chromatography. *Anal. Biochem.*, **219**, 380–381.
 33. Stetefeld, J., McKenna, S.A. and Patel, T.R. (2016) Dynamic light scattering: a practical guide and applications in biomedical sciences. *Biophys. Rev.*, **8**, 409–427.
 34. Blom, J., Kübrich, M., Rassow, J., Voos, W., Dekker, P.J., Maarse, A.C., Meijer, M. and Pfanner, N. (1993) The essential yeast protein MIM44 (encoded by MPI1) is involved in an early step of preprotein translocation across the mitochondrial inner membrane. *Mol. Cell. Biol.*, **13**, 7364–7371.
 35. Schneider, H.C., Berthold, J., Bauer, M.F., Dietmeier, K., Guiard, B., Brunner, M. and Neupert, W. (1994) Mitochondrial Hsp70/MIM44 complex facilitates protein import. *Nature*, **371**, 768–774.
 36. Polkinghorne, A., Ziegler, U., González-Hernández, Y., Pospischil, A., Timms, P. and Vaughan, L. (2008) Chlamydomonas pneumoniae HflX belongs to an uncharacterized family of conserved GTPases and associates with the Escherichia coli 50S large ribosomal subunit. *Microbiology*, **154**, 3537–3546.
 37. Jain, N., Dhimole, N., Khan, A.R., De, D., Tomar, S.K., Sajish, M., Dutta, D., Parrack, P. and Prakash, B. (2009) E. coli HflX interacts with 50S ribosomal subunits in presence of nucleotides. *Biochem. Biophys. Res. Commun.*, **379**, 201–205.
 38. Basu, A. and Yap, M.-N.F. (2017) Disassembly of the Staphylococcus aureus hibernating 100S ribosome by an evolutionarily conserved GTPase. *Proc. Natl. Acad. Sci. U.S.A.*, **114**, E8165–E8173.
 39. Duval, M., Dar, D., Carvalho, F., Rocha, E.P.C., Sorek, R. and Cossart, P. (2018) HflXr, a homolog of a ribosome-splitting factor, mediates antibiotic resistance. *Proc. Natl. Acad. Sci. U.S.A.*, **115**, 13359–13364.
 40. Rudra, P., Hurst-Hess, K.R., Cotten, K.L., Partida-Miranda, A. and Ghosh, P. (2020) Mycobacterial HflX is a ribosome splitting factor that mediates antibiotic resistance. *Proc. Natl. Acad. Sci. U.S.A.*, **117**, 629–634.
 41. Haag, S., Sloan, K.E., Ranjan, N., Warda, A.S., Kretschmer, J., Blessing, C., Hubner, B., Seikowski, J., Dennerlein, S., Rehling, P. et al. (2016) NSUN3 and ABH1 modify the wobble position of mt-tRNA^{Met} to expand codon recognition in mitochondrial translation. *EMBO J.*, **35**, 2104–2119.
 42. Tsuboi, M., Morita, H., Nozaki, Y., Akama, K., Ueda, T., Ito, K., Nierhaus, K.H. and Takeuchi, N. (2019) EF-G2mt Is an Exclusive Recycling Factor in Mammalian Mitochondrial Protein Synthesis. *Mol. Cell*, **35**, 502–510.
 43. Soleimanpour-Lichaei, H.R., Kühl, I., Gaisne, M., Passos, J.F., Wydro, M., Rorbach, J., Temperley, R., Bonnefoy, N., Tate, W., Lightowers, R. et al. (2007) mtRF1a is a human mitochondrial translation release factor decoding the major termination codons UAA and UAG. *Mol. Cell*, **27**, 745–757.
 44. Richter, R., Rorbach, J., Pajak, A., Smith, P.M., Wessels, H.J., Huynen, M.A., Smeitink, J.A., Lightowers, R.N. and Chrzanoska-Lightowers, Z.M. (2010) A functional peptidyl-tRNA hydrolase, ICT1, has been recruited into the human mitochondrial ribosome. *EMBO J.*, **29**, 1116–1125.
 45. Godefroy-Colburn, T., Wolfe, A.D., Dondon, J., Grunberg-Manago, M., Dessen, P. and Pantaloni, D. (1975) Light-scattering studies showing the effect of initiation factors on the reversible dissociation of Escherichia coli ribosomes. *J. Mol. Biol.*, **94**, 461–478.
 46. Srinivasan, K., Dey, S. and Sengupta, J. (2019) Structural modules of the stress-induced protein HflX: an outlook on its evolution and biological role. *Curr. Genet.*, **65**, 363–370.
 47. Metodiev, M.D., Spähr, H., Loguerio Polosa, P., Meharg, C., Becker, C., Altmueller, J., Habermann, B., Larsson, N.-G. and Ruzzenente, B. (2014) NSUN4 is a dual function mitochondrial protein required for both methylation of 12S rRNA and coordination of mitoribosomal assembly. *PLoS Genet.*, **10**, e1004110.
 48. Brown, A., Rathore, S., Kimanius, D., Aibara, S., Bai, X.-C., Rorbach, J., Amunts, A. and Ramakrishnan, V. (2017) Structures of the human mitochondrial ribosome in native states of assembly. *Nat. Struct. Mol. Biol.*, **24**, 866–869.

49. Huang,B., Wu,H., Hao,N., Blombach,F., van der Oost,J., Li,X., Zhang,X.C. and Rao,Z. (2010) Functional study on GTP hydrolysis by the GTP-binding protein from *Sulfolobus solfataricus*, a member of the HflX family. *J. Biochem.*, **148**, 103–113.
50. Sato,A., Kobayashi,G., Hayashi,H., Yoshida,H., Wada,A., Maeda,M., Hiraga,S., Takeyasu,K. and Wada,C. (2005) The GTP binding protein Obg homolog ObgE is involved in ribosome maturation. *Genes Cells*, **10**, 393–408.
51. Rorbach,J., Richter,R., Wessels,H.J., Wydro,M., Pekalski,M., Farhoud,M., Kuhl,I., Gaisne,M., Bonnefoy,N., Smeitink,J.A. *et al.* (2008) The human mitochondrial ribosome recycling factor is essential for cell viability. *Nucleic Acids Res.*, **36**, 5787–5799.
52. Chadani,Y., Ono,K., Kutsukake,K. and Abo,T. (2011) *Escherichia coli* YaeJ protein mediates a novel ribosome-rescue pathway distinct from SsrA- and ArfA-mediated pathways. *Mol. Microbiol.*, **80**, 772–785.
53. Handa,Y., Inaho,N. and Nameki,N. (2011) YaeJ is a novel ribosome-associated protein in *Escherichia coli* that can hydrolyze peptidyl-tRNA on stalled ribosomes. *Nucleic Acids Res.*, **39**, 1739–1748.
54. Gagnon,M.G., Seetharaman,S.V., Bulkley,D. and Steitz,T.A. (2012) Structural basis for the rescue of stalled ribosomes: structure of YaeJ bound to the ribosome. *Science*, **335**, 1370–1372.
55. Akabane,S., Ueda,T., Nierhaus,K.H. and Takeuchi,N. (2014) Ribosome rescue and translation termination at non-standard stop codons by ICT1 in mammalian mitochondria. *PLoS Genet*, **10**, e1004616.
56. Wesolowska,M.T., Richter-Dennerlein,R., Lightowers,R.N. and Chrzanoska-Lightowers,Z.M.A. (2014) Overcoming stalled translation in human mitochondria. *Front. Microbiol.*, **5**, 374.
57. Antonicka,H., Ostergaard,E., Sasarman,F., Weraarpachai,W., Wibrand,F., Pedersen,A.M.B., Rodenburg,R.J., van der Knaap,M.S., Smeitink,J.A.M., Chrzanoska-Lightowers,Z.M. *et al.* (2010) Mutations in C12orf65 in patients with encephalomyopathy and a mitochondrial translation defect. *Am. J. Hum. Genet.*, **87**, 115–122.
58. Greber,B.J., Boehringer,D., Leibundgut,M., Bieri,P., Leitner,A., Schmitz,N., Aebersold,R. and Ban,N. (2014) The complete structure of the large subunit of the mammalian mitochondrial ribosome. *Nature*, **515**, 283–286.
59. Brown,A., Amunts,A., Bai,X.-C., Sugimoto,Y., Edwards,P.C., Murshudov,G., Scheres,S.H.W. and Ramakrishnan,V. (2014) Structure of the large ribosomal subunit from human mitochondria. *Science*, **346**, 718–722.
60. Ayyub,S.A., Gao,F., Lightowers,R.N. and Chrzanoska-Lightowers,Z.M. (2020) Rescuing stalled mammalian mitoribosomes – what can we learn from bacteria? *J. Cell. Sci.*, **133**, jcs231811.
61. Vawter,M.P., Harvey,P.D. and DeLisi,L.E. (2007) Dysregulation of X-linked gene expression in Klinefelter's syndrome and association with verbal cognition. *Am. J. Med. Genet.*, **144B**, 728–734.
62. Koripella,R.K., Sharma,M.R., Risteff,P., Keshavan,P. and Agrawal,R.K. (2019) Structural insights into unique features of the human mitochondrial ribosome recycling. *Proc. Natl. Acad. Sci. U.S.A.*, **116**, 8283–8288.
63. Rorbach,J., Gammage,P.A. and Minczuk,M. (2012) C7orf30 is necessary for biogenesis of the large subunit of the mitochondrial ribosome. *Nucleic Acids Res.*, **40**, 4097–4109.
64. Wanschers,B.F.J., Szklarczyk,R., Pajak,A., van den Brand,M.A.M., Gloerich,J., Rodenburg,R.J.T., Lightowers,R.N., Nijtmans,L.G. and Huynen,M.A. (2012) C7orf30 specifically associates with the large subunit of the mitochondrial ribosome and is involved in translation. *Nucleic Acids Res.*, **40**, 4040–4051.
65. Jain,N., Vithani,N., Rafay,A. and Prakash,B. (2013) Identification and characterization of a hitherto unknown nucleotide-binding domain and an intricate interdomain regulation in HflX-a ribosome binding GTPase. *Nucleic Acids Res.*, **41**, 9557–9569.
66. Wu,H., Sun,L., Blombach,F., Brouns,S.J.J., Snijders,A.P.L., Lorenzen,K., van den Heuvel,R.H.H., Heck,A.J.R., Fu,S., Li,X. *et al.* (2009) Structure of the ribosome associating GTPase HflX. *Proteins*, **348**, 705–713.

Dual function of GTPBP6 in biogenesis and recycling of human mitochondrial ribosomes

Elena Lavdovskaia^{1,3}, Kärt Denks^{2,3}, Franziska Nadler¹, Emely Steube¹, Andreas Linden^{4,5}, Henning Urlaub^{4,5}, Marina V. Rodnina^{2,3} and Ricarda Richter-Dennerlein^{1,3*}

Supplementary data

Table S1: Key reagents

	SOURCE	IDENTIFIER
Antibodies		
Rabbit polyclonal anti-uS7m	Sigma Prestige	Cat#HPA023007
Rabbit polyclonal anti-uS14m	ProteinTech	Cat#16301-1-AP
Rabbit polyclonal anti-uS15m	ProteinTech	Cat#17006-1-AP
Rabbit polyclonal anti-bS16m	ProteinTech	Cat#16735-1-AP
Rabbit polyclonal anti-mS25	ProteinTech	Cat#15277-1-AP
Rabbit polyclonal anti-mS27	ProteinTech	Cat#17280-1-AP
Rabbit polyclonal anti-uL1m	self made	PRAB4964
Rabbit polyclonal anti-uL3m	ProteinTech	Cat#16584-1- AP
Rabbit polyclonal anti-bL12m	ProteinTech	Cat#14795-1-AP
Rabbit polyclonal anti-uL13m	ProteinTech	Cat#16241-1-AP
Rabbit polyclonal anti-bL20m	ProteinTech	Cat#16969-1-AP
Rabbit polyclonal anti-uL23m	self made	PRAB1716
Rabbit polyclonal anti-bL32m	self made	PRAB4957
Rabbit polyclonal anti-mL44	ProteinTech	Cat#16394-1-AP
Rabbit polyclonal anti-mL45	ProteinTech	Cat#15682-1-AP
Rabbit polyclonal anti-mL62	ProteinTech	Cat#10403-1-AP
Rabbit polyclonal anti-MALSU1	ProteinTech	Cat#22838-1-AP
Rabbit polyclonal anti-NSUN4	ProteinTech	Cat#16320-1-AP
Rabbit polyclonal anti-GTPBP5 (MTG2)	Sigma Prestige	Cat#HPA047379
Rabbit polyclonal anti-GTPBP7 (MTG1)	ProteinTech	Cat#13742-1-AP
Rabbit polyclonal anti-GTPBP10	Novusbio	Cat#NBP1-85055
Mouse monoclonal anti-FLAG	Sigma Prestige	Cat#F1804
Rabbit polyclonal anti-MFN2	ProteinTech	Cat#12186-1-AP
Rabbit polyclonal anti-TIM23	self made	PRAB1527
Rabbit polyclonal anti-TIM44	ProteinTech	Cat#13859-1-AP
Mouse monoclonal anti-COX1	Invitrogen	Cat#459600

Mouse monoclonal anti-COX2	Abcam	Cat#ab110258
Mouse monoclonal anti-Calnexin	Proteintech	Cat#66903-1-Ig
Mouse monoclonal anti-SDHA	Invitrogen	Cat#459200
Mouse monoclonal anti-GAPDH	Santa Cruz	Cat#sc-32233
Rabbit polyclonal anti-MTERF4	Sigma Prestige	Cat#HPA027097
Chemicals		
Anti-FLAG M2 Affinity Gel	Sigma-Aldrich	A2220
L-[³⁵ S]methionine	Hartmann Analytic	SCM-01
EasyTides® Adenosine 5'-triphosphate, [γ - ³² P]	PerkinElmer	BLU502Z250UC
Emetine dihydrochloride hydrate	Roth	
Lipofectamine 3000	Invitrogen	L3000-015
GeneJuice	Novagen	70967-3
Alt-R® CRISPR-Cas9 tracrRNA, ATTO™ 550	Integrated DNA technologies	1075927
Alt-R® S.p. Cas9 Nuclease V3	Integrated DNA technologies	1081058
Glutathione Sepharose™ 4B beads	GE Healthcare	17-0756-01
PreScission™ protease	GE Healthcare	27-0843-01
TRizol® Reagent	Ambion	15596018
Critical Commercial Assays		
Alt-R® Genome Editing Detection Kit	Integrated DNA technologies	1075932
Rapid DNA Ligation Kit	ThermoFisher Scientific	K1423
T4 Polynucleotide Kinase (T4 PNK)	ThermoFisher Scientific	EK0031
Wizard® Plus SV Minipreps DNA Purification System	Promega	A1460
Wizard® SV Gel and PCR Clean-Up System	Promega	A9282
QuikChange Lightning Site-Directed Mutagenesis Kit	Agilent Technologies	210519-5
Cell Lines		
HEK293-Flp-In T-Rex	ThermoFisher Scientific	R78007
HEK293-Flp-In T-Rex- <i>Gtbbp6</i> ^{-/-} cl.1	This study	N/A
HEK293-Flp-In T-Rex- <i>Gtbbp6</i> ^{-/-} cl.2	This study	N/A
HEK293-Flp-In T-Rex-GTPBP6 ^{FLAG}	This study	N/A
HEK293-Flp-In T-Rex-GTPBP6 ^{K187A-FLAG}	This study	N/A
HEK293-Flp-In T-Rex-GTPBP6 ^{D199A-FLAG}	This study	N/A
HEK293-Flp-In T-Rex-GTPBP6 ^{G352P-FLAG}	This study	N/A
HEK293-Flp-In T-Rex-GTPBP6 ^{S437P-FLAG}	This study	N/A

Oligonucleotides		
Guide RNA: targeting the Exon 1 of GTPBP6: 5'-AGATGCGGACGAGAACGCCG-3'	This study; Integrated DNA technologies	N/A
Primer: Generation of the FLAG-tagged version of GTPBP6 Forward: 5'-TATAAAGCTTATGTGGGCCTGCGGGCCGCGTACGCC-3'	This study; Microsynth	N/A
Primer: Generation of the FLAG-tagged version of GTPBP6 Reverse: 5'-TATAGATATCTTACTTGTCATCGTCGTCC TTGTAGTCTCCTGGAAAGAGCTTCCGGA ATTTGCCG-3'	This study; Microsynth	N/A
Primer: Generation of the FLAG-tagged mutant (K187A) version of GTPBP6 Forward: 5'-GCTGCCCGACCAAGGCAGAACTGGAA GCCGCCTGGGGCGTG-3'	This study; Microsynth	N/A
Primer: Generation of the FLAG-tagged mutant (K187A) version of GTPBP6 Reverse: 5'-GGCGGCTTCCAGTTCTGCCTTGGTCGGG GCAGCCATCCTCTC-3'	This study; Microsynth	N/A
Primer: Generation of the FLAG-tagged mutant (D199A) version of GTPBP6 Forward: 5'-GGCGTGGAGGTGTTTGCCCGCTTACGG TCGTCTGCACATC-3'	This study; Microsynth	N/A
Primer: Generation of the FLAG-tagged mutant (D199A) version of GTPBP6 Reverse: 5'-GACGACCGTGAAGCGGGCAAACACCTCC ACGCCCCAGGCGGC-3'	This study; Microsynth	N/A
Primer: Generation of the FLAG-tagged mutant (G352P) version of GTPBP6 Forward: 5'-GTACGTGGACACCATCCCTTCTCTCC CAGCTGCCGCACGGC-3'	This study; Microsynth	N/A
Primer: Generation of the FLAG-tagged mutant (G352P) version of GTPBP6 Reverse: 5'-CAGCTGGGAGAGGAAGGGGATGGTGTC CACGTACAGGACGGTC-3'	This study; Microsynth	N/A
Primer: Generation of the FLAG-tagged mutant (S437P) version of GTPBP6 Forward: 5'-GAACGTCGTGCCCGTGCCTGCCCTGCG GGGCCACGGGCTCCAG-3'	This study; Microsynth	N/A

Primer: Generation of the FLAG-tagged mutant (S437P) version of GTPBP6 Reverse: 5'- GTGGCCCCGCAGGGCAGGCACGGGCAC GACGTTTCGGTCCG-3'	This study; Microsynth	N/A
Probe for northern blot: targeting MTRNR1 (12S rRNA) 5'- TCGATTACAGAACAGGCTCCTCTAG-3'	This study; Microsynth	N/A
Probe for northern blot: targeting MTRNR2 (16S rRNA) 5'- GTTTGGCTAAGGTTGTCTGGTAGTA-3'	This study; Microsynth	N/A
Probe for northern blot: targeting MTCO1 5'- GTCAGTTGCCAAAGCCTCCGATTATG-3'	This study; Microsynth	N/A
Probe for northern blot: targeting MTCO2 5'- GACGTCCGGGAATTGCATCTGTTTT-3'	This study; Microsynth	N/A
Probe for northern blot: targeting 18S-rRNA 5'- TTTACTTCCTCTAGATAGTCAAGTTCGAC C-3'	(1); Microsynth	
Recombinant DNA		
pOG44 Flp-Recombinase Expression Vector	ThermoFisher Scientific	V600520
pcDNA5/FRT/TO	ThermoFisher Scientific	V6520-20
pGex-6P-1	Merck	GE28-9546-48
Software and Algorithms		
ImageJ	https://imagej.nih.gov/ij/	
ImageQuant TL 7.0	GE Healthcare http://www.gelifesciences.com/webapp/wcs/stores/servlet/catalog/en/GELifeSciences-de/products/AlternativeProductStructure_16016/	

Table S2: Apparent rate constant (k_{app}) of 70S ribosome recycling catalyzed by human GTPBP6 and *E.coli* RRF-EF-G (related to Figure 3)

Complex	k_{app1} (s^{-1})	k_{app2} (s^{-1})
preHC + GTPBP6	0.05 ± 0.006	
postHC + GTPBP6	0.08 ± 0.012	
70S + GTPBP6	0.09 ± 0.006	
preHC + RRF + EF-G	0.31 ± 0.05	0.02 ± 0.003
postHC + RRF + EF-G	0.34 ± 0.02	
70S + RRF + EF-G	0.33 ± 0.04	

n = 3; mean \pm standard deviation.

Table S3: Label-free quantitative mass spectrometry analyses of mtLSU complexes in *Gtpbp6*^{-/-} cells vs. WT (related to Figure 5) (see excel file)

Figure S1: Sequence alignment of human GTPBP6 and the bacterial homolog HflX from *E. coli*, *B. subtilis* and *S. aureus* using ClustalW2 (related to Figure 1).

Mutated residues analyzed in this study are indicated in red.

Figure S2: Elevated expression of GTPBP6 does not affect mtLSU assembly factors (related to Figure 2).

Mitochondrial lysates (0.5 mg) isolated from cells overexpressing GTPBP6^{FLAG} were dissected by sucrose density gradient centrifugation in comparison to wild type. Fractions were analyzed by western blotting using indicated antibodies. Figure represents an extended version of Figure 1D. In addition to markers of the mtLSU and mtSSU, the levels and distribution of the assembly factors NSUN4, MALSU1 and GTPBP10 have been determined using specific antibodies.

Figure S3: 70S subunit dissociation facilitated by RRF and EF-G (related to Figure 3).

(A) Time courses of ribosome dissociation measured upon addition of RRF (2.5 μM) and EF-G (2 μM) to 70S ribosomes (0.05 μM). For method details, see Figure 3C and Methods.

(B) Dissociation of different ribosomal complexes facilitated by RRF-EF-G. Complexes were prepared as in Figure 3E. Concentrations are as in (A).

(C) Ribosome dissociation upon addition of IF3 (1 μM) to 70S ribosomes (0.05 μM). 70S + IF3: $k_{\text{app}} = 0.04 \text{ s}^{-1}$. Experiment was performed as in 3C and S3A.

Figure S4: Characterization of CRISPR/Cas9 generated *Gtpbp6* knock out cell lines (related to Figure 4).

(A) Genotyping of the *Gtpbp6*^{-/-} clone 1 genomic DNA by Sanger sequencing. Chromatogram represents an amplicon generated by PCR covering the guide RNA target site in the first exon of GTPBP6 in *Gtpbp6*^{-/-} clone 1. Resolving the double peaks suggests that *Gtpbp6*^{-/-} clone 1 has heterozygous single (allele 1) or double (allele 2) nucleotide deletions.

(B) Sequence alignment of the first exons of GTPBP6-WT and *Gtpbp6*^{-/-} clone 2. The absence of the double peaks in chromatogram of *Gtpbp6*^{-/-} clone 2 indicates the presence of the homozygous 332 bp insertion.

(C) Schematic representation of the affected *Gtpbp6* locus (upper panel) and corresponding translation frames (lower panel). Full-length GTPBP6 consists of 516 amino acid residues. The presence of frame shift mutations leading to the premature stop codons formation in *Gtpbp6*^{-/-} clone 1 results in formation of 2 truncated protein variants (113 aa – allele 1 and 102 aa – allele 2). Insertion in *Gtpbp6*^{-/-} clone 2 leads to formation of 112 aa protein.

(D-E) GTPBP6^{FLAG} expression in *Gtpbp6*^{-/-} cells. Expression of GTPBP6^{FLAG} in *Gtpbp6*^{-/-} cells clone 1 (D) and clone 2 (E) was induced with different concentration of tetracycline as indicated. Whole cell protein extracts were isolated and analyzed by western blotting. Relative expression levels of GTPBP6^{FLAG} were determined using FLAG antibodies. Calnexin was used as a loading control.

(F) GTPBP6 loss does not affect mt-RNA levels. RNA was isolated from HEK293T-wild type (WT) and *Gtpbp6*^{-/-} cells and analyzed by Northern blotting using specific probes against *MTRNR1* (12S rRNA), *MTRNR2* (16S rRNA), *MTCO1* (COX1 mRNA), *MTCO2* (COX2 mRNA) and 18S rRNA (loading control).

(G) RNA levels were visualized using Typhoon imaging system (GE Healthcare) and quantified with ImageQuant TL software. Steady state RNA levels from wild type cells are marked as dashed line (100%). (n = 3; mean ± SEM).

Figure S5. HflX binds on *E. coli* 50S subunit to the site that is also conserved in human 39S mtLSU.

(A) Superimposition of human mitochondrial 39S mtLSU (yellow, PDB 3J9M, (2)), HflX-bound *E. coli* 50S LSU (blue, PDB 5ADY, (3)) and free *E. coli* 50S LSU (green, PDB 4YBB, (4)). View from the small subunit side. HflX is shown in transparent blue.

(B) HflX contacts conserved elements of 50S subunit, such as 23S rRNA helix 69 (H69), L7/L12 stalk, sarcin-ricin loop (SRL) and peptidyl transferase center (3).

(C, D). In addition to SRL (panel B), also A- and P-loop at the PTC are structurally similar in 39S and 50S; as well as H89, which was shown to form extensive interactions with HflX on 50S subunit (3).

(E) HflX induces a displacement of H69 that forms intersubunit bridge B2a both in bacterial and mitochondrial ribosome. Its flexible loop is not resolved in 39S mtLSU.

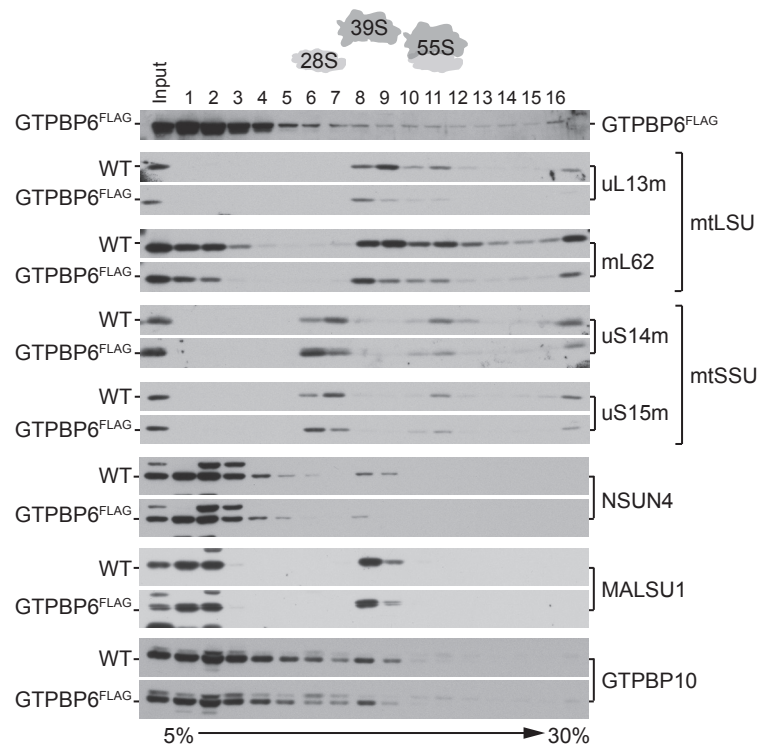
(F) Large conformational changes also occur on L7/L12 stalk of 50S upon the binding of HflX. This is illustrated with the displacement of uL11 (blue).

References

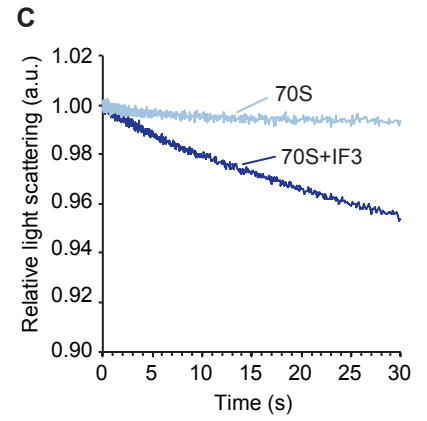
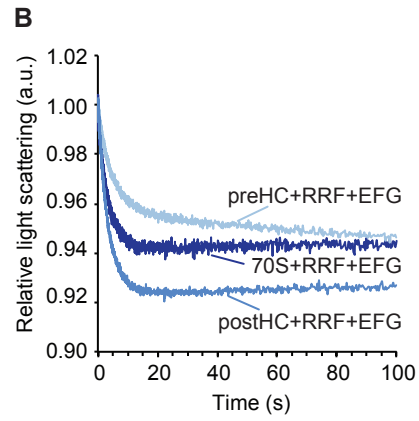
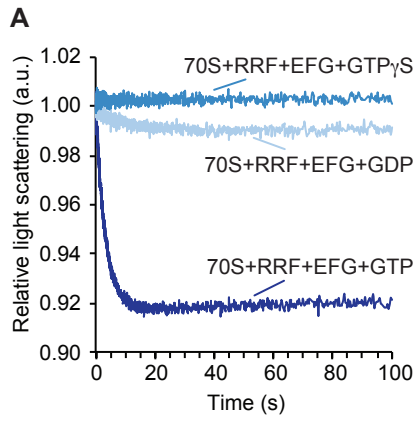
1. Larburu,N., Montellese,C., O'Donohue,M.-F., Kutay,U., Gleizes,P.-E. and Plisson-Chastang,C. (2016) Structure of a human pre-40S particle points to a role for RACK1 in the final steps of 18S rRNA processing. *Nucleic Acids Research*, **44**, 8465–8478.
2. Amunts,A., Brown,A., Toots,J., Scheres,S.H.W. and Ramakrishnan,V. (2015) Ribosome. The structure of the human mitochondrial ribosome. *Science*, **348**, 95–98.
3. Zhang,Y., Mandava,C.S., Cao,W., Li,X., Zhang,D., Li,N., Zhang,Y., Zhang,X., Qin,Y., Mi,K., *et al.* (2015) HflX is a ribosome-splitting factor rescuing stalled ribosomes under stress conditions. *Nat. Struct. Mol. Biol.*, **22**, 906–913.
4. Noeske,J., Wasserman,M.R., Terry,D.S., Altman,R.B., Blanchard,S.C. and Cate,J.H.D. (2015) High-resolution structure of the Escherichia coli ribosome. *Nat. Struct. Mol. Biol.*, **22**, 336–341.

GTPBP6_HUMAN	MWALRAAVRPLRLSRVGRGRSAPRAAAPSCPARALAAVGRRSPGNLEGPWGGGRGLRAD	60
HFLX_ECOLI	-----	0
HFLX_BACSU	-----	0
HFLX_STAAU	-----	0
ND1 (ATPase)		
GTPBP6_HUMAN	GGRSRTGDDEEPEADENAEELLRGEPLLPAGTQRVCLVHPDVKWGPGKSQMTRAEWQ	120
HFLX_ECOLI	-----MFDRYDAGEQA-----VLVHIYF---TQDKDM---ED	26
HFLX_BACSU	-----MNEQETIQEKA-----ILVGCQL---PHITDE-HFENS	29
HFLX_STAAU	----MYNMAQQQIHDTKNKLEKA-----VLVGVHA---QDDKQF-NFEST	37
	: * : ** :	
GTPBP6_HUMAN	VAEATALVHTLDGWSVVQTMVSTKTPDRKLI FGKGNFEHLTEKIRGSPDITCVFLNVER	180
HFLX_ECOLI	LQEFESLVS-SAGVEALQVITGSRKAPHPKYFVGEKAVEIAEAVKATGA-SVVL-FDHA	83
HFLX_BACSU	MEELASLTK-TADGKVLTSVTQKRNRAAATYIGKGVKVELKALVEELEA-DLLI-FNDE	86
HFLX_STAAU	MEELSSLSE-TCQLEVLGQITQNRDRVDRKYVVGKGIETQAFIEFKDI-DVVI-TNDE	94
	: * : * : * : * : . : . : .	
α-helical linker		
GTPBP6_HUMAN	MAAPT K KELEAAWGVVEFDRFTVVLHIFRCNARTKEARLQVALAEMPLHRSNLKRDVAHL	240
HFLX_ECOLI	LSPA Q ER N LRLCECRV I DR T GLILDIFAQAR T HEGKLVQELAQLRHLATRLVRGWTHL	143
HFLX_BACSU	LSP S QL K SLATAIEVK M DR T QLILDIFAKRARTREGKLVQELAQYALPRLTGQGINL	146
HFLX_STAAU	LT T AQ S KLNEALGV K I D RTQLILEIFALRARSKEGKLVQELAQLDYLLPRLQGHGKSL	154
	: : . * . : : * * : * : * * . * * : * : * * : * : * . *	
GTPBP6_HUMAN	YRGVGSRYIMSGESFMQLQORLLREKEAKIRKALDRLRKRRHLRRQRTRREFPVISVV	300
HFLX_ECOLI	ERQGGIGLRGPGETQLETDRLLRNRIVQIQSRLEVEKQREQGRQSRIKADVPTVSLV	203
HFLX_BACSU	SRQGGIGARGPGETKLETDRRHIRNRIHEINTQLSTVIRHRSRYRERRKKNGLVQIALV	206
HFLX_STAAU	SRLGGIGTRGPGETKLEMDRRHIRTRMNEIKHQLRVTEEHRERYRNKRQNQVQVALV	214
	* * . * * : : : * : * : * . * : : * * . * : . : : *	
ND2 (GTPase)		
GTPBP6_HUMAN	GYTNCGKTTLIKALTGDAAIQPRDQLFATLDVTAHAGTLP SRMTVLYVDT G FLS Q LPHG	360
HFLX_ECOLI	GYTNAGKSTLFNRI T EA-RVYAADQLFATLDPTLRIDVADVGETVLADTV G FIRH L PHD	262
HFLX_BACSU	GYTNAGKSTWFNRL T SA-DSYEEDLLFATLDPMTRK M VLPSGYSVLLSDTV G FIQ L PTT	265
HFLX_STAAU	GYTNAGKSSWFNVL A NE-ETYEKDQLFATLDPKTRQIQINDGFNLIISDTV G FIQ L PTT	273
	* * * . * * : : : : * * * * * : : . : * * : * * : . * *	
GTPBP6_HUMAN	LIESFSATLEDVAHSDLILHVRDVSHPEAELQKCSVLSTLRGLQLPAPLLDSMVVHNKV	420
HFLX_ECOLI	LVAAFKATLQETRQATLLLVHVIDAADVRVQENIEAVNTVLEEIDAHE---IPTLLVMNKI	319
HFLX_BACSU	LIAAFRSTLEEVKEADLILHLIDSSNEDYAGHEKTVLRLLEELEADD---IPMLTAYNKR	322
HFLX_STAAU	LIAAFKSTLEEAKGADLLVHVVDSSHPEYRTQYDVTNDLIKQLDMSH---ISQIVIFNKK	330
	* : * * * : . : * : * : * . : : * : . : : : * *	
GTPBP6_HUMAN	DLVPG--YSP-----TEPNVVPV S ALRGHGLQELKAELDAAVLKATGRQILTLRVRL-	470
HFLX_ECOLI	DMLED--FEPRIDREENKPNRVWL S AQTGAGIPQLFQAL T ERL---SG-EVAQHTLR L P	373
HFLX_BACSU	DQKLPD-FIPTAGRD-----HIMV S AKFEDDAAAFKEAIQRYL---RQEL L TSFEAHVP	372
HFLX_STAAU	DLCDHASNRPASDLP-----NVFV S SKNDGDKLLVKT L FIDEI---K-RQLTY D E A IA	380
	* * : : * : . . : : : : : :	
GTPBP6_HUMAN	--AGAQLSWLYKEATVQEVVDVIPEDGAADV R VIIISNSAYGKFRK L FPG-----	516
HFLX_ECOLI	PQEGRLRSR F YQL Q AIE-KEWMEEDGSVSLQVRMP I VDWRR L CK Q EPALIDY L I---	426
HFLX_BACSU	ASEG L LSRIK S ET M VD-RFYFNEENE Q -----YDISGYV Q EE Q SI G EL K K Y M	420
HFLX_STAAU	TNNADRL Y FLK Q HT L V T -ELKYDE I ENV-----YRIK G F K K-----	415
	. : . : * :	

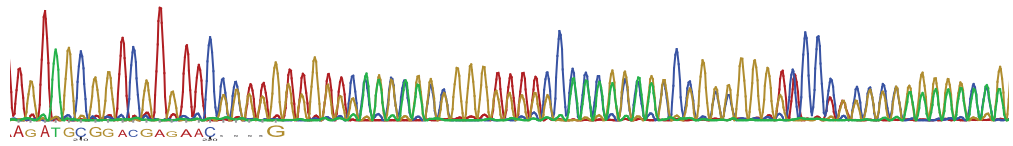
Lavdovskaia et al. Figure S1



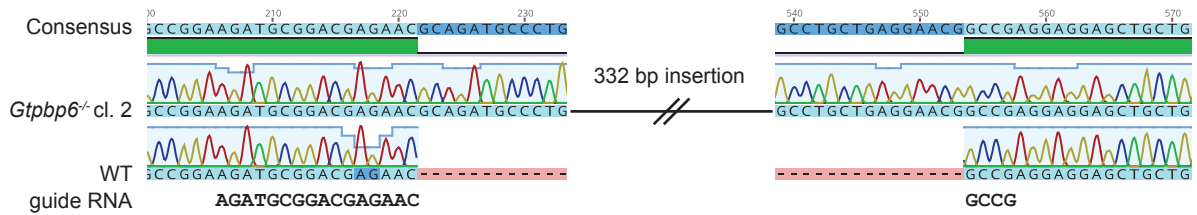
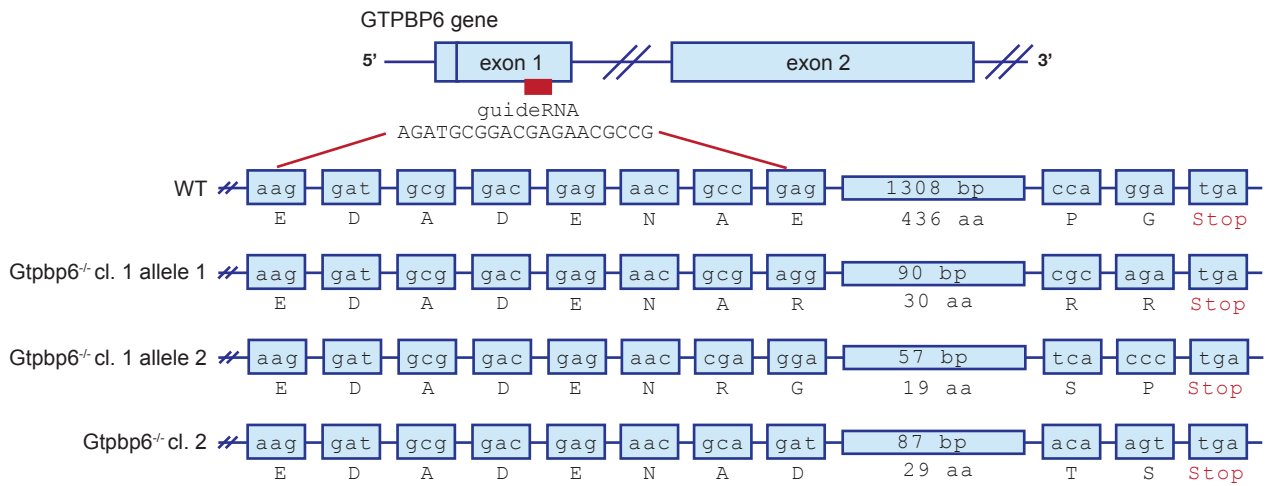
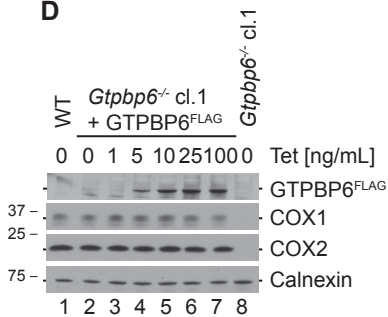
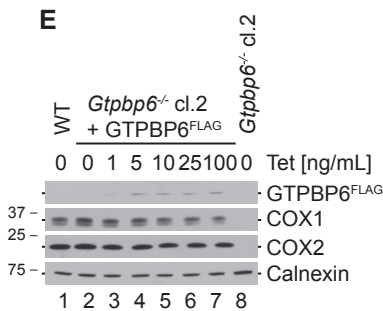
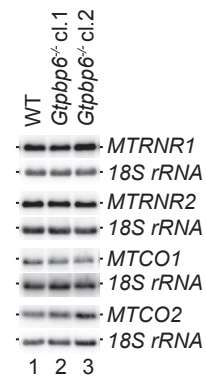
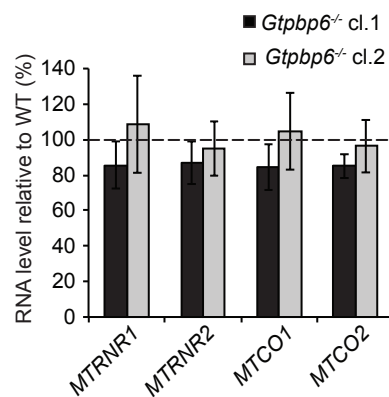
Lavdovskaia et al. Figure S2

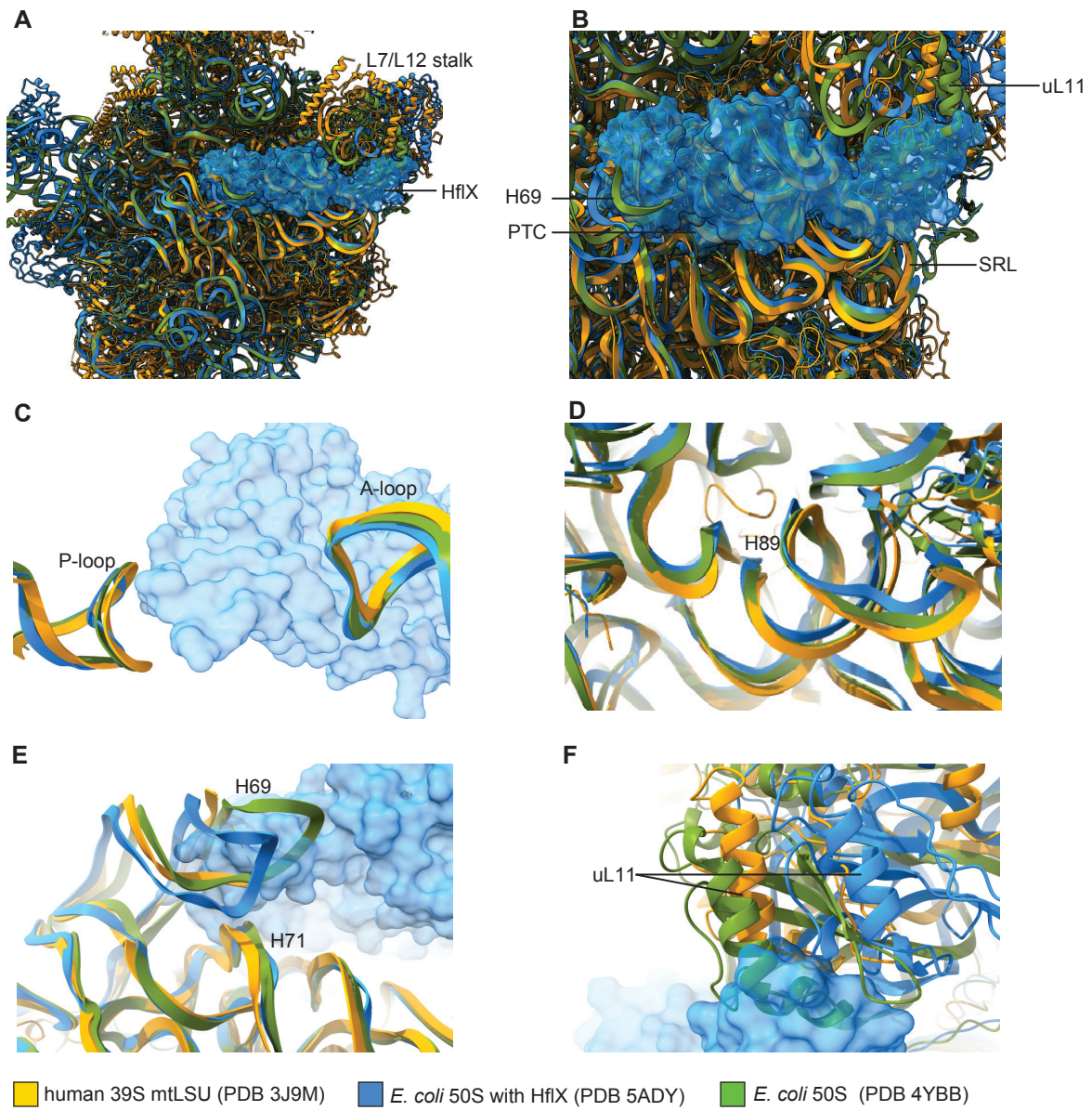


Lavdovskaia et al. Figure S3

A

Gtpbp6^{-/-} cl. 1 allele 1 AGATGCGGACGAGAACGC-GAGGAGGAGCTGCTGCGGGGAGAGCCCTCTGCTGCCGGCGGGGACCCAGCGCGTGTGTCT
Gtpbp6^{-/-} cl. 1 allele 2 AGATGCGGACGAGAAC-C-GAGGAGGAGCTGCTGCGGGGAGAGCCCTCTGCTGCCGGCGGGGACCCAGCGCGTGTGTCT
 WT AGATGCGGACGAGAACGCCGAGGAGGAGCTGCTGCGGGGAGAGCCCTCTGCTGCCGGCGGGGACCCAGCGCGTGTGTCT
 guide RNA AGATGCGGACGAGAACGCCG

B**C****D****E****F****G**



Lavdovskaia et al. Figure S5

4.3 Publication 3

Hillen, H., Lavdovskaia, E., Nadler, F., Hanitsch, E., Linden, A., Bohnsack, K., Urlaub, H., and Richter-Dennerlein, R. (2021). Structural basis of GTPase-mediated mitochondrial ribosome biogenesis and recycling. *Nature communications* 12. doi: 10.1038/s41467-021-23702-y.

Copyright license: according to the publisher's web-site and Copyright Clearance Center's RightsLink®, this is an open access article distributed under the terms of the [Creative Commons CC BY](#) license, which permits unrestricted use, distribution, and reproduction in any medium, provided the original work is properly cited.

Authors contribution:

Figure 1. Cell culture maintenance and ribosome isolation from *Gtpbp6*^{-/-} cell line (E.L.). Sample preparation for cryo-EM, data collection and processing, model building and refinement (H.S.H.).

Figure 2. Cell culture maintenance and ribosome isolation from *Gtpbp6*^{-/-} cell line (E.L.). Sample preparation for cryo-EM, data collection and processing, model building and refinement (H.S.H.).

Figure 3. Cell culture maintenance and ribosome isolation from *Gtpbp6*^{-/-} cell line, *in vitro* reconstitution experiments (E.L.). Purification of recombinant GTPBP6 protein, sample preparation for cryo-EM, data collection and processing, model building and refinement (H.S.H.).

Figure 4. A model for the mtLSU PTC maturation (H.S.H., R.R.-D.).

Figure 5. Cell culture maintenance and ribosome isolation from HEK293F WT cell line, *in vitro* reconstitution experiments (F.N.). Purification of recombinant GTPBP6 protein, sample preparation for cryo-EM, data collection and processing, model building and refinement (H.S.H.).

Extended data Figure 1 and Figure 2. Authors contribution according to the main text Figure 1; western blot analysis of mitoribosomal complexes isolated from *Gtpbp6*^{-/-} cells (E.L.)

Extended data Figure 3 and Figure 4. Authors contribution according to the main text Figure 3.

Extended data Figure 5. Authors contribution according to the main text Figure 5.

Extended data Figure 6. Analysis of GTPBP6 conformations (H.S.H.), bisulfite sequencing (K.E.B.).

Other experimental contribution: method development (mitochondrial ribosome isolation from cultured cells) (E.H.), mass spectrometry data analysis (A.L., H.U.).

Non-experimental contribution: data analysis and visualization (H.S.H., E.L., A.L., E.K.B. and R.R.-D.), project supervision (R.R.-D., H.S.H. and H.U.); study conceptualization (R.R.-D. and H.S.H.), manuscript writing (H.S.H. and R.R.-D. with the contribution of all the co-authors).

Structural basis of GTPase-mediated mitochondrial ribosome biogenesis and recycling

Hauke S. Hillen ^{1,2,3✉}, Elena Lavdovskaia ^{1,2}, Franziska Nadler¹, Elisa Hanitsch¹, Andreas Linden^{4,5}, Katherine E. Bohnsack ⁶, Henning Urlaub ^{4,5} & Ricarda Richter-Dennerlein ^{1,2✉}

Ribosome biogenesis requires auxiliary factors to promote folding and assembly of ribosomal proteins and RNA. Particularly, maturation of the peptidyl transferase center (PTC) is mediated by conserved GTPases, but the molecular basis is poorly understood. Here, we define the mechanism of GTPase-driven maturation of the human mitochondrial large ribosomal subunit (mtLSU) using endogenous complex purification, in vitro reconstitution and cryo-EM. Structures of transient native mtLSU assembly intermediates that accumulate in GTPBP6-deficient cells reveal how the biogenesis factors GTPBP5, MTERF4 and NSUN4 facilitate PTC folding. Addition of recombinant GTPBP6 reconstitutes late mtLSU biogenesis in vitro and shows that GTPBP6 triggers a molecular switch and progression to a near-mature PTC state. Additionally, cryo-EM analysis of GTPBP6-treated mature mitochondrial ribosomes reveals the structural basis for the dual-role of GTPBP6 in ribosome biogenesis and recycling. Together, these results provide a framework for understanding step-wise PTC folding as a critical conserved quality control checkpoint.

¹Department of Cellular Biochemistry, University Medical Center Goettingen, Goettingen, Germany. ²Cluster of Excellence “Multiscale Bioimaging: from Molecular Machines to Networks of Excitable Cells” (MBExC), University of Goettingen, Goettingen, Germany. ³Research Group Structure and Function of Molecular Machines, Max Planck Institute for Biophysical Chemistry, Goettingen, Germany. ⁴Bioanalytical Mass Spectrometry Group, Max Planck Institute for Biophysical Chemistry, Goettingen, Germany. ⁵Bioanalytics, Institute for Clinical Chemistry, University Medical Center Goettingen, Goettingen, Germany. ⁶Department of Molecular Biology, University Medical Center Goettingen, Goettingen, Germany. ✉email: hauke.hillen@med.uni-goettingen.de; ricarda.richter@med.uni-goettingen.de

The human mitochondrial ribosome (mitoribosome) synthesizes 13 essential subunits of the oxidative phosphorylation (OXPHOS) system. Defects in mitoribosome biogenesis or function result in OXPHOS deficiency and cause severe early-onset mitochondrial diseases¹. The mitoribosome is composed of a small and a large ribosomal subunit (mtSSU and mtLSU, respectively), which each contain a ribosomal RNA (12S, 16S rRNA) and a number of mitoribosomal proteins (MRPs). Structural analyses of the mitoribosome have revealed its overall architecture and differences to cytoplasmic and bacterial ribosomes^{2,3}. However, little is known about the mechanisms of mitoribosome assembly.

Biogenesis of the large ribosomal subunit (LSU) in all translation systems proceeds through distinct steps in which the formation of the peptidyl transferase center (PTC), the active site of the ribosome, represents the last and most critical step and requires the assistance of assembly factors^{4–7}. In particular, universally conserved GTPases, which act as quality control and antiassociation factors, play key roles during late LSU assembly stages and ensure proper maturation of the PTC⁸. In human mitochondria, the GTPases GTPBP5, GTPBP6, GTPBP7, and GTPBP10 mediate mtLSU maturation, as their deletion results in a loss of active mitoribosomes and stalls mtLSU biogenesis at distinct states^{8–14}. In particular, ablation of either GTPBP5 or GTPBP6 in human cells results in the accumulation of late mtLSU assembly intermediates containing GTPBP7, GTPBP10, MALSU1, MTERF4, NSUN4 and, in the case of GTPBP6 loss, GTPBP5^{9,12,14}. MTERF4 is a putative RNA-binding protein that forms a stable complex with the methyltransferase NSUN4^{15,16}, which modifies the 12S rRNA during mtSSU biogenesis¹⁷. However, the role of the MTERF4-NSUN4 complex in mtLSU assembly is unclear. Previous structural studies of mtLSU assembly intermediates purified from wild-type human cells revealed premature rRNA conformations and showed that MALSU1 forms a submodule with LOR8F8 and mtACP that binds to the mtLSU and likely prevents premature subunit association⁵. These results indicate that the GTPases act hierarchically and cooperate with other maturation factors during mtLSU biogenesis. However, the mechanistic basis of GTPase-driven LSU biogenesis and PTC folding is not known.

Here, we combine genetic perturbation and endogenous complex purification with *in vitro* reconstitution and cryo-electron microscopy (cryo-EM) to dissect the molecular basis of GTPase-mediated human mtLSU maturation and mitoribosome recycling.

Results and discussion

Two distinct mtLSU biogenesis intermediates accumulate in the absence of GTPBP6. We isolated mtLSU complexes from a human cell line lacking GTPBP6, which accumulate assembly intermediates that contain GTPBP7, GTPBP10, and GTPBP5 as well as MALSU1, MTERF4, and NSUN4¹². Mass-spectrometric analyses confirmed the presence of these proteins as well as all 52 MRPs (Supplementary Fig. 1a, Supplementary Data 1). We then analyzed the intermediates by single-particle cryo-EM (dataset 1). Particle classification yielded two distinct reconstructions of mtLSU assembly intermediates at overall resolutions of 2.2 and 2.5 Å, respectively, which led to refined structures (Supplementary Fig. 1b–e, Supplementary Table 1).

Compared to the mature mtLSU, both reconstructions show an extra density close to the L1 stalk and a distinct folding of the interfacial rRNA (Supplementary Fig. 1c). The density could be unambiguously fit with the crystal structure of the complex of the RNA-binding protein MTERF4 and the methyltransferase NSUN4^{15,16}, with some adjustments (Supplementary Fig. 2a, b).

Additionally, both structures contain all MRPs as well as the MALSU1-LOR8F8-mtACP module, which prevents premature subunit association⁵. However, they differ in their PTC conformation, and the second reconstruction showed an additional density above the PTC. Based on its resemblance to bacterial Obg¹⁸, we identified it as GTPBP5 (Supplementary Fig. 2c). Thus, two distinct mtLSU biogenesis intermediates accumulate in the absence of GTPBP6, one containing MTERF4-NSUN4 and one additionally containing GTPBP5.

MTERF4 binds subunit-bridging elements in the rRNA. The structure of the MTERF4-NSUN4-bound assembly intermediate reveals a distinct rRNA conformation, which appears to be stabilized by binding of MTERF4-NSUN4 to the interfacial side of the 16S rRNA (Fig. 1a, b). MTERF4 interacts with the mtLSU through contacts with h75 in the L1 stalk (nucleotides 2743–2756 and 2792–2804) and with the C-terminal tail of uL2m (residues 275–300) (Fig. 1c). In the mature mtLSU, this tail runs in between h68 and h66³. In the MTERF4-bound state, it is rearranged beneath MTERF4 and forms a helix (residues 290–295) that binds α 12 of MTERF4. Compared to previous crystal structures, the curvature of MTERF4 is altered by an inward rotation of helices α 1–8, resulting in a narrower RNA-binding groove (Supplementary Fig. 2b). NSUN4 binds to the mtLSU on top of the P loop/h80 (nucleotides 2815–2821) and h81 (nucleotides 2841–2853) (Fig. 1c), next to bL33m. The N-terminal part of mL64 runs above NSUN4, but this region is invisible, as in previous structures³. The active site of NSUN4 is positioned above h81, but the closest RNA base is more than 15 Å away from its SAM-binding site^{15,16}, suggesting that NSUN4 does not methylate the 16S rRNA, as had been shown previously¹⁹.

MTERF4 additionally contacts the interfacial rRNA segment that forms h68–h70 in the mature mtLSU. In the MTERF4-NSUN4 assembly intermediate, this region is partially unfolded and wraps over the outward-facing RNA-binding groove of MTERF4 (Fig. 1d). Although the density did not allow for atomic modeling, comparison shows that helices h68 and h69 would clash with MTERF4 in their mature conformation (Fig. 1d), indicating that MTERF4 binds a premature conformation of the interfacial rRNA. In the mature mitoribosome, h68–h70 form seven of the fifteen intersubunit bridges². MTERF4-NSUN4 may thus act as a quality-control checkpoint by sequestering the interfacial rRNA to prevent subunit joining prior to final mtLSU maturation.

GTPBP5 and NSUN4 cooperate to facilitate PTC folding. The structure of the second mtLSU intermediate reveals the structure and function of the Obg domain of GTPBP5 (Fig. 2a, b). GTPBP5 binds above the PTC and interacts primarily with the rRNA (Supplementary Fig. 2d). It consists of an N-terminal Obg domain and a C-terminal GTPase domain (Fig. 2b). The GTPase domain is poorly resolved, but the density indicates that it resides between uL11m and the sarcin-ricin loop (SRL, h95). The Obg domain extends along the PTC and contains three conserved loops at its tips (loop 1: residues 93–103, loop 2: residues 140–145, loop 3: residues 191–205)¹⁸ (Fig. 2b, Supplementary Fig. 2c, d). These loops reach into the PTC, where we additionally observe density for the N-terminal tail of NSUN4 (residues 26–37), which was invisible in the intermediate lacking GTPBP5 but becomes ordered in the presence of GTPBP5 (Fig. 2c, d).

Comparison of the two assembly intermediates shows that they differ in their PTC maturation state. In the intermediate lacking GTPBP5, the PTC is partially disordered and adopts a premature conformation (Fig. 2c). In particular, h72 (2692–2695), the PTC loop (nucleotides 2936–2946 and 2977–2992), h39 (nucleotides

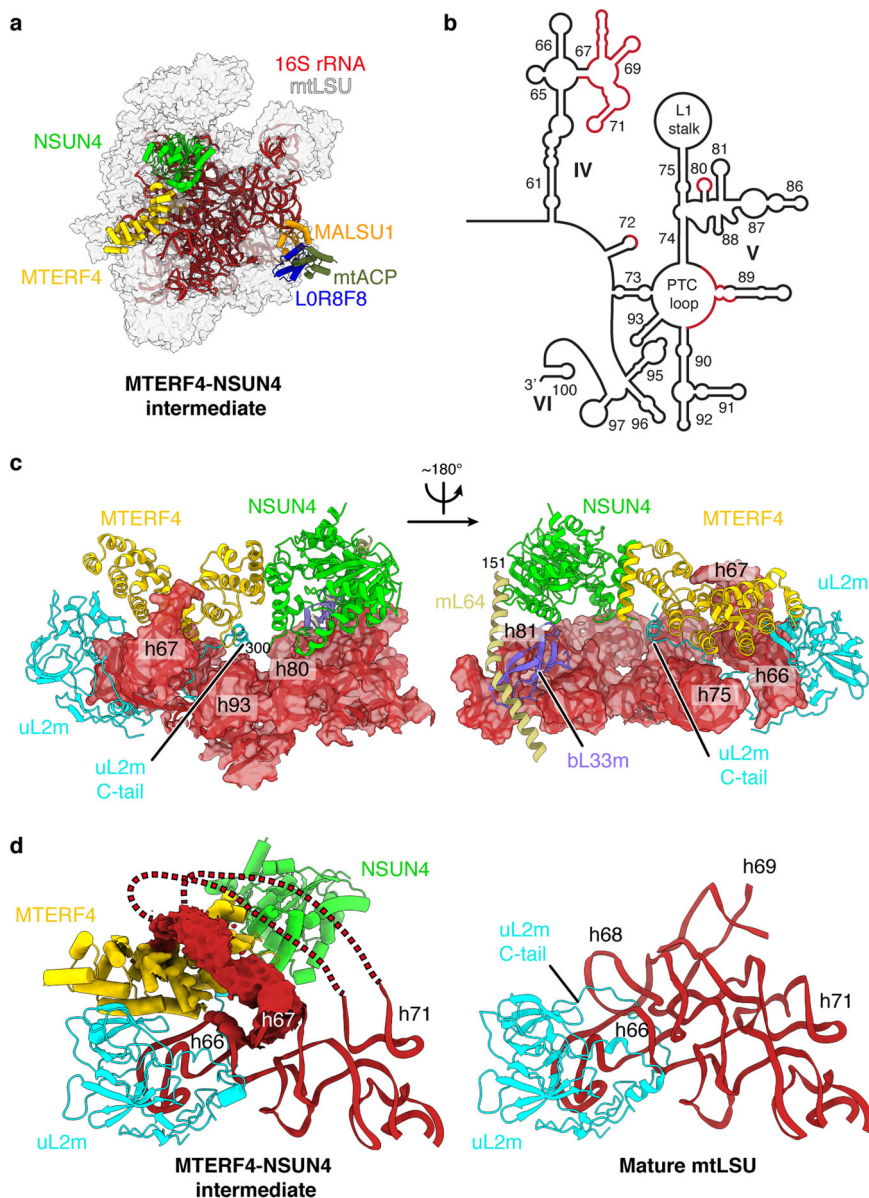


Fig. 1 Structure of the MTERF4-NSUN4-bound mtLSU assembly intermediate. **a** Cryo-EM structure of the MTERF4-NSUN4-bound large mitochondrial subunit (mtLSU) intermediate (dataset 1). The 16S rRNA (red) and indicated biogenesis factors are shown as cartoon and the remaining mitochondrial proteins (MRPs) are shown as gray transparent surface. NSUN4: lime green, MTERF4: yellow, MALSU1: orange, mtACP: olive, LOR8F8: blue. **b** Schematic depiction of the mature 16S rRNA secondary structure with domains IV–VI as indicated. Regions with distinct fold in the MTERF4-NSUN4 intermediate are depicted in red. **c** Interaction of the MTERF4-NSUN4 complex with the mtLSU. Regions of the 16S rRNA interacting with MTERF4-NSUN4 are shown as cartoon and as transparent surface. MTERF4, NSUN4, uL2m, bL33m, and mL64 are shown in cartoon representation. Coloring as in **a** and as follows: uL2m: cyan, bL33m: violet, mL64: sand. **d** (Left) In the MTERF4-NSUN4 assembly intermediate, the 16S rRNA region encompassing h68–h71 wraps above MTERF4, as indicated by red lines. The density is shown as red surface. (Right) Closeup view of the 16S rRNA region 2469–2659 in the mature mtLSU (PDB 3J7Y)³. The fold observed in the mature mtLSU would clash with MTERF4-NSUN4.

2108–2115), and the P loop/h80 (nucleotides 2814–2818) adopt distinct conformations. The PTC loop is partially mobile, and nucleotides 2975–2995 form a loop that base pairs with the tip of the P loop/h80 (Fig. 2c). In the GTPBP5-containing intermediate, the PTC adopts a more mature-like conformation in which the PTC loop forms the base of h89, and the h80 tip is shifted upward (Fig. 2d). The structures show how GTPBP5 and the NSUN4 tail facilitate these rearrangements. First, GTPBP5 and the NSUN4 tail disrupt the interaction between the PTC loop and h80, which allows the PTC loop to refold. NSUN4 sequesters bases G2817 and G2814 through stacking interactions with W31 and Y27, respectively (Fig. 2d), and GTPBP5 binds G2816 through stacking

interactions with F92 and sandwiches A3089 between F100, A202 and F92. Second, GTPBP5 stabilizes the refolded PTC conformation through backbone and base interactions with charged residues in loop 1 and loop 3 (R97, K98, E95, E99, and R201) (Fig. 2d). These rearrangements also lead to ordering of ribosomal protein elements, which are disordered in the intermediate without GTPBP5, including parts of mL63 (residues 9–21), uL10m (residues 30–36), and uL16m (residues 47–69 and 134–148).

PTC maturation also involves 2'-O-methylation of bases within the P loop/h80 (G2815) and the A loop/h92 (U3039 and G3040) catalyzed by MRM1, MRM2 and MRM3, respectively^{14,20,21}.

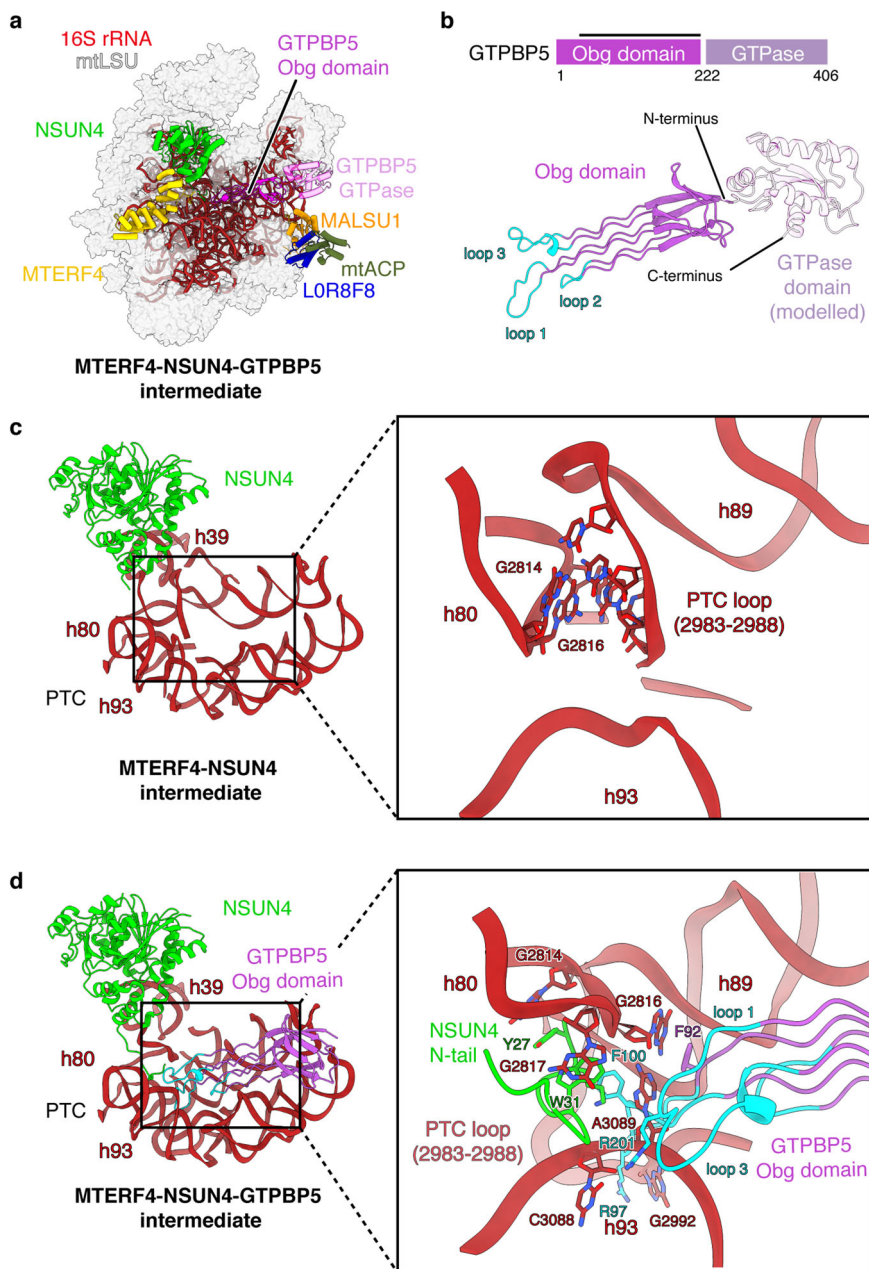


Fig. 2 GTPBP5 cooperates with NSUN4 to mature the PTC. **a** Cryo-EM structure of MTERF4-NSUN4-GTPBP5-bound large mitoribosomal subunit (mtLSU) intermediate (dataset 1). Depiction as in Fig. 1a with GTPBP5 shown in pink. **b** Structure of human GTPBP5. The protein is depicted schematically on top, with domain annotation indicated by coloring and residue numbers. The black bar above represents regions modeled in the structure. A homology model of the GTPase domain is shown transparently, but was not included in the final model. The conserved loops 1-3 that contact bases of the peptidyl transferase center (PTC) are shown in cyan. **c, d** The P loop/h80, h93, and PTC loop undergo rearrangements upon GTPBP5 binding. Closeup view of the PTC in the NSUN4-MTERF4 (**c**) and NSUN4-MTERF4-GTPBP5 (**d**) mtLSU assembly intermediates. The rRNA and proteins are shown as cartoons, with coloring as in Fig. 1. Selected bases that undergo rearrangements are indicated and highlighted as sticks. Loop 1 and 3 of GTPBP5 and the N-terminal tail of NSUN4 are shown as cartoons and residues that interact with the indicated bases are shown as sticks.

Methylation of U3039 is one of the last steps in PTC maturation and requires GTPBP5¹⁴. The cryo-EM reconstructions show density consistent with 2'-O-methylation at all these residues (Supplementary Fig. 2e), suggesting that GTPBP6 acts downstream of MRM1-3 and GTPBP5, in agreement with previous data¹². In a complementary study, Cipullo et al.²² report structures of mtLSU intermediates in complex with GTPBP5 and MRM2, which lack density for 2'-O-methylated U3039, thus indicating that these intermediates represent assembly states

upstream of the MTERF4-NSUN4-GTPBP5 intermediate described here. This suggests that MRM2 may be independently released upon catalysis while GTPBP5 can remain bound, at least in the absence of GTPBP6.

Taken together, the cryo-EM structures reveal how GTPBP5 and NSUN4 facilitate maturation of the PTC and suggest sequential PTC methylation and folding (Supplementary Movie 1). They also explain the dual-role of NSUN4 as a methyltransferase in mtSSU assembly¹⁷ and as a biogenesis factor

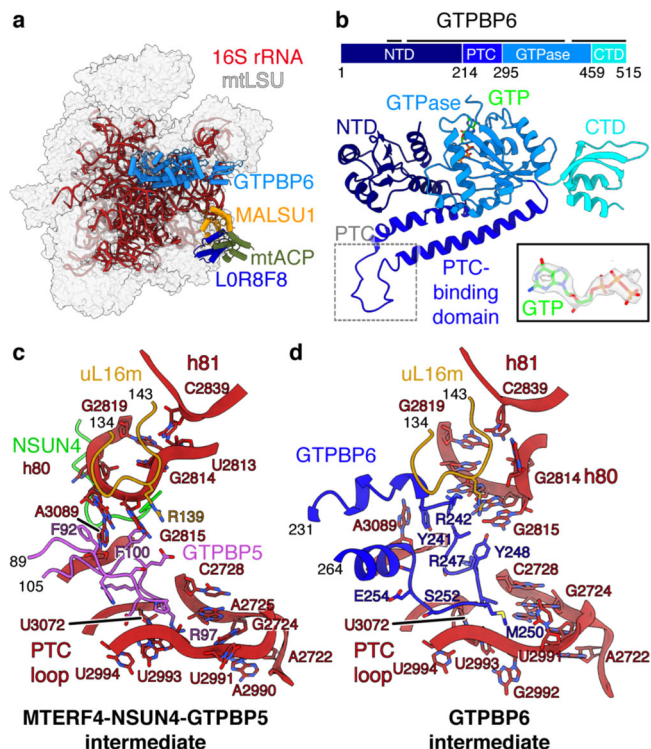


Fig. 3 GTPBP6 binding causes rearrangements in the PTC. **a** Cryo-EM structure of the GTPBP6-bound large mitoribosomal subunit (mtLSU) assembly intermediate (dataset 2). Depiction as in Fig. 1a with GTPBP6 in marine. **b** Structure of human GTPBP6. The protein is depicted schematically on top, with domain annotation indicated by coloring and residue numbers. The black bar above represents regions modeled in the structure. The density for the bound GTP is shown as indent. **c, d** Rearrangements in the peptidyl transferase center (PTC) upon GTPBP6 binding. The PTC region is shown enlarged in the MTERF4-NSUN4-GTPBP5 (**c**) and the GTPBP6 (**d**) mtLSU assembly intermediates. The rRNA and proteins are shown as cartoons, with coloring as in Fig. 2 and uL16m in ocher. NTD N-terminal domain, CTD C-terminal domain.

in mtLSU maturation, because the latter function is mediated by its N-terminal tail, which is not conserved in homologous methyltransferases that act only as small-subunit biogenesis factors, such as bacterial rsmB.

GTPBP6 displaces GTPBP5 and MTERF4-NSUN4. We next aimed to investigate the role of GTPBP6 during mtLSU biogenesis. For this, we reconstituted mtLSU maturation *in vitro* by complementing the biogenesis intermediates from GTPBP6-deficient cells with recombinant GTPBP6 in the presence of GTP and ATP. Subsequent cryo-EM analysis again revealed the MTERF4-NSUN4- and the MTERF4-NSUN4-GTPBP5-bound mtLSU complexes (dataset 2; Supplementary Fig. 3, Supplementary Table 2), which were largely identical as before but showed improved density for the interfacial rRNA and the GTPBP5 GTPase domain (see experimental procedures) (Supplementary Fig. 4a–d). In addition, classification yielded a 2.6 Å reconstruction that lacks MTERF4-NSUN4 and GTPBP5 but shows a new density that corresponds to GTPBP6 in close proximity to the L12 stalk, which allowed us to build a molecular model (Fig. 3a, b, Supplementary Figs. 3, 4e). GTPBP6 contains a N-terminal nucleotide-binding domain (NTD), a PTC-binding linker domain, a GTPase domain and a C-terminal domain (CTD) (Fig. 3b). Like GTPBP5, it binds above the PTC and primarily

interacts with rRNA (Supplementary Fig. 4f). The NTD stacks against h71, which appears stabilized compared to the MTERF4-NSUN4 state. By analogy with its bacterial homolog HflX¹², the NTD of GTPBP6 is predicted to be a putative ATP-dependent RNA helicase domain. However, we did not observe density for a bound ATP molecule, suggesting that ATP is not required for its function during ribosome biogenesis. The PTC-binding domain resides between h89 and h92, and inserts a loop (residues 241–255) deep into the PTC. The GTPase domain is located next to the NTD, on top of h89, and shows clear density for a bound GTP molecule, suggesting that GTP hydrolysis is not required for GTPBP6 binding (Fig. 3b, Supplementary Fig. 4g). The CTD is positioned between the SRL (h95) and uL11m, in a similar position as the GTPase domain of GTPBP5 (Supplementary Fig. 4f, h).

Comparison of the GTPBP6- and GTPBP5-bound structures suggests a mechanism for the hierarchical action of these factors during mtLSU biogenesis. Superimposition shows that both factors share the same binding site, and that the NTD of GTPBP6 would clash with NSUN4 (Supplementary Fig. 4h). Thus, binding of GTPBP6 and GTPBP5/MTERF4-NSUN4 is mutually exclusive, suggesting that these factors act sequentially and that GTPBP6 either triggers the release of GTPBP5/MTERF4-NSUN4 from the mtLSU or binds after their dissociation.

GTPBP6 mediates PTC maturation. Comparison to the GTPBP5-bound state also reveals that GTPBP6 further folds the PTC. The PTC-binding loop of GTPBP6 occupies the same position as loop 1 of GTPBP5, between the P loop/h80 and the PTC loop and in vicinity to uL16m (residues 134–143), and causes rearrangements in the elements (Fig. 3c, d, Supplementary Movie 1). In particular, the tip of the P loop/h80 (residues 2814–2819) refolds, which leads to elimination of a basepair between G2819 and U2813 and replacement of the latter by C2839 from h81. G2814 is flipped out of the loop to face outward, and G2815 is rearranged and may contact Y248 in GTPBP6 and R139 in uL16m. Binding of GTPBP6 also leads to movement of A3089 by replacing its interaction with F92 in GTPBP5 by a stacking interaction with Y241 in GTPBP6. Finally, nucleotides 2990–2994, 2722–2728 and U3072 in the PTC loop undergo conformational changes, which may be induced by a change in chemical environment upon exchange of maturation factors, as GTPBP6 places hydrophobic residues (L249, M250) at the position previously occupied by R97 of GTPBP5. Collectively, these rearrangements lead to a nearly mature PTC conformation.

A molecular model of GTPase-mediated PTC maturation. These structural snapshots allow us to deduce a model for GTPase-mediated mtLSU assembly and PTC maturation, which we have summarized in a molecular movie (Fig. 4, Supplementary Movie 1). First, early biogenesis factors assemble a core mtLSU with a premature PTC and partially unfolded interfacial rRNA that lacks late-stage MRPs as well as 2'-O-methylations within the PTC¹⁴. This mtLSU intermediate contains the MALSU1-LOR8F8-mtACP module and the MTERF4-NSUN4 complex, which both prevent premature subunit joining⁵. PTC methylations are then introduced by MRM1 and MRM2, leading to the intermediate with methylated but unfolded PTC. Next, GTPBP5 and NSUN4 act in concert to establish the basic architecture of the PTC. Both GTPBP5 and the MTERF4-NSUN4 are then replaced by GTPBP6, which induces further conformational changes that lead to a near-mature PTC. The release of MTERF4-NSUN4 liberates the rRNA region h68–h71, which can then adopt its final conformation to facilitate subunit joining. Final maturation steps must then involve dissociation of GTPBP6 and the MALSU1-

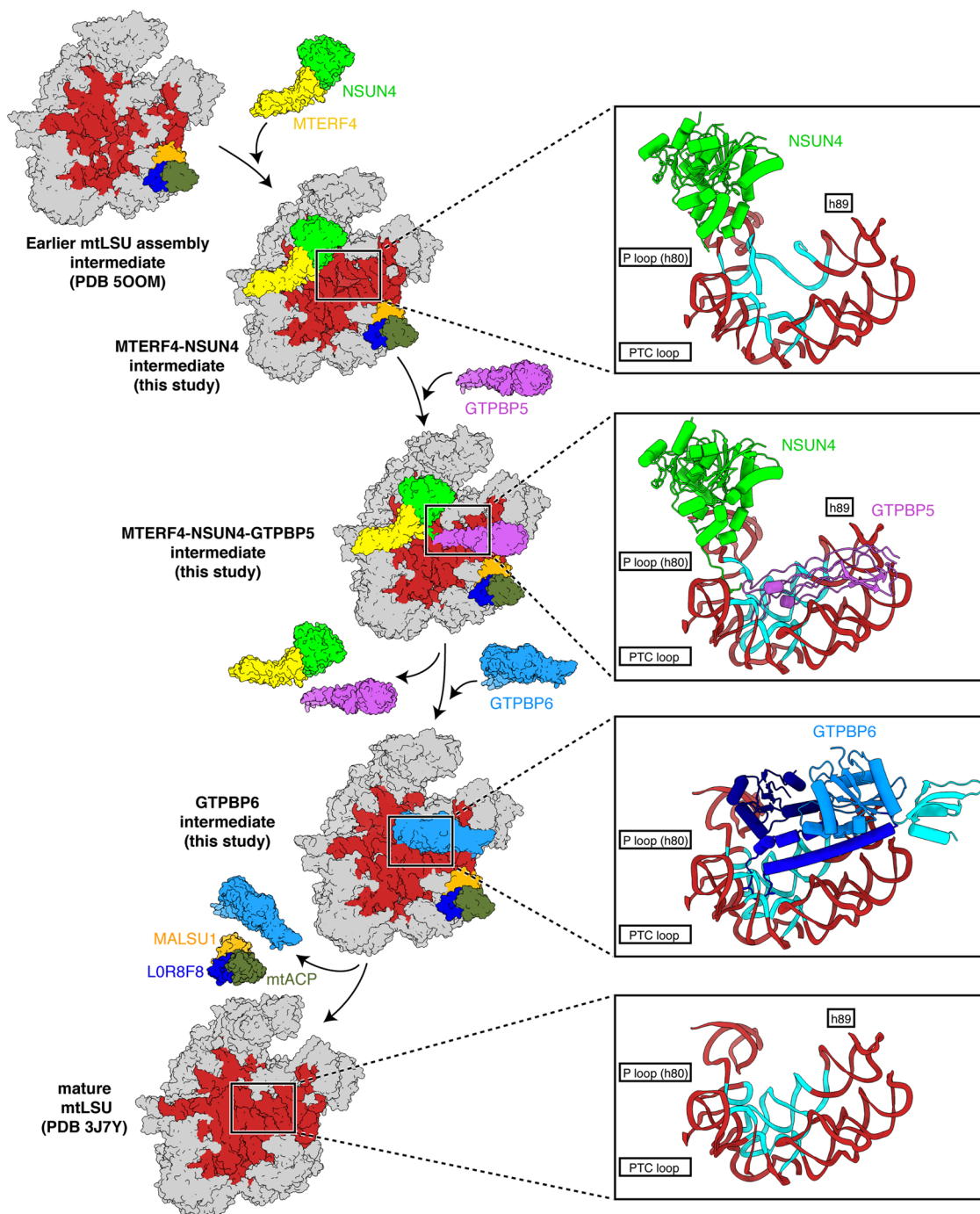


Fig. 4 Model of GTPase-mediated maturation of human mtLSU. Intermediate states of the mtLSU are depicted as surface with coloring as in Figs. 1–3. Models of immature and mature mtLSU were derived from previous studies (PDB 500M, 3J7Y)^{3,5}. Closeup views illustrate GTPase-mediated rearrangements in the peptidyl transferase center (PTC). PTC intermediate states are depicted as in Fig. 2 and Supplementary Fig. 4, with the regions undergoing conformational changes highlighted in cyan.

LOR8F8-mtACP module to allow formation of the functional 55S mitoribosome.

In addition to GTPBP5, we also observed the accumulation of GTPBP7 and GTPBP10 in the mtLSU samples isolated from GTPBP6-deficient cells (Supplementary Data 1). However, despite extensive classification efforts, we did not identify particle populations with these factors present in our cryo-EM datasets. During the revision of our manuscript, several complementary studies were published showing the binding site of these GTPases on the mtLSU^{22–24}. Like GTPBP5, GTPBP10 is a homolog of bacterial ObgE and accommodates

the same position on the mtLSU, which suggests that binding of GTPBP5 and GTPBP10 is mutually exclusive²³. Previous studies indicate that GTPBP10 is among the first GTPases that binds to the mtLSU to facilitate the final maturation steps, and thus likely acts before GTPBP5^{8,11,13}. This could explain the absence of GTPBP10-containing assembly intermediates in our datasets, as assembly of the mtLSU may progress past the GTPBP10-bound state even in GTPBP6-deficient cells. GTPBP7 appears to be somewhat flexible and may bind to the mtLSU in different orientations^{22,24,25}. The absence of detectable GTPBP7-containing particles in our mtLSU intermediates purified from

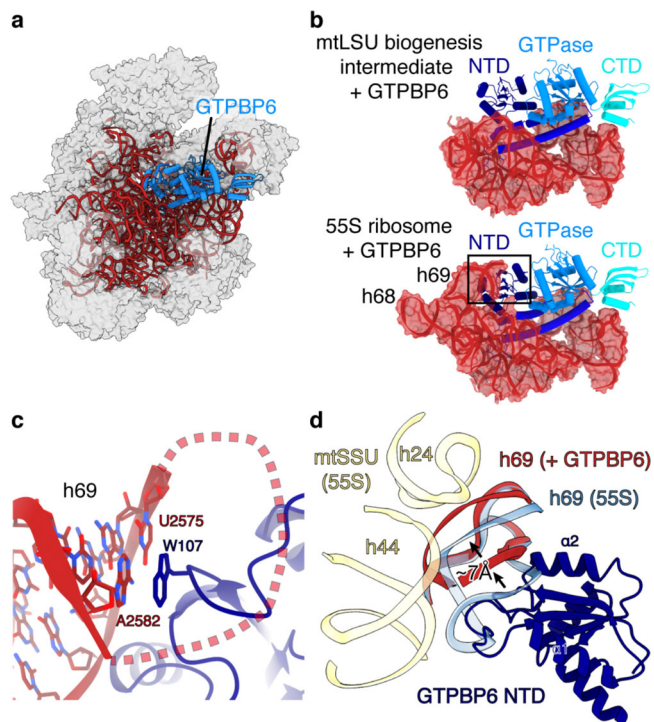


Fig. 5 Structural basis of ribosome recycling by GTPBP6. **a** Cryo-EM structure of GTPBP6 bound to the mature large mitoribosomal subunit (mtLSU) (dataset 3). The 16 s rRNA and GTPBP6 are shown as cartoon and colored as in Fig. 3. **b** Comparison of 16 rRNA interactions of GTPBP6 during biogenesis (top) and ribosome splitting (bottom). **c** GTPBP6 interacts with h69. Closeup view of h69 in the split mature mtLSU bound to GTPBP6. W107, which forms stacking interactions with h69, is shown as sticks. **d** Comparison of intersubunit-bridging elements in the 55S mitoribosome and the GTPBP6-bound split mtLSU. The GTPBP6-bound split mtLSU structure was superimposed with the structure of the elongating 55S ribosome (PDB 6ZSG)⁵². h69 is shown in blue (55S mitoribosome) or red (GTPBP6-bound mtLSU). GTPBP6 binding causes a shift of h69 by -7 \AA leading to clashes with h24 and h44 (yellow) in the small mitoribosomal subunit (mtSSU). NTD: N-terminal domain, CTD C-terminal domain.

GTPBP6-deficient cells indicates that under these conditions, GTPBP7-binding may be highly transient.

Mechanism of GTPBP6-mediated ribosome recycling. In addition to its role in mtLSU biogenesis, GTPBP6 also facilitates the dissociation of intact 55S mitoribosomes into subunits, which might be required to rescue stalled ribosomes¹². To determine the mechanism of GTPBP6-mediated ribosome splitting, we treated 55S mitoribosomes with recombinant GTPBP6 in the presence of GTP and ATP. Subsequent cryo-EM analysis revealed the presence of complete mitoribosomes as well as free mtLSU and mtSSU particles (Supplementary Fig. 5, Supplementary Table 3). Classification of the mtLSU particle population led to a reconstruction at an overall resolution of 2.7 \AA , which shows that GTPBP6 binds to the mature mtLSU in the same location as during ribosome biogenesis (Fig. 5a, b). As before, we observe GTP bound to the GTPase domain but no ATP in the NTD. This is in agreement to previous data, which showed that GTPBP6-mediated ribosome recycling requires GTP, but no ATP¹². In addition to the previously observed contacts, GTPBP6 also interacts with h69 in the mature mtLSU (Fig. 5b, c), which was unfolded in the biogenesis intermediates but forms intersubunit

contacts with the mtSSU in the 55S mitoribosome. The NTD of GTPBP6 binds to h69 and inserts a tryptophan residue (W107) next to the U2575-A2582 basepair at its tip. Superimposition with the intact mitoribosome shows that h69 is shifted by $\sim 7 \text{ \AA}$ in the GTPBP6-bound state, which would lead to clashes with h44 in the mtSSU (Fig. 5d). Thus, GTPBP6 dissociates the ribosome by rearranging elements that mediate intersubunit interactions, as has been suggested for HflX and ribosome recycling factors^{26–29}. However, its mechanism is distinct, because W107 is not conserved and HflX does not form direct contacts with bases in h69, yet causes a more prominent displacement (13 vs 7 \AA)²⁸.

The structure of GTPBP6 bound to the mature mtLSU also reveals two distinct conformations of the PTC-binding loop (Supplementary Fig. 6a). While the first is similar to that observed during mtLSU biogenesis, the second shows rearrangements in $\alpha 7$ and $\alpha 8$ and a register shift in $\alpha 5$ that translates into the PTC. This is accompanied by rearrangements of PTC bases, including A3089 (E. coli: A2602), U3072 (E. coli: 2585), and U2993 (E. coli: U2993) (Supplementary Fig. 6b), which play key roles during peptide bond formation and peptide release^{30–34} and undergo conformational changes during elongation and termination in bacteria^{32,33}. However, it is not clear whether GTPBP6 induces these rearrangements or recognizes different PTC configurations that occur during the peptide elongation cycle.

The preferred substrates of GTPBP6 are vacant ribosomes or posthydrolysis complexes with a deacylated tRNA in the P site¹². Our structural data explain this preference, as a peptidyl tRNA in the P site would prevent GTPBP6 binding. To recycle ribosomes, release factors that trigger peptide hydrolysis such as ICT1/mL62 must therefore act prior to GTPBP6, as has been suggested recently^{12,28,35}. Alternatively, GTPBP6-mediated ribosome recycling may require spontaneous hybrid P/E state formation, in agreement with *in vitro* data¹².

In summary, these results provide the structural and mechanistic basis of late mtLSU maturation by showing how universally conserved and mitochondria-specific assembly factors act in concert to mediate the step-wise folding of the PTC. This provides an important step towards understanding ribosome biogenesis in general, as GTPase-driven PTC maturation appears to be a conserved quality-control step during ribosome biogenesis throughout different domains of life. This is underscored by the high degree of structural similarity between bacterial and human mitochondrial ribosome biogenesis factors. However, their mechanisms appear to have at least partially diverged. Recent structural studies suggest that the bacterial GTPBP5/GTPBP10 homolog ObgE cooperates with the MALSU1-homolog RsfS and with factors that are not conserved in human mitochondria to prevent premature subunit joining and facilitate folding of h89³⁶. In contrast, GTPBP5 acts in concert with the mitochondria-specific N-terminal tail of NSUN4, which in turn binds MTERF4 that prevents interfacial rRNA maturation. Thus, human mitochondria appear to combine conserved ribosome maturation factor folds with organelle-specific mechanisms to achieve mtLSU maturation.

Our findings are supported by several recently published complementary studies, which provide detailed structural snapshots of earlier mtLSU maturation steps mediated by GTPBP7, GTPBP10 and GTPBP5 in conjunction with MRM2^{22–25}. Taken together, a comprehensive mechanistic picture of late mtLSU biogenesis now emerges from this large body of structural and functional information.

Methods

No statistical methods were used to predetermine sample size. The experiments were not randomized, and the investigators were not blinded to allocation during experiments and outcome assessment.

Cell culture conditions. HEK293-Flp-In T-Rex wild-type (WT) (Thermo Fisher Scientific) and *Gtpbp6*^{-/-} cell lines were grown under standard cultivation conditions¹². Briefly, cells were cultured in Dulbecco's modified Eagle's medium (DMEM) with supplements (10% FBS (Sigma), 2 mM L-glutamine (GIBCO), 1 mM sodium pyruvate (GIBCO), 50 µg/ml uridine (Sigma-Aldrich)) in 5% CO₂ humidified atmosphere at 37 °C.

Mitoplasts isolation. Cells from 100–120 cell culture plates (15 cm) were harvested and homogenized in trehalose buffer (300 mM trehalose, 10 mM KCl, 10 mM HEPES-KOH pH 7.4) with addition of 1 mM PMSF and 0.2% BSA using Homogenplus Homogenizer (Schuett-Biotec, Germany). After each homogenization step mitochondria were separated from cell debris and nuclei at 1000 × g for 10 min, 4 °C. Obtained mitochondria were pelleted for large-scale mitoplast preparation. To isolate mitoplasts, mitochondria were subjected to digitonin/proteinase K treatment (detergent to protein ratio 1:4, proteinase K to protein ratio 1:200), washed 4 times with trehalose buffer and pelleted at 25,000 × g for 15 min, 4 °C (SS34 Rotor, Beckman Coulter).

Purification of mitoribosomes. Mitoplasts were lysed in lysis buffer (20 mM Tris-HCl (pH 7.4), 100 mM NH₄Cl, 15 mM MgCl₂, 2 mM DTT, 1% Triton X-100) with detergent to protein ratio 2.5:1 and the resulting lysate was clarified by centrifugation at 16,000 × g for 15 min, 4 °C. To enrich mitoribosomal particles and to eliminate other mitochondrial protein complexes contaminants, the collected supernatant was subjected to a two-step sucrose cushion (1 M sucrose cushion/1.75 M sucrose cushion) and centrifuged for 15 h at 148,000 × g at 4 °C. Fractions were collected from top to bottom of the cushion and the fraction containing mitoribosomal particles was concentrated and subsequently washed with 5 volumes of wash buffer (100 mM NH₄Cl, 15 mM MgCl₂, 20 mM Tris-HCl (pH 7.4), 2 mM DTT) in order to reduce the sucrose concentration and the sample volume. Concentrated sample was loaded on a 15–30% sucrose gradient (15–30% (w/v) sucrose, 100 mM NH₄Cl, 15 mM MgCl₂, 20 mM Tris-HCl (pH 7.4)), centrifuged at 115,600 × g for 16 h 10 min, 4 °C (SW41Ti rotor, Beckman Coulter) and 16 fractions were collected. Each fraction was measured at 260 nm and fractions corresponding to the mtLSU or 55S mitoribosome were further concentrated and washed with wash buffer as described above. Purified mitoribosomal complexes were analysed by western blotting and stored at –80 °C, or used directly for grid preparation or for in vitro reconstitutions followed by cryo-EM analyses.

To monitor the structural rearrangements in the mtLSU upon GTPBP6-binding 0.1–0.18 µM of 39 s/55 s particles purified from *Gtpbp6*^{-/-} or WT cell lines were mixed with 20-fold molar excess of purified GTPBP6 protein in the presence of nucleotides (1 mM ATP/1 mM GTP) in reaction buffer (2 mM DTT, 100 mM NH₄Cl, 15 mM MgCl₂, 20 mM Tris-HCl (pH 7.4)). Mixtures were incubated at 4 °C for 30 min and were used directly for grid preparation.

Western blotting and immunodetection. After separation of the mitoribosomal complexes by sucrose gradient ultracentrifugation, 16 fractions were collected and analyzed by western blotting. For each fraction, ~1.4% of the total volume was resuspended in loading buffer containing 2% (w/v) SDS and 50 mM DTT (final concentration) and loaded on a 10–18% SDS Tris-Tricine gel. Ten micrograms of crude mitochondria isolated from HEK293T WT cells were used as a control. Proteins were transferred to nitrocellulose membrane Amersham™ Protran™ 0.2 µm NC (GE Healthcare) and visualized using specific antibodies. Primary polyclonal anti-rabbit antibodies used in this study (dilution is indicated in brackets): anti-NSUN4 [1:1000] (ref. ¹² Proteintech; #16320-1-AP), anti-MTERF4 [1:1000] (refs. ^{12,14} Sigma Prestige; #HPA027097; RRID:AB_10603879), anti-MALSU1 [1:1000] (ref. ¹¹ Proteintech; #22838-1-AP; RRID:AB_11182483), anti-GTPBP5 [1:1000] (refs. ^{12,14} Sigma Prestige; #HPA047379; RRID:AB_10965845), anti-GTPBP10 [1:1000] (ref. ¹¹ Novusbio; #NBP1-85055; RRID:AB_11037644), anti-bL32m [1:1000] (ref. ¹¹ gift from Prof. P. Rehling; PRAB4957), anti-uS14m [1:1000] (Proteintech; #16301-1-AP; RRID:AB_2878240). Primary monoclonal anti-mouse antibody used in this study (dilution is indicated in brackets): anti-uL3 [1:500] (Proteintech; #66130-1-IG; RRID: AB_2881529).

Cryo-EM sample preparation, data collection, and processing. Purified mtLSU or 55S mitoribosome samples (4 µL) were applied to freshly glow discharged R 3.5/1 holey carbon grids (Quantifoil) that were precoated with a 2–3 nm carbon layer using a Leica EM ACE600 coater. Prior to flash freezing in liquid ethane, the samples were incubated on the grid for 30 s in a Vitrobot MarkIV (Thermo Fisher Scientific) at 4 °C and 100% humidity and subsequently blotted for 3 s seconds with a blot force of 0. Cryo-EM data collection was performed with SerialEM³⁷ using a Titan Krios transmission electron microscope (Thermo Fisher Scientific) operated at 300 keV. Images were acquired in EFTEM mode with a slit width of 20 eV using a GIF quantum energy filter and a K3 direct electron detector (Gatan) at a nominal magnification of 81,000× corresponding to a calibrated pixel size of 1.05 Å/pixel. Exposures were recorded in counting mode with a dose rate of ~20 e⁻/px/s resulting in a total dose of 36–40 e⁻/Å² (see Supplementary Table 1–3) that was fractionated into 40 movie frames. Motion correction, CTF-estimation, particle picking were

performed on the fly using Warp³⁸. Particle extraction was performed with Relion³⁹ (dataset 1; 3-fold binned) or with Warp (dataset 2, dataset 3; unbinned).

For dataset 1 and dataset 2, particles were subjected to 2D classification followed by consensus 3D refinement using ab initio model created in cryoSPARC⁴⁰ as reference. Particles were then subjected to 3D classification without image alignment. In addition to the assembly factor-containing particles, both datasets contained two classes that resemble the mtLSU assembly intermediates previously observed in wild-type cells, which both contain the MALSU1-L0R8F8-mtACAP module and differ in their rRNA folding state and the presence of bL36m^{5,14}.

The assembly factor-containing particles were unbinned by re-extraction (dataset 1) and subjected to 3D classification using a soft mask around the interfacial rRNA region where extra density for factors was visible (Supplementary Fig. 1, 3). Particle subsets were then subjected to CTF refinement (dataset 1 and 2) and Bayesian polishing (dataset 1). Further separation of particle populations with differing PTC conformations or subtle conformational differences within factors was achieved by using soft masks and a regularization parameter of T = 100 in Relion. Final maps were obtained by gold-standard 3D refinement followed by post-processing in Relion. Focused refinements using soft masks were used to obtain improved maps for conformationally flexible regions. For dataset 3, 2D classification and initial further steps were carried out in cryoSPARC (Supplementary Fig. 5). Good classes were selected and a subset of 150,000 particles was used to generate three ab initio models, which clearly resembled the full 55S mitoribosome, the mtLSU and the mtSSU. Particles were classified into these three classes by supervised classification in cryoSPARC and the mtLSU particle subset subject to consensus 3D refinement in Relion using the model from cryoSPARC as reference. Particles were further classified without image alignment, followed by focused classification with a soft mask around the interfacial rRNA and focused classification using a mask around GTPBP6 and T = 100. This led to three particle subsets containing GTPBP6. The first two represented different PTC conformations and were refined to high resolution, while the third resembled PTC conformation 1 but lacked clear density for h69. Final maps were obtained by gold-standard 3D refinement followed by post-processing in Relion. Local resolution was estimated using Relion. Figures were prepared with Chimera⁴¹ and ChimeraX⁴².

Model building and refinement. An initial model for the MTERF4-NSUN4 intermediate was obtained by rigid-body fitting the previously reported structure of a mtLSU assembly intermediate (PDB 5OOL)⁵ and the previously reported crystal structure of the MTERF4-NSUN4 complex (PDB 4FZV)¹⁶ into the density in Chimera. The model was manually adjusted and rebuilt in Coot⁴³ and served as a starting model for the remaining structures. The model of GTPBP5 was generated by docking a homology model generated with SwissModel⁴⁴ into the density followed by manual rebuilding in Coot. The GTPase domain of GTPBP5 showed poor density and only allowed for docking and adjusting of the homology mode and was therefore omitted from the final model. The final model contains residues 74–221 of GTPBP5. The model of GTPBP6 was generated by docking a homology model generated by SwissModel into the density followed by manual rebuilding in Coot. The final model of GTPBP6 comprises residues 94–515, but residues 106–118, 424–431 and the loop contacting h69 (106–118) are invisible in the mtLSU biogenesis intermediate containing GTPBP6. Models were built and interpreted using both the unsharpened and post-processed maps. Refinement was carried out using the unsharpened maps in phenix.real_space_refine⁴⁵ with restraints for 2'-methyl-UMP generated by phenix.elbow⁴⁶. Model quality was assessed with MolProbity within the phenix suite⁴⁷. Figures were generated with ChimeraX.

Notably, the reconstructions obtained from dataset 1 lack density for parts of uL24m, bL20m and mL42, while they show strong density in the reconstructions from dataset 2. In addition, we observed extra densities close to a number of surface-exposed cysteine residues in the reconstructions from dataset 1, accompanied by slight rearrangements of some protein and RNA loops. We speculate that these densities may represent covalent adducts to the sulfhydryl groups of cysteines, which may be a result of partial oxidation during sample preparation. Overall, we observed the following major differences between the MTERF4-NSUN4 and MTERF4-NSUN4-GTPBP5 intermediates from the first and the second dataset. First, the rRNA wrapping over MTERF4 is better resolved in dataset 2, showing that it forms a helical structure (Supplementary Fig. 4a). This is supported by basic residues in MTERF4 that form a charge-complementary binding groove, as well as two potential base-binding pockets (Supplementary Fig. 4b). Second, a part of the uL2m C-tail (residues 270–284) occupies a different path than in dataset 1 (Supplementary Fig. 4c). Third, the GTPase domain of GTPBP5 is better resolved in dataset 2, which allowed rigid-body fitting of a homology model (Supplementary Fig. 4d).

Expression and purification of human GTPBP6. Human Δ43GTPBP6 was cloned into the pET-derived vector 14-C (gift from Scott Gradia; Addgene plasmid #48309; <http://n2t.net/addgene:48309>; RRID:Addgene_48309) via ligation-independent cloning (primer sequences: Supplementary Table 4). 6xHis-MPB-tagged Δ43GTPBP6 was expressed in *E.coli* BL21 (DE3) RIL cells (Merck Millipore) grown in LB media. Cells were grown to an optical density at 600 nm of 0.5 at

37 °C and protein expression was subsequently induced with 0.15 mM isopropyl β -D-1-thiogalactopyranoside at 16 °C for 18 h. Cells were collected by centrifugation, resuspended in lysis buffer (300 mM NaCl, 50 mM Na-HEPES pH 7.4, 10% (v/v) glycerol, 30 mM imidazole pH 8.0, 2 mM DTT, 0.284 μ g/ml leupeptin, 1.37 μ g/ml pepstatin, 0.17 mg/ml PMSF, and 0.33 mg/ml benzamidine) and immediately used for protein purification performed at 4 °C. The cells were lysed by sonication and the lysate was cleared by centrifugation (87,200 \times g, 4 °C, 30 min). The supernatant was applied to a HisTrap HP 5 ml column (GE Healthcare), preequilibrated in lysis buffer. The column was washed with 9.5 CV high-salt buffer (1000 mM NaCl, 50 mM Na-HEPES pH 7.4, 10% (v/v) glycerol, 30 mM imidazole pH 8.0, 2 mM DTT, 0.284 μ g/ml leupeptin, 1.37 μ g/ml pepstatin, 0.17 mg/ml PMSF, and 0.33 mg/ml benzamidine), and 9.5 CV low-salt buffer (150 mM NaCl, 50 mM Na-HEPES pH 7.4, 10% (v/v) glycerol, 30 mM imidazole pH 8.0 and 2 mM DTT). The sample was then eluted using nickel elution buffer (150 mM NaCl, 50 mM Na-HEPES pH 7.4, 10% (v/v) glycerol, 500 mM imidazole pH 8.0 and 2 mM DTT). The eluted protein was dialysed overnight in dialysis buffer (150 mM NaCl, 50 mM Na-HEPES pH 7.4, 15 mM imidazole pH 8.0, 10% (v/v) glycerol and 2 mM DTT) in the presence of 4 mg His-tagged TEV protease at 4 °C. The dialysed sample was applied to a HiTrap Heparin HP 5 ml column (GE Healthcare), preequilibrated in Buffer A (20 mM Na-HEPES pH 7.4, 10% (v/v) glycerol, 2 mM DTT) with 7.5 % Buffer B (2 M NaCl, 20 mM Na-HEPES pH 7.4, 10% (v/v) glycerol, 2 mM DTT). The protein was eluted with a linear salt gradient from 7.5–50% Buffer B and peak fractions containing GTPBP6 were collected and reappplied to a His Trap HP 5 ml column in the presence of 40 mM imidazole pH 8.0 to remove cleaved His-tagged MBP and TEV protease. The flow-through containing GTPBP6 was collected and applied to a Superdex 75 10/300 GL column (GE Healthcare) equilibrated in size exclusion buffer (70 mM NH₄Cl, 30 mM KCl, 7 mM MgCl₂, 20 mM TRIS-HCl pH 7.4, 10% (v/v) glycerol, 5 mM DTT). Peak fractions were assessed by SDS-PAGE and Coomassie staining and pooled. The protein was concentrated to ~65 mM using a MWCO 30,000 Amicon Ultra Centrifugal Filter (Merck), flash-frozen and stored at –80 °C until use.

LC-MS/MS analysis. Proteins were separated by polyacrylamide gel electrophoresis on a 4–12% gradient gel (NuPAGE, Invitrogen). After Coomassie staining, lanes were cut into 12 slices and proteins were reduced by dithiothreitol, alkylated by iodoacetamide, and digested with trypsin in-gel. Extracted peptides were vacuum-dried and subsequently resuspended in 2% acetonitrile (ACN, v/v)/0.05% trifluoroacetic acid (TFA, v/v). Peptides were measured on a QExactive HF Mass Spectrometer coupled to a Dionex UltiMate 3000 UHPLC system (both Thermo Fisher Scientific) equipped with an in-house-packed C18 column (ReproSil-Pur 120 C18-AQ, 1.9 μ m pore size, 75 μ m inner diameter, 30 cm length, Dr. Maisch GmbH). Peptides were separated applying the following gradient: mobile phase A consisted of 0.1% formic acid (FA, v/v), mobile phase B of 80% ACN/0.08% FA (v/v). The gradient started at 5% B, increasing to 10% B within 3 min, followed by a continuous increase to 46% B within 45 min, and then keeping B constant at 90% for 8 min. After each gradient the column was again equilibrated to 5% B for 2 min. The flow rate was set to 300 nL/min. MS1 full scans were acquired with a resolution of 60,000, an injection time (IT) of 50 ms and an automatic gain control (AGC) target of 1×10^6 . Dynamic exclusion (DE) was set to 30 s. MS2 spectra were acquired of the 30 most abundant precursor ions; the resolution was set to 15,000; the IT was set to 60 ms and the AGC target to 1×10^5 . Fragmentation was enforced by higher-energy collisional dissociation (HCD) at 28% NCE. Acquired raw data were analyzed by MaxQuant⁴⁸ (v. 1.6.0.1) applying default settings and enabled ‘match between runs’ option. Proteins were quantified based on their iBAQ value.

The mass spectrometry proteomics data have been deposited to the ProteomeXchange Consortium via the PRIDE⁴⁹ partner repository with the dataset identifier PXD023502. Project Name: GTPase-driven maturation of the human mitochondrial peptidyl transferase center; Project accession: PXD023502.

Bisulfite sequencing to monitor 12S-m⁵C1488 and 12S-m⁴C1486. To ensure that the accumulation of NSUN4 on the mtLSU in GTPBP6-deficient cells does not affect its second function as a methyltransferase modifying the 12S rRNA at position 1488, we analyzed the modification status of 12S-m⁵C1488 and, as a control, 12S-m⁴C1486, by subjecting DNase-treated total RNA from HEK293T wild-type and *Gtpbp6*^{-/-} cells to bisulfite sequencing^{50,51}. Bisulfite treatment was performed using the EpiTect Bisulfite kit (Qiagen) according to the manufacturer’s instructions. Deamination was performed by three cycles of incubation at 70 °C for 5 min and at 60 °C for 60 min. Samples were purified using mini Quick spin RNA columns (Roche) and the desulphonated in Tris pH 9.0 for 30 min at 37 °C. RNA was extracted using phenol:chloroform, precipitated and reverse transcribed from the 12S-m⁵C841_RT primer (Primer sequences: Supplementary Table 4) using Superscript III reverse transcriptase (Thermo) according to the manufacturer’s instructions. A 70-nt fragment of the 12S rRNA was amplified by PCR (Primer sequences: Supplementary Table 4) and cloned using a TOPO-TA kit (Thermo). Clones were sequenced at Eurofins Genomics using the T7 primer and only sequences in which all cytosines (disregarding C1486 and C1488) were converted to uracil/thymine were used for the presented analysis (Supplementary Fig. 6c).

Reporting summary. Further information on research design is available in the Nature Research Reporting Summary linked to this article.

Data availability

The electron density reconstructions and structure coordinates were deposited with the Electron Microscopy Database (EMDB) under accession codes EMD-12865, EMD-12872, EMD-12867, EMD-12868, EMD-12870, EMD-12869, EMD-12871, and with the Protein Data Bank (PDB) under accession codes 7OF0 [<https://doi.org/10.2210/pdb7OF0/pdb>], 7OF7 [<https://doi.org/10.2210/pdb7OF7/pdb>], 7OF2 [<https://doi.org/10.2210/pdb7OF2/pdb>], 7OF3 [<https://doi.org/10.2210/pdb7OF3/pdb>], 7OF5 [<https://doi.org/10.2210/pdb7OF5/pdb>], 7OF4 [<https://doi.org/10.2210/pdb7OF4/pdb>], and 7OF6 [<https://doi.org/10.2210/pdb7OF6/pdb>]. The mass spectrometry proteomics data have been deposited to the ProteomeXchange Consortium with the dataset identifier PXD023502. Material will be available upon reasonable request. Source data are provided with this paper.

Received: 2 March 2021; Accepted: 7 May 2021;

Published online: 16 June 2021

References

- Ferrari, A., Del’Olio, S. & Barrientos, A. The diseased mitoribosome. *FEBS Lett.* **233**, 657 (2020).
- Amunts, A., Brown, A., Toots, J., Scheres, S. H. W. & Ramakrishnan, V. Ribosome. The structure of the human mitochondrial ribosome. *Science* **348**, 95–98 (2015).
- Brown, A. et al. Structure of the large ribosomal subunit from human mitochondria. *Science* **346**, 718–722 (2014).
- Jaskolowski, M. et al. Structural insights into the mechanism of mitoribosomal large subunit biogenesis. *Mol. Cell* **79**, 629–644 (2020).
- Brown, A. et al. Structures of the human mitochondrial ribosome in native states of assembly. *Nat. Struct. Mol. Biol.* **24**, 866–869 (2017).
- Nikolay, R. et al. Structural visualization of the formation and activation of the 50 s ribosomal subunit during In vitro reconstitution. *Mol. Cell* **70**, 881–893.e3 (2018).
- Kummer, E. & Ban, N. Mechanisms and regulation of protein synthesis in mitochondria. *Nat. Rev. Mol. Cell Biol.* <https://doi.org/10.1038/s41580-021-00332-2> (2021).
- Maiti, P., Lavdovskaia, E., Barrientos, A. & Richter-Dennerlein, R. Role of GTPases in driving mitoribosome assembly. *Trends Cell Biol.* **31**, 284–297 (2021).
- Cipullo, M. et al. Human GTPBP5 is involved in the late stage of mitoribosome large subunit assembly. *Nucleic Acids Res.* **242**, 2172 (2020).
- Kim, H.-J. & Barrientos, A. MTG1 couples mitoribosome large subunit assembly with intersubunit bridge formation. *Nucleic Acids Res.* **46**, 8435–8453 (2018).
- Lavdovskaia, E. et al. The human Obg protein GTPBP10 is involved in mitoribosomal biogenesis. *Nucleic Acids Res.* **46**, 8471–8482 (2018).
- Lavdovskaia, E. et al. Dual function of GTPBP6 in biogenesis and recycling of human mitochondrial ribosomes. *Nucleic Acids Res.* **48**, 12929–12942 (2020).
- Maiti, P., Kim, H.-J., Tu, Y.-T. & Barrientos, A. Human GTPBP10 is required for mitoribosome maturation. *Nucleic Acids Res.* **46**, 11423–11437 (2018).
- Maiti, P., Antonicka, H., Gingras, A.-C., Shoubridge, E. A. & Barrientos, A. Human GTPBP5 (MTG2) fuels mitoribosome large subunit maturation by facilitating 16 s rRNA methylation. *Nucleic Acids Res.* **348**, 95 (2020).
- Spähr, H., Habermann, B., Gustafsson, C. M., Larsson, N.-G. & Hallberg, B. M. Structure of the human MTERF4-NSUN4 protein complex that regulates mitochondrial ribosome biogenesis. *Proc. Natl Acad. Sci. USA* **109**, 15253–15258 (2012).
- Yakubovskaya, E. et al. Structure of the essential MTERF4:NSUN4 protein complex reveals how an MTERF protein collaborates to facilitate rRNA modification. *Structure* **20**, 1940–1947 (2012).
- Metodieva, M. D. et al. NSUN4 is a dual function mitochondrial protein required for both methylation of 12 s rRNA and coordination of mitoribosomal assembly. *PLoS Genet.* **10**, e1004110 (2014).
- Feng, B. et al. Structural and functional insights into the mode of action of a universally conserved Obg GTPase. *PLoS Biol.* **12**, e1001866 (2014).
- Metodieva, M. D. et al. NSUN4 is a dual function mitochondrial protein required for both methylation of 12 s rRNA and coordination of mitoribosomal assembly. *PLoS Genet.* **10**, e1004110–e1004111 (2014).
- Lee, K.-W. & Bogenhagen, D. F. Assignment of 2'-O-methyltransferases to modification sites on the mammalian mitochondrial large subunit 16 s ribosomal RNA (rRNA). *J. Biol. Chem.* **289**, 24936–24942 (2014).
- Rorbach, J. et al. MRM2 and MRM3 are involved in biogenesis of the large subunit of the mitochondrial ribosome. *Mol. Biol. Cell* **25**, 2542–2555 (2014).

22. Cipullo, M., Gesé, G. V., Khawaja, A., Hällberg, B. M. & Rorbach, J. Structural basis for late maturation steps of the human mitoribosomal large subunit. *Nat. Commun.* <https://doi.org/10.1038/s41467-021-23617-8> (2021).
23. Cheng, J., Berninghausen, O. & Beckmann, R. A distinct assembly pathway of the human 39 s late pre-mitoribosome. *bioRxiv* <https://doi.org/10.1101/2021.03.17.435838> (2021).
24. Chandrasekaran, V. et al. Visualising formation of the ribosomal active site in mitochondria. *bioRxiv* <https://doi.org/10.1101/2021.03.19.436169> (2021).
25. Lenarcic, T. et al. Stepwise maturation of the peptidyl transferase region of human mitoribosomes. *Nat. Commun.* <https://doi.org/10.1038/s41467-021-23811-8> (2021).
26. Gao, N. et al. Mechanism for the disassembly of the posttermination complex inferred from cryo-EM studies. *Mol. Cell* **18**, 663–674 (2005).
27. Koriopella, R. K., Sharma, M. R., Risteff, P., Keshavan, P. & Agrawal, R. K. Structural insights into unique features of the human mitochondrial ribosome recycling. *Proc. Natl Acad. Sci. USA* **116**, 8283–8288 (2019).
28. Zhang, Y. et al. HflX is a ribosome-splitting factor rescuing stalled ribosomes under stress conditions. *Nat. Struct. Mol. Biol.* **22**, 906–913 (2015).
29. Zhou, D., Tanzawa, T., Lin, J. & Gagnon, M. G. Structural basis for ribosome recycling by RRF and tRNA. *Nat. Struct. Mol. Biol.* **27**, 25–32 (2020).
30. Polacek, N. et al. The critical role of the universally conserved A2602 of 23 s ribosomal RNA in the release of the nascent peptide during translation termination. *Mol. Cell* **11**, 103–112 (2003).
31. Schmeing, T. M., Huang, K. S., Strobel, S. A. & Steitz, T. A. An induced-fit mechanism to promote peptide bond formation and exclude hydrolysis of peptidyl-tRNA. *Nature* **438**, 520–524 (2005).
32. Voorhees, R. M., Weixlbaumer, A., Loakes, D., Kelley, A. C. & Ramakrishnan, V. Insights into substrate stabilization from snapshots of the peptidyl transferase center of the intact 70 s ribosome. *Nat. Struct. Mol. Biol.* **16**, 528–533 (2009).
33. Weixlbaumer, A. et al. Insights into translational termination from the structure of RF2 bound to the ribosome. *Science* **322**, 953–956 (2008).
34. Youngman, E. M., Brunelle, J. L., Kochaniak, A. B. & Green, R. The active site of the ribosome is composed of two layers of conserved nucleotides with distinct roles in peptide bond formation and peptide release. *Cell* **117**, 589–599 (2004).
35. Richter, R. et al. A functional peptidyl-tRNA hydrolase, ICT1, has been recruited into the human mitochondrial ribosome. *EMBO J.* **29**, 1116–1125 (2010).
36. Nikolay, R. et al. Snapshots of native pre-50 s ribosomes reveal a biogenesis factor network and evolutionary specialization. *Mol. Cell* **81**, 1200–1215.e9 (2021).
37. Mastrorarde, D. N. Automated electron microscope tomography using robust prediction of specimen movements. *J. Struct. Biol.* **152**, 36–51 (2005).
38. Tegunov, D. & Cramer, P. Real-time cryo-electron microscopy data preprocessing with Warp. *Nat. Methods* **16**, 1146–1152 (2019).
39. Zivanov, J., Nakane, T. & Scheres, S. H. W. A Bayesian approach to beam-induced motion correction in cryo-EM single-particle analysis. *IUCr* **6**, 5–17 (2019).
40. Punjani, A., Rubinstein, J. L., Fleet, D. J. & Brubaker, M. A. cryoSPARC: algorithms for rapid unsupervised cryo-EM structure determination. *Nat. Methods* **14**, 290–296 (2017).
41. Huang, C. C., Meng, E. C., Morris, J. H., Pettersen, E. F. & Ferrin, T. E. Enhancing UCSF Chimera through web services. *Nucleic Acids Res.* **42**, W478–W484 (2014).
42. Pettersen, E. F. et al. UCSF ChimeraX: structure visualization for researchers, educators, and developers. *Protein Sci.* **30**, 70–82 (2021).
43. Emsley, P., Lohkamp, B., Scott, W. G. & Cowtan, K. Features and development of Coot. *Acta Crystallogr. D Biol. Crystallogr.* **66**, 486–501 (2010).
44. Waterhouse, A. et al. SWISS-MODEL: homology modelling of protein structures and complexes. *Nucleic Acids Res.* **46**, W296–W303 (2018).
45. Afonine, P. V. et al. Real-space refinement in PHENIX for cryo-EM and crystallography. *Acta Crystallogr. D Biol. Crystallogr.* **74**, 531–544 (2018).
46. Moriarty, N. W., Grosse-Kunstleve, R. W. & Adams, P. D. Electronic Ligand Builder and Optimization Workbench (eLBOW): a tool for ligand coordinate and restraint generation. *Acta Crystallogr. D Biol. Crystallogr.* **65**, 1074–1080 (2009).
47. Williams, C. J. et al. MolProbity: More and better reference data for improved all-atom structure validation. *Protein Sci.* **27**, 293–315 (2018).
48. Cox, J. & Mann, M. MaxQuant enables high peptide identification rates, individualized p.p.b.-range mass accuracies and proteome-wide protein quantification. *Nat. Biotechnol.* **26**, 1367–1372 (2008).
49. Perez-Riverol, Y. et al. The PRIDE database and related tools and resources in 2019: improving support for quantification data. *Nucleic Acids Res.* **47**, D442–D450 (2018).
50. Schaefer, M., Pollex, T., Hanna, K. & Lyko, F. RNA cytosine methylation analysis by bisulfite sequencing. *Nucleic Acids Res.* **37**, e12–e12 (2009).
51. Haag, S. et al. NSUN3 and ABH1 modify the wobble position of mt-tRNA^{Met} to expand codon recognition in mitochondrial translation. *EMBO J.* **35**, 2104–2119 (2016).
52. Aibara, S., Singh, V., Modelska, A. & Amunts, A. Structural basis of mitochondrial translation. *elife* **9**, 531 (2020).

Acknowledgements

We thank Peter Rehling for providing antibodies. We thank Christian Dienemann and Ulrich Steuerwald for support with cryo-EM sample preparation and data acquisition. This work was funded by the Deutsche Forschungsgemeinschaft by the Emmy-Noether grant [RI 2715/1-1 to R.R.-D.]; the Excellence Cluster [EXC 2067/1-390729940 to R.R.-D. and H.S.H.]; the Forschergruppe 2848 [to H.S.H.], the Collaborative Research Center [SFB860 to R.R.-D., K.E.B., and H.U.; SFB1190 to H.S.H.]; and the Max Planck Society [to H.U.]. We acknowledge support by the Open Access Publication Funds of the Göttingen University.

Author contributions

R.R.-D. and H.S.H. designed the study. H.S.H. prepared samples for cryo-EM, collected and processed cryo-EM data, built and interpreted structural models. E.L. and F.N. isolated ribosome complexes from human cells. E.H. established ribosome purification strategy. A.L. and H.U. performed mass spectrometry analysis. K.E.B. performed the bisulfite sequencing. H.S.H., E.L., and R.R.-D. prepared figures. H.S.H. and R.R.-D. wrote the manuscript.

Funding

Open Access funding enabled and organized by Projekt DEAL.

Competing interests

The authors declare no competing interests.

Additional information

Supplementary information The online version contains supplementary material available at <https://doi.org/10.1038/s41467-021-23702-y>.

Correspondence and requests for materials should be addressed to H.S.H. or R.R.-D.

Peer review information *Nature Communications* thanks Sebastian Klinge, Robert Lightowers, and other, anonymous, reviewers for their contributions to the peer review of this work. Peer review reports are available.

Reprints and permission information is available at <http://www.nature.com/reprints>

Publisher's note Springer Nature remains neutral with regard to jurisdictional claims in published maps and institutional affiliations.



Open Access This article is licensed under a Creative Commons Attribution 4.0 International License, which permits use, sharing, adaptation, distribution and reproduction in any medium or format, as long as you give appropriate credit to the original author(s) and the source, provide a link to the Creative Commons license, and indicate if changes were made. The images or other third party material in this article are included in the article's Creative Commons license, unless indicated otherwise in a credit line to the material. If material is not included in the article's Creative Commons license and your intended use is not permitted by statutory regulation or exceeds the permitted use, you will need to obtain permission directly from the copyright holder. To view a copy of this license, visit <http://creativecommons.org/licenses/by/4.0/>.

© The Author(s) 2021

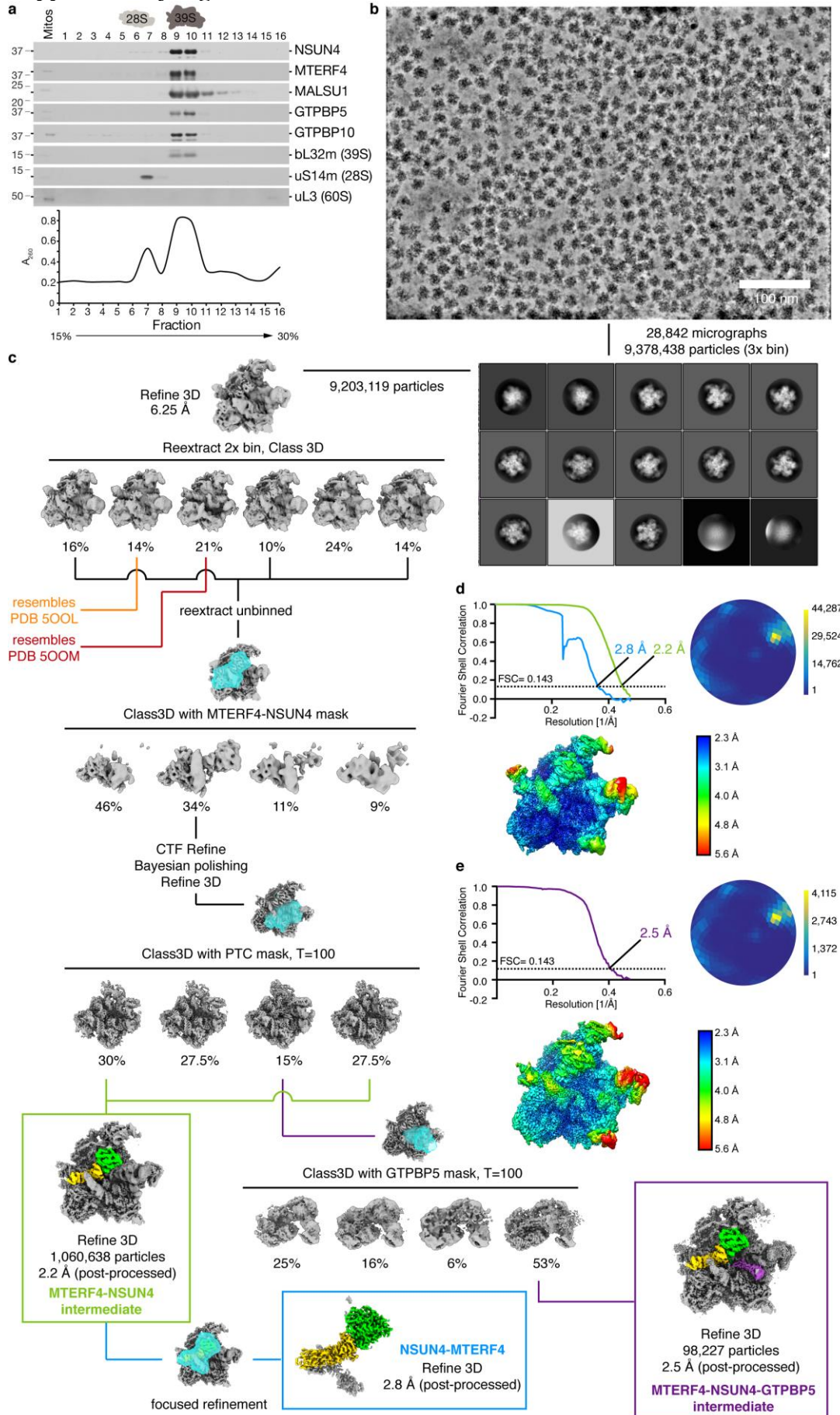
Structural basis of GTPase-mediated mitochondrial ribosome biogenesis and recycling

Hauke S. Hillen^{1,2,3,*}, Elena Lavdovskaia^{1,2}, Franziska Nadler¹, Elisa Hanitsch¹, Andreas Linden^{4,5}, Katherine E. Bohnsack⁶, Henning Urlaub^{4,5} and Ricarda Richter-Dennerlein^{1,2,*}

SUPPLEMENTARY DATA

Structural basis of GTPase-mediated mitochondrial ribosome biogenesis and recycling

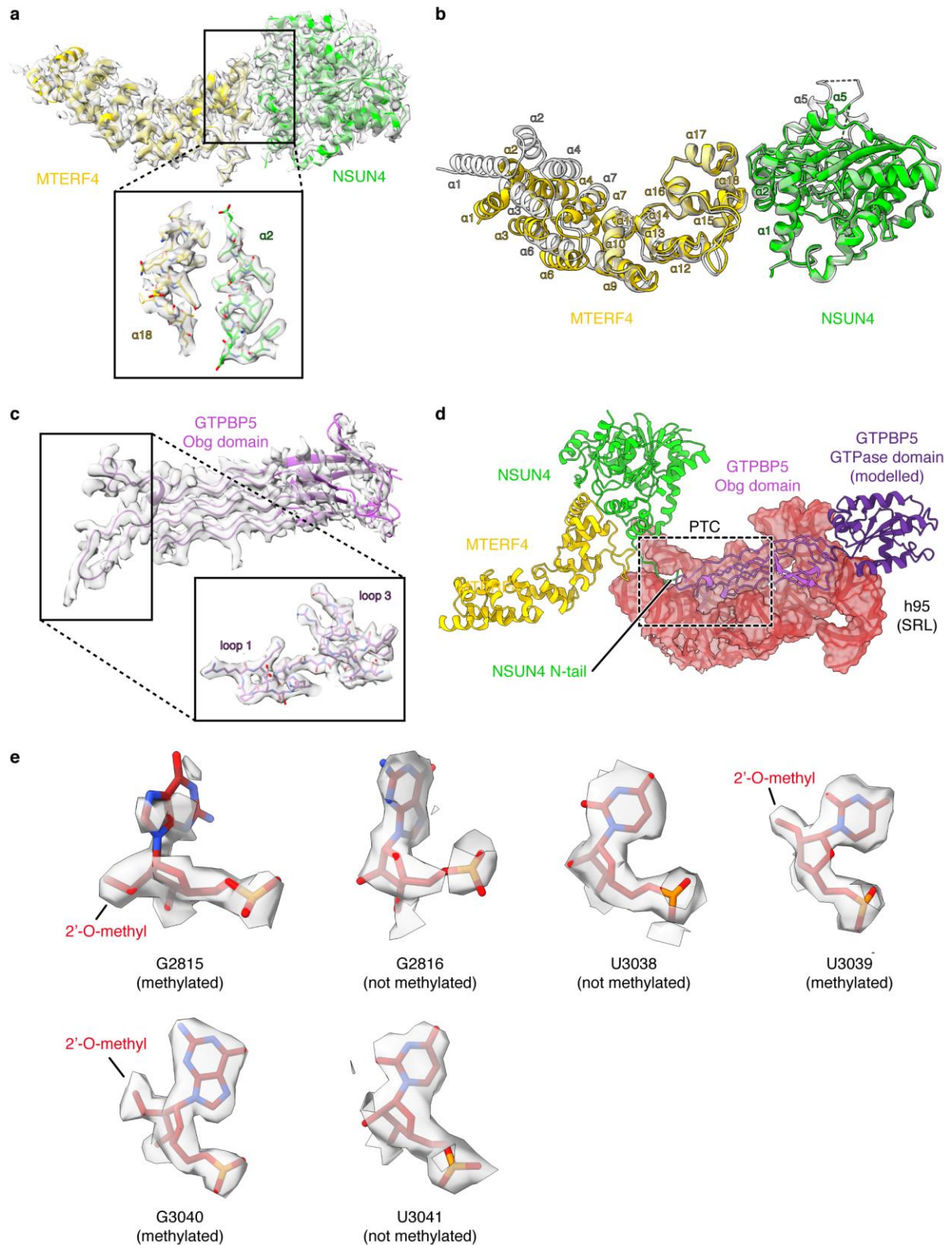
Supplementary Figures



Supplementary Fig. 1 | Purification and Cryo EM data processing first dataset.

(a) Gradient fractions (1-16) upon ribosome isolation were analyzed by western blotting using indicated antibodies. uL3 (component of the cytosolic 60S large ribosomal subunit (LSU)) was used as a control to assess the level of contamination with cytosolic ribosomes. Absorbance was measured for each fraction at 260 nm. Fractions 8 and 9 were used for further analyses. The experiment was performed twice with reproducible outcome. Source data are provided as a Source Data file. (b) Example denoised micrograph calculated from two independently measured half sets of 40 frames each. Scale bar, 100 nm. (c) 2D class averages and Cryo-EM processing tree. (d) Fourier shell correlation (FSC) plot, Angular distribution plot and local resolution distribution for the MTERF4-NSUN4 large mitoribosomal subunit (mtLSU) intermediate. Scale for the angular distribution plot shows the number of particles assigned to a particular angular bin. Blue, a low number of particles; yellow, a high number of particles. (e) FSC plot, Angular distribution plot and local resolution distribution for the MTERF4-NSUN4-GTPBP5 mtLSU intermediate. Scale for the angular distribution plot shows the number of particles assigned to a particular angular bin. Blue, a low number of particles; yellow, a high number of particles.

Structural basis of GTPase-mediated mitochondrial ribosome biogenesis and recycling



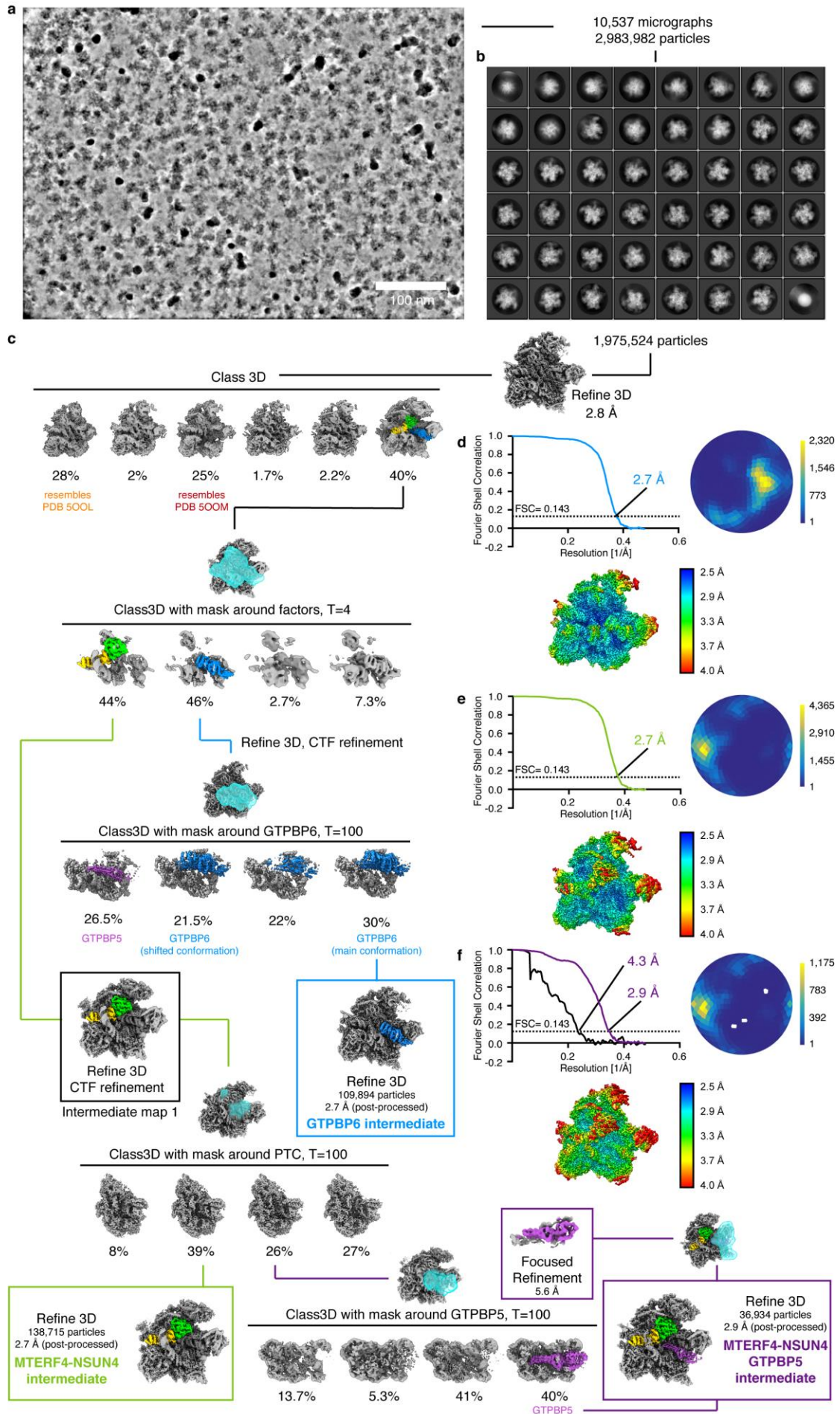
Supplementary Fig. 2 | Structural details of MTERF4, NSUN4 and ribosomal RNA.

(a) Density fit of MTERF4-NSUN4. The model of MTERF4-NSUN4 is shown as cartoon with coloring as in Fig. 1. The post-processed cryo-EM density from focused refinement is shown as transparent grey surface. The region at the interface between MTERF4 and NSUN4 is enlarged and shown as sticks. **(b)** Comparison between the MTERF4-NSUN4 complex bound to the large mitoribosomal subunit (mtLSU) and the previous crystal structure (PDB 4FP9)¹⁵. The two structures are shown superimposed as cartoon. The mtLSU-bound structure is colored

Structural basis of GTPase-mediated mitochondrial ribosome biogenesis and recycling

as in Fig. 1 and the free crystal structure is colored in grey and shown transparently. Secondary structure elements in MTERF4 and that adopt different conformations in NSUN4 are indicated. The helical repeats of MTERF4 form a widened curve when bound to the ribosome. **(c)** Density fit of GTPBP5. The model of GTPBP5 is shown as cartoon with coloring as in Fig. 2. The post-processed cryo-EM density is shown as transparent grey surface. The PTC-interacting loops described in Fig. 2 are shown enlarged as sticks. **(d)** Interaction of GTPBP5 with the mtLSU. Regions of the 16S rRNA interacting with MTERF4-NSUN4 are shown as cartoon and as transparent surface. MTERF4, NSUN4 and GTPBP5 are shown as cartoons. SRL: sarcin-ricin loop. **(e)** G2815, U3039 and G3040 are methylated. G2815, U3039 and G3040 are shown as sticks with the post-processed cryo-EM density of the MTERF4-NSUN4-GTPBP5 mtLSU intermediate (dataset 1) shown as transparent surface. Neighboring non-methylated bases are shown for comparison.

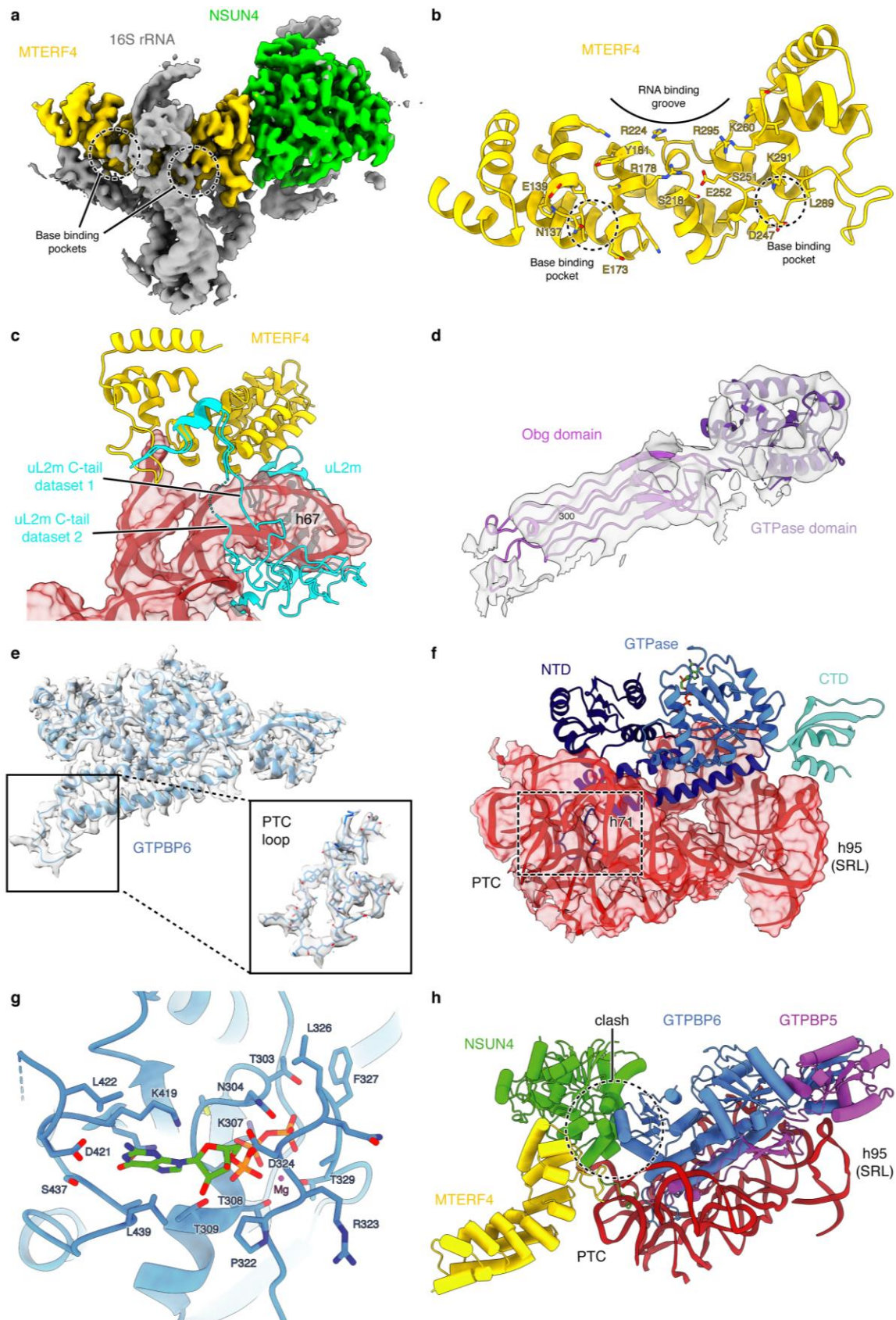
Structural basis of GTPase-mediated mitochondrial ribosome biogenesis and recycling



Supplementary Fig. 3 | Cryo-EM data processing second dataset.

(a) Example denoised micrograph calculated from two independently measured half sets of 40 frames each. Scale bar, 100 nm. (b) 2D class averages. (c) Cryo-EM processing tree. (d) Fourier shell correlation (FSC) plot, Angular distribution plot and local resolution distribution for the GTPBP6-bound large mitoribosomal subunit (mtLSU) intermediate. Scale for the angular distribution plot shows the number of particles assigned to a particular angular bin. Blue, a low number of particles; yellow, a high number of particles. (e) Fourier shell correlation (FSC) plot, Angular distribution plot and local resolution distribution for the MTERF4-NSUN4 mtLSU intermediate. Scale for the angular distribution plot shows the number of particles assigned to a particular angular bin. Blue, a low number of particles; yellow, a high number of particles. (f) FSC plot, Angular distribution plot and local resolution distribution for the MTERF4-NSUN4-GTPBP5 mtLSU intermediate. Scale for the angular distribution plot shows the number of particles assigned to a particular angular bin. Blue, a low number of particles; yellow, a high number of particles.

Structural basis of GTPase-mediated mitochondrial ribosome biogenesis and recycling



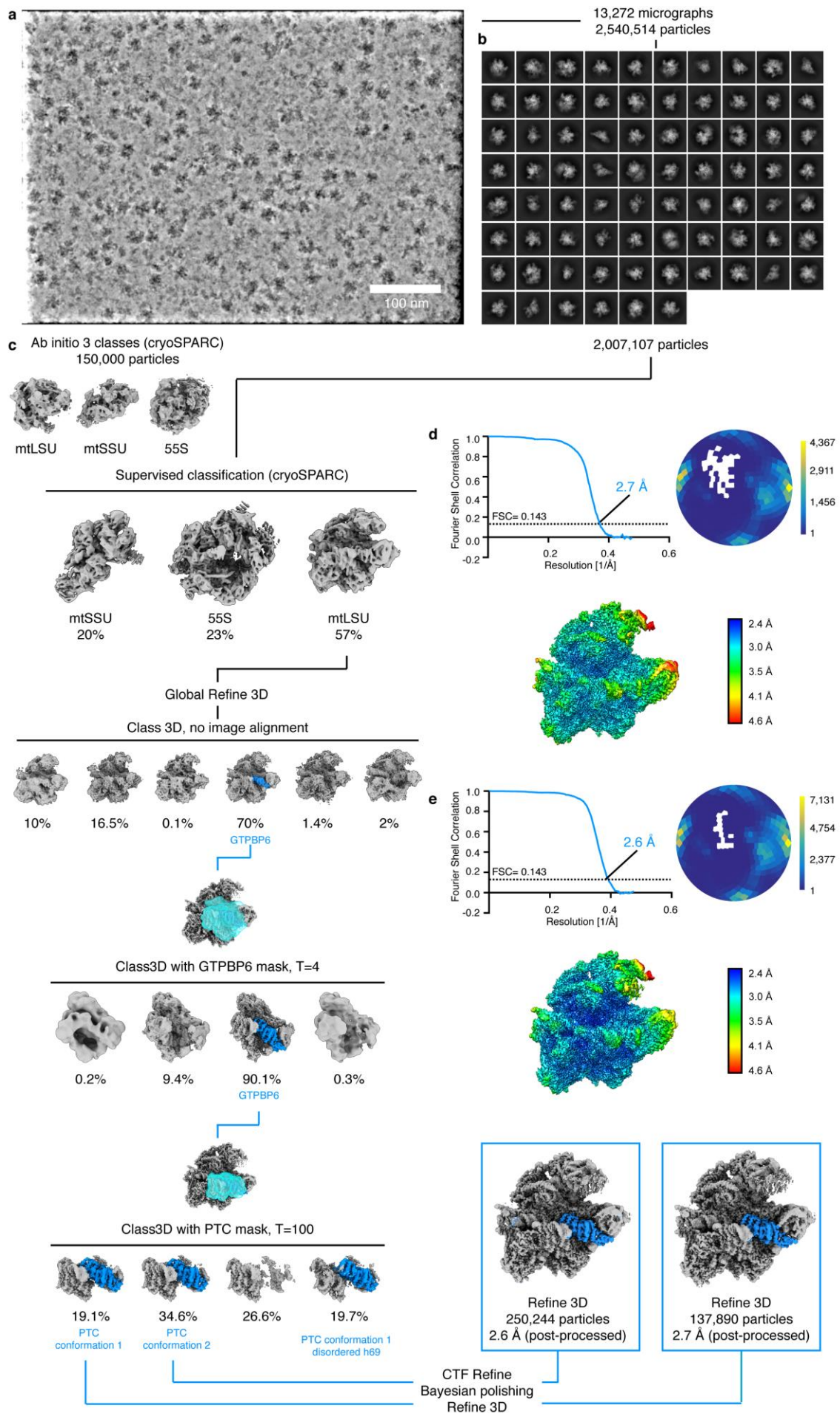
Supplementary Fig. 4 | Structural details of MTERF4, NSUN4, GTPBP5 and GTPBP6 in the second dataset.

(a) Improved density for the 16 rRNA region wrapping over MTERF4. A region of the cryo-EM reconstruction (Intermediate map 1, Supplementary Fig. 3) of MTERF4-NSUN4

Structural basis of GTPase-mediated mitochondrial ribosome biogenesis and recycling

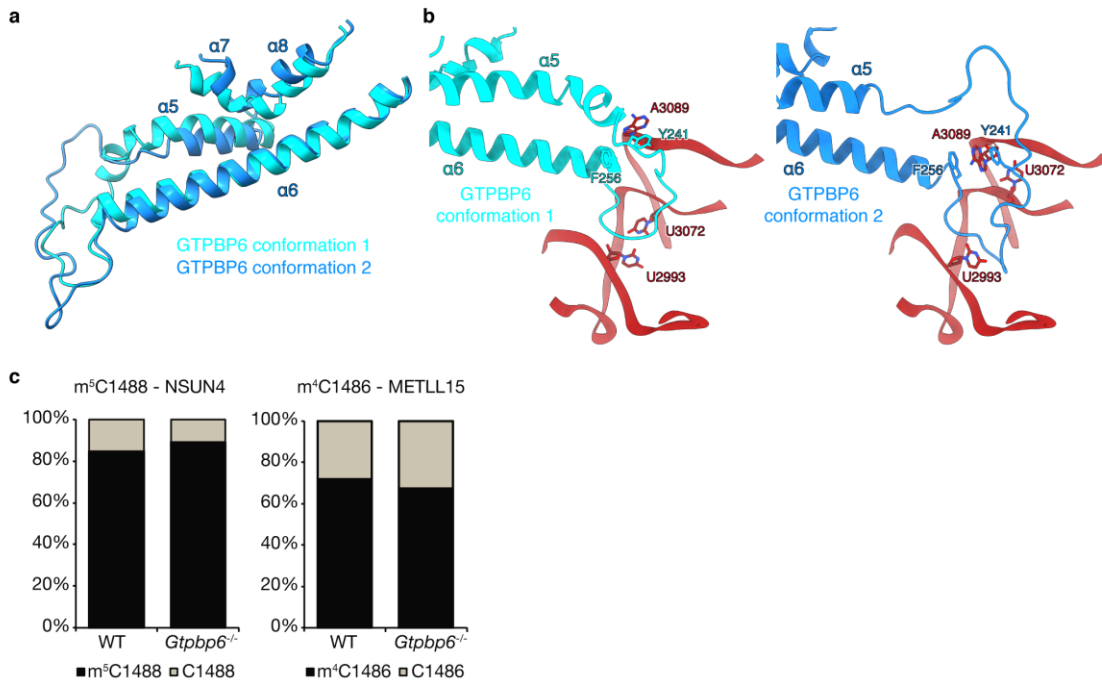
containing particles from dataset 2 is shown as surface and colored as follows: NSUN4: lime green, MTERF4: yellow, 16S rRNA: grey. The region of the rRNA wrapping above MTERF4 adopts a helical fold and may form base-mediated interactions with MTERF4 (indicated). **(b)** Close-up view of the RNA-binding groove of MTERF4. MTERF4 is shown as cartoon in yellow and residues close to the RNA density observed in (a) are shown as sticks. The potential base-binding pockets are indicated. **(c)** The C-tail of uL2m occupies different paths in the MTERF4-NSUN4 mtLSU intermediate from dataset 1 and dataset 2. MTERF4 and uL2m are shown as cartoons and the 16S rRNA elements interacting with them are shown as cartoon and transparent surface. Coloring as in Fig. 1. **(d)** Improved density for the GTPBP5 GTPase domain in dataset 2. GTPBP5 is shown as cartoon and colored as in Fig. 2. The cryo-EM density obtained from focused refinement of the GTPBP5-containing particle set in dataset 2 is shown as transparent grey surface. **(e)** Density fit of GTPBP6. GTPBP6 is shown as cartoon and colored in blue. The post-processed cryo-EM density of the GTPBP6-bound mtLSU intermediate structure is shown as transparent grey surface. The PTC loop described in Fig. 3 is shown enlarged as sticks. **(f)** Interaction of GTPBP6 with the mtLSU. Regions of the 16S rRNA interacting with GTPBP6 are shown as cartoon and as transparent surface. GTPBP6 is shown as cartoon. **(g)** GTP binding pocket of GTPBP6. The GTP binding site of GTPBP6 is shown as cartoon and colored as in Fig. 3. Residues within 4 Å of GTP are shown as sticks. GTP is shown in green as sticks. **(h)** GTPBP6 occupies the same binding site as GTPBP5 on the mtLSU and would clash with NSUN4. The structure of the MTERF4-NSUN4-GTPBP5 intermediate and the GTPBP6 intermediate were superimposed with their 16S rRNA. The peptidyl transferase center (PTC) and factors are shown as cartoons and colored as in Fig. 1-3. SRL: sarcin-ricin loop.

Structural basis of GTPase-mediated mitochondrial ribosome biogenesis and recycling



Supplementary Fig. 5 | Cryo-EM data processing third dataset.

(a) Example denoised micrograph calculated from two independently measured half sets of 40 frames each. Scale bar, 100 nm. (b) 2D class averages. (c) Cryo-EM processing tree. (d) Fourier shell correlation (FSC) plot, Angular distribution plot and local resolution distribution for the GTPBP6-bound split large mitoribosomal subunit (mtLSU) with peptidyl transferase center (PTC) conformation 1. Scale for the angular distribution plot shows the number of particles assigned to a particular angular bin. Blue, a low number of particles; yellow, a high number of particles. (e) FSC plot, Angular distribution plot and local resolution distribution for the GTPBP6-bound split mtLSU with PTC conformation 2. Scale for the angular distribution plot shows the number of particles assigned to a particular angular bin. Blue, a low number of particles; yellow, a high number of particles.



Supplementary Fig. 6 | GTPBP6 conformations.

(a) The PTC-binding loop of GTPBP6 can adopt two conformations. Superimposition of GTPBP6 in the PTC conformation 1 and PTC conformation 2 structures observed after ribosome splitting (dataset 3). GTPBP6 is shown as cartoon. GTPBP6 conformation 1, which is also observed during mtLSU biogenesis, is shown in cyan and GTPBP6 conformation 2 in maroon. **(b)** Close-up of PTC interactions in GTPBP6 PTC conformation 1 and 2. Depiction as in a, with the region of the 16S rRNA differing between the two states shown as cartoon. Bases that adopt different conformations as well as interacting GTPBP6 residues are shown as sticks. **(c)** Methylation of 12S rRNA is not affected in GTPBP6-deficient cells. Total RNA from wild type (WT) or *Gtpbp6*^{-/-} was treated with bisulfite, reverse transcribed and a region of the 16S rRNA containing m^5C1488 and m^4C1486 was amplified, cloned and sequenced. The relative proportions of unconverted cytosine reflecting m^5C/m^4C (black) and thymine reflecting converted, unmodified cytosine (grey) are shown. Data derived from sequencing of 46 individual clones per sample are presented. Source data are provided as a Source Data file.

Supplementary Tables

Supplementary Table 1 | Cryo-EM data collection and refinement for dataset 1.

	MTERF4-NSUN4 intermediate (PDB: 7OF0)	MTERF4-NSUN4- GTPBP5-intermediate (PDB: 7OF7)
Data collection and processing		
Magnification		81,000
Voltage (kV)		300
Electron exposure (e-/Å ²)		36
Defocus range (μm)		0.3 – 2.8
Pixel size (Å)		1.05
Symmetry imposed		C1
Initial particle images (no.)		9,378,438
Final particle images (no.)	1,060,638	98,227
Map resolution (Å)	2.2	2.5
FSC threshold	0.143	0.143
Map sharpening <i>B</i> factor (Å ²)	-50	-39.5
Map resolution range (Å)	5.6 – 2.2	5.6 – 2.2
Refinement		
Model resolution (Å)	2.3	2.7
FSC threshold	0.5	0.5
Model composition		
Non-hydrogen atoms	99,476	101,032
Protein/Nucleotide residues	8,446 / 1,432	8,655 / 1,432
Ligands	ZN: 3, MG: 61	ZN:3, MG:74
<i>B</i> factors (Å ²)		
Protein/Nucleotide	107.39 / 97.44	94.53 / 71.94
Ligand	62.66	46.80
R.m.s. deviations		
Bond lengths (Å)	0.006	0.006
Bond angles (°)	0.859	0.874
Validation		
MolProbity score	1.54	1.52
Clashscore	7.28	5.58
Poor rotamers (%)	0.00	0.00
Ramachandran plot		
Favored (%)	97.26	96.61
Allowed (%)	2.74	3.39
Disallowed (%)	0.00	0.00

Supplementary Table 2 | Cryo-EM data collection and refinement for dataset 2.

	GTPBP6 intermediate (PDB: 7OF2)	MTERF4- NSUN4 intermediate (PDB: 7OF3)	MTERF4- NSUN4- GTPBP5- intermediate (PDB: 7OF5)
Data collection and processing			
Magnification		81,000	
Voltage (kV)		300	
Electron exposure (e-/Å ²)		37	
Defocus range (µm)		0.3 – 2.1	
Pixel size (Å)		1.05	
Symmetry imposed		C1	
Initial particle images (no.)		2,983,982	
Final particle images (no.)	109,894	138,715	36,934
Map resolution (Å)	2.7	2.7	2.9
FSC threshold	0.143	0.143	0.143
Map sharpening <i>B</i> factor (Å ²)	-52	-58	-53
Map resolution range (Å)	4.0 – 2.5	4.0 – 2.5	4.0 – 2.5
Refinement			
Model resolution (Å)	2.8	2.9	3.0
FSC threshold	0.5	0.5	0.5
Model composition			
Non-hydrogen atoms	101,195	101,226	102,785
Protein/Nucleotide residues	8,560 / 1,466	8,627 / 1,442	8,829 / 1,445
Ligands	GTP: 3, ZN: 3, MG: 85	GTP: 2, ZN: 3, MG: 58	GTP: 2, ZN: 3, MG: 70
<i>B</i> factors (Å ²)			
Protein/Nucleotide	84.56 / 65.75	94.62 / 76.45	102.28 / 84.03
Ligand	59.47	69.93	72.24
R.m.s. deviations			
Bond lengths (Å)	0.004	0.04	0.004
Bond angles (°)	0.815	0.804	0.812
Validation			
MolProbity score	1.39	1.50	1.45
Clashscore	4.30	5.64	4.93
Poor rotamers (%)	0.01	0.00	0.00
Ramachandran plot			
Favored (%)	96.93	96.81	96.83
Allowed (%)	3.07	3.18	3.17
Disallowed (%)	0.00	0.01	0.00

Supplementary Table 3 | Cryo-EM data collection and refinement for dataset 3.

	Mature mtLSU with GTPBP6 – PTC state 1 (PDB: 7OF4)	Mature mtLSU with GTPBP6 – PTC state 2 (PDB: 7OF6)
Data collection and processing		
Magnification		81,000
Voltage (kV)		30
Electron exposure (e-/Å ²)		40
Defocus range (µm)		0.2 – 2.7
Pixel size (Å)		1.05
Symmetry imposed		C1
Initial particle images (no.)		2,540,514
Final particle images (no.)	137,890	250,244
Map resolution (Å)	2.7	2.6
FSC threshold	0.143	0.143
Map sharpening <i>B</i> factor (Å ²)	-57	-66
Map resolution range (Å)	4.6 – 2.4	4.6 – 2.4
Refinement		
Model resolution (Å)	2.8	2.7
FSC threshold	0.5	0.5
Model composition		
Non-hydrogen atoms	100,322	100,321
Protein/Nucleotide residues	8,320 / 1,519	8,320 / 1,519
Ligands	GTP: 3, ZN: 3, MG: 89	GTP:3, ZN: 3, MG: 88
<i>B</i> factors (Å ²)		
Protein/Nucleotide	92.56 / 73.81	86.71 / 69.37
Ligand	70.84	65.35
R.m.s. deviations		
Bond lengths (Å)	0.005	0.003
Bond angles (°)	0.818	0.805
Validation		
MolProbity score	1.45	1.38
Clashscore	4.92	4.18
Poor rotamers (%)	0.00	0.01
Ramachandran plot		
Favored (%)	96.83	96.99
Allowed (%)	3.17	3.01
Disallowed (%)	0.00	0.00

Supplementary Table 4 | Primers

Primer	Sequence
12S-m ⁵ C841_RT	5'-TTTAATTAAATATCCTTTAAAATATAC-3'
12S forward	5'-TTTAATTAAATATCCTTTAAAATATAC-3'
12S reverse	5'-AATAGGGTTTTGAAGTGTGTATATA-3'
GTPBP6 LIC for	5'-TACTTCCAATCCAATGCaccgggaatctggaggggcc-3'
GTPBP6 LIC rev	5'-TTATCCACTTCCAATGTTATTAtcctggaaagagcttccggaatttgc-3'

5 Discussion

5.1 Identification of the human mitoribosome assembly GTPases

Even though the mitochondrial genome and mitoribosomes were discovered more than 50 years ago (O'Brien and Kalf, 1967; Schatz et al., 1964), our knowledge about the mechanisms of mitochondrial gene expression is still far from being complete or comprehensive. For example, more than 250 factors are predicted to be required for the proper formation and function of the human mitochondrial translation apparatus (Pearce et al., 2017), but only a few of them have been precisely characterized. In recent years, advantages into cryo-EM approaches have allowed resolving the detailed structure of the mitoribosomes from mammals and other organisms and, in combination with biochemical studies, have advanced our understanding of the mitochondrial translation and the mitoribosome assembly pathway.

The evolutionary conserved RA-GTPases of the Obg/HflX superfamily are involved in a plethora of functions in bacteria, including the biogenesis and recycling of ribosomes (Leipe et al., 2002; reviewed by Bennison et al., 2019; Verstraeten et al., 2011). Bioinformatic analysis predicted the existence of homologous factors in eukaryotic genomes, however, their function remained unexplored. The first evidence about TRAFAC GTPases engagement into the mitochondrial gene expression has started to emerge nearly two decades ago. For example, Barrientos et al. (2003) suggested a role of Mtg1 in protein biosynthesis in yeast mitochondria and Hirano et al. (2006) characterized two human ObgE homologs GTPBP5 and GTPBP10 as factors required for the maintenance of the mitochondrial and nuclear architecture, respectively. Further development of the biochemical approaches allowed the characterization of the other essential GTPases involved in the mitoribosome assembly pathway in humans and mice. Thus, it was demonstrated that ERAL1 and MTG3 are involved in the mtSSU biogenesis (Dennerlein et al., 2010; He et al., 2012; Kolanczyk et al., 2011); GTPBP5 and GTPBP7 were suggested to be required for mitochondrial translation (Kotani et al., 2013). Moreover, mass spectrometry analysis of the mitoribosome and known mitoribosome assembly factors interactome revealed numerous uncharacterized proteins allocated to the ribosome biogenesis centers within the mitochondrion (Antonicka and Shoubridge, 2015; Tu and Barrientos, 2015). For example, GTPBP6 and GTPBP10, as well as the other GTPases (GTPBP5, GTPBP7 and GTPBP8), were identified as factors associated with the mitoribosome assembly RNA helicase DDX28 and with the MRP mL62 (Tu and Barrientos, 2015, Richter-Dennerlein, unpublished data). Based on homology to the bacterial or yeast (mito)ribosome assembly factors, their role in human mitochondria was extensively investigated during the last years.

Currently, the list of the TRAFAC GTPases involved in human mitoribosome biogenesis has been expanded and accounts for 6 members (reviewed by Maiti et al., 2021). Unveiling the function of GTPBP6 and GTPBP10 in human mitochondrial gene expression represents the direct contribution of this doctoral study to the field. Moreover, the structural analysis in collaboration with Prof. Dr. Hauke Hillen expanded the understanding of the late mtLSU biogenesis steps and revealed the precise role of the MTERF4-NSUN4 complex and the GTPases GTPBP5 and GTPBP6 during mtLSU maturation.

5.2 GTPBP6 and GTPBP10 as TRAFAC RA-GTPases

5.2.1 The structure of the GTPase domain

The typical G-domain structure of TRAFAC GTPases includes 5 conserved motifs (G1-G5), which are involved into phosphate binding (G1-G3) and specific interactions with the guanidine ring (G4-G5). Alignment of human GTPBP6 and GTPBP10 with their homologs and the classical RA-GTPase of the TRAFAC class EF-Tu highlights the conservation of the functional motifs and crucial amino acid residues of the GTPase domain (Figure 13). The most notable difference between classical GTPases such as Ras and trGTPases is the substitution of the catalytic Glu in the switch II domain by His (Koripella et al., 2015; reviewed by Maracci and Rodnina, 2016) and, therefore, different mechanism of catalysis. However, GTPBP6 and GTPBP10, as well as their bacterial homologs, have a hydrophobic amino acid at the position corresponding to His in trGTPases, so called hydrophobic amino acid substituted for catalytic Glutamine GTPases (HAS-GTPases). Different amino acids were proposed to serve as a catalytic residue in HAS-GTPases (Batra et al., 2020; reviewed by Goto et al., 2013). Although we lack experimental evidence of the exact GTP-hydrolysis mechanism by GTPases involved into ribosome biogenesis, it is reasonable to speculate that it is different from both the canonical GTPases and trGTPases family. His-9 in RbgA was recently confirmed to serve as a catalytic residue in a structural study (Seffouh et al., 2019). However, this residue is not conserved in GTPBP6 or GTPBP10, and further biochemical analysis is required to establish the catalytic mechanism of these GTPases.

suggest that GTPBP6 probably uses a tRNA mimicry strategy similarly to HflX and release factors to associate with the mitoribosomal PTC (Nakamura and Ito, 2011; Zhang et al., 2015). How does the GTPase activity of GTPBP6 correlate with its function in mitoribosome assembly and recycling? Our analysis shows that binding to the 55S mitoribosome or the 39S mtLSU does not stimulate GTP hydrolysis by GTPBP6 as we trapped the factor bound to the mtLSU in a complex with GTP during biogenesis and after 55S dissociation (Hillen et al., 2021). This is in contrast to many other RA-GTPases, including assembly factors (for example, RbgA and GTPBP7) and trGTPases (Gulati et al., 2013; Kotani et al., 2013; reviewed by Maracci and Rodnina, 2016 for trGTPases). It implies an essential role of GTPBP6 as an anti-association factor, which stays bound to the mtLSU until its conformation or action of a specific mediator (including translationally competent mtSSU) favor the factor release probably coupled with GTP-hydrolysis as it was suggested for HflX (Dey et al., 2018; Zhang et al., 2015). In contrast to the typical RA-associated GTPases such as trGTPases and GTPBP5/GTPBP10, the GTPase/ND2 domain of GTPBP6 occupies the position on top of the helix 89 and is spatially remoted from the GAC (Hillen et al., 2021). Instead, the canonical position between the L7/L12 stalk base and the SRL is filled with GTPBP6 CTD. This observation suggests that the mechanism of GTPBP6 GTPase activation by the mitoribosome is strikingly different from the aforementioned RA-associated GTPases but similar to HflX, which possesses the same domain location on 50S LSU (Zhang et al., 2015). Thus, GTP hydrolysis by GTPBP6 is activated by a mechanism, which does not involve the action of the SRL. Alternatively, the GTPase domain displacement toward the GAC precedes GTP hydrolysis by the factor.

Another member of the Obg/HflX superfamily, GTPBP10, a human homolog of bacterial ObgE/CtgA, was previously suggested to localize to the nucleolus (Hirano et al., 2006). However, our study revealed that GTPBP10 resides within the mitochondrion as a peripheral component of the IMM which is typical for the other mitoribosome assembly factors. Further analysis of the GTPBP10 interactome showed that the factor associates specifically with the mtLSU, and the other study confirmed that this interaction is significantly increased in the presence of non-hydrolysable GTP analog (Busch et al., 2019). The factor has a domain composition characteristic to Obg GTPases family: the N-terminal Obg-fold, middle GTPase domain and C-terminal domain (Leipe et al., 2002; reviewed by Verstraeten et al., 2011). Mutation analysis of the factor demonstrates that both Obg domain and GTPase domain are critical for its interaction with the mtLSU. GTPBP10 GTPase domain is situated into mitoribosomal GAC between the L7/L12 stalk base and the SRL while the N-terminal Obg-fold protrudes toward the PTC and lies beneath the helix 89 (Cheng et al., 2021). GTP hydrolysis potentially precedes GTPBP10 release from the mtLSU as it was shown for its bacterial homolog ObgE (Feng et al., 2014).

Nucleotide exchange is important to shift a GTPase into an active GTP-bound state and to induce rearrangements into the protein structure. Many RA-GTPases do not need a GEF to exchange GDP molecule for GTP because of the higher abundance of the latter in the cell. This is especially relevant for the GTPases involved into ribosome assembly in bacteria since they are able to sense the stringent response mediator (p)ppGpp and adjust the ribosome assembly process accordingly (Corrigan et al., 2016; reviewed by Bennison et al., 2019). However, the situation is more complicated in the case of human mitochondrial ribosome biogenesis GTPases. As the mitoribosome synthesizes the 13 core OXPHOS proteins, the other OXPHOS components are imported from the cytosol. Therefore, the protein synthesis into mitochondria adapts to the influx of the nuclear encoded proteins and serves as a rate-limiting step for OXPHOS assembly (Bogenhagen and Haley, 2020; Richter-Dennerlein et al., 2016). Thus, the expression of the mitochondrial and nuclear genomes must be tightly coordinated. To achieve this, the synthesis of the mtDNA-encoded OXPHOS proteins is regulated via a feedback loop assured by the action of OXPHOS assembly factors, although the exact mechanism of mitochondrial translation pausing remains elusive (Richter-Dennerlein et al., 2016; Wang et al., 2020). It is tempting to speculate that the translation rate may also be regulated at the step of mitoribosome assembly, and that the nuclear-encoded mitoribosome assembly factors may play an important role in this process. The guanine nucleotide exchange rate regulation may act as a limiting step, preventing an assembly GTPase activation and thereby formation of the translationally competent mitoribosomes. However, although it was proposed that GTPBP7 utilizes the GEF activity of mtSSU integrated dible-homology (DH) domain-containing MRP mS27 (Kim and Barrientos, 2018) and RCC1L may act as a GEF for GTPBP10 and MTG3 or ERAL1 (Reyes et al., 2020), the biochemical and physiological relevance of these findings remains to be addressed further.

5.3 The role of the Obg/HflX superfamily GTPases in human mitoribosome biogenesis

5.3.1 The role of GTPBP10

Members of the Obg-family GTPases ObgE/CtgA are essential factors involved in a plethora of intracellular processes, including the biogenesis of the bacterial ribosomal LSU (Feng et al., 2014; reviewed by Bennison et al., 2019; Verstraeten et al., 2011). Based on the sequence homology to ObgE, two putative GTPases were identified in the human genome: GTPBP5 and GTPBP10. Although both proteins resemble ObgE domain organization, GTPBP10 has 2 extended deletions in the loops of the Obg-fold. Since the loops are crucial for the Obg GTPases interaction with the (mito)ribosomal PTC rRNA helices, their altered structure in GTPBP10 may suggest that the homologs have evolved distinct molecular mechanisms for mitoribosome association.

GTPBP10 is essential for late stages of mtLSU maturation when all MRPs with the exception of bL36m are incorporated. Our analysis of GTPBP10 interactome revealed that the function of GTPBP10 at late stages of mtLSU biogenesis is tightly coupled with DDX28, MRM3, TRMT61B, MTERF4-NSUN4, GTPBP7, pseudouridine synthase and MALSU1 modules (Lavdovskaia et al., 2018). Recent structural analysis of the GTPBP10-containing mt-LSU assembly intermediate has confirmed that the factor acts concomitantly to DDX28, MRM3 and MALSU1 module (Cheng et al., 2021). This highly complex interplay of GTPBP10 with the other biogenesis factors resembles the process of mtLSU functional centers maturation in bacteria, where ObgE cooperates with RsfS (homologous to MALSU1) and RluD (pseudouridine synthase) to facilitate the formation of the CP and the PTC (Nikolay et al., 2021). Remarkably, GTPBP10 does not associate with GTPBP5 (Lavdovskaia et al., 2018). Our cryo-EM analysis of the mtLSU assembly intermediates resolved the binding site for GTPBP5 (Hillen et al., 2021) and the group of Prof. Dr. Roland Beckman (Cheng et al., 2021) obtained the structure of the pre-mtLSU with bound GTPBP10. Both factors, similarly to GTPBP6 and ObgE use tRNA mimicry strategy to interact with the mtLSU immature PTC. Indeed, the association of the factors with the mtLSU appeared to be spatially mutually exclusive.

Structural analysis suggests that GTPBP10 dissociates from the mtLSU leaving the PTC in nearly mature conformation (Cheng et al., 2021). However, our data indicate that downstream collaborative action of GTPBP5 and NSUN4 is required for additional refolding of the P-loop and ensures the correct ordering of the surrounding MRP elements (Hillen et al., 2021). Thus, GTPBP10 may act as a placeholder for GTPBP5 in the vicinity of helix 89. Importantly, overexpression of GTPBP10 is deleterious for the levels of the 55S mitoribosome, shifting the equilibrium towards the free subunits and further emphasizing its role as an anti-association factor similarly to ObgE which abstracts helix 69 from its mature position thereby preventing premature subunit joining (Feng et al., 2014).

Moreover, GTPBP10 is essentially required for the 16S rRNA stability (Lavdovskaia et al., 2018). As a model for our study, we used a variant of GTPBP10 containing the mutations of conserved Arg-64 and Lys-65 residues in Obg-fold. Our results support the importance of the electrostatic interactions formed between the charged amino acids of the Obg-fold and the PTC rRNA helices as it was previously shown for *E. coli* ObgE (Feng et al., 2014). In a study by Prof. Dr. Barrientos' group (Maiti et al., 2018), the complete ablation of GTPBP10 revealed that the factor is involved in the processing of the 12S rRNA-tRNA^{Val}-16S rRNA transcript, providing an exciting link between the assembly of the mitoribosomal subunits. Taking together, it is reasonable to speculate that in addition to GTPBP10 function during late stages of mtLSU biogenesis where aforementioned factors mature the CP and the PTC at the

intersubunit interface of the mtLSU, GTPBP10 also facilitates the early assembly of the MRP clusters on a nascent rRNA transcript probably guiding the separation of 12S and 16S-tRNA^{Val}.

Although both GTPBP10 and GTPBP5 are involved into late stages of mtLSU maturation and can substitute for ObgE depletion in bacterial strains (reviewed by Maiti et al., 2021), our findings emphasize that the homologs have acquired distinct functions in human mitoribosome biogenesis. In other words, the function of ObgE in bacterial ribosome biogenesis appeared to be shared between GTPBP5 and GTPBP10 in human mitochondria and the factors cannot compensate for each other.

5.3.2 The role of GTPBP6

The members of the HflX GTPases family are not essential in prokaryotes under physiological conditions and are involved in stress-activated ribosome recycling pathway (reviewed by Bennison et al., 2019; Srinivasan et al., 2019; Verstraeten et al., 2011). While HflX expression is typically nearly non-detectable, it dramatically increases upon heat-shock (*E. coli*, *S. aureus*), antibiotic treatment (*L. monocytogenes*, *Mycobacterium spp.*) or manganese stress (*E. coli*) (Duval et al., 2018; Rudra et al., 2020; Sengupta et al., 2018; Zhang et al., 2015). In contrast, GTPBP6 constitutively expresses in all human tissues (reviewed by Srinivasan et al., 2019). Our findings explain the permanent expression of the factor since, in addition to its conserved role during ribosome recycling (discussed in section 5.5), GTPBP6 has acquired a crucial function as a mitoribosome maturation factor (Lavdovskaia et al., 2020). Thus, ablation of GTPBP6 is detrimental to mitochondrial protein synthesis. The molecular mechanism of the translation deficiency originates from the impaired mtLSU biogenesis. GTPBP6 loss results into the formation of mtLSU particles, which comprise a full set of the MRPs and are enriched in the assembly factors such as MTERF4-NSUN4 and the MALSU1 module, and the GTPases GTPBP5, GTPBP7 and GTPBP10 (Lavdovskaia et al., 2020). The accumulation of these factors and the presence of all 52 MRPs suggests that the assembly of the particle stalls at a very late stage during biogenesis resulting in a nearly mature mtLSU, which, however, is incompetent for subunit joining. Structural analysis of this assembly intermediate further confirmed that GTPBP6 associates with the mtLSU, which has been previously modified by the concomitant action of MTERF4-NSUN4 and GTPBP5 (Hillen et al., 2021). As the binding of MTERF4-NSUN4, GTPBP5 and GTPBP6 is mutually exclusive, GTPBP6 probably triggers a molecular switch and facilitates the release of the factors. GTPBP6 mediates the PTC rRNA elements maturation allowing them to adopt conformations resembling the state characteristic to the nearly mature mtLSU particle. Finally, the binding of GTPBP6 keeps the mitoribosome functional center blocked against a premature occupation by the translation factors and prevents intersubunit bridge formation (Hillen et al., 2021).

Although the mass spectrometry analysis has revealed the presence of GTPBP10 in GTPBP6-deficient mtLSU assembly intermediate(s), we could not visualize any biogenesis complexes containing the factor. This might suggest that the GTPBP10-bound pre-mtLSU population is not abundant in GTPBP6-depleted cells, thereby indirectly confirming that the GTPBP10 and GTPBP6 action is temporally separated. The other curious observation is a significant (more than 7-fold) accumulation of GTPBP7-containing mtLSU biogenesis intermediates upon GTPBP6 ablation (Lavdovskaia et al., 2020). Biochemical analysis suggested a role of GTPBP7 in coupling mtLSU biogenesis with mB6 intersubunit bridge formation, thereby meaning that the factor is involved into the very final steps of assembly directly preceding intersubunit association (Kim and Barrientos, 2018). Despite the fact that we were not able to detect any density corresponding to GTPBP7 in our isolated pre-mtLSU particles, which might be due to the high flexibility of the GTPBP7, it is reasonable to speculate that GTPBP6 and GTPBP7 may simultaneously accommodate in the particle and their release promote B2a and mB6 bridge formation, respectively, finally completing 55S mitoribosome assembly.

5.4 GTPase-driven structural transitions during mtLSU biogenesis

Towards to understanding of the mtLSU late biogenesis intermediates structure

Biogenesis of the mitochondrial ribosomes is a complex and highly dynamic process that involves the assembly of individual MRP or MRP blocks on an rRNA scaffold and proper folding of both rRNA and protein components. While MRPs can drive rRNA folding on their own in early stages of mitoribosome assembly, in many cases, additional assembly factors are required to overcome the kinetic traps allowing the biogenesis process to proceed further. However, the relative order of assembly factors involvement, as well as the conformational and compositional transitions induced by the factors remained obscure due to lack of structural details. The recent progress of the single particle cryo-EM approach started to fill this gap. High resolution cryo-EM has significantly enhanced our understanding of the structural composition and remodeling of the pre-mtLSU particles during late stages of biogenesis. Thus, detailed resolution of the mtLSU assembly intermediates suggests that the majority of the known biogenesis factors are engaged into late stages of maturation acting on the intersubunit interface. The final steps of the mtLSU production are reminiscent of bacterial ribosomal LSU synthesis and involve intensive tuning of the intersubunit interface and formation of the main functional centers such as CP and PTC. In contrast, the solvent side resides into a completely mature conformation in agreement with the hierarchical order of MRP clusters incorporation (Bogenhagen et al., 2018). Thus, the resolved biogenesis intermediates contain the mature domains I-III (with the exception of helices 34-35 of the domain II) and VI of the 16S rRNA,

thereby providing insights into the folding of the domains IV and V and subsequent incorporation of the late-binding MPRs such as bL33m, bL35m and bL36m.

The first structure of the native mtLSU assembly intermediates isolated from WT cells represent the least mature pre-mtLSU obtained so far and contains completely misfolded interfacial rRNA (Brown et al., 2017). The particles were largely devoid of the mitoribosome biogenesis factors on the structure except for the MALSU1-L0R0F8-mtACP module. The study revealed a conserved function of the module as an anti-association factor required to prevent premature subunit association similarly to bacterial RsfS and cytosolic eIF6 (Brina et al., 2015; Brown et al., 2017; Gartmann et al., 2010; Nikolay et al., 2021). However, mass spectrometry analysis detected several assembly factors associated with the intermediate (e.g., NSUN4, GTPBP5, MRM3 and DDX28). Thus, the pre-mtLSU particles likely represent a mixture of the distinct biogenesis states corresponding to the action of each assembly factor or complex of factors. Indeed, recent extensive studies of the mtLSU assembly intermediates associated with the aforementioned biogenesis factors allowed to arrange the assembly states in the most plausible order based on the 16S rRNA maturation status induced by the respective assembly factor.

DDX28, MRM3 and GTPBP10 cooperate to promote the CP and the PTC initial rRNA folding

The least mature mtLSU intermediate (Figure 14, state A) revealed how the cooperative action of DDX28, MRM3 and GTPBP10 initiates the maturation of the CP and the PTC (Cheng et al., 2021). Thus, bound DDX28 stabilizes the CP into immature conformation by keeping the scaffolding rRNA helices 80-88 upwards from their actual position on the mature mtLSU (Cheng et al., 2021). In turn, GTPBP10 Obg-fold stacks against helix 89 and dislodges it from the mature position, thereby providing access for methyltransferase MRM3 active site toward its target at helix 92. The cooperation of GTPBP10 and MRM3 to modify the A-loop represents a striking example of a GTPase-assisted rRNA modification.

The simultaneous involvement of DDX28 and GTPBP10 suggests that the CP and the PTC maturation may be coupled in human mitoribosome as it was observed for bacterial 50S LSU, although the functional centers are composed of independent assembly blocks of MRPs (Bogenhagen et al., 2018; Nikolay et al., 2018). Dissociation of DDX28 facilitates helices 80-88 to fold into the position closely resembling the mature state and allowing simultaneous incorporation of bL33m and bL35m, further cementing the CP structure (Cheng et al., 2021).

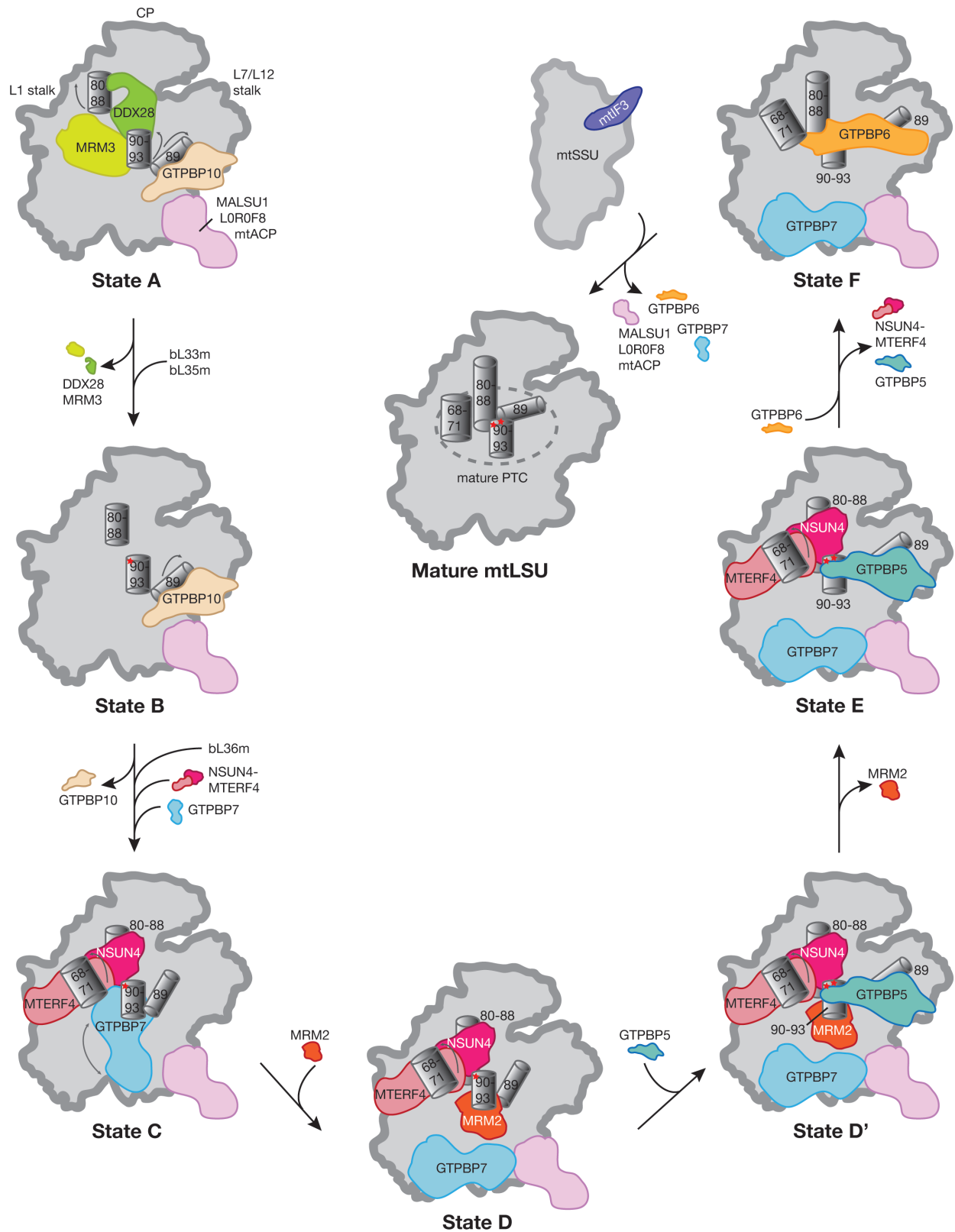


Figure 14. A model of the hierarchical GTPase-driven maturation of the mtLSU functional centers. Different states are designated in the most plausible order based on the maturation status of the rRNA segments (shown as grey cylinders) and the surrounding MRPs. Arrows on the mtLSU indicate a shift from the mature position of the respective rRNA helices. In the case of GTPBP7, double-headed arrow reflects the proposed flexibility of the factor. Red stars at the helix 92 (A-loop) indicate its methylation status. For detailed description of the states, please refer to the text.

Further, GTPBP10, similarly to ObgE, facilitates helix 89 to adopt its mature-like position most likely after the release of MRM3 and DDX28 and hallmarks the transition to state B (Figure 14) (Cheng et al., 2021). Interestingly, in bacteria, incorporation of uL16 is spatially possible only after helix 89 adopts its mature position guided by the action of ObgE (Nikolay et al., 2021). However, this is not the case for the human mtLSU where uL16m is already incorporated when GTPBP10 still holds the helix 89 into the immature conformation (Cheng et al., 2021).

The release of GTPBP10 finally allows an incorporation of bL36m which additionally stabilizes the PTC rRNA together with uL16m acting as an evolutionary conserved 'molecular glue' (Brown et al., 2017; Nikolay et al., 2021). However, at this stage, the incorporation of the MRP might be transient as it was suggested that bL36m stably associates with the mtLSU only downstream to GTPBP7 and GTPBP5 (Kim and Barrientos, 2018; Maiti et al., 2020). Thus, in state C (Figure 14), helices 89-93 accommodate their positions inside the PTC, and the only segment of the 16S rRNA which remains completely disordered are helices 68-71.

MTERF4-NSUN4 module prevents the PTC cleft folding

The rRNA segments corresponding to the mature helices 68-71 are stabilized by the MTERF4-NSUN4 when mtLSU assembly intermediate proceeds through the states C-E (Figure 14) (Cheng et al., 2021). NSUN4, a methyltransferase that introduces the modification to the C1488 of the 12S rRNA, possesses a dual function during mitoribosome assembly. It cooperates with MTERF4, an RNA-binding protein, to associate with the mtLSU preventing premature subunit joining. Although it was previously suggested that MTERF4-NSUN4 might bar the 16S rRNA fragment required for intersubunit bridge formation, the molecular basis of this interaction remained unclear (Metodiev et al., 2014). Our structural analysis has confirmed the hypothesis (Hillen et al., 2021). Thus, the position of MTERF4 on the pre-mtLSU particle overlaps with the helices 68-69 on the mature mtLSU. In agreement with the previous data (Metodiev et al., 2014; Spåhr et al., 2012; Yakubovskaya et al., 2012), our structural work confirms that NSUN4 does not methylate 16S rRNA since no potential target base was observed in the active site of the methyltransferase. In addition, from this position NSUN4 cannot reach the 12S rRNA providing further evidence that the function of NSUN4 as a 12S rRNA methyltransferase and a scaffolding function during mtLSU biogenesis are distinct and spatial-temporal separated (Hillen et al., 2021).

At the states C-E (Figure 14), certain PTC-forming helices maintain non-matured conformations/interactions and require further folding and modification. For example, the A-loop at state C (Figure 14), despite being previously modified at the position G3040, lacks additional methylation of U3039 introduced by MRM2. MTERF4 binds to the helices 68-71 of the domain IV, displacing them from their mature position and exposing the PTC for the dedicated assembly factors which facilitate the modification.

Methylation of the A-loop: concerted function of GTPBP5 and MRM2?

The function of MTERF4 in abstracting helix 71 provides an essential example of the biogenesis factors cooperation allowing the A-loop to be targeted by the methyltransferase MRM2 to modify U3039 (Figure 14, state D) (Cipullo et al., 2021a; Lenarcic et al., 2021). In the reported structures, the MRM2 active site is positioned towards U3039; however, the methyl donor S-Adenosyl methionine (SAM) is not present. Previously, it has been shown that GTPBP5 is required to facilitate U3039 2-O-methylation by MRM2 (Maiti et al., 2020). The other solved mtLSU intermediate structure simultaneously accommodates MRM2 and GTPBP5 (Figure 14, state D'), but the positioning of the MRM2 active site towards its target nucleotide base is achievable only without bound GTPBP5 otherwise the factor would abstract the A-loop from its interaction with MRM2 (Lenarcic et al., 2021; Cipullo et al., 2021a). Although we did not detect the interaction of MRM2 with our assembly intermediate, the methylation of the helix 92 is completed in our mtLSU*GTPBP5 structure (Figure 14, state E), confirming that it took place before or in parallel to GTPBP5 binding (Hillen et al., 2021). Thus, the solved intermediate structures rather suggest that GTPBP5 serves as a quality control factor to ensure the correct U3039 base modification but the molecular details that would unveil how GTPBP5 promotes the U3039 methylation by MRM2 remain unclear.

Additionally, the Obg domain of GTPBP5 stabilizes the mature-like PTC conformation and cooperates with the N-terminal domain of NSUN4 to refold the PTC-loop by disrupting its interaction with the P-loop tip (state E, Figure 14) (Cipullo et al., 2021a; Hillen et al., 2021; Lenarcic et al., 2021).

GTPBP6 provides the final quality control check point during mtLSU maturation

Our *in vitro* reconstitution of the mtLSU assembly pathway by adding the recombinant GTPBP6 to the pre-mtLSU intermediate isolated from GTPBP6 deficient cells allowed us to track the final tuning steps preceding the formation of translationally competent mtLSU particle. Thus, when MTERF4-NSUN4 and GTPBP5 nearly complete the PTC maturation, GTPBP6 binding displaces the factors from the particle and hallmarks the transition to state F (Figure 14). Even though the position of the GTPase domain of GTPBP5 in the GAC would allow for stimulating the GTP hydrolysis by a conventional SRL-mediated mechanism, the kinetic evidence implies that the GTPBP5 GTPase activity is not enhanced by mitoribosomal particles (Kotani et al., 2013) and the dissociation of the factor from the ribosome does not rely on GTP hydrolysis and is likely promoted by another factor (Cipullo et al., 2021b). Therefore, GTPBP6 is a perfect candidate to displace GTPBP5 during the last steps of the mtLSU maturation. Finally, GTPBP6-mediated MTERF4-NSUN4 dissociation liberates the helices 68-71, and further release of GTPBP6 may finally allow them to fall into the mature position within the PTC. Thus,

the mtLSU biogenesis is complete and critical intersubunit bridges between the 16S rRNA helices and 12S rRNA can form.

The intriguing function of GTPBP7

Interestingly, a combination of biochemical and structural analysis suggests that GTPBP6 might not be the last GTPase to dissociate from the mature mtLSU complex. Previously, GTPBP7 was suggested to facilitate the mB6 intersubunit bridge formation (Kim and Barrientos, 2018). Structural analysis of the mtLSU assembly intermediates has revealed that GTPBP7 binding to the pre-mtLSU particles takes place simultaneously to MTERF4-NSUN4 (Cipullo et al., 2021a; Chandrasekaran et al., 2021). GTPBP7 accommodates in the vicinity of the A- and P-loops of the PTC, assisting the folding of helices 89-93, and directly contacts the methylation site of MRM2 and MTERF4-NSUN4 dimer (Chandrasekaran et al., 2021). Slight rearrangements within GTPBP7 would also allow the factor to verify the methylation status of G3040. In the structure obtained by Chandrasekaran et al. (2021), the position of GTPBP7 bound to the assembly intermediate is reminiscent of *B. subtilis* RbgA and *T. brucei* GTPBP7/Mtg1 position although it is shifted more to the bottom of the mtLSU and the exact binding sites of the factor appeared to be not conserved (Jaskolowski et al., 2020; Seffouh et al., 2019; Tobiasson et al., 2021). Remarkably, in the aforementioned structures, the GTPase domain of GTPBP7/Mtg1 is remoted from the conventional position within the GAC of the mitoribosomes.

However, in a complex with GTPBP5 and MRM2 the factor appeared to be displaced and the only contact to the PTC is mediated by disordered helix 68 (Cipullo et al., 2021a). In this conformation GTPBP7 is unlikely to induce any conformational changes within the PTC or promote the other factors to bind or dissociate. Thus, it is reasonable to speculate that GTPBP7 associates with mtLSU intermediates in a highly flexible manner which in turn authorizes the GTPase to ensure the proper folding of the PTC-loop and modifications in the A-loop and to expose the rRNA core of the PTC for the action of the other biogenesis factors when required. Although we could not detect any density which might correspond to GTPBP7 in our GTPBP6-containing assembly intermediate, the allocation of GTPBP7 on the mtLSU bottom would not interfere with GTPBP6. Moreover, since the GTP-hydrolysis by GTPBP7 is stimulated by the mature mtLSU and even more significantly by the 55S mitoribosome (Kotani et al., 2013), it is tempting to assume that the GTPase activity is required for GTPBP7 dissociation from the mature particle in parallel with GTPBP6.

Limitations of the mitoribosome assembly complexes analysis by cryo-EM

Recent progress in cryo-EM allowed to improve the resolution limit and advanced image classification approaches now make it possible to characterize even minor particle populations. Even though trapping of the native assembly complexes appeared to be a challenge since the intermediates trapped on their native pathway in WT cells were largely devoid of biogenesis factors (Brown et al., 2017). Several strategies have been recently applied to overcome this issue and unveil the role of the dedicated factors into mtLSU maturation. The first approach implies the genetic perturbation of the mtLSU biogenesis pathway by deletion of an assembly factor and subsequent structural analysis of accumulated assembly intermediates. However, one of the apparent limitations of the strategy is that it has to be further determined that the intermediate is competent for further progression into the mature subunit and represents the actual substrate for the factor binding. For example, in bacteria, the ribosomal particles formed upon depletion of GTPases YjeQ or Era largely represent off-pathway intermediates incompetent for the external recombinant factors binding. Consequently, around a half of the particles are not able to progress to form the mature 30S SSU (Thurlow et al., 2016). Accounting that many of the late mtLSU biogenesis factors serve to stabilize rRNA into specific non-native conformations, which further facilitate the proper folding of the PTC, it is reasonable to expect that in the absence of the factor, rRNA would spontaneously fold into the most thermodynamically stable conformation and might represent even a downstream intermediate. Additionally, there is a possibility of activation of an alternative assembly pathway to overcome the artificial block.

In our study, we used mtLSU biogenesis intermediates purified from the GTPBP6-deficient cells (Hillen et al., 2021). To prove that the particles are on-pathway intermediates we reconstituted the assembly process by adding recombinant GTPBP6 and consequently observed a portion of the intermediates bound to the factor and resembled nearly mature mtLSU. In a similar study by Cipullo et al. (2021a) the structure of the GTPBP5-deficient mtLSU assembly intermediates was characterized and further compared to the intermediates isolated via affinity tagged GTPBP5, thus combining the first strategy with the second approach, which implies affinity purification of the pre-mtLSU particles containing tagged assembly factor(s) bound to the complex (Cipullo et al., 2021a; Cheng et al., 2021; Lenarcic et al., 2021). Although the using of the affinity purification is preferable since it reflects the on-pathway it remains speculative whether the observed structural transitions represent the direct effect of an assembly factor and do not happen spontaneously or as a result of another factor, which was not possible to trap during structural analysis. Additionally, the strategy is probably not applicable to every biogenesis factor. For example, since ribosome assembly GTPases possess an anti-association activity (reviewed by Bennison et al., 2019; Maiti et al., 2021), their overexpression affects (mito)ribosome biogenesis and might lead to the formation of non-

native intermediates hindering their further progression. Thus, expression of the affinity tagged biogenesis GTPases should be accurately titrated to avoid possible adverse effects and artifacts.

The other challenge on the way to unveil the mitoribosome assembly pathway using the single particle cryo-EM technology is indeed the preparation of the samples suitable for the structural analysis. Assembly intermediates are usually low abundant, heterogeneous and possess compromised stability. Thus, improving the purification conditions, grids preparation and particle classification techniques will allow to strictly determine the actual composition of the assembly intermediates. For example, as it was discussed previously, the biochemical data suggest that GTPBP7 associates with the pre-mtLSU particle simultaneously to MTERF4-NSUN4 module and most likely stays bound until the subunit completes its maturation. However, GTPBP7 was detected only in half of the intermediates potentially corresponding to the factor-bound state (found in the studies by Cipullo et al., 2021a; Chandrasekaran et al., 2021; absent in the studies by Hillen et al., 2021; Lenarcic et al., 2021). Despite we observe a significant accumulation of GTPBP7 on the mtLSU biogenesis intermediates purified from GTPBP6-deficient cells (Lavdovskaia et al., 2020), the factor was not identified in the structure probably due to its high flexibility or minor pre-mtLSU*GTPBP7 particle sub-population.

Another challenge is to sieve any artifacts arising during sample preparation. The paradigm suggesting that the ribosome should be devoid of association with translation factors during the biogenesis process appeared to be shifted in the case of the mitoribosome assembly in humans. For example, in a study by Cheng et al. (2021) a tRNA was detected in the E-site in certain assembly intermediates. The authors could not withdraw the possibility that the tRNA binding occurred accidentally, although a possible function in monitoring the maturation status of the CP was suggested (Cheng et al., 2021). Another unexpected finding is the association of mtEF-Tu with the maturing mtLSU particle together with GTPBP5 (Cipullo et al., 2021a). Although the authors claim that mtEF-Tu provides a binding platform for GTPBP5, it appeared to be dispensable for GTPBP5 association in our study (Hillen et al., 2021) and in the study by Lenarcic et al. (2021). Further biochemical analysis is required to solve this discrepancy.

5.5 Novel recycling pathway for human mitoribosomes

The canonical mitoribosome recycling system has evolved from its bacterial counterpart and consists of mtRRF, mtEF-G2 and mtIF3. However, our data indicate the existence of an alternative ribosome recycling pathway in human mitochondria actively mediated by GTPBP6. Therefore, the ribosome recycling activity is conserved among the HflX-family GTPases. GTPBP6 is able to promote dissociation of both bacterial- and mito-ribosomes, and *in vitro* assays show that the factor splits vacant ribosomes or ribosomal complexes with deacylated tRNA in the P-site. Notably, the presence of peptidyl-tRNA would sterically clash with GTPBP6,

thereby ensuring that actively translating ribosomes are protected from GTPBP6-mediated splitting. This mechanism is reminiscent of HflX and mtRRF-mtEF-G2 since both factors preferably bind the rotated conformation of the ribosome with deacylated tRNA in the P-site, which is subsequently shifted into the P/E hybrid state (Aibara et al., 2020; Koripella et al., 2019b; Koripella et al., 2021; Koripella et al., 2020; Kummer et al., 2021; Zhang et al., 2015).

Rapid kinetic measurements suggest that GTPBP6 actively separates ribosomal subunits without the assistance of any other factor with a dissociation rate constant comparable to HflX (Lavdovskaia et al., 2020). Remarkably, GTPBP6 splitting activity essentially depends on GTP-binding but does not require GTP hydrolysis, similarly to HflX and mtRRF-mtEF-G2 (Lavdovskaia et al., 2020; Koripella et al., 2019b; Tsuboi et al., 2009; Zhang et al., 2015; Koripella et al., 2020; Koripella et al., 2021) but contrary to bacterial RRF/EF-G (reviewed by Rodnina, 2018). Our structural analysis of the split mtLSU with bound GTPBP6*GTP has revealed that the target site for GTPBP6-mediated mitoribosome recycling is a conserved intersubunit bridge B2a formed by helix 44 of the 12S rRNA and helix 69 of the 16S rRNA from the mtSSU and mtLSU side, respectively (Hillen et al., 2021). GTPBP6 contacts helix 69 via Trp-107 of the NTD and shifts it towards the position occupied by helix 44 in the intact mitoribosome. This mechanism of helix 69 displacement is reminiscent of HflX, although the latter does not directly contact this helix (Dey et al., 2018; Zhang et al., 2015). Apparently, the critical B2a bridge disruption by helix 69 dislocation is a basic underlying mechanism of ribosome subunit dissociation among different recycling systems. However, the canonical recycling machinery in both bacteria and human abstracts helix 69 by capturing it between domain I and II of mtRRF/RRF and directly lift it from helix 44 acting as tweezers (Fu et al., 2016; Kummer et al., 2021; Koripella et al., 2021; Zhou et al., 2020). This motion is induced by mtEF-G2 or EF-G, respectively, coupled with GTP hydrolysis by EF-G in the bacterial recycling system. Thus, the more prominent way of helix 69 displacement by canonical recycling system explains its efficiency, which exceeds GTPBP6-mediated splitting activity by ~4.25 fold under our experimental conditions. It remains to be further clarified if GTPBP6 binding stabilizes the rotated state of the mitoribosome in a manner similar to mtEF-G2, which favors further intersubunit bridges disruption (Koripella et al., 2020; Koripella et al., 2021).

The post-splitting complex of mtLSU*GTPBP6*GTP captured in our structural analysis probably represents the final recycling product of the mtLSU. Deferred GTP hydrolysis by GTPBP6 after mitoribosome dissociation highlights an additional role of GTPBP6 as an anti-association factor for mtLSU during mitoribosome recycling. Similarly, (mt)IF3 prevents premature (mt)SSU engagement into a new round of translation (Koripella et al., 2021; Koripella et al., 2019b; reviewed by Ayyub and Varshney, 2019). However, the exact mechanism that triggers GTP hydrolysis and subsequent release of GTPBP6 from mtLSU during both biogenesis and recycling remains to be clarified. It is tempting to speculate that

pre-IC2 (mtSSU*mtIF2*mtIF3) joining promotes further SRL shift towards GTPBP6 GTPase/ND2 domain, thereby activating GTP hydrolysis and GTPBP6*GDP release from the mtLSU in a similar way suggested for mtLSU*mtRRF*mtEF-G2*GTP complex (Koripella et al., 2020; Koripella et al., 2019b). Thus, GTPBP6 provides an elegant link between the mitoribosome rescue and the formation of a translationally competent mitoribosome after recycling.

Although our findings suggest an active role of GTPBP6 in mitoribosome recycling, its physiological relevance is unclear. In accordance to the HflX function in bacteria (reviewed by Bennison et al., 2019; Srinivasan et al., 2019; Verstraeten et al., 2011), it is reasonable to speculate that GTPBP6 is involved in the rescue of the ribosomes stalled upon aberrant non-stop mRNA translation or due to aminoacyl-tRNA starvation. Recently, the novel mitoribosome-associated quality control pathway has been reported (Desai et al., 2020). Mitoribosomes stalled during translation elongation due to tRNA depletion appeared to be split, resulting in mtLSU particles with a peptidyl tRNA in the P-site. These mtLSU complexes are rescued by C12ORF65 (mtRF-R) and C6ORF203 (MTRES1). mtRF-R facilitates the hydrolysis of the nascent polypeptide chain according to its function as a release factor and MTRES1 removes the remaining tRNA. The preceding mitoribosome dissociating mechanism remains unclear. However, it is unlikely that the subunit splitting result from the GTPBP6 activity since the post splitting complex still contains peptidyl tRNA in the P-site thereby sterically excluding GTPBP6 binding. GTPBP6 binding would be only possible if the peptidyl-tRNA would spontaneously adopt the P/E hybrid state.

Another scenario implies the possible role of GTPBP6-driven mitoribosome recycling in rescuing mitoribosomes stalled on non-stop mRNAs. The pathway is initiated by an action of a mitochondrial codon-unspecific tRNA hydrolase, ICT1 (mL62) (Feaga et al., 2016; Kummer et al., 2021). ICT1 binds specifically to the mitoribosomes with a partially empty mRNA channel. Associated with the A-site, ICT1 probes the mRNA channel from the PTC to the mRNA entry site with its C-terminal domain. Although the mitoribosome substrates are different for ICT1 and the canonical mitochondrial release factor mtRF1a (Soleimanpour-Lichaei et al., 2007; Richter et al., 2010), their mechanism of binding to the mitoribosome and of a nascent polypeptide chain release appeared to be strikingly similar (Kummer et al., 2021). ICT1 is a human homolog of bacterial ArfB (YaeJ). The latter factor rescues ribosomes stalled on non-stop truncated mRNAs (Chan et al., 2020) and was proposed to precede the HflX-mediated splitting of stalled 70S ribosomes (Zhang et al., 2015). Thus, it is tempting to assume that the action of ICT1 precedes GTPBP6-mediated mitoribosome recycling activity in a similar scenario. Available structural data do not allow to distinguish architectural features of post-hydrolysis mitoribosome complexes that would specifically favor recycling by GTPBP6 instead of the canonical recycling system. Therefore, the choice of a recycling pathway is probably

defined by physiological conditions rather than by the structure of the mitoribosome complex itself.

5.6 Structural basis of the dual function of GTPBP6 in human mitochondria

GTPBP6 possesses the basic domain architecture characteristic to the other members of the HflX GTPases family. The family is characterized by the presence of a highly conserved GTPase domain (ND2) generally responsible for the ribosome binding (reviewed by Srinivasan et al., 2019). On the contrary, there are certain structural differences between ND1 domains among species. Those differences probably reflect functional adaptations of the HflX family GTPases to operate within distinct stress response pathways. For example, *E. coli* HflX is devoted to rescue stalled ribosomes in heat-stress and apply its ND2 GTPase activity to dissociate the ribosome, whereas ND1 together with the linker domain is capable of binding ATP and serves as a helicase to unwind damaged rRNA (Dey et al., 2018; Zhang et al., 2015). Although only GTP-binding is essential for HflX interaction with 70S ribosomes or 50S LSU, ATP facilitates the PTC-binding domain to come into close contact to the P- loop, thereby promoting rRNA refolding (Dey et al., 2018; Zhang et al., 2015). HflX was not characterized as a classical ATPase (Jain et al., 2013); however, several amino-acid residues in the ND1 domain were bioinformatically predicted to be crucial for ATP docking, including Arg-90 and Asp-102 (*E. coli* numbering) (Srinivasan et al., 2019). Arg-90 and Asp-102 correspond to Lys-187 and Asp-199 in human GTPBP6. However, none of the residues are crucial for GTPBP6 function as a ribosome biogenesis factor (Lavdovskaia et al., 2020). Moreover, a combination of rapid kinetic measurements and cryo-EM analysis suggest that GTPBP6 fulfills its function in driving the PTC maturation and ribosome recycling without complementation of adenosine nucleotides (Hillen et al., 2021; Lavdovskaia et al., 2020). In contrast, Asp-199 appeared to be critical for GTPBP6 recycling activity, suggesting that although the residue does not promote ATP binding, it is probably required for correct positioning of GTPBP6 Trp-107 towards the mitoribosome intersubunit bridge resulting in mitoribosome dissociation (Hillen et al., 2021; Lavdovskaia et al., 2020). The importance of the Asp-199 for the GTPBP6 recycling function further emphasizes the evolutionary conserved involvement of the ND1 domain of HflX-related GTPases into the stress-induced rescuing pathways of (mito)ribosomes.

Structural analysis of the GTPBP6-bound mtLSU biogenesis and recycling complexes revealed that the factor executes its dual function in a complex with GTP, suggesting that association with the co-factor is a prerequisite for its interaction with the mtLSU (Hillen et al., 2021). Mutational analysis of the GTPBP6 GTPase domain indicates the importance of the Ser-437 for the factor dissociation activity on 70S ribosomes *in vitro* (Lavdovskaia et al., 2020). Despite the exact function of the residue in mitoribosome assembly GTPases remains to be

elucidated, it is tempting to speculate that as a part of the G5 motif it is involved into interactions with the guanine ring. Previously, we have shown that the corresponding Ser-325 into GTPBP10 is crucial for its binding to the mitoribosome (Lavdovskaia et al., 2018). In contrast to the loss of the ribosome recycling activity, the GTPBP6 S437P mutant retains its mitoribosome biogenesis function, although to a lower extent (Lavdovskaia et al., 2020). A possible explanation for this discrepancy can be (i) even though S437P attenuates GTP-binding, GTPBP6 is able to associate with the mtLSU without a bound nucleotide as it was demonstrated for *S. solfataricus* HflX (Blombach et al., 2011) and complement the subunit biogenesis to a certain extent. In contrast, GTPBP6 interaction with the 55S mitoribosome indispensably requires GTP-binding; (ii) alternatively, S437P does not abolish the nucleotide binding itself but disrupts complex inter-domain interactions of GTPBP6 which are specifically required for 55S splitting but not for mtLSU maturation. The recycling function of HflX on 70S ribosomes essentially relies on the extensive inter-domain interactions mediated by salt bridges (Jain et al., 2013). Although the residues involved in the HflX inter-domain communication are not conserved in GTPBP6, it is reasonable to assume that the same mechanism of a cross-talk also exists.

Our previous observation that GTPBP6 function in mitoribosome recycling essentially requires GTP-binding but not GTP hydrolysis is further supported by mutational analysis. Conserved Gly-325 (Gly-352 in GTPBP6 numbering) in G4 motif was found to be essential for GTP hydrolysis by *S. solfataricus* HflX (Huang et al., 2010). In agreement with the residue function, G352P substitution completely abolishes GTPBP6 function as a ribosome biogenesis factor. In contrast, the mutant retains a rate of ribosome recycling activity comparable to WT protein. Indeed, the GTP-hydrolysis and subsequent dissociation of GTPBP6*GDP is an essential prerequisite of the subunits joining and translationally competent mitoribosome formation but is not required for mitoribosome splitting.

In summary, our data suggest that mitoribosome biogenesis and recycling activities of GTPBP6 are independent of each other and involve different regions of the factor.

6 Summary and outlook

In conclusion, a combination of high resolution structural analysis with biochemical and genome editing techniques allowed to propose a hierarchical model for the folding of the mitoribosome functional center and to unveil the role of the biogenesis factors in driving the structural transitions within the mtLSU interface. Thus, at least 4 GTPases are involved into the late stages of mtLSU assembly to form the PTC: GTPBP5, GTPBP6, GTPBP7 and GTPBP10. They protect the catalytic site from the premature binding of translation factors and serve as assembly check points, probing the maturation status of the respective rRNA domains. GTPases extensively collaborate with other assembly factors as exemplified by DDX28-GTPBP10 and MRM2-GTPBP5 interactions. However, we still lack the mechanistic details of these interactions since the structural data obtained so far are controversial. Remarkably, the aforementioned GTPases tightly associate with the mtLSU in a GTP-dependent manner, but their departure most likely implies distinct underlying mechanisms. Further biochemical analysis will clarify the link between GTP binding vs. hydrolysis and mitoribosome association of the assembly GTPases. Moreover, the mtLSU assembly GTPases serve as anti-association factors to prevent premature subunit joining. In this case, GTPBP6 represents the first identified example of how the mitoribosome recycling might be coupled with the assembly of a new functional 55S particle.

Why are so many GTPases required to guide the last steps of the mtLSU maturation? Bacterial ribosome assembly machinery accounts for at least 4 GTPases which assist the PTC maturation (despite their presence in species may vary) (reviewed by Bennison et al., 2019; Verstraeten et al., 2011). Certain proteins do not have homologs in higher eukaryotes; for example, the Der-related GTPases are not present in mammalian genomes. Instead, the function of the bacterial ObgE is distributed between two homologs – GTPBP5 and GTPBP10; GTPBP6 has acquired an additional role of a mitoribosome biogenesis factor in humans. An extensive investigation of the mitoribosome assembly GTPases shows that the role of each factor is unique and indispensable. As it was demonstrated by the structural studies, the functional center of the mitoribosome is the final region of the mtLSU to be matured. It has an essential physiological relevance since the universally conserved PTC is critical for ensuring the accuracy and fidelity of translation. Therefore, aberrantly assembled particles must be prevented from being engaged into the (mito)ribosome. The mtLSU biogenesis GTPases facilitate its maturation and also fulfill the quality control function. Since the factors use a tRNA mimicry strategy to associate with the PTC, this raises the hypothesis that the mechanism implicates a ‘translation test-drive’ of the mitoribosome functional center to dissect the correctly assembled particles to progress into the mature translationally competent subunits. The same strategy was suggested for the assembly GTPases of the cytosolic 60S LSU (Bussiere et al.,

2012). Apparently, GTPases appeared to be an indispensable evolutionary conserved tool to regulate ribosome biogenesis.

What is the regulatory mechanism of mitoribosome assembly GTPases? In bacteria, ribosome assembly GTPases are sensors of the stringent response alarmone (p)ppGpp. A GTPase bound to the co-factor blocks the ribosome maturation at late stages by acting as an anti-association factor. Indeed, this driving mechanism cannot be applied to their mitochondrial counterparts. Do the mitochondrial GTPases sense the intracellular levels of guanosine nucleotides? Alternatively, does their activity rely on the GEFs? These questions remain to be addressed in the future and will provide the mechanism of how the assembly GTPases adjust the biogenesis of the mammalian mitoribosome in response to the cellular/organellar needs.

7 References

1. Achila, D., Gulati, M., Jain, N., and Britton, R.A. (2012). Biochemical characterization of ribosome assembly GTPase RbgA in *Bacillus subtilis*. *J Biol Chem* 287, 8417–8423.
2. Agaronyan, K., Morozov, Y.I., Anikin, M., and Temiakov, D. (2015). Mitochondrial biology. Replication-transcription switch in human mitochondria. *Science* 347, 548–551.
3. Aibara, S., Singh, V., Modelska, A., and Amunts, A. (2020). Structural basis of mitochondrial translation. *eLife* 9.
4. Akabane, S., Ueda, T., Nierhaus, K.H., and Takeuchi, N. (2014). Ribosome rescue and translation termination at non-standard stop codons by ICT1 in mammalian mitochondria. *PLoS Genet* 10, e1004616.
5. Amunts, A., Brown, A., Toots, J., Scheres, S.H.W., and Ramakrishnan, V. (2015). The structure of the human mitochondrial ribosome. *Science* 348, 95–98.
6. Antonicka, H., and Shoubridge, E.A. (2015). Mitochondrial RNA Granules Are Centers for Posttranscriptional RNA Processing and Ribosome Biogenesis. *CellReports* 10, 920–932.
7. Antonicka, H., Choquet, K., Lin, Z.-Y., Gingras, A.-C., Kleinman, C.L., and Shoubridge, E.A. (2017). A pseudouridine synthase module is essential for mitochondrial protein synthesis and cell viability. *EMBO Rep* 18, 28–38.
8. Antonicka, H., Sasarman, F., Nishimura, T., Paupe, V., and Shoubridge, E.A. (2013). The mitochondrial RNA-binding protein GRSF1 localizes to RNA granules and is required for posttranscriptional mitochondrial gene expression. *Cell Metabolism* 17, 386–398.
9. Arai, T., Ishiguro, K., Kimura, S., Sakaguchi, Y., Suzuki, T., and Suzuki, T. (2015). Single methylation of 23S rRNA triggers late steps of 50S ribosomal subunit assembly. *Proc. Natl. Acad. Sci. U.S.a.* 112, E4707–E4716.
10. Arroyo, J.D., Jourdain, A.A., Calvo, S.E., Ballarano, C.A., Doench, J.G., Root, D.E., and Mootha, V.K. (2016). A Genome-wide CRISPR Death Screen Identifies Genes Essential for Oxidative Phosphorylation. *Cell Metabolism* 24, 875–885.
11. Ayyub, S.A., and Varshney, U. (2019). Translation initiation in mammalian mitochondria- a prokaryotic perspective. *RNA Biology* 17, 165–175.
12. Ayyub, S.A., S L, A., Dobriyal, D., Aluri, S., Spremulli, L.L., and Varshney, U. (2018). Fidelity of translation in the presence of mammalian mitochondrial initiation factor 3. *Mitochondrion* 39, 1–8.
13. Babu, V.M.P., Sankari, S., Budnick, J.A., Caswell, C.C., and Walker, G.C. (2020). *Sinorhizobium meliloti* YbeY is a zinc-dependent single-strand specific endoribonuclease that plays an important role in 16S ribosomal RNA processing. *Nucleic Acids Research* 48, 332–348.
14. Ban, N., Nissen, P., Hansen, J., Moore, P.B., and Steitz, T.A. (2000). The complete atomic structure of the large ribosomal subunit at 2.4 Å resolution. *Science* 289, 905–920.
15. Bar-Yaacov, D., Frumkin, I., Yashiro, Y., Chujo, T., Ishigami, Y., Chemla, Y., Blumberg, A., Schlesinger, O., Bieri, P., Greber, B., et al. (2016). Mitochondrial 16S rRNA Is Methylated by tRNA Methyltransferase TRMT61B in All Vertebrates. *PLoS Biol* 14, e1002557.
16. Barrientos, A. (2015). Mitochondriolus: assembling mitoribosomes. *Oncotarget* 6, 16800–16801.
17. Barrientos, A., Korr, D., Barwell, K.J., Sjulsen, C., Gajewski, C.D., Manfredi, G., Ackerman, S., and Tzagoloff, A. (2003). MTG1 codes for a conserved protein required for mitochondrial translation. *Mol Biol Cell* 14, 2292–2302.
18. Barchiesi, A., and Vascotto, C. (2019). Transcription, Processing, and Decay of

- Mitochondrial RNA in Health and Disease. *International Journal of Molecular Sciences* 20, 2221.
19. Batra, S., Kumar, A., Prakash, B. Alternative catalytic mechanisms driven by structural plasticity is an emerging theme in HAS-GTPases, Era and FeoB. (2020). bioRxiv. doi: 10.1101/2020.08.16.253419.
 20. Bennison, Irving, and Corrigan (2019). The Impact of the Stringent Response on TRAFAC GTPases and Prokaryotic Ribosome Assembly. *Cells* 8, 1313–1324.
 21. Bhargava, K., and Spremulli, L.L. (2005). Role of the N- and C-terminal extensions on the activity of mammalian mitochondrial translational initiation factor 3. *Nucleic Acids Research* 33, 7011–7018.
 22. Bieri, P., Greber, B.J., and Ban, N. (2018). High-resolution structures of mitochondrial ribosomes and their functional implications. *Curr Opin Struct Biol* 49, 44–53.
 23. Blombach, F., Launay, H., Zorraquino, V., Swarts, D.C., Cabrita, L.D., Benelli, D., Christodoulou, J., Londei, P., and van der Oost, J. (2011). An HflX-type GTPase from *Sulfolobus solfataricus* binds to the 50S ribosomal subunit in all nucleotide-bound states. *Journal of Bacteriology* 193, 2861–2867.
 24. Bogenhagen, D.F., and Haley, J.D. (2020). Pulse-chase SILAC-based analyses reveal selective oversynthesis and rapid turnover of mitochondrial protein components of respiratory complexes. *J Biol Chem* 295, 2544–2554.
 25. Bogenhagen, D.F., Martin, D.W., and Koller, A. (2014). Initial steps in RNA processing and ribosome assembly occur at mitochondrial DNA nucleoids. *Cell Metabolism* 19, 618–629.
 26. Bogenhagen, D.F., Ostermeyer-Fay, A.G., Haley, J.D., and Garcia-Diaz, M. (2018). Kinetics and Mechanism of Mammalian Mitochondrial Ribosome Assembly. *CellReports* 22, 1935–1944.
 27. Bohnsack, M.T., and Sloan, K.E. (2018). The mitochondrial epitranscriptome: the roles of RNA modifications in mitochondrial translation and human disease. *Cell Mol Life Sci* 75, 241–260.
 28. Bonekamp, N.A., and Larsson, N.-G. (2018). SnapShot: Mitochondrial Nucleoid. *Cell* 172, 388–388.e1.
 29. Borowski, L.S., Dziembowski, A., Hejnowicz, M.S., Stepień, P.P., and Szczesny, R.J. (2013). Human mitochondrial RNA decay mediated by PNPase-hSuv3 complex takes place in distinct foci. *Nucleic Acids Research* 41, 1223–1240.
 30. Bourne, H.R., Sanders, D.A., and McCormick, F. (1990). The GTPase superfamily: a conserved switch for diverse cell functions. *Nature* 348, 125–132.
 31. Bourne, H.R., Sanders, D.A., and McCormick, F. (1991). The GTPase superfamily: conserved structure and molecular mechanism. *Nature* 349, 117–127.
 32. Brina, D., Miluzio, A., Ricciardi, S., and Biffo, S. (2015). eIF6 anti-association activity is required for ribosome biogenesis, translational control and tumor progression. *Biochim Biophys Acta* 1849, 830–835.
 33. Britton, R.A. (2009). Role of GTPases in bacterial ribosome assembly. *Annu Rev Microbiol* 63, 155–176.
 34. Brown, A., Amunts, A., Bai, X.C., Sugimoto, Y., Edwards, P.C., Murshudov, G., Scheres, S.H.W., and Ramakrishnan, V. (2014). Structure of the large ribosomal subunit from human mitochondria. *Science* 346, 718–722.
 35. Brown, A., Rathore, S., Kimanius, D., Aibara, S., Bai, X.-C., Rorbach, J., Amunts, A., and Ramakrishnan, V. (2017). Structures of the human mitochondrial ribosome in native states of assembly. *Nat Struct Mol Biol* 24, 866–869.
 36. Bruni, F., Gramegna, P., Oliveira, J.M.A., Lightowlers, R.N., and Chrzanowska-

- Lightowers, Z.M.A. (2013). REXO2 is an oligoribonuclease active in human mitochondria. *PLoS One* 8, e64670.
37. Bruni, F., Lightowers, R.N., and Chrzanowska-Lightowers, Z.M. (2017). Human mitochondrial nucleases. *Febs J* 284, 1767–1777.
38. Brzezniak, L.K., Bijata, M., Szczesny, R.J., and Stepien, P.P. (2011). Involvement of human ELAC2 gene product in 3' end processing of mitochondrial tRNAs. *RNA Biology* 8, 616–626.
39. Busch, J.D., Cipullo, M., Atanassov, I., Bratic, A., Silva Ramos, E., Schöndorf, T., Li, X., Pearce, S.F., Milenkovic, D., Rorbach, J., et al. (2019). MitoRibo-Tag Mice Provide a Tool for In Vivo Studies of Mitoribosome Composition. *CellReports* 29, 1728–1738.e1729.
40. Bussiere, C., Hashem, Y., Arora, S., Frank, J., and Johnson, A.W. (2012). Integrity of the P-site is probed during maturation of the 60S ribosomal subunit. *J Cell Biol* 197, 747–759.
41. Bügl, H., Fauman, E.B., Staker, B.L., Zheng, F., Kushner, S.R., Saper, M.A., Bardwell, J.C., and Jakob, U. (2000). RNA methylation under heat shock control. *Mol Cell* 6, 349–360.
42. Cavdar Koc, E., Burkhart, W., Blackburn, K., Moseley, A., and Spremulli, L.L. (2001a). The small subunit of the mammalian mitochondrial ribosome. Identification of the full complement of ribosomal proteins present. *Journal of Biological Chemistry* 276, 19363–19374.
43. Cavdar Koc, E., Ranasinghe, A., Burkhart, W., Blackburn, K., Koc, H., Moseley, A., and Spremulli, L.L. (2001b). A new face on apoptosis: death-associated protein 3 and PDCD9 are mitochondrial ribosomal proteins. *FEBS Lett* 492, 166–170.
44. Cámara, Y., Asin-Cayuela, J., Park, C.B., Metodiev, M.D., Shi, Y., Ruzzenente, B., Kukat, C., Habermann, B., Wibom, R., Hultenby, K., et al. (2011). MTERF4 regulates translation by targeting the methyltransferase NSUN4 to the mammalian mitochondrial ribosome. *Cell Metabolism* 13, 527–539.
45. Chan, K.-H., Petrychenko, V., Mueller, C., Maracci, C., Holtkamp, W., Wilson, D.N., Fischer, N., and Rodnina, M.V. (2020). Mechanism of ribosome rescue by alternative ribosome-rescue factor B. *Nature Communications* 11, 4106–4111.
46. Chandrasekaran, V., Desai, N., Burton, N., Yang, H., Price, J., Miska, E.A., Ramakrishnan, V. (2021). Visualising formation of the active site in the mitochondrial ribosome. *eLife* 10:e68806.
47. Chen, H., Shi, Z., Guo, J., Chang, K.-J., Chen, Q., Yao, C.-H., Haigis, M.C., and Shi, Y. (2020). The human mitochondrial 12S rRNA m4C methyltransferase METTL15 is required for mitochondrial function. *J Biol Chem* 295, 8505–8513.
48. Chen, S.S., and Williamson, J.R. (2013). Characterization of the ribosome biogenesis landscape in *E. coli* using quantitative mass spectrometry. *Journal of Molecular Biology* 425, 767–779.
49. Cheng, J., Berninghausen, O., Beckmann, R. (2021). A distinct assembly pathway of the human 39S late pre-mitoribosome. *Nature Communications* 12.
50. Chicherin, I.V., Baleva, M.V., Levitskii, S.A., Dashinimaev, E.B., and Krasheninnikov, I.A. (2019). Mitochondrial Translation Initiation Factor 3: Structure, Functions, Interactions, and Implication in Human Health and Disease. *Biochemistry (Mosc)* 84, 1143–1150.
51. Christian, B.E., and Spremulli, L.L. (2009). Evidence for an active role of IF3mt in the initiation of translation in mammalian mitochondria. *Biochemistry* 48, 3269–3278.
52. Chrzanowska-Lightowers, Z., Rorbach, J., and Minczuk, M. (2017). Human mitochondrial ribosomes can switch structural tRNAs - but when and why? *RNA Biology* 14, 1668–1671.
53. Cipullo, M., Pearce, S.F., Lopez Sanchez, I.G., Gopalakrishna, S., Krüger, A., Schober,

- F., Busch, J.D., Li, X., Wredenber, A., Atanassov, I., et al. (2021b). Human GTPBP5 is involved in the late stage of mitoribosome large subunit assembly. *Nucleic Acids Research* 49, 354–370.
54. Cipullo, M., Gesé, G. V., Khawaja, A., Hällberg, B. M. & Rorbach, J. (2021a). Structural basis for late maturation steps of the human mitoribosomal large subunit. *Nature Communications* 12.
55. Coatham, M.L., Brandon, H.E., Fischer, J.J., Schümmer, T., and Wieden, H.-J. (2016). The conserved GTPase HflX is a ribosome splitting factor that binds to the E-site of the bacterial ribosome. *Nucleic Acids Research* 44, 1952–1961.
56. Corrigan, R.M., Bellows, L.E., Wood, A., and Gründling, A. (2016). ppGpp negatively impacts ribosome assembly affecting growth and antimicrobial tolerance in Gram-positive bacteria. *Proc Natl Acad Sci USA* 113, E1710–E1719.
57. Dalla Rosa, I., Durigon, R., Pearce, S.F., Rorbach, J., Hirst, E.M.A., Vidoni, S., Reyes, A., Brea-Calvo, G., Minczuk, M., Woellhaf, M.W., et al. (2014). MPV17L2 is required for ribosome assembly in mitochondria. *Nucleic Acids Research* 42, 8500–8515.
58. Datta, K., Fuentes, J.L., and Maddock, J.R. (2005). The yeast GTPase Mtg2p is required for mitochondrial translation and partially suppresses an rRNA methyltransferase mutant, *mrm2*. *Mol Biol Cell* 16, 954–963.
59. Davis, J.H., and Williamson, J.R. (2017). Structure and dynamics of bacterial ribosome biogenesis. *Phil. Trans. R. Soc. B* 372, 20160181–20160189.
60. Davydov, I.I., Wohlgemuth, I., Artamonova, I.I., Urlaub, H., Tonevitsky, A.G., and Rodnina, M.V. (2019). Evolution of the protein stoichiometry in the L12 stalk of bacterial and organellar ribosomes. *Nature Communications* 10.
61. Demirci, H., Murphy, F., Belardinelli, R., Kelley, A.C., Ramakrishnan, V., Gregory, S.T., Dahlberg, A.E., and Jogl, G. (2010). Modification of 16S ribosomal RNA by the KsgA methyltransferase restructures the 30S subunit to optimize ribosome function. *RNA* 16, 2319–2324.
62. Dennerlein, S., Rozanska, A., Wydro, M., Chrzanowska-Lightowlers, Z.M.A., and Lightowlers, R.N. (2010). Human ERAL1 is a mitochondrial RNA chaperone involved in the assembly of the 28S small mitochondrial ribosomal subunit. *Biochem J* 430, 551–558.
63. Desai, N., Brown, A., Amunts, A., and Ramakrishnan, V. (2017). The structure of the yeast mitochondrial ribosome. *Science* 355, 528–531.
64. Desai, N., Yang, H., Chandrasekaran, V., Kazi, R., Minczuk, M., and Ramakrishnan, V. (2020). Elongational stalling activates mitoribosome-associated quality control. *Science* 370, 1105–1110.
65. Desmond, E., Brochier-Armanet, C., Forterre, P., and Gribaldo, S. (2011). On the last common ancestor and early evolution of eukaryotes: reconstructing the history of mitochondrial ribosomes. *Research in Microbiology* 162, 53–70.
66. Dey, S., Biswas, C., and Sengupta, J. (2018). The universally conserved GTPase HflX is an RNA helicase that restores heat-damaged *Escherichia coli* ribosomes. *J Cell Biol* 217, 2519–2529.
67. Dohme, F., and Nierhaus, K.H. (1976). Total reconstitution and assembly of 50 S subunits from *Escherichia coli* Ribosomes in vitro. *Journal of Molecular Biology* 107, 585–599.
68. D'Souza, A.R., and Minczuk, M. (2018). Mitochondrial transcription and translation: overview. *Essays Biochem* 62, 309–320.
69. D'Souza, A.R., Van Haute, L., Powell, C.A., Mutti, C.D., Páleníková, P., Rebelo-Guimar, P., Rorbach, J., and Minczuk, M. (2021). YbeY is required for ribosome small subunit assembly and tRNA processing in human mitochondria. *Nucleic Acids Research* 49,

5798-5812.

70. Duval, M., Dar, D., Carvalho, F., Rocha, E.P.C., Sorek, R., and Cossart, P. (2018). HflXr, a homolog of a ribosome-splitting factor, mediates antibiotic resistance. *Proc Natl Acad Sci USA* *115*, 13359–13364.
71. Ekstrand, M.I., Falkenberg, M., Rantanen, A., Park, C.B., Gaspari, M., Hultenby, K., Rustin, P., Gustafsson, C.M., and Larsson, N.-G. (2004). Mitochondrial transcription factor A regulates mtDNA copy number in mammals. *Hum Mol Genet* *13*, 935–944.
72. Englmeier, R., Pfeffer, S., and Förster, F. (2017). Structure of the Human Mitochondrial Ribosome Studied In Situ by Cryoelectron Tomography. *Structure* *25*, 1574–1581.e2.
73. Falkenberg, M., Gaspari, M., Rantanen, A., Trifunovic, A., Larsson, N.-G., and Gustafsson, C.M. (2002). Mitochondrial transcription factors B1 and B2 activate transcription of human mtDNA. *Nat Genet* *31*, 289–294.
74. Farge, G., and Falkenberg, M. (2019). Organization of DNA in Mammalian Mitochondria. *Ijms* *20*, 2770–14.
75. Feaga, H.A., Quickel, M.D., Hankey-Giblin, P.A., and Keiler, K.C. (2016). Human Cells Require Non-stop Ribosome Rescue Activity in Mitochondria. *PLoS Genet* *12*, e1005964.
76. Feng, B., Mandava, C.S., Guo, Q., Wang, J., Cao, W., Li, N., Zhang, Y., Zhang, Y., Wang, Z., Wu, J., et al. (2014). Structural and functional insights into the mode of action of a universally conserved Obg GTPase. *PLoS Biol* *12*, e1001866.
77. Ferrari, A., Del’Olio, S. and Barrientos, A. (2020). The diseased mitoribosome. *FEBS Lett.* *233*, 657.
78. Fu, Z., Kaledhonkar, S., Borg, A., Sun, M., Chen, B., Grassucci, R.A., Ehrenberg, M., and Frank, J. (2016). Key Intermediates in Ribosome Recycling Visualized by Time-Resolved Cryoelectron Microscopy. *Structure* *24*, 2092–2101.
79. Fung, S., Nishimura, T., Sasarman, F., and Shoubridge, E.A. (2013). The conserved interaction of C7orf30 with MRPL14 promotes biogenesis of the mitochondrial large ribosomal subunit and mitochondrial translation. *Mol Biol Cell* *24*, 184–193.
80. Gartmann, M., Blau, M., Armache, J.-P., Mielke, T., Topf, M., and Beckmann, R. (2010). Mechanism of eIF6-mediated inhibition of ribosomal subunit joining. *J Biol Chem* *285*, 14848–14851.
81. Gaur, R., Grasso, D., Datta, P.P., Krishna, P.D.V., Das, G., Spencer, A., Agrawal, R.K., Spremulli, L., and Varshney, U. (2008). A single mammalian mitochondrial translation initiation factor functionally replaces two bacterial factors. *Mol Cell* *29*, 180–190.
82. Ghosal, A., Köhrer, C., Babu, V.M.P., Yamanaka, K., Davies, B.W., Jacob, A.I., Ferullo, D.J., Gruber, C.C., Vercruyssen, M., and Walker, G.C. (2017). C21orf57 is a human homologue of bacterial YbeY proteins. *Biochem Biophys Res Commun* *484*, 612–617.
83. Ghosh, A., Dutta, D., Bandyopadhyay, K., and Parrack, P. (2016). Characterization of the autophosphorylation property of HflX, a ribosome-binding GTPase from *Escherichia coli*. *FEBS Open Bio* *6*, 651–659.
84. Goto, S., Muto, A., and Himeno, H. (2013). GTPases involved in bacterial ribosome maturation. *The Journal of Biochemistry* *153*, 403–414.
85. Greber, B.J., and Ban, N. (2016). Structure and Function of the Mitochondrial Ribosome. *Annu. Rev. Biochem.* *85*, 103–132.
86. Greber, B.J., Bieri, P., Leibundgut, M., Leitner, A., Aebersold, R., Boehringer, D., and Ban, N. (2015). Ribosome. The complete structure of the 55S mammalian mitochondrial ribosome. *Science* *348*, 303–308.
87. Greber, B.J., Boehringer, D., Leibundgut, M., Bieri, P., Leitner, A., Schmitz, N., Aebersold, R., and Ban, N. (2014). The complete structure of the large subunit of the mammalian mitochondrial ribosome. *Nature* *515*, 283–286.

88. Gulati, M., Jain, N., Anand, B., Prakash, B., and Britton, R.A. (2013). Mutational analysis of the ribosome assembly GTPase RbgA provides insight into ribosome interaction and ribosome-stimulated GTPase activation. *Nucleic Acids Research* 41, 3217–3227.
89. Gupta, A., Gupta, K., and Habib, S. (2020). YihA GTPases localize to the apicoplast and mitochondrion of the malaria parasite and interact with LSU of organellar ribosomes. *Mol Biochem Parasitol* 236, 111265.
90. Haque, M.E., Elmore, K.B., Tripathy, A., Koc, H., Koc, E.C., and Spremulli, L.L. (2010a). Properties of the C-terminal tail of human mitochondrial inner membrane protein Oxa1L and its interactions with mammalian mitochondrial ribosomes. *J Biol Chem* 285, 28353–28362.
91. Haque, M.E., Grasso, D., and Spremulli, L.L. (2008). The interaction of mammalian mitochondrial translational initiation factor 3 with ribosomes: evolution of terminal extensions in IF3mt. *Nucleic Acids Research* 36, 589–597.
92. Haque, M.E., Spremulli, L.L., and Fecko, C.J. (2010b). Identification of protein-protein and protein-ribosome interacting regions of the C-terminal tail of human mitochondrial inner membrane protein Oxa1L. *J Biol Chem* 285, 34991–34998.
93. Hällberg, B.M., and Larsson, N.-G. (2014). Making Proteins in the Powerhouse. *Cell Metabolism* 20, 226–240.
94. He, J., Cooper, H.M., Reyes, A., Di Re, M., Kazak, L., Wood, S.R., Mao, C.C., Fearnley, I.M., Walker, J.E., and Holt, I.J. (2012). Human C4orf14 interacts with the mitochondrial nucleoid and is involved in the biogenesis of the small mitochondrial ribosomal subunit. *Nucleic Acids Research* 40, 6097–6108.
95. Helm, M., Brulé, H., Friede, D., Giegé, R., Pütz, D., and Florentz, C. (2000). Search for characteristic structural features of mammalian mitochondrial tRNAs. *RNA* 6, 1356–1379.
96. Hillen, H., Lavdovskaia, E., Nadler, F., Hanitsch, E., Linden, A., Bohnsack, K., Urlaub, H., and Richter-Dennerlein, R. (2021). Structural basis of GTPase-mediated mitochondrial ribosome biogenesis and recycling. *Nature Communications* 12.
97. Hillen, H.S., Parshin, A.V., Agaronyan, K., Morozov, Y.I., Graber, J.J., Chernev, A., Schwinghammer, K., Urlaub, H., Anikin, M., Cramer, P., et al. (2017). Mechanism of Transcription Anti-termination in Human Mitochondria. *Cell* 171, 1082–1093.e13.
98. Hillen, H.S., Morozov, Y.I., Sarfallah, A., Temiakov, D., and Cramer, P. (2017). Structural Basis of Mitochondrial Transcription Initiation. *Cell* 171, 1072–1081.e10.
99. Hirano, Y., Ohniwa, R.L., Wada, C., Yoshimura, S.H., and Takeyasu, K. (2006). Human small G proteins, ObgH1, and ObgH2, participate in the maintenance of mitochondria and nucleolar architectures. *Genes Cells* 11, 1295–1304.
100. Holzmann, J., Frank, P., Löffler, E., Bennett, K.L., Gerner, C., and Rossmann, W. (2008). RNase P without RNA: identification and functional reconstitution of the human mitochondrial tRNA processing enzyme. *Cell* 135, 462–474.
101. Huang, B., Wu, H., Hao, N., Blombach, F., van der Oost, J., Li, X., Zhang, X.C., and Rao, Z. (2010). Functional study on GTP hydrolysis by the GTP-binding protein from *Sulfolobus solfataricus*, a member of the HflX family. *J Biochem* 148, 103–113.
102. Itoh, Y., Andréll, J., Choi, A., Richter, U., Maiti, P., Best, R.B., Barrientos, A., Battersby, B.J., and Amunts, A. (2021). Mechanism of membrane-tethered mitochondrial protein synthesis. *Science* 371, 846–849.
103. Jacob, A.I., Köhler, C., Davies, B.W., RajBhandary, U.L., and Walker, G.C. (2013). Conserved bacterial RNase YbeY plays key roles in 70S ribosome quality control and 16S rRNA maturation. *Mol Cell* 49, 427–438.
104. Jain, N., Vithani, N., Rafay, A., and Prakash, B. (2013). Identification and characterization of a hitherto unknown nucleotide-binding domain and an intricate

- interdomain regulation in HflX-a ribosome binding GTPase. *Nucleic Acids Research* *41*, 9557–9569.
105. Jaskolowski, M., Ramrath, D.J.F., Bieri, P., Niemann, M., Mattei, S., Calderaro, S., Leibundgut, M., Horn, E.K., Boehringer, D., Schneider, A., et al. (2020). Structural Insights into the Mechanism of Mitoribosomal Large Subunit Biogenesis. *Mol Cell* *79*, 629–644.e4.
106. Jiang, M., Datta, K., Walker, A., Strahler, J., Bagamasbad, P., Andrews, P.C., and Maddock, J.R. (2006). The *Escherichia coli* GTPase CgtAE is involved in late steps of large ribosome assembly. *Journal of Bacteriology* *188*, 6757–6770.
107. Jomaa, A., Jain, N., Davis, J.H., Williamson, J.R., Britton, R.A., and Ortega, J. (2014). Functional domains of the 50S subunit mature late in the assembly process. *Nucleic Acids Research* *42*, 3419–3435.
108. Jourdain, A.A., Boehm, E., Maundrell, K., and Martinou, J.-C. (2016). Mitochondrial RNA granules: Compartmentalizing mitochondrial gene expression. *J Cell Biol* *212*, 611–614.
109. Jourdain, A.A., Koppen, M., Wydro, M., Rodley, C.D., Lightowers, R.N., Chrzanowska-Lightowers, Z.M., and Martinou, J.-C. (2013). GRSF1 regulates RNA processing in mitochondrial RNA granules. *Cell Metabolism* *17*, 399–410.
110. Kaledhonkar, S., Fu, Z., Caban, K., Li, W., Chen, B., Sun, M., Gonzalez, R.L., and Frank, J. (2019). Late steps in bacterial translation initiation visualized using time-resolved cryo-EM. *Nature* *570*, 400–404.
111. Karbstein, K. (2007). Role of GTPases in ribosome assembly. *Biopolymers* *87*, 1–11.
112. Karimi, R., Pavlov, M.Y., Buckingham, R.H., and Ehrenberg, M. (1999). Novel roles for classical factors at the interface between translation termination and initiation. *Mol Cell* *3*, 601–609.
113. Kaushal, P.S., Sharma, M.R., Booth, T.M., Haque, E.M., Tung, C.S., Sanbonmatsu, K.Y., Spremulli, L.L., and Agrawal, R.K. (2014). Cryo-EM structure of the small subunit of the mammalian mitochondrial ribosome. *Proc Natl Acad Sci USA* *111*, 7284–7289.
114. Khawaja, A., Itoh, Y., Remes, C., Spähr, H., Yukhnovets, O., Höfig, H., Amunts, A., and Rorbach, J. (2020). Distinct pre-initiation steps in human mitochondrial translation. *Nature Communications* *11*, 2932–10.
115. Kim, H.-J., and Barrientos, A. (2018). MTG1 couples mitoribosome large subunit assembly with intersubunit bridge formation. *Nucleic Acids Research* *46*, 8435–8453.
116. Kogure, H., Handa, Y., Nagata, M., Kanai, N., Güntert, P., Kubota, K., and Nameki, N. (2014). Identification of residues required for stalled-ribosome rescue in the codon-independent release factor YaeJ. *Nucleic Acids Research* *42*, 3152–3163.
117. Kolanczyk, M., Pech, M., Zemojtel, T., Yamamoto, H., Mikula, I., Calvaruso, M.-A., van den Brand, M., Richter, R., Fischer, B., Ritz, A., et al. (2011). NOA1 is an essential GTPase required for mitochondrial protein synthesis. *Mol Biol Cell* *22*, 1–11.
118. Koripella, R.K., Deep, A., Agrawal, E.K., Keshavan, P., Banavali, N.K., Agrawal, R.K. (2021). Distinct mechanisms of the human mitoribosome recycling and antibiotic resistance. *Nature Communications* *14*.
119. Koripella, R.K., Sharma, M.R., Haque, M.E., Risteff, P., Spremulli, L.L., and Agrawal, R.K. (2019a). Structure of Human Mitochondrial Translation Initiation Factor 3 Bound to the Small Ribosomal Subunit. *Iscience* *12*, 76–86.
120. Koripella, R.K., Sharma, M.R., Risteff, P., Keshavan, P., and Agrawal, R.K. (2019b). Structural insights into unique features of the human mitochondrial ribosome recycling. *Proc. Natl. Acad. Sci. U.S.A.* *116*, 8283–8288.
121. Koripella, R.K., Holm, M., Dourado, D., Mandava, C.S., Flores, S., and Sanyal, S. (2015). A conserved histidine in switch-II of EF-G moderates release of inorganic phosphate. *Sci Rep* *5*, 12970–10.

122. Koriyella, R.K., Sharma, M.R., Bhargava, K., Datta, P.P., Kaushal, P.S., Keshavan, P., Spremulli, L.L., Banavali, N.K., and Agrawal, R.K. (2020). Structures of the human mitochondrial ribosome bound to EF-G1 reveal distinct features of mitochondrial translation elongation. *Nature Communications* 11.
123. Kotani, T., Akabane, S., Takeyasu, K., Ueda, T., and Takeuchi, N. (2013). Human G-proteins, ObgH1 and Mtg1, associate with the large mitochondrial ribosome subunit and are involved in translation and assembly of respiratory complexes. *Nucleic Acids Research* 41, 3713–3722.
124. Kukat, C., Davies, K.M., Wurm, C.A., Spähr, H., Bonekamp, N.A., Kühl, I., Joos, F., Polosa, P.L., Park, C.B., Posse, V., et al. (2015). Cross-strand binding of TFAM to a single mtDNA molecule forms the mitochondrial nucleoid. *Proc. Natl. Acad. Sci. U.S.A.* 112, 11288–11293.
125. Kummer, E., and Ban, N. (2020). Structural insights into mammalian mitochondrial translation elongation catalyzed by mtEFG1. *EMBO J* 39, e104820.
126. Kummer, E., and Ban, N. (2021). Mechanisms and regulation of protein synthesis in mitochondria. *Nat Rev Mol Cell Biol* 22, 307–325.
127. Kummer, E., Leibundgut, M., Rackham, O., Lee, R.G., Boehringer, D., Filipovska, A., and Ban, N. (2018). Unique features of mammalian mitochondrial translation initiation revealed by cryo-EM. *Nature* 560, 263–267.
128. Kummer, E., Schubert, K.N., Schoenhut, T., Scaiola, A., and Ban, N. (2021). Structural basis of translation termination, rescue, and recycling in mammalian mitochondria. *Mol Cell* 81(12), 2566-2582.e6.
129. Laptev, I., Dontsova, O., and Sergiev, P. (2020a). Epitranscriptomics of Mammalian Mitochondrial Ribosomal RNA. *Cells* 9.
130. Laptev, I., Shvetsova, E., Levitskii, S., Serebryakova, M., Rubtsova, M., Bogdanov, A., Kamenski, P., Sergiev, P., and Dontsova, O. (2020b). Mouse Trmt2B protein is a dual specific mitochondrial methyltransferase responsible for m5U formation in both tRNA and rRNA. *RNA Biology* 17, 441–450.
131. Lavdovskaia, E., Denks, K., Nadler, F., Steube, E., Linden, A., Urlaub, H., Rodnina, M.V., and Richter-Dennerlein, R. (2020). Dual function of GTPBP6 in biogenesis and recycling of human mitochondrial ribosomes. *Nucleic Acids Research* 48, 12929–12942.
132. Lavdovskaia, E., Kolander, E., Steube, E., Mai, M.M.-Q., Urlaub, H., and Richter-Dennerlein, R. (2018). The human Obg protein GTPBP10 is involved in mitoribosomal biogenesis. *Nucleic Acids Research* 46, 8471–8482.
133. Lee, K.-W., and Bogenhagen, D.F. (2014). Assignment of 2'-O-methyltransferases to modification sites on the mammalian mitochondrial large subunit 16 S ribosomal RNA (rRNA). *J Biol Chem* 289, 24936–24942.
134. Lee, K.-W., Okot-Kotber, C., LaComb, J.F., and Bogenhagen, D.F. (2013). Mitochondrial ribosomal RNA (rRNA) methyltransferase family members are positioned to modify nascent rRNA in foci near the mitochondrial DNA nucleoid. *J Biol Chem* 288, 31386–31399.
135. Lee, S.R., and Han, J. (2017). Mitochondrial Nucleoid: Shield and Switch of the Mitochondrial Genome. *Oxid Med Cell Longev* 2017, 8060949.
136. Lee, Y., Bang, W.Y., Kim, S., Lazar, P., Kim, C.W., Bahk, J.D., and Lee, K.W. (2010). Molecular modeling study for interaction between *Bacillus subtilis* Obg and Nucleotides. *PLoS One* 5, e12597.
137. Leipe, D.D., Wolf, Y.I., Koonin, E.V., and Aravind, L. (2002). Classification and evolution of P-loop GTPases and related ATPases. *Journal of Molecular Biology* 317, 41–72.
138. Lenarcic, T., Jaskolowski, M., Leibundgut, M., Scaiola, A., Schönhut, T., Saurer, M.,

- Lee, R., Rackham, O., Filipovska, A., Ban N. (2021). Stepwise maturation of the peptidyl transferase region of human mitoribosomes. *Nature Communications* 12.
139. Litonin, D., Sologub, M., Shi, Y., Savkina, M., Anikin, M., Falkenberg, M., Gustafsson, C.M., and Temiakov, D. (2010). Human mitochondrial transcription revisited: only TFAM and TFB2M are required for transcription of the mitochondrial genes in vitro. *J Biol Chem* 285, 18129–18133.
140. Liu, Q., and Fredrick, K. (2016). Intersubunit Bridges of the Bacterial Ribosome. *Journal of Molecular Biology* 428, 2146–2164.
141. Liu, X., Shen, S., Wu, P., Li, F., Liu, X., Wang, C., Gong, Q., Wu, J., Yao, X., Zhang, H., et al. (2019). Structural insights into dimethylation of 12S rRNA by TFB1M: indispensable role in translation of mitochondrial genes and mitochondrial function. *Nucleic Acids Research* 47, 7648–7665.
142. Lopez Sanchez, M.I.G., Krüger, A., Shiriaev, D.I., Liu, Y., and Rorbach, J. (2021). Human Mitoribosome Biogenesis and Its Emerging Links to Disease. *International Journal of Molecular Sciences* 22, 3827.
143. Lopez Sanchez, M.I.G., Cipullo, M., Gopalakrishna, S., Khawaja, A., Rorbach, L. (2020). Methylation of Ribosomal RNA: A Mitochondrial Perspective. *Frontiers in Genetics* 11, 761.
144. Maiti, P., Antonicka, H., Gingras, A.-C., Shoubridge, E.A., and Barrientos, A. (2020). Human GTPBP5 (MTG2) fuels mitoribosome large subunit maturation by facilitating 16S rRNA methylation. *Nucleic Acids Research* 48, 7924–7943.
145. Maiti, P., Kim, H.-J., Tu, Y.-T., and Barrientos, A. (2018). Human GTPBP10 is required for mitoribosome maturation. *Nucleic Acids Research* 46, 11423–11437.
146. Maiti, P., Lavdovskaia, E., Barrientos, A., and Richter-Dennerlein, R. (2021). Role of GTPases in Driving Mitoribosome Assembly. *Trends in Cell Biology* 31, 284–297.
147. Maracci, C., and Rodnina, M.V. (2016). Review: Translational GTPases. *Biopolymers* 105, 463–475.
148. Maracci, C., Wohlgemuth, I., and Rodnina, M.V. (2015). Activities of the peptidyl transferase center of ribosomes lacking protein L27. *RNA* 21, 2047–2052.
149. Martin, R., Straub, A.U., Doebele, C., and Bohnsack, M.T. (2013). DExD/H-box RNA helicases in ribosome biogenesis. *RNA Biology* 10, 4–18.
150. Márquez, V., Fröhlich, T., Armache, J.-P., Sohmen, D., Dönhöfer, A., Mikolajka, A., Berninghausen, O., Thomm, M., Beckmann, R., Arnold, G.J., et al. (2011). Proteomic characterization of archaeal ribosomes reveals the presence of novel archaeal-specific ribosomal proteins. *Journal of Molecular Biology* 405, 1215–1232.
151. Melnikov, S., Ben-Shem, A., de Loubresse, N.G., Jenner, L., Yusupova, G., and Yusupov, M. (2012). One core, two shells: bacterial and eukaryotic ribosomes. *Nat Struct Mol Biol* 1–8.
152. Metodiev, M.D., Lesko, N., Park, C.B., Cámara, Y., Shi, Y., Wibom, R., Hultenby, K., Gustafsson, C.M., and Larsson, N.-G. (2009). Methylation of 12S rRNA is necessary for in vivo stability of the small subunit of the mammalian mitochondrial ribosome. *Cell Metabolism* 9, 386–397.
153. Metodiev, M.D., Spåhr, H., Loguercio Polosa, P., Meharg, C., Becker, C., Altmueller, J., Habermann, B., Larsson, N.-G., and Ruzzenente, B. (2014). NSUN4 is a dual function mitochondrial protein required for both methylation of 12S rRNA and coordination of mitoribosomal assembly. *PLoS Genet* 10, e1004110.
154. Milón, P., and Rodnina, M.V. (2012). Kinetic control of translation initiation in bacteria. *Crit Rev Biochem Mol Biol* 47, 334–348.
155. Minczuk, M., He, J., Duch, A.M., Ettema, T.J., Chlebowski, A., Dzionek, K., Nijtmans,

- L.G.J., Huynen, M.A., and Holt, I.J. (2011). TEFM (c17orf42) is necessary for transcription of human mtDNA. *Nucleic Acids Research* 39, 4284–4299.
156. Nagaike, T., Suzuki, T., Tomari, Y., Takemoto-Hori, C., Negayama, F., Watanabe, K., and Ueda, T. (2001). Identification and characterization of mammalian mitochondrial tRNA nucleotidyltransferases. *Journal of Biological Chemistry* 276, 40041–40049.
157. Nakamura, Y., and Ito, K. (2011). tRNA mimicry in translation termination and beyond. *Wiley Interdiscip Rev RNA* 2, 647–668.
158. Ni, X., Davis, J.H., Jain, N., Razi, A., Benlekbir, S., McArthur, A.G., Rubinstein, J.L., Britton, R.A., Williamson, J.R., and Ortega, J. (2016). YphC and YsxC GTPases assist the maturation of the central protuberance, GTPase associated region and functional core of the 50S ribosomal subunit. *Nucleic Acids Research* 44, 8442–8455.
159. Nierhaus, K.H., and Dohme, F. (1974). Total reconstitution of functionally active 50S ribosomal subunits from *Escherichia coli*. *Proc Natl Acad Sci USA* 71, 4713–4717.
160. Nikolay, R., Hilal, T., Qin, B., Mielke, T., Bürger, J., Loerke, J., Textoris-Taube, K., Nierhaus, K.H., and Spahn, C.M.T. (2018). Structural Visualization of the Formation and Activation of the 50S Ribosomal Subunit during In Vitro Reconstitution. *Mol Cell* 70, 881–893.e883.
161. Nikolay, R., Hilal, T., Schmidt, S., Qin, B., Schwefel, D., Vieira-Vieira, C.H., Mielke, T., Bürger, J., Loerke, J., Amikura, K., et al. (2021). Snapshots of native pre-50S ribosomes reveal a biogenesis factor network and evolutionary specialization. *Mol Cell* 81, 1200–1215.e1209.
162. Nissen, P., Hansen, J., Ban, N., Moore, P.B., and Steitz, T.A. (2000). The structural basis of ribosome activity in peptide bond synthesis. *Science* 289, 920–930.
163. Nozaki, Y., Matsunaga, N., Ishizawa, T., Ueda, T., and Takeuchi, N. (2008). HMRF1L is a human mitochondrial translation release factor involved in the decoding of the termination codons UAA and UAG. *Genes Cells* 13, 429–438.
164. O'Brien, T.W., and Kalf, G.F. (1967). Ribosomes from rat liver mitochondria. II. Partial characterization. *Journal of Biological Chemistry* 242, 2180–2185.
165. O'Brien, T.W. (2002). Evolution of a protein-rich mitochondrial ribosome: implications for human genetic disease. *Gene* 286, 73–79.
166. Ogle, J.M., Brodersen, D.E., Clemons, W.M., Tarry, M.J., Carter, A.P., and Ramakrishnan, V. (2001). Recognition of cognate transfer RNA by the 30S ribosomal subunit. *Science* 292, 897–902.
167. Ojala, D., Montoya, J., and Attardi, G. (1981). tRNA punctuation model of RNA processing in human mitochondria. *Nature* 290, 470–474.
168. Ott, M., Amunts, A., and Brown, A. (2016). Organization and Regulation of Mitochondrial Protein Synthesis. *Annu. Rev. Biochem.* 85, 77–101.
169. Pearce, S.F., Rebelo-Guimar, P., D'Souza, A.R., Powell, C.A., Van Haute, L., and Minczuk, M. (2017). Regulation of Mammalian Mitochondrial Gene Expression: Recent Advances. *Trends in Biochemical Sciences* 42, 625–639.
170. Perks, K.L., Rossetti, G., Kuznetsova, I., Hughes, L.A., Ermer, J.A., Ferreira, N., Busch, J.D., Rudler, D.L., Spähr, H., Schöndorf, T., et al. (2018). PTC1D1 Is Required for 16S rRNA Maturation Complex Stability and Mitochondrial Ribosome Assembly. *CellReports* 23, 127–142.
171. Petrov, A.S., Wood, E.C., Bernier, C.R., Norris, A.M., Brown, A., and Amunts, A. (2018). Structural Patching Fosters Divergence of Mitochondrial Ribosomes. *Molecular Biology and Evolution* 36, 207–219.
172. Polacek, N., and Mankin, A.S. (2005). The ribosomal peptidyl transferase center: structure, function, evolution, inhibition. *Crit Rev Biochem Mol Biol* 40, 285–311.

173. Powell, C.A., and Minczuk, M. (2020). TRMT2B is responsible for both tRNA and rRNA m5U-methylation in human mitochondria. *RNA Biology* 17, 451–462.
174. Rackham, O., Busch, J.D., Matic, S., Siira, S.J., Kuznetsova, I., Atanassov, I., Ermer, J.A., Shearwood, A.-M.J., Richman, T.R., Stewart, J.B., et al. (2016). Hierarchical RNA Processing Is Required for Mitochondrial Ribosome Assembly. *CellReports* 16, 1874–1890.
175. Ramrath, D.J.F., Niemann, M., Leibundgut, M., Bieri, P., Prange, C., Horn, E.K., Leitner, A., Boehringer, D., Schneider, A., and Ban, N. (2018). Evolutionary shift toward protein-based architecture in trypanosomal mitochondrial ribosomes. *Science* 362, eaau7735–11.
176. Rey, T., Zaganelli, S., Cuillery, E., Vartholomaiou, E., Croisier, M., Martinou, J.-C., and Manley, S. (2020). Mitochondrial RNA granules are fluid condensates positioned by membrane dynamics. *Nat Cell Biol* 22, 1180–1186.
177. Reyes, A., Favia, P., Vidoni, S., Petruzzella, V., and Zeviani, M. (2020). RCC1L (WBSCR16) isoforms coordinate mitochondrial ribosome assembly through their interaction with GTPases. *PLoS Genet* 16, e1008923.
178. Richter, R., Rorbach, J., Pajak, A., Smith, P.M., Wessels, H.J., Huynen, M.A., Smeitink, J.A., Lightowers, R.N., and Chrzanowska-Lightowers, Z.M. (2010). A functional peptidyl-tRNA hydrolase, ICT1, has been recruited into the human mitochondrial ribosome. *EMBO J* 29, 1116–1125.
179. Richter-Dennerlein, R., Oeljeklaus, S., Lorenzi, I., Ronsör, C., Bareth, B., Schendzielorz, A.B., Wang, C., Warscheid, B., Rehling, P., and Dennerlein, S. (2016). Mitochondrial Protein Synthesis Adapts to Influx of Nuclear-Encoded Protein. *Cell* 167, 471–483.e10.
180. Rodnina, M.V., Stark, H., Savelsbergh, A., Wieden, H.J., Mohr, D., Matassova, N.B., Peske, F., Daviter, T., Gualerzi, C.O., and Wintermeyer, W. (2000). GTPases mechanisms and functions of translation factors on the ribosome. *Biological Chemistry* 381, 377–387.
181. Rodnina, M.V. (2018). Translation in Prokaryotes. *Cold Spring Harbor Perspectives in Biology* 10, a032664.
182. Rodnina, M.V., Fischer, N., Maracci, C., and Stark, H. (2017). Ribosome dynamics during decoding. *Philos Trans R Soc Lond B Biol Sci* 372.
183. Rodnina, M.V., Peske, F., Peng, B.-Z., Belardinelli, R., and Wintermeyer, W. (2019). Converting GTP hydrolysis into motion: versatile translational elongation factor G. *Biological Chemistry* 401, 131–142.
184. Roger, A.J., Muñoz-Gómez, S.A., and Kamikawa, R. (2017). The Origin and Diversification of Mitochondria. *Curr Biol* 27, R1177–R1192.
185. Rorbach, J., Boesch, P., Gammage, P.A., Nicholls, T.J.J., Pearce, S.F., Patel, D., Hauser, A., Perocchi, F., and Minczuk, M. (2014). MRM2 and MRM3 are involved in biogenesis of the large subunit of the mitochondrial ribosome. *Mol Biol Cell* 25, 2542–2555.
186. Rorbach, J., Gammage, P.A., and Minczuk, M. (2012). C7orf30 is necessary for biogenesis of the large subunit of the mitochondrial ribosome. *Nucleic Acids Research* 40, 4097–4109.
187. Rorbach, J., Gao, F., Powell, C.A., D'Souza, A., Lightowers, R.N., Minczuk, M., and Chrzanowska-Lightowers, Z.M. (2016). Human mitochondrial ribosomes can switch their structural RNA composition. *Proc. Natl. Acad. Sci. U.S.A.* 113, 12198–12201.
188. Rorbach, J., Richter, R., Wessels, H.J., Wydro, M., Pekalski, M., Farhoud, M., Kühl, I., Gaisne, M., Bonnefoy, N., Smeitink, J.A., et al. (2008). The human mitochondrial ribosome recycling factor is essential for cell viability. *Nucleic Acids Research* 36, 5787–5799.
189. Rozanska, A., Richter-Dennerlein, R., Rorbach, J., Gao, F., Lewis, R.J., Chrzanowska-Lightowers, Z.M., and Lightowers, R.N. (2017). The human RNA-binding protein RBFA

- promotes the maturation of the mitochondrial ribosome. *Biochem J* 474, 2145–2158.
190. Rudra, P., Hurst-Hess, K.R., Cotten, K.L., Partida-Miranda, A., and Ghosh, P. (2020). Mycobacterial HflX is a ribosome splitting factor that mediates antibiotic resistance. *Proc Natl Acad Sci USA* 117, 629–634.
191. Sanchez, M.I.G.L., Mercer, T.R., Davies, S.M.K., Shearwood, A.-M.J., Nygård, K.K.A., Richman, T.R., Mattick, J.S., Rackham, O., and Filipovska, A. (2011). RNA processing in human mitochondria. *Cell Cycle* 10, 2904–2916.
192. Schatz, G., Haslbrunner, E., and Tuppy, H. (1964). Deoxyribonucleic acid associated with yeast mitochondria. *Biochem Biophys Res Commun* 15, 127–132.
193. Seffouh, A., Jain, N., Jahagirdar, D., Basu, K., Razi, A., Ni, X., Guarné, A., Britton, R.A., and Ortega, J. (2019). Structural consequences of the interaction of RbgA with a 50S ribosomal subunit assembly intermediate. *Nucleic Acids Research* 47, 10414–10425.
194. Sengupta, S., Mondal, A., Dutta, D., and Parrack, P. (2018). HflX protein protects *Escherichia coli* from manganese stress. *J Biosci* 43, 1001–1013.
195. Sharma, M.R., Koc, E.C., Datta, P.P., Booth, T.M., Spremulli, L.L., and Agrawal, R.K. (2003). Structure of the mammalian mitochondrial ribosome reveals an expanded functional role for its component proteins. *Cell* 115, 97–108.
196. Smits, P., Smeitink, J.A.M., van den Heuvel, L.P., Huynen, M.A., and Ettema, T.J.G. (2007). Reconstructing the evolution of the mitochondrial ribosomal proteome. *Nucleic Acids Research* 35, 4686–4703.
197. Soleimanpour-Lichaei, H.R., Kühl, I., Gaisne, M., Passos, J.F., Wydro, M., Rorbach, J., Temperley, R., Bonnefoy, N., Tate, W., Lightowlers, R., et al. (2007). mtRF1a is a human mitochondrial translation release factor decoding the major termination codons UAA and UAG. *Mol Cell* 27, 745–757.
198. Spåhr, H., Habermann, B., Gustafsson, C.M., Larsson, N.-G., and Hällberg, B.M. (2012). Structure of the human MTERF4-NSUN4 protein complex that regulates mitochondrial ribosome biogenesis. *Proc. Natl. Acad. Sci. U.S.A.* 109, 15253–15258.
199. Srinivasan, K., Dey, S., and Sengupta, J. (2019). Structural modules of the stress-induced protein HflX: an outlook on its evolution and biological role. *Current Genetics* 65, 363–370.
200. Summer, S., Smirnova, A., Gabriele, A., Toth, U., Fasemore, A.M., Förstner, K.U., Kuhn, L., Chicher, J., Hammann, P., Mitulović, G., et al. (2020). YBEY is an essential biogenesis factor for mitochondrial ribosomes. *Nucleic Acids Research* 48, 9762–9786.
201. Svidritskiy, E., and Korostelev, A.A. (2018). Conformational Control of Translation Termination on the 70S Ribosome. *Structure* 26, 821–828.e823.
202. Szczepanowska, K., Maiti, P., Kukat, A., Hofsetz, E., Nolte, H., Senft, K., Becker, C., Ruzzenente, B., Hornig-Do, H.-T., Wibom, R., et al. (2016). CLPP coordinates mitoribosomal assembly through the regulation of ERAL1 levels. *EMBO J* 35, 2566–2583.
203. Tamaru, D., Amikura, K., Shimizu, Y., Nierhaus, K.H., and Ueda, T. (2018). Reconstitution of 30S ribosomal subunits in vitro using ribosome biogenesis factors. *RNA* 24, 1512–1519.
204. Tan, J., Jakob, U., and Bardwell, J.C.A. (2002). Overexpression of two different GTPases rescues a null mutation in a heat-induced rRNA methyltransferase. *Journal of Bacteriology* 184, 2692–2698.
205. Temperley, R.J., Wydro, M., Lightowlers, R.N., and Chrzanowska-Lightowlers, Z.M. (2010a). Human mitochondrial mRNAs--like members of all families, similar but different. *Biochim Biophys Acta* 1797, 1081–1085.
206. Temperley, R., Richter, R., Dennerlein, S., Lightowlers, R.N., and Chrzanowska-Lightowlers, Z.M. (2010b). Hungry codons promote frameshifting in human mitochondrial

ribosomes. *Science* 327, 301–301.

207. Thurlow, B., Davis, J.H., Leong, V., Moraes, T.F., Williamson, J.R., and Ortega, J. (2016). Binding properties of YjeQ (RsgA), RbfA, RimM and Era to assembly intermediates of the 30S subunit. *Nucleic Acids Research* 44, 9918–9932.
208. Tobiasson, V., and Amunts, A. (2020). Ciliate mitoribosome illuminates evolutionary steps of mitochondrial translation. *eLife* 9, 4–15.
209. Tobiasson, V., Gahura, O., Aibara, S., Baradaran, R., Zíková, A., and Amunts, A. (2021). Interconnected assembly factors regulate the biogenesis of mitoribosomal large subunit. *EMBO J* 40, e106292.
210. Traub, P., and Nomura, M. (1968). Structure and function of *E. coli* ribosomes. V. Reconstitution of functionally active 30S ribosomal particles from RNA and proteins. *Proc Natl Acad Sci USA* 59, 777–784.
211. Tsuboi, M., Morita, H., Nozaki, Y., Akama, K., Ueda, T., Ito, K., Nierhaus, K.H., and Takeuchi, N. (2009). EF-G2mt is an exclusive recycling factor in mammalian mitochondrial protein synthesis. *Mol Cell* 35, 502–510.
212. Tu, Y.-T., and Barrientos, A. (2015). The Human Mitochondrial DEAD-Box Protein DDX28 Resides in RNA Granules and Functions in Mitoribosome Assembly. *CellReports* 10, 854–864.
213. van der Sluis, E.O., Bauerschmitt, H., Becker, T., Mielke, T., Frauenfeld, J., Berninghausen, O., Neupert, W., Herrmann, J.M., and Beckmann, R. (2015). Parallel Structural Evolution of Mitochondrial Ribosomes and OXPHOS Complexes. *Genome Biology and Evolution* 7, 1235–1251.
214. van Esveld, S.L., and Huynen, M.A. (2018). Does mitochondrial DNA evolution in metazoa drive the origin of new mitochondrial proteins? *IUBMB Life* 70, 1240–1250.
215. Van Haute, L., Hendrick, A.G., D'Souza, A.R., Powell, C.A., Rebelo-Guiomar, P., Harbour, M.E., Ding, S., Fearnley, I.M., Andrews, B., and Minczuk, M. (2019). METTL15 introduces N4-methylcytidine into human mitochondrial 12S rRNA and is required for mitoribosome biogenesis. *Nucleic Acids Research* 47, 10267–10281.
216. Verstraeten, N., Fauvart, M., Versées, W., and Michiels, J. (2011). The universally conserved prokaryotic GTPases. *Microbiol Mol Biol Rev* 75, 507–42.
217. Vetter, I.R., and Wittinghofer, A. (1999). Nucleoside triphosphate-binding proteins: different scaffolds to achieve phosphoryl transfer. *Q Rev Biophys* 32, 1–56.
218. Vetter, I.R., and Wittinghofer, A. (2001). The guanine nucleotide-binding switch in three dimensions. *Science* 294, 1299–1304.
219. Vilardo, E., Nachbagauer, C., Buzet, A., Taschner, A., Holzmann, J., and Rossmann, W. (2012). A subcomplex of human mitochondrial RNase P is a bifunctional methyltransferase—extensive moonlighting in mitochondrial tRNA biogenesis. *Nucleic Acids Research* 40, 11583–11593.
220. Voorhees, R.M., Weixlbaumer, A., Loakes, D., Kelley, A.C., and Ramakrishnan, V. (2009). Insights into substrate stabilization from snapshots of the peptidyl transferase center of the intact 70S ribosome. *Nat Struct Mol Biol* 16, 528–533.
221. Waltz, F., and Giegé, P. (2020). Striking Diversity of Mitochondria-Specific Translation Processes across Eukaryotes. *Trends in Biochemical Sciences* 45, 149–162.
222. Waltz, F., Soufari, H., Bochler, A., Giegé, P., and Hashem, Y. (2020). Cryo-EM structure of the RNA-rich plant mitochondrial ribosome. *Nat Plants* 6, 377–383.
223. Wang, C., Richter-Dennerlein, R., Pacheu-Grau, D., Liu, F., Zhu, Y., Dennerlein, S., and Rehling, P. (2020). MITRAC15/COA1 promotes mitochondrial translation in a ND2 ribosome-nascent chain complex. *EMBO Rep* 21, e48833.
224. Wanschers, B.F.J., Szklarczyk, R., Pajak, A., van den Brand, M.A.M., Gloerich, J.,

- Rodenburg, R.J.T., Lightowers, R.N., Nijtmans, L.G., and Huynen, M.A. (2012). C7orf30 specifically associates with the large subunit of the mitochondrial ribosome and is involved in translation. *Nucleic Acids Research* 40, 4040–4051.
225. Wesolowska, M.T., Richter-Dennerlein, R., Lightowers, R.N., and Chrzanowska-Lightowers, Z.M.A. (2014). Overcoming stalled translation in human mitochondria. *Front Microbiol* 5, 374.
226. Wittinghofer, A., and Vetter, I.R. (2011). Structure-Function Relationships of the G Domain, a Canonical Switch Motif. *Annu. Rev. Biochem.* 80, 943–971.
227. Yakubovskaya, E., Guja, K.E., Mejia, E., Castano, S., Hambardjieva, E., Choi, W.S., and Garcia-Diaz, M. (2012). Structure of the essential MTERF4:NSUN4 protein complex reveals how an MTERF protein collaborates to facilitate rRNA modification. *Structure* 20, 1940–1947.
228. Yoshizawa, S., Fourmy, D., and Puglisi, J.D. (1999). Recognition of the codon-anticodon helix by ribosomal RNA. *Science* 285, 1722–1725.
229. Zaganelli, S., Rebelo-Guimar, P., Maundrell, K., Rozanska, A., Pierredon, S., Powell, C.A., Jourdain, A.A., Hulo, N., Lightowers, R.N., Chrzanowska-Lightowers, Z.M., et al. (2017). The Pseudouridine Synthase RPUSD4 Is an Essential Component of Mitochondrial RNA Granules. *Journal of Biological Chemistry* 292, 4519–4532.
230. Zaremba-Niedzwiedzka, K., Caceres, E.F., Saw, J.H., Bäckström, D., Juzokaite, L., Vancaester, E., Seitz, K.W., Anantharaman, K., Starnawski, P., Kjeldsen, K.U., et al. (2017). Asgard archaea illuminate the origin of eukaryotic cellular complexity. *Nature* 541, 353–358.
231. Zeng, R., Smith, E., and Barrientos, A. (2018). Yeast Mitoribosome Large Subunit Assembly Proceeds by Hierarchical Incorporation of Protein Clusters and Modules on the Inner Membrane. *Cell Metabolism* 27, 645–656.e647.
232. Zhang, Y., Mandava, C.S., Cao, W., Li, X., Zhang, D., Li, N., Zhang, Y., Zhang, X., Qin, Y., Mi, K., et al. (2015). HflX is a ribosome-splitting factor rescuing stalled ribosomes under stress conditions. *Nat Struct Mol Biol* 22, 906–913.
233. Zhou, D., Tanzawa, T., Lin, J., and Gagnon, M.G. (2020). Structural basis for ribosome recycling by RRF and tRNA. *Nat Struct Mol Biol* 27, 25–32.

8 List of figures

Figure 1. Overview of the human mitoribosome structure.....	16
Figure 2. Structure of the mitoribosomal central protuberance	17
Figure 3. Schematic representation of the PTC structure	18
Figure 4. Structure of the human mitoribosome bound to the OXA1L insertase.....	19
Figure 5. The mammalian mitochondrial mRNA channel.....	21
Figure 6. The mitochondrial genome and RNAs	23
Figure 7. Translation cycle in human mitochondria	25
Figure 8. Compartmentalization of the mitochondrial gene expression.....	29
Figure 9. The assembly map of the human mitoribosome	33
Figure 10. Structure of the G-domain	37
Figure 11. The GTPase cycle.....	39
Figure 12. The domain architecture of the ribosome assembly GTPases	40
Figure 13. Conserved sequence motifs of the ribosome-associated GTPases	123
Figure 14. A model of the hierarchical GTPase-driven maturation of the mtLSU functional centers.....	130

Elena Lavdovskaia

Curriculum Vitae

Address: Humboldtallee 22, 37073 Göttingen, Germany

Phone: +4915773403945

E-mail: lavdovskaia@gmail.com

Education

- 2017 – present** **PhD**
PhD program 'GGNB Molecular Biology of Cells', University Medical Centre Göttingen, Department of Cellular Biochemistry (Germany)
- 2011 – 2013** **M.S. in Molecular Genetics (with honors)**
St. Petersburg State University, Faculty of Biology and Soil Sciences, Department of Genetics (Russia)
- 2007 – 2011** **B.S. in Biology (area of specialization: Genetics)**
St. Petersburg State University, Faculty of Biology and Soil Sciences, Department of Genetics (Russia)

Academic & Research Experience

- 2017 – present** **PhD Student (full funded academic position)**
University Medical Centre Göttingen, Department of Cellular Biochemistry (Germany)
Supervisor: Dr. Ricarda Richter-Dennerlein
PhD Thesis: 'The role of GTPases in human mitochondrial ribosome biogenesis'
- 2014 – 2016** **Research Assistant (full funded academic position)**
I.P. Pavlov First St. Petersburg State Medical University and N.N. Petrov Institute of Oncology (Russia)
Supervisor: Prof. Dr. Evgeny Imyanitov and Dr. Aglaya Ievleva
Project: 'EGFR T790M Mutation in TKI-Naïve Clinical Samples: Frequency, Tissue Mosaicism, Predictive Value and Awareness on Artifacts'
- 2011 – 2013** **Graduate Student and Senior Lab Technician**
St. Petersburg State University, Faculty of Biology and Soil Sciences, Department of Genetics (Russia)
Project: Influence of *sup35* allele combinations on stability and maintenance of prion [*PSI*⁺] in yeast *Saccharomyces cerevisiae*

Publications

Peer-reviewed journal articles

Lavdovskaia E., Kolander E., Steube E., Mai M.M., Urlaub H., Richter-Dennerlein R. (2018). The human Obg protein GTPBP10 is involved in mitoribosomal biogenesis. *Nucleic Acids Res.* 46(16):8471-8482. doi: 10.1093/nar/gky701.

Lavdovskaia ED, Iyevleva AG, Sokolenko AP, Mitiushkina NV, Preobrazhenskaya EV, Tiurin VI, Ivantsov AO, Bizin IV et al. (2018). EGFR T790M Mutation in TKI-Naïve Clinical Samples: Frequency, Tissue Mosaicism, Predictive Value and Awareness on Artifacts. *Oncol Res Treat.* 41(10):634-642. doi: 10.1159/000491441.

Lavdovskaia E., Denks K., Nadler F., Steube E., Linden A., Urlaub H., Rodnina M.V., Richter-Dennerlein R. (2020). Dual function of GTPBP6 in biogenesis and recycling of human mitochondrial ribosomes. *Nucleic Acids Res.* 48(22):12929-12942. doi: 10.1093/nar/gkaa1132.

Hillen, H., **Lavdovskaia, E.**, Nadler, F., Hanitsch, E., Linden, A., Bohnsack, K., Urlaub, H., and Richter-Dennerlein, R. (2021). Structural basis of GTPase-mediated mitochondrial ribosome biogenesis and recycling. *Nature Communications* 12. doi: 10.1038/s41467-021-23702-y.

Review Articles

Maiti, P., **Lavdovskaia, E.**, Barrientos, A., and Richter-Dennerlein, R. (2021). Role of GTPases in Driving Mitoribosome Assembly. *Trends in Cell Biology* 31, 284–297. doi: 10.1016/j.tcb.2020.12.008.

Awards & Honors

- | | |
|----------------|---|
| 09.2019 | GGNB Travel Grant (956 €)
Supporting travel to EMBO/FEBS Lecture Course ‘Mitochondria in Life, Death and Disease’, Herceg Novi, Montenegro |
| 05.2018 | GGNB Travel Grant (1.450 €)
Supporting travel to EMBO Workshop ‘Molecular Biology of Mitochondrial Gene Expression’, Svartsjö, Sweden |
| 04.2016 | Diploma – 1st Place Award
Podium presentation at the LXXVII International Practical Conference of Young Scientists ‘The Actual Questions of Experimental and Practical Medicine’
St. Petersburg, Russia |
| 06.2013 | M.S. Diploma with Honors |
| 07.2012 | Certificate of Completion
Intensive Scientific English Language Training, U.S. Civilian Research |

Development Foundation (CRDF)
Yekaterinburg, Russia

Conferences

Podium Presentations

- 23.05.2018** **Lavdovskaia E.**, Kolander E., Steube E., Richter-Dennerlein R. Ribosome biogenesis in human mitochondria.
EMBO Workshop 'Molecular Biology of Mitochondrial Gene Expression', Svartsjö, Sweden
- 06.02.2018** **Lavdovskaia E.**, Kolander E., Steube E., Richter-Dennerlein R. GTPases in human mitochondrial ribosome biogenesis.
SFB860 Retreat 2018, Hirschegg, Austria
- 16.04.2016** **Lavdovskaia E.**, Iyevleva A., Mitushkina N., Zaitcev I. Determination of the EGFR T790M frequency in lung cancer samples from Russian patients with the use of wild type allele amplification inhibitors.
LXXVII Practical Conference of Young Scientists 'The actual questions of Experimental and Practical Medicine', St. Petersburg, Russia

Selected Poster Presentations

- 25.09.2018** **Lavdovskaia E.**, Hanitsch E., Steube E., Richter-Dennerlein R. Role of GTPases in mitochondrial ribosome biogenesis.
EMBO/FEBS Lecture Course 'Mitochondria in Life, Death and Disease', Herceg Novi, Montenegro
- 21.04.2016** **Lavdovskaia E.**, Iyevleva A., Mitushkina N., Raskin G., Zaitcev I., Korzhenevskaja M., Imyanitov E. Detection of the EGFR T790M mutation in lung cancer samples from Russian patients using highly sensitive PNA-mediated real-time PCR clamping technology.
20th International Pushchino School Conference of Young Scientists "Biology – the Science of the XXI Century", Pushchino, Russia

Teaching Experience

- 2019** **Georg-August University Göttingen**
Practical course: 'Investigating macromolecular complexes by density gradient centrifugation' (GGNB Doctoral program)
Göttingen, Germany
- 2017 – 2018** **Georg-August University, University Medical Center Göttingen**
Undergraduate practical course: Seminars in medical biochemistry (Faculty of Medicine, 1st academic semester)

Göttingen, Germany

2014 – 2016

I.P. Pavlov First St. Petersburg State Medical University

Undergraduate course: Seminars in medical biology (Faculty of Medicine, 1st and 2nd academic semester)

St. Petersburg, Russia